**Determination of the Effective Bond Strength for Near-Surface Mounted
Titanium-Alloy Bars in Reinforced Concrete**

by

Jack Christian Flowers

A thesis submitted to the Graduate Faculty of
Auburn University
in partial fulfillment of the
requirements for the Degree of
Master of Science

Auburn, Alabama
May 4, 2024

Keywords: Bond strength, Bridge Strengthening, Reinforced Concrete, Near Surface Mounting,
Titanium-Alloy Bars,

Approved by

Kadir C. Sener, Chair, Assistant Professor of Civil Engineering
Anton K. Schindler, Professor of Civil Engineering
Robert W. Barnes, Professor of Civil Engineering

ABSTRACT

The repair and strengthening of existing structures have become active research areas in civil engineering with the objective of developing efficient means to extend the service life of bridges to avoid the high cost of replacing transportation infrastructure. Strengthening reinforced concrete members using near-surface mounted (NSM) titanium-alloy bars (TiABs) has recently emerged as a feasible option to provide a simple and economical solution over other alternatives such as carbon fiber-reinforced polymers. However, experimental investigations are still needed to establish and verify design procedures and to enable structural reliability studies. The AASHTO Guide for Design and Construction of Near-Surface Mounted Titanium-alloy Bars for Strengthening Concrete Structures provides an assumed average bond strength of 1 ksi for TiABs that have hooked anchorage. The AASHTO Guide does not provide any information on any other type of anchorage or TiAB mounting method. This project investigated: (i) the effective bond strength for bonded TiAB with hooked anchorage (hooked-bonded) to achieve yielding and the assumed 1 ksi of bond strength, (ii) the effective bond strength for bonded TiAB with no hooked anchorage at the bar ends (straight-bonded) to achieve yielding, and (iii) the flexural behavior of TiAB that are unbonded along the length of the bar with hooked anchorage (hooked-unbonded).

Fifteen test specimens, including one control, with varying TiAB anchorage types and bond lengths were tested. Average bond strengths of 1.09 ksi, 0.82 ksi, and 0.55 ksi yielded a hooked-bonded #4 TiAB in a NSM flexural bending application. The specimen that exhibited 1.09 ksi of average bond strength achieved the expected strength from the AASHTO Guide's nominal moment equation adapted for the use of NSM TiAB. However, improved ductility was observed with longer bonded lengths that represent a lower average bond strength such as 0.82

ksi. The AASHTO Guide average bond strength recommendation of 1.0 ksi for hooked-bonded anchorage method appears to be a reasonable effective bond strength designation based on the testing conducted in this research, but large-scale testing is recommended to gain greater confidence for use in design documents. Average bond strengths of 0.55 ksi, 0.41 ksi, and 0.34 ksi yielded a straight-bonded #4 TiABs in a NSM flexural bending application. The specimen that exhibited the 0.55 ksi of average bond strength achieved the expected strength from the AASHTO Guide's nominal moment equation adapted for the use of NSM TiAB for hooked-bonded anchorage. However, more ductile behavior was observed with longer bonded lengths that represent a lower average bond strength such as 0.41 ksi. 0.5 ksi for straight-bonded anchorage methods appears to be a reasonable effective bond strength designation based on the testing conducted in this research, but large-scale testing is recommended to gain greater confidence for use in design documents. Specimens mounted with hooked-unbonded TiAB achieved yielding and similar capacities as the hooked-bonded and straight-bonded strengthening methods with larger crack widths and a lower stiffness. The observed low stiffness and large crack widths supports other researchers' recommendations to use hooked-unbonded TiAB for temporary operations.

ACKNOWLEDGEMENTS

TABLE OF CONTENTS

TABLE OF FIGURES

TABLE OF TABLES

CHAPTER 1: INTRODUCTION

1.1 General Background

According to National Bridge Inventory (NBI) data, over 60 percent of US bridges are made of concrete, and bridges built before 1970 are nearing the end of their service life; additionally, the rapid growth in the volume and weight of truck traffic during recent decades is seriously affecting the long-term performance of bridges (Nowak and Latsko, 2018). Many bridges that were built in the 1950s and 1960s had inadequate reinforcement detailing (Adkins and George, 2017). Thus, repair and strengthening of deteriorated structures have become active research areas in civil engineering with the objective of developing efficient means to extend the service life of bridges to avoid the high cost of replacing transportation infrastructure. Therefore, improvements to the load carrying capacity or fatigue performance may be required for existing reinforced concrete (RC) bridges to extend their service life further or adapt to new serviceability conditions. Common reasons for bridge strengthening include: (i) outdated design or detailing practices, (ii) repurposing of the bridge, (iii) increase in traffic volume, (iv) increase in the weight of vehicles crossing the bridge, and (v) damage (e.g., fire, vehicle collision, corrosion, delamination, material fatigue, and chemical degradation).

Several strengthening methods have emerged for RC bridges because repairing/strengthening a bridge is more economical than replacing one. Common repair/strengthening methods include increasing member size, external post-tensioning, rebar planting, externally bonded plates, externally bonded carbon fiber reinforced polymer (CFRP) sheets, near-surface mounting (NSM) of CFRP strips/bars, among others. Increases in self-weight, requirements of skilled labor, complicated stressing procedures, careful and lengthy

surface preparations, as well as non-ductile failure modes are all drawbacks to current techniques (Vavra, 2016). Near-surface mounting of CFRP is a common repair/strengthening method because it results in minimal damage to the structure, does not require skilled labor, and does not increase the self-weight of the bridge. In the NSM method, a groove is cut into the tension side of the concrete and then the reinforcement is epoxied into the center of the groove, see Figure 1.1. CFRP is used because it has high mechanical strength, high corrosion resistance, and low unit weight. NSM with FRP is not a perfect solution because the stress-strain performance of the FRP is brittle (Subagia and Kim, 2014).

Researchers at Oregon State University (OSU) tested titanium-alloy bars (TiABs) as reinforcement by using the NSM method. Titanium has similar advantages as CFRP because it is highly resistant to corrosion, but it also exhibits a ductile stress-strain response like steel and can be anchored by mechanical hooks. The inelastic deformations after the TiABs yield results in a ductile failure mode that is consistent with how RC is designed to fail in flexure. The mechanical anchors allow stresses in the bar to develop with shorter embedment lengths. The mechanical anchors also add redundancy to the system by connecting the TiAB to the concrete with bearing forces on the inside of the hooks in addition to the bond with the epoxy. OSU researchers successfully strengthened a bridge in Mosier Oregon with NSM TiABs (Higgins et al., 2015b). A design guide for NSM TiABs was developed by the OSU researchers and Oregon DOT engineers based on their experience and published by The American Association of State Highway and Transportation Officials, the ASHTO Guide for Design and Construction of Near-Surface Mounted Titanium-alloy Bars for Strengthening Concrete Structures (AASHTO, 2020). The AASHTO Guide assumes an average bond strength of 1.0 ksi is achieved in hooked-bonded

applications based on conclusions drawn for FRP strengthening in the Guide for the Design and

and Construction of Externally Bonded FRP systems (ACI Committee 440, 2017).
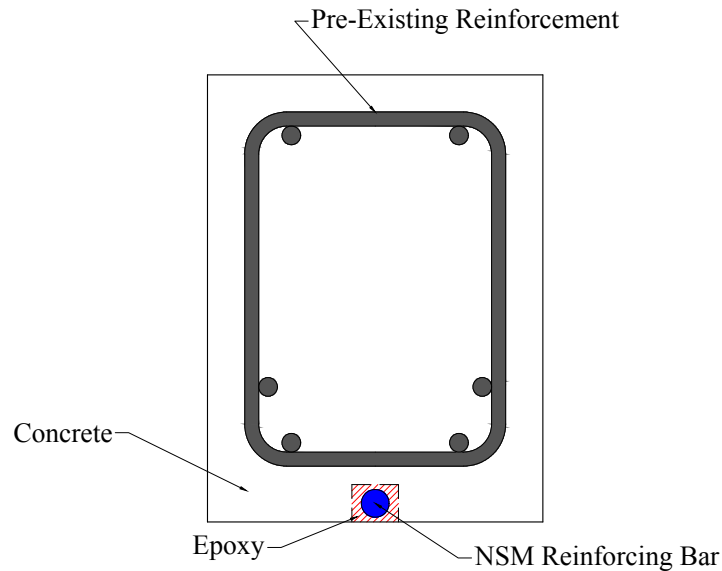
Figure 1.1 – Near Surface Mounting of Reinforcement

Most of the research regarding NSM TiABs investigated mounting the bars into an

epoxied groove with hooks penetrating the concrete (hooked-bonded). There are common

constraints that have led to the investigation of other mounting methods. These constraints

include (i) shallow decks that the TiAB hooks could penetrate through, (ii) unknown location of

original mild reinforcing steel that could interfere with TiAB hook holes, and (iii) time of

installation due to lane or railroad closure costs. One investigated method is to epoxy the TiAB

into the groove without having hooked end anchorage (straight-bonded). This method provides

little disturbance to the existing concrete because drilling holes for the hooks is not required. The

straight-bonded method can also be useful in shallow deck conditions where there is not

adequate depth for a standard hooked anchorage. The effective bond strength of straight-bonded

NSM TiABs is unknown and needs to be investigated. Another investigated method that

mitigates these constraints is to mount the TiAB to the concrete by epoxying the hooked ends into the concrete exclusively and unbonded along the length of the bar (hooked-unbonded). This method significantly reduces installation time becuase the groove cutting process is not required. Minimal research has been conducted on this mounting method aside from OSU. The hooked-unbonded installation method's minimal research accompanied by the potential industry impact motivated a further investigation.

1.2 Research Objectives

Different mounting methods for NSM TiAB as strengthening applications for reinforced concrete bridges with flexural strength deficiencies are evaluated in this thesis. The main objectives are listed below:

1. Determine the effective bond strength to achieve yielding of NSM TiABs with hooked-bonded anchorage and compare it to the assumed 1.0 ksi of average bond strength mentioned in the current standard.

2. Determine the effective bond strength to achieve yielding of NSM TiABs with unhooked straight-bonded anchorage and develop effective bond strength recommendations for design.

3. Investigate the behavior of hooked-unbonded NSM TiABs and provide design recommendations.

1.3 Research Implementation

This study is part of comprehensive research where the goal is to strengthen strength-deficient RC bridges in Alabama. The overall research project includes 5 project-tasks. Task 1 – material-level experimental studies, task 2 – member-level experimental studies, task 3 - analytical mode development and verification, task 4 - preparation of strengthening guidelines and bid

documentation, and task 5 – preparation of final project report. Task 1 is the focus of this thesis. The results from this thesis were taken under consideration when deciding embedment lengths of the TiABs for task 2.

1.4 Research Methodology

This study was conducted to experimentally investigate the bond behavior of near surface mounted Titanium-alloy bars used to strengthen concrete beams. Hooked-bonded, straight-bonded, and hooked-unbonded mounting methods were observed on 15 different concrete beams. The concrete beams were cast in Auburn, Alabama on November 16, 2021. The specimens were pre-cracked prior to the installation of the TiABs. The strengthened specimens were loaded until failure, which was defined as a 5% reduction in strength. The loading of the concrete beam commenced from May to August of 2022. The displacement, reinforcing bar strains, and curvature were recorded to evaluate the bond behavior. Conclusions were drawn based on a comparison to a control beam that was not reinforced with NSM TiABs, a numerical model that accounted for the additional TiAB, and the nominal capacities of the strengthened concrete utilizing equations from the AASHTO Guide for Design and Construction of Near-Surface Mounted Titanium-alloy Bars for Strengthening Concrete (AASHTO, 2020).

1.5 Thesis Organization

Chapter 2 provides a literature review of the use of NSM TiABs, with an emphasis on research conducted at Oregon State University and University of Pittsburgh. Chapter 3 discusses a strength-deficient bridge in Coleman, Alabama that is the potential candidate for the first bridge in Alabama to be strengthened using NSM TiABs. Chapter 4 presents the specimen design and test matrix to achieve the research objectives. Chapter 5 discusses the mechanical properties of the materials used and the construction of the specimens. Chapter 6 includes the testing program

where the instrumentation and load protocol are outlined. Chapter 7 presents the specimen preparation for bond strength testing including the pre-cracking of the specimens and the installation of the NSM TiAB. Chapter 8 present the results of the strengthened beam tests of each bond method and provides outcomes on effective bond strength. Chapter 9 includes the conclusions of this study and recommendations for future research.

CHAPTER 2: LITERATURE REVIEW

2.1 Introduction

The development of economic and reliable concrete strengthening techniques has gained

popularity in the last decades. This is motivated by the growing need to repair our current

bridges and infrastructure as mentioned in Chapter 1. This chapter discusses common concrete

strengthening techniques, titanium corrosive properties, research on the flexural performance of

NSM TiABs, research on the bond performance of NSM TiABs, NSM TiAB bond research

needs, failure modes of concrete with NSM reinforcement, and current standards regarding the

use of strengthening with TiABs.

2.2 NSM FRP

The most common method used to strengthen existing RC structures is the addition of fiber-

reinforced polymer (FRP) composite materials externally bonded using adhesives (e.g., epoxy).

The design method and the implementation alternatives in construction for FRP have

significantly advanced over the past two decades. ACI Committee 440 created a Guide for the

design and construction of externally bonded FRP systems for strengthening concrete structures

(ACI Committee 440, 2017). Carbon fiber reinforced polymers (CFRP) are a type of FRP that

are commonly used because of their high modulus, high strength, good creep resistance, high

corrosion resistance, and low unit weight (Subagia & Kim, 2014). There are four common

implementations for retrofitting and repair with FPR: (i) sheets (Nurbaiah et al., 2010) and (Choi

et al., 2022), (ii) laminates (Bertolotti, 2012) and (Hassan & Rizkalla, 2003), (iii) near-surface

mounted (NSM) bars (Al-Mahmoud et al., 2009) and (Nurbaiah et al., 2010), and (iv) hybrid

solutions of the aforementioned (Maheswaran et al., 2022) and Hadi et al., (2022).

2.3 NSM with CFRP

CFRP reinforcement, as mentioned in section 2.2 above, has a reasonably high modulus, high strength, good creep resistance, high corrosion resistance, and low unit weight. It has become a popular repair application for these reasons. Despite the advantages of having a high structural performance to weight ratio, CFRPs are (i) brittle due to a lack of a mechanical yield plateau (Subagia & Kim, 2014) (ii) as a fiber unable to form hooks for anchorage. Subagia and Kim (2104) tested CFRP, basalt fiber-reinforced polymer (BFRP), and hybrid composites for tensile strengths in a universal testing machine in accordance with ASTM D 638 (2022); the results are seen in Figure 2.1.
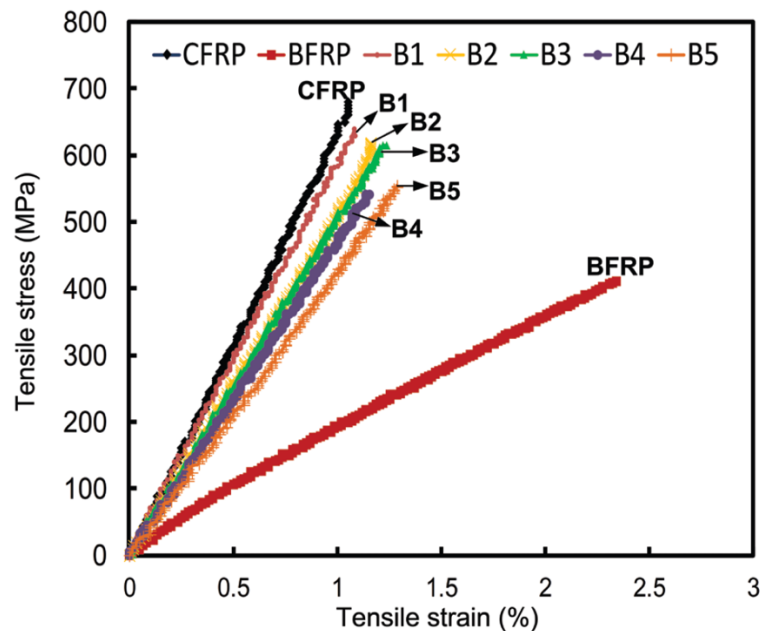
Figure 2.1 – Stress Strain Curve of CFRP and Other Fibers (Subagia and Kim, 2014)

Figure 2.1 demonstrates the tensile strength of CFRP can reach 689.7 MPa (100 ksi). The maximum tensile strain for CFRP in this case is slightly above 1%. It has become an accepted strengthening method because it is capable of reaching significant strengths. However, as illustrated in the figure, CFRP does not have a yield plateau. This causes significant amounts of

8

energy to be stored in the CFRP as it undergoes strain with no inelastic deformation. The stored

energy is released upon rupture or potential debonding of the CFRP. The lack of yielding for

CFRP results in failures at the peak load without any warnings or post-peak displacement, which

is provided by conventional RC design that can be designed to fail in a tension-controlled failure

mode. Figure 2.2 displays laboratory test beams that were reinforced with different ratios of

CFRP (Bertolotti, 2012). The last two numbers in the specimen's name indicate the ratio of

CFRP reinforcement. LS6F00 had a yield plateau, because it did not have any NSM CFRP strips

(i.e., is the control specimen) whereas the specimens with NSM-bonded CFRP failed at peak

load.
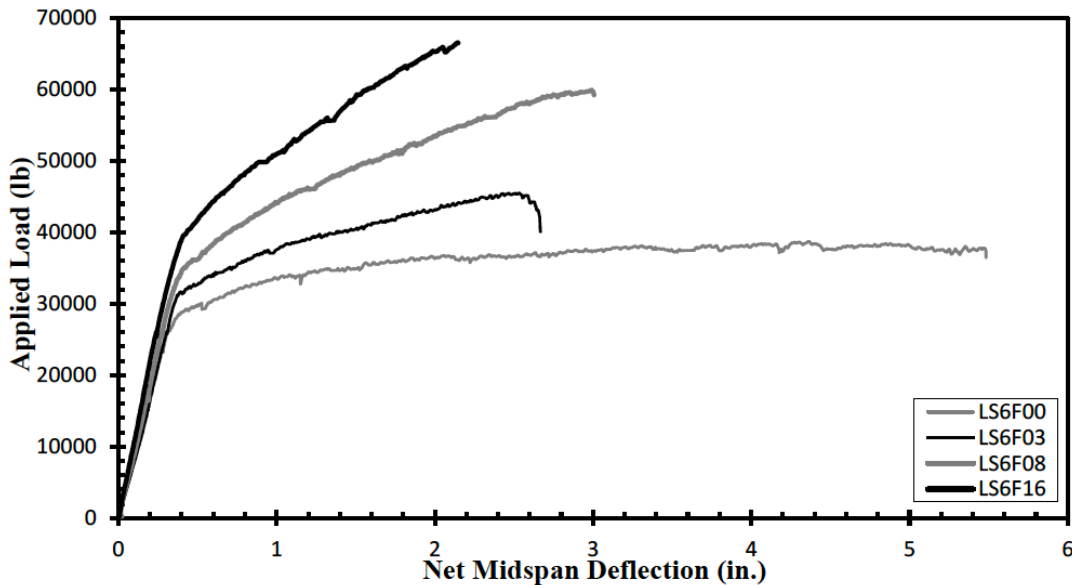
Figure 2.2 – Load vs Deflection FRP Reinforced Bridge Girder (Bertolotti, 2012)

CFRP is available as sheets, laminates, and bars, therefore cannot be bent into hooks

capable of having high anchorage resistance. On the other hand, metal NSM reinforcement can

bend into forming such anchorages that can potentially provide shorter development lengths and desirable debonding failures (Barker, 2014).

2.4 NSM with TiAB

Strengthening using NSM titanium-alloy bars has emerged as a feasible option to provide a simple and economical solution over conventional alternatives such as CFRP because of its steel-like stress strain behavior, see Figure 2.3, and ability to be bent to achieve additional hooked anchors.
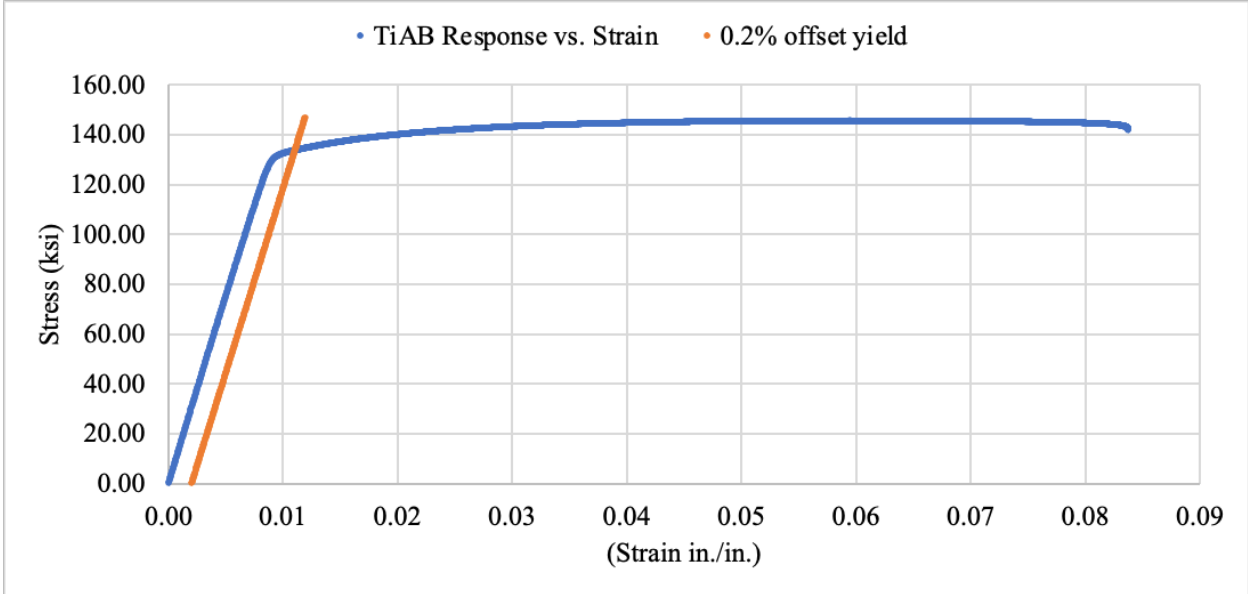
Figure 2.3 – Stress Strain Curve of TiAB with 0.2% offset yield

Flexural strengthening with NSM TiABs has the potential to provide additional load carrying capacity while maintaining the ductile behavior of RC members. TiAB reinforcement has advantageous properties as a retrofit material due to its: (i) high nominal yield strength (120-130 ksi) (ASTM B1009 2020), (ii) steel-like stress-strain response with a well-defined yield point and significant ductility as displayed in Figure 2.3, (iii) robust corrosion resistance and high durability to environmental exposure conditions (Bomberger et al., 1954), (iv) no galvanic

induced corrosions with black steel (Platt and Harries, 2018), (v) high deformability to allow bending of bars into mechanical anchors (Perryman Company, 2021), and (vi) cost-effectiveness compared to other alternatives (Higgins et al., 2017). Higgins et al. (2017) reported an application of NSM TiAB for the strengthening of a reinforced concrete bridge that was completed at a 30% cost savings compared to alternative solutions (CFRP).

2.5 Corrosion Resistance of Titanium

Titanium as a material has proven to be incredibly resistant to marine environments as well as galvanic corrosion (S. Platt & Harries, 2018). This makes it a great material for NSM applications because it is placed close to the face of the concrete where reinforcement is more susceptible to atmospheric conditions. The NSM of titanium requires it to be in close contact with the existing reinforcing steel. If galvanic corrosion were to occur, then the state of the existing reinforcing steel could become compromised making the resisting strength of the RC lesser than before the titanium was introduced to the system.

2.5.1 Bomberger, Cambourelis, and Hutchinson (1954)

Bomberger, Cambourelis, and Hutchinson (1954) published Corrosion Properties of Titanium in Marine Environments. Commercially produced cold-rolled titanium strips that were 6 x 1.5 x 1/32 or 1/16 inches were tested for titanium's corrosion properties. The titanium was exposed to industrial and rural atmospheres during the 1950's for approximately five years and sea water up to four and a half years. The conclusion was that the titanium appeared to be completely unaffected by these exposure conditions.

2.5.2 Platt and Harries (2018)

Platt and Harries (2018) published the Study of galvanic corrosion potential of NSM titanium reinforcing bars. This study assessed the effects of coupling Ti-6Al-4V titanium-alloy and ASTM A615 black steel in NSM applications. Sixty-two concrete prisms were tested, each having a single embedded No.4 ASTM A615 black steel bar. A 0.5 in. diameter titanium bar, CFRP, or 2205 stainless steel NSM bar was embedded along one side of the prism into NSM slots. For two years the specimens were conditioned in a cyclic temperature and humidity environment where half-cell potential and macro couple current were monitored. The conclusion was that the presence of Ti-6Al-4V reinforcing bars in proximity or in electrical contact with A615 steel reinforcing bars did not result in any change in the rate or nature of corrosion.

2.6 Flexural Strengthening Studies using NSM TiAB

Oregon State University provided a series of studies using NSM TiABs. These studies evaluated both positive and negative flexural moment strengthening as well as factors such as freeze/thaw and fatigue cycles. Their research, as well as a study from the University of Bath, are highlighted in this section

2.6.1 Laura Barker (2014)

Barker (2014) conducted a study in 2014 on metal NSM techniques to strengthen bridge girders with inadequate moment capacity due to poor rebar detailing. The objective of this study was to develop methods for NSM metallic bars as a retrofit for old bridges with inadequate detailing and develop a design guide. Seven inverted T-beams were tested and meant to simulate bridge girders from the 1950's with poorly detailed flexural steel. Two different metals were used as the NSM reinforcement - titanium and stainless steel. Different detailing inadequacies were simulated in the beams. The inadequacies were created by inducing a crack in the beam,

terminating a bar before development, or by leaving a gap between the longitudinal rebar at

midspan to simulate inadequate lap splicing. Figure 2.4 illustrates a 45° crack with terminating

reinforcing steel that was retrofitted with NSM TiAB. The beam in Figure 2.4 held 420.5 kips

and displaced 1.12 inches at failure while the unreinforced comparison held 358.9 kips and

displaced 0.98 inches at failures.
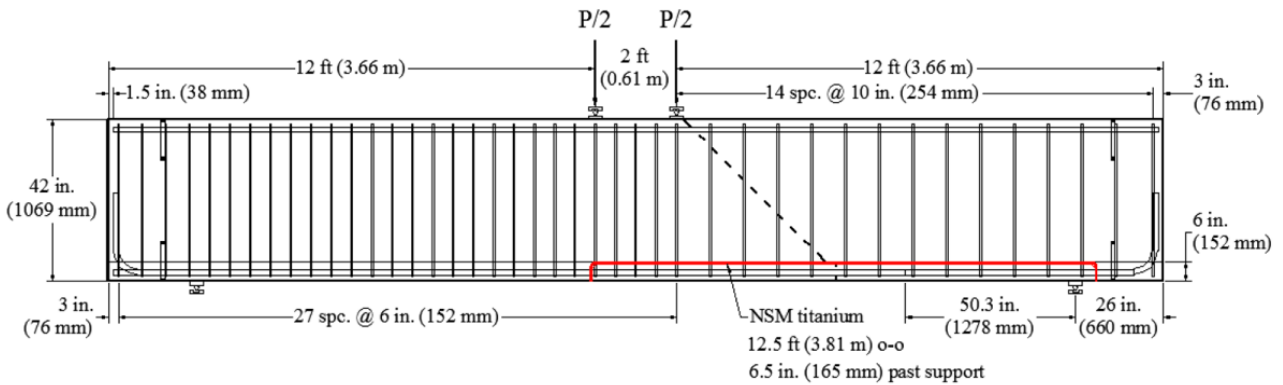
Figure 2.4 – NSM TiAB Retrofitted Beam with Inadequate Detailing (- Moment) (Barker, 2014)

The test results were that the NSM retrofitted with metallurgic bars of stainless steel and

titanium-alloy led to 17% to 39% increase in flexural capacity, respectively, a higher overall

deformation capacity, and a greater distribution of cracking compared to the control specimens.

The failures of the control specimens were shifted from non-ductile diagonal-tension failures to

ductile flexural failures. Out of the two metallurgic bars, titanium-alloy bars had the high

ultimate strength and was deemed by the researchers as the most suitable metal for NSM

strengthening.

2.6.2 Deanna Amneus (2014)

Another thesis from Oregon State University was on a similar project by Amneus (2014). This thesis covered three more specimens (two TiAB and one stainless steel) that were retrofitted to increase positive moment capacity of beams with flexural deficiency. These beams were the same as the ones tested in Barker's study but were not inverted so the positive moment capacity could be tested. Figure 2.5 displays one of the beams that were retrofitted for positive moment capacity.
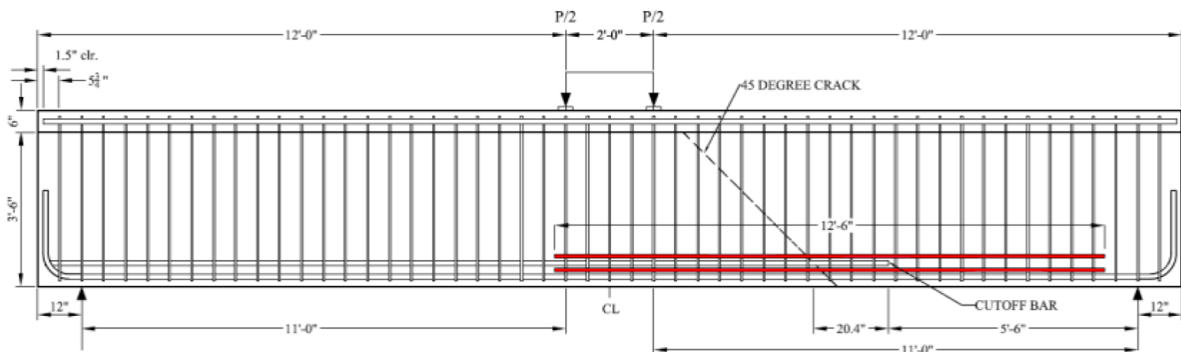
Figure 2.5 - NSM TiAB Retrofitted Beam with Inadequate Detailing (+ Moment) (Amneus, 2014)

Amneus (2014) tested these beams and analyzed the performance of the NSM reinforcing bars. The results demonstrated that the NSM metallurgic bar reinforcement led to an increased moment capacity of up to 44% and ductility increase of up to 174% compared to the baseline specimen. The failures were shifted from non-ductile diagonal-tension failures to ductile flexural failures. The stainless-steel specimen could increase the capacity as much as the titanium-alloy but required twice the reinforcing area. Therefore titanium-alloy bars were deemed as a more suitable option for NSM strengthening.

2.6.3 Higgins, Amneus, and Barker (2015)

In the appendix of both Amneus and Barkers' theses there includes a case study conducted by

Oregon State that successfully repaired a bridge in Mosier Oregon using NSM TiAB. This

research is summarized in the conference article by Higgins et al. (2015b).

A four – span bridge that over crosses I-84 in Mosier, Oregon built in the 1950s was

identified during a biennial bridge inspection in 2013 to have large cracks (0.03 inches), see

Figure 2.6. The Oregon Department of Transportation conducted a test by sweeping truck

models over the span with the prescribed rating. It was determined that the demand at the critical

section was 219 k-ft. This was 46 k-ft above the AASHTO designed moment capacity.

Figure 2.6 - Mosier Bridge with Critical Section circled (Higgins et al., 2015b)

Higgins et al. (2015b) tested three beams to evaluate the NSM TiAB repair application

experimentally before implementing it on the Mosier bridge. The beams were called Mosier 1,

Mosier 2, and Mosier 3, Mosier 1 was a replica of the bridge as it was without any strengthening,

Mosier 2 implements the NSM TiAB after failing the reinforcing steel anchorages, and Mosier 3

applies the TiAB with the steel anchorages fully intact. Figure 2.7 illustrates the location of the

added NSM TiAB reinforcement.
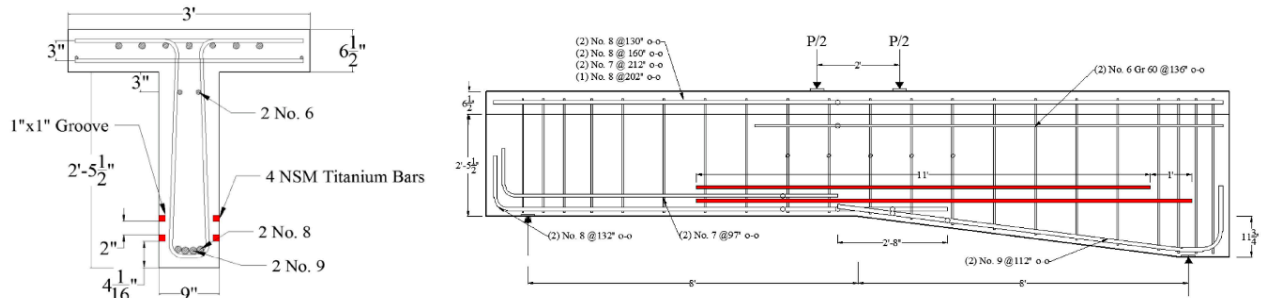
Figure 2.7 - Mosier Girder and Cross Section with NSM TiAB (Higgins et al., 2015b)

The results proved that repairing the Mosier bridge with NSM TiAB would ensure that no shoring or even weight restrictions would be necessary in the future. The experimental girders held more than double the required 219 k-ft. Based on the researchers estimates, the Mosier bridge was strengthened with NSM TiAB at a cost of 30% less than a CFRP alternative. Upon completion of the strengthening of the bridge with NSM TiABs, the weight restrictions were lifted. This process made the Mosier bridge the first bridge to ever be reinforced with NSM titanium-alloy reinforcement.

2.6.4 Platt, Harries, and McCabe (2019)

Plat et al. (2019) conducted a study on flexural strengthening of RC slabs using NSM TiAB method by intentionally damaging four slabs by cutting two of four #5 steel reinforcing bars, which reduced the flexural capacity by 40%. The goal was to see if the capacity could be restored by using NSM TiAB. Four slabs approximately six feet in length were tested/compared to an undamaged control slab of the same length. Two slabs were reinforced with 72-inch straight TiABs. One of the slabs with straight bars had one #5 TiAB and the other had four straight #5 TiAB. Two slabs were reinforced with 16-inch hooked TiABs. One of the slabs with hooked bars had one #5 TiAB and the other had four hooked #5 TiABs. The elevation view of

the retrofits as well as the cuts made to the longitudinal rebar to damage the slab is shown in Figure 2.8. The dimensions provided in Figure 2.8 are in millimeters.
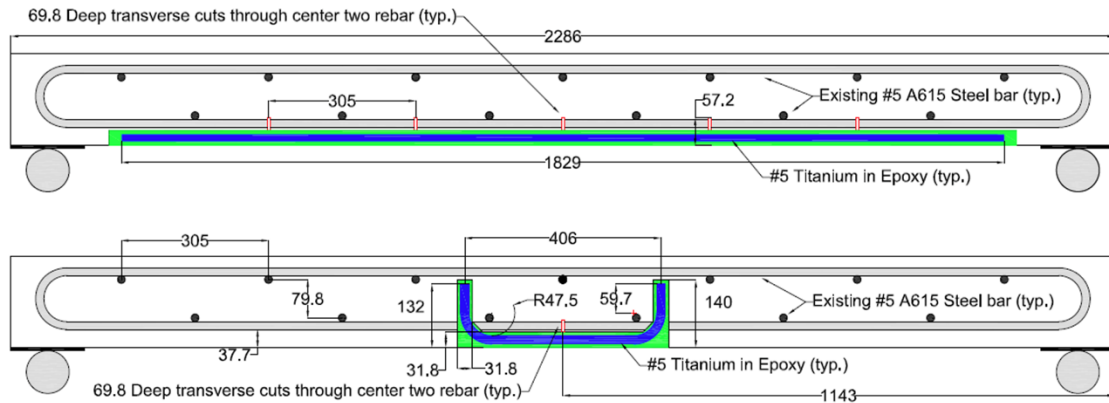
Figure 2.8 - Straight Bar (Top) and Hooked Bar (Bottom) NSM Retrofit (Platt et al., 2019)

These slabs were then tested under 3-point loading until failure and compared to the control slab. The researchers concluded that NSM TiABs could be used for repairing the slabs. The reinforced slabs exceeded the capacity of the original slab with the exception of the singular hooked TiAB slab.

2.6.5 Eric Vavra (2016) – Fatigue/Freeze-Thaw

Vavra (2016) studied NSM TiAB performance during freeze-thaw cycles and simultaneous fatigue cycles. The specimens tested for fatigue/freeze thaw identical to the T.45.Ld3(10) beam tested by Amneus (2014) from Oregon State that can be seen in Figure 2.5 (named T.45.Ld3(10) NSM.FTG/FT in this study). This beam was subject to 1,600,000 cycles to simulate a 50-year service life using Miner's rule with assumed concrete cracking occurred from an 80,000 lb semi-truck. The cycles occurred at a rate of 1.2 Hz and were designed to take the internal reinforcement to 20 ksi which was considered as the upper bound for maintaining long-life in internal steel reinforcement. The mean load for these cycles was 80 kips in a 3-point loading test

set up. Three pseudo static cycles were run from 3 kips to 210 kips at the beginning of the test

and at every 250,000 cycles. These tests occurred in an environmental chamber that

simultaneously underwent freeze/thaw cycles. The temperature range was from 45°F to 21°F

with a 30-minute ramp time between the two extreme temperatures and a 60-minute hold time at

the extreme temperatures. This was equivalent to 8 cycles a day (200 total cycles over 25 days).

Once a day, during the thaw portion of the cycle, the beam was wetted to ensure that there was

enough moisture present to penetrate the cracks and freeze.

After the fatigue and freeze thaw cycles were completed, the beam was moved to the

strong floor where it was failed monotonically in four-point bending. The results of the test are

shown in Table 2.1.

Table 2.1 - Results and Comparison of Fatigue and Freeze/Thaw Test (Vavra, 2016)

Specimen	Applied Load (kip) [kN]	V_{APP} (kip) [kN]	V_{DL} (kip) [kN]	V_{EXP} (kip) [kN]	Midspan Disp. (in) [mm]	Failure Crack Angle (deg)
T.45.Ld3(10)	299.5 [1332]	149.8 [666]	3.1 [14]	152.9 [680]	1.14 [29]	33
T.45.Ld3(10).Ti	392.9 [1748]	196.5 [874]	3.5 [16]	200 [890]	2.11 [54]	33
T.45.Ld(10).Ti.FT/FTG	395.5 [1759]	197.8 [880]	3.6 [16]	201.4 [896]	2.09 [53]	33

This table displays that the fatigue and freeze/thaw cycles had negligible impacts on the

performance of the beam with the NSM TiABs. The applied load was 1% greater and the final

displacement was 1% less than an identical beam that did not undergo the fatigue and

freeze/thaw cycles. Compared to the beam without the NSM TiABs, the capacity was increased

by 32% and the midspan displacement by 83%. The results of Vavra's study demonstrates NSM

using TiAB is negligibly affected by fatigue and freeze/thaw cycles.

2.6.6 Eric Vavra (2016) – Hooked-Unbonded

The thesis by Vavra (2016) mentioned in Section 2.6.5 also tested NSM TiAB using a hooked-unbonded mounting method. The hooked-unbonded method was tested using two identical beams that had three #11 longitudinal bars as positive moment reinforcement in the stem of the beam. Two of the three #11 bars were cut in the middle of the beam to create a weak region. Two different methods of hooked-unbonded bars were observed in this study - epoxy anchors and anchors using prestressing chucks. Both methods were prestressed using deflectors as shown in Figure 2.9. The prestressing force in each bar ranged from 1.6 kips to 5.9 kips.
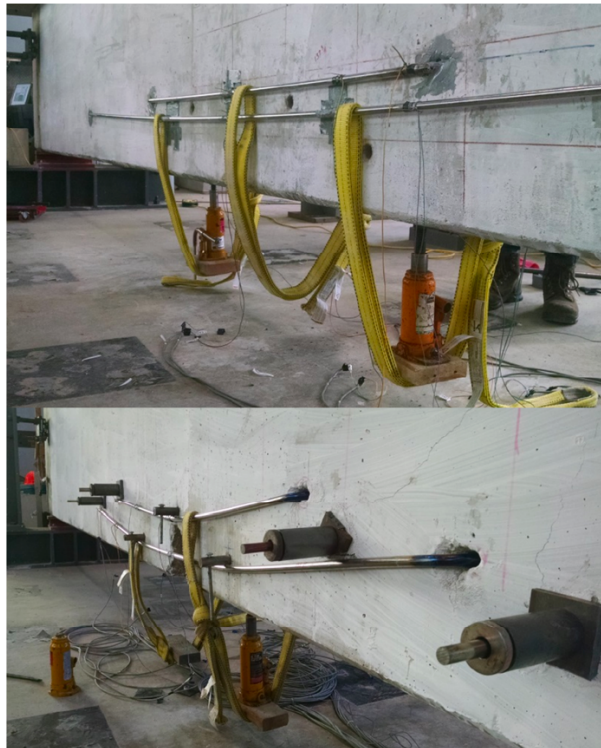
Figure 2.9 – Epoxy Anchors (top) and Prestressing Chuck Anchors (Bottom) (Vavra, 2016)

Response2000 software was used to determine the final load and displacement of an unreinforced beam. Both specimens failed from concrete crushing in the compression zone. The epoxied anchors exhibited slipping which resulted in softening and an overall lower capacity

than compared to the beam with the prestressing chuck anchorage. The control specimen using the software failed at 106.1 kips and 5.12 inches of displacement, the epoxy anchored specimen failed at 171.3 kips (161% increase) and 4.76 inches of displacement, and the prestressing chuck anchored specimen failed at 216.3 kips (204% increase) and 5.06 inches of displacement. The results proved that flexural capacity can be increased using unbonded TiABs. Vavra (2016) recommended that it be used as a temporary fix and not to be used as a long-term solution because of the low stiffness of the system and large crack widths.

2.7 NSM TiAB Bond Strength Test

This section will review experimental studies regarding the bond stress created by NSM TiAB. The theses by Barker (2014) and Amneus (2014) from Oregon State University mentioned in previous sections also performed varying levels of bond studies and those tests will be mentioned in this section.

2.7.1 Barker (2014) – Bond Test

Barker (2014) conducted a study on negative-moment member-level NSM TiAB flexural strengthening- as discussed in Section 2.5.1. This study also conducted pull-out tests to evaluate the strength of several titanium-epoxy interfaces. Five TiABs with different surface deformations/treatments were tested. The surface deformation/treatments were surface blasted, rough finish, as well as light turn, light turn blasted, and heavy turn. "Turn" indicated threading along the bar to increase friction and bond performance. The pull-out test consisted of a 0.75 in. diameter hole drilled 5 in. deep. The hole was filled halfway with epoxy and the bar was set perpendicular to the concrete and allowed to cure for seven days. The pull-out test setup is shown in Figure 2.10.

Figure 2.10 - Pull-out test (Barker, 2014)

The light and heavy turn deformations performed best in the pull-out test. The bars with blasted and rough surface deformations failed between 1.0 and 1.5 ksi of average bond stress and the light turned, heavy turned, and light turned blasted failed above 4.5 ksi of average bond stress calculate from Equation 2.1 Barker (2014).

$$\mu_{avg} = \frac{\Delta f_s d_b}{4 \Delta l}$$ **Equation 2.1**

where

μ_{avg} = average bond stress

Δf_s = change in stress

d_b = diameter of the bar

Δl = change in length over which the stress was measured

Based on the pull-out tests and tensile tests the researchers determined that heavy-turns surface deformation on TiABs provided the best performance.

2.7.2 Amneus (2014) – Bond Test

Amneus (2014) commenced member-level work in 2014 highlighted in section 2.6.2. The member-level study reported an average bond strength of 1.2 ksi for TiABs in flexure. Amneus also tested bond lengths of NSM TiABs at a smaller scale. The bond tests used an adapted version of ASTM A944 (2010). Six 9 x 12 x 4 in. blocks were constructed with a 15/16" groove cut into the top. Three 4 in. embedded #5 TiAB and three 12 in. embedded #5 TiAB were epoxied into the groove of these blocks and pulled with a 110-kip actuator. The test configuration can be seen in Figure 2.11.
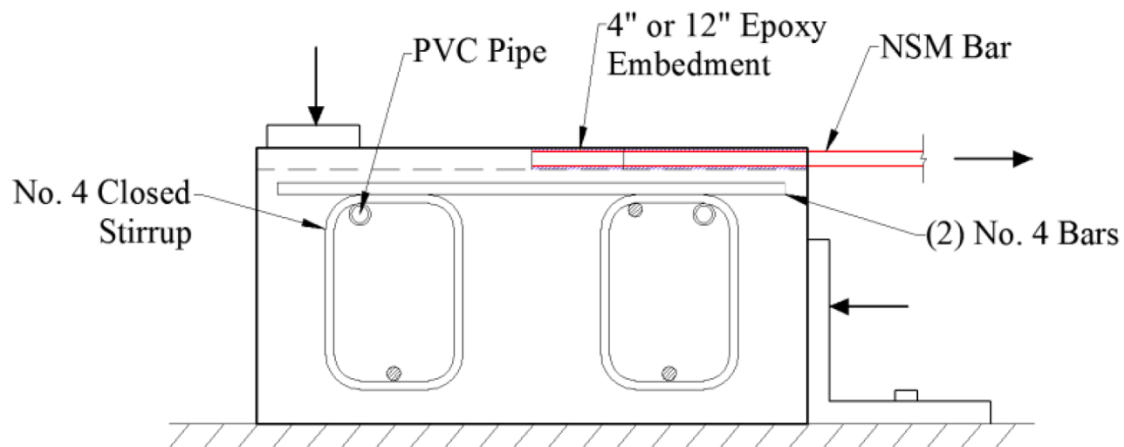
Figure 2.11 - Modified ASTM A944 (2010) for Development Length (Amneus, 2014)

The 4 in. tests failed along the concrete-epoxy interface. The average bond stress was 2.091 ksi using Equation 2.1. The bars embedded 12 inches experienced failures at similar loads as the 4 in. tests and the TiABs did not yield. The failure mode was a 37° plane in the concrete

that was equal in depth to the concrete groove. The average bond stress experienced by the 12 in. embedded bars before failure using Equation 2.5 was 0.802 ksi. The specimen design ended up being the limiting factor of the test rather than the bond interfaces, limiting the researcher's conclusions regarding bond performance of a singular TiAB. However, the development length for a # 5TiAB was determined to be greater than 4 inches.

2.7.3 Vavra (2016) – Bond Test

Vavra (2016) had performed bond stress tests for NSM TiAB called the inverted half-beam test. This test was designed to exhibit slender flexural response under four-point loading with a 12 in. constant moment region. The inverted half beams were 56" long, 14" tall, and 6" wide. Figure 2.12 displays the test configuration.
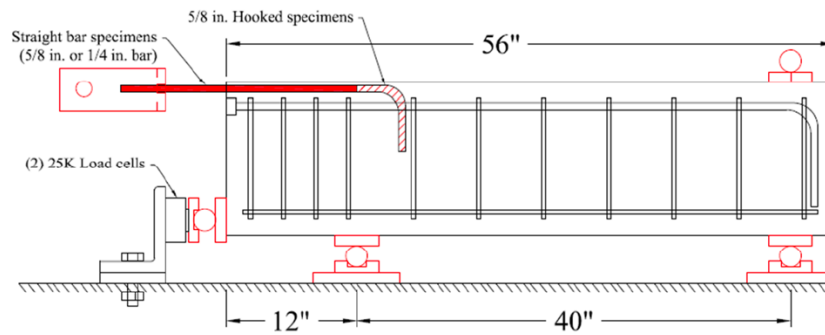
Figure 2.12 - Inverted Half Beam Bond Test Setup (Vavra, 2016)

Vavra tested straight-bonded bars using 4, 6, 8, and 12-inch embedment lengths. Each embedment length was test three times for a total of 12 straight-bonded tests. Three hooked-bonded bars were also tested with embedment lengths of 4, 6, and 8 inches and 90° hooks. #5 TiAB were chosen for these tests.

The straight-bonded bars experienced an average bond stress from 0.5 ksi to 0.6 ksi, also calculated using Equation 2.1, before failing. The failure mechanism for the straight-bonded bars

in this study were a wedge-shaped concrete failure plane from the embedded end of the bar to the free face of the beam. The hooked bars exhibited similar results. The hook-bonded specimens failed in bar pull-out and crushing of the concrete at the hook bearing area. The TiABs achieved an average bar stress of 80 ksi (all three performed similarly) which equates to about 62% of the 130 ksi yield stress. The bond stress was not measured in the hooked specimens.

2.8 NSM FRP Bond Test

This section includes a study of NSM CFRP bond that was used as the basis for the bond study of NSM TiABs commenced in this study.

2.8.1 Hassan and Rizkalla (2003)

A study of the development length of NSM CFRP was conducted by Hassan and Rizkalla (2003) that used a small member-level test under three-point loading. The members were 106 inches (2700 mm) long, 12 inches (300 mm) tall, and had a 6 in. (150 mm) web with a flange that was 12 inches (300 mm) wide and 2 inches (50 mm) deep. An 8 in. (200 mm) weak region existed in the center of the beam. The beam side view and cross section are shown in Figure 2.13.
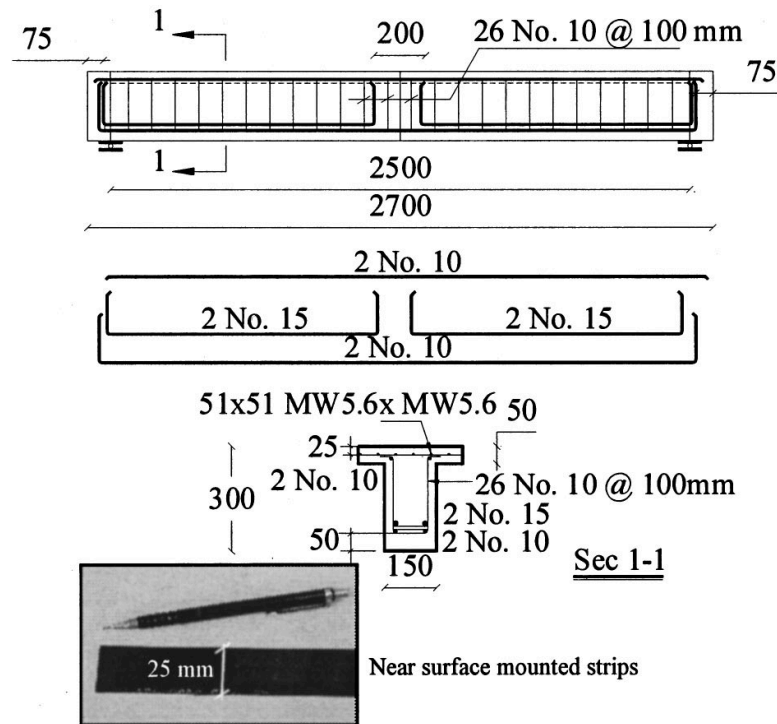
Figure 2.13 - Test Specimen and Reinforcement (Hassan and Rizkalla, 2003)

There were nine specimens tested by Hassan and Rizkalla (2003) with varying embedment lengths of NSM CFRP. The maximum stress achieved by each CFRP strip was graphed versus the embedment lengths as shown in Figure 2.14. From the results collected, it was concluded that a minimum embedment length of 850 mm created full composite interaction and longer strips of embedded CFRP would not increase the load carrying capacity for the test configuration.
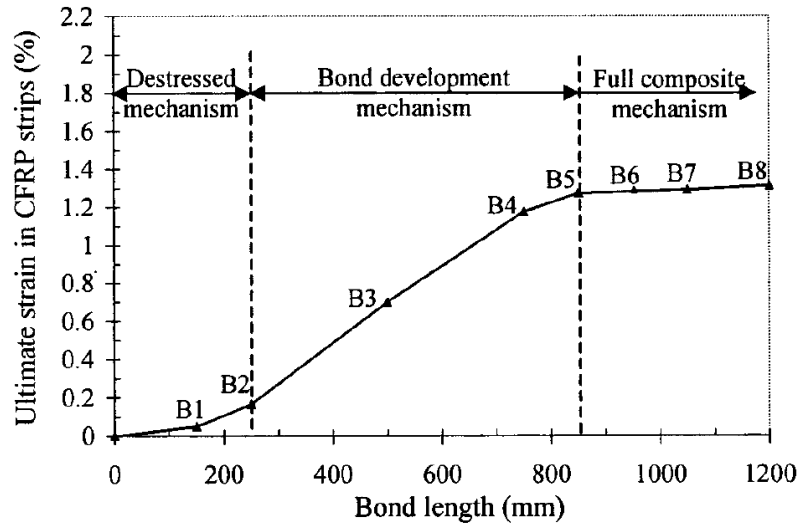
Figure 2.14 - Ultimate Strain vs Bond Length (Hassan and Rizkalla, 2003)

2.9 TiAB Bond Research Needs

This literature review has discussed the overall effectiveness of NSM TiAB as a flexural strengthening method. Understanding the development length of TiAB is necessary for adequate implementation of the NSM TiAB strengthening method.

The AASHTO Guide provides an assumed average bond strength of 1.0 ksi for hook-bonded anchorage cases. The expected average bond strength of 1.0 ksi is referenced from ACI440.R2 regarding FRP (ACI Committee 440, 2017). This value was calibrated using the maximum debonding strain for CFRP of 0.0117 in./in. because the concrete-epoxy interface is typically the limiting factor in NSM reinforcing and not the ultimate strain (Amneus, 2014). Amneus's (2014) study reported an average bond strength of 1.2 ksi for TiABs in flexure, congruent with the AASHTO Guide. The 1.0 ksi of average bond strength for TiABs with hooked-bonded anchorage has been reported in a member-level study, but attempts at determining the bond limits of an isolated TiAB with hooked-bonded and straight-bonded anchorage have not been successful.

26

Research determining the maximum effective bond strength of a singular TiAB that yielded with hooked-bonded or straight-bonded anchorage has not been conducted. The ease of installation and the increased strength observed in Vavra's studies in 2016 prompt further investigation of the hooked-unbonded anchorage method. Therefore, this research aims to use a reconfigured version of the test conducted by Hassan (2003) to conduct tests that achieve yielding. The embedment length will be incrementally changed in a 3-point loading set-up to determine the effective bond strengths of TiABs with hooked-bonded and straight-bonded anchorage methods as well as the performance of the hooked-unbonded anchorage method.

2.10 Failure Modes of NSM Reinforcement

Due to the limited TiAB NSM research, this section includes failure modes exhibited by NSM FRP. Strengthened members can fail as a result of (i) debonding of the reinforcement , (ii) rupture of the reinforcement, (iii) failure in the concrete, or any combination of these modes (Bertolotti, 2012). FRP are unable to form anchors, but the OSU researchers observed anchorage failure of the NSM TiAB (iv). Intermediate crack debonding, epoxy rupture, critical diagonal crack, and end debonding are further classifications of the reinforcement debonding failure modes that are discussed in the following sections.

2.10.1 Rupture of NSM Reinforcement

Rupture of the NSM reinforcement occurs whenever the strains of the NSM reinforcement exceed its tensile strain capacity and the reinforcement ruptures.

2.10.2 Concrete Failure

If the strength of the concrete is low enough or if a large amount of NSM reinforcement is used, the concrete can fail before any failure occurs in the NSM reinforcement. Concrete failure can

occur due to concrete crushing in the compressive region of the member or due to shear failure (Bertolotti, 2012).

2.10.3 Intermediate-Crack (IC) Debonding

Intermediate-Crack (IC) occurs when a flexural crack, typically at or near the maximum moment region, induces high local interfacial shear stresses because of the geometric discontinuity (Zhang et al., 2017). IC debonding can be further classified into either interfacial debonding or cover separation. IC interfacial debonding can occur between the concrete-concrete interface or more commonly the epoxy-concrete interface. IC cover separation debonding occurs when the failure plane is along the depth of the cover region. The two different types of IC debonding can be seen in Figure 2.15.
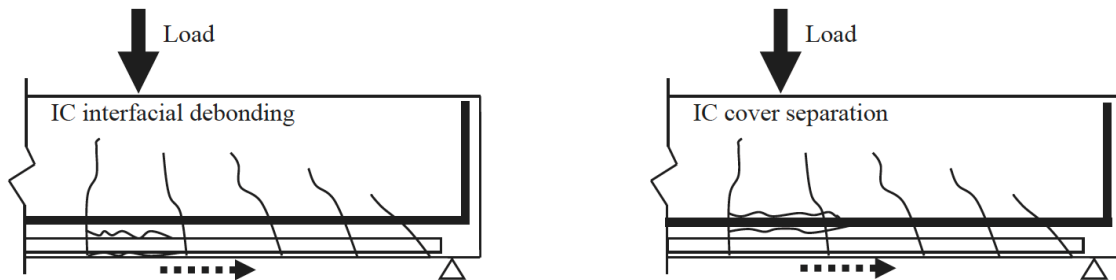
Figure 2.15 - IC Debonding (Zhang et al., 2017)

2.10.4 Epoxy Rupture

Epoxy rupture is initiated by flexural cracks in the epoxy. More cracks propagate within the epoxy and eventually a continuous failure plane is created, and the epoxy shatters. An example of this failure was observed in a study of NSM CFRP rods conducted by Al-Mahmoud, et. al (2009). The epoxy rupture failure in that study is shown in Figure 2.16.

Figure 2.16 – Epoxy Rupture (Al-Mahmoud, et al. 2009)

2.10.5 Critical-Diagonal-Crack (CDC) Debonding

Critical-diagonal-crack (CDC) debonding is similar to IC interfacial debonding but occurs from a diagonal shear crack (Coelho et al., 2015). When the crack reaches the NSM reinforcement, it propagates along the length of the NSM system toward the closest extremity. This can be further classified as either interfacial debonding or cover separation depending on the failure plane.

2.10.6 End Debonding

In this failure mode, the debonding of the NSM reinforcement starts from the terminus and propagates to the mid-span of the beam. This failure mode is mainly due to the high interfacial shear and normal stresses caused by the abrupt termination of the NSM reinforcement (Zhang et al., 2017). It can also be further classified as end cover separation if the crack separates the NSM reinforcement and cover from the core of the beam. Figure 2.17 displays end debonding.
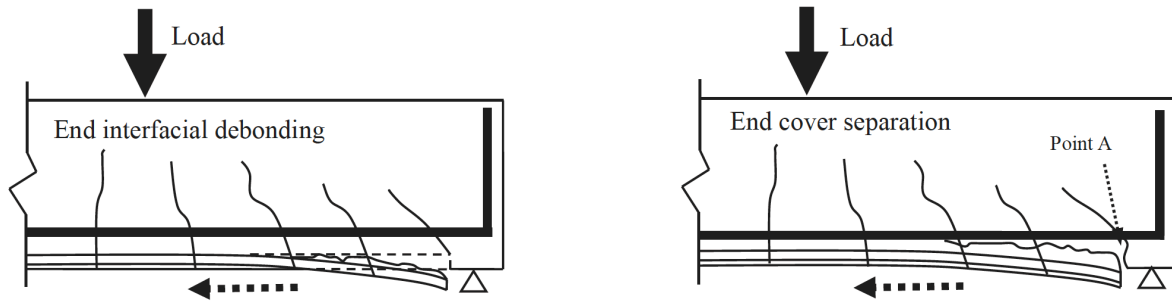
Figure 2.17 - End Debonding (Zhang et al., 2017)

2.10.7 Anchorage Slip

Anchorage slip of hooked reinforcement describes the process of the hook losing its seat and deforming in the direction of the tensile forces. Under increased loading, crushing of the concrete at the inner radius of the bend begins resulting in a loss of bond along the outer radius (Vavra, 2016). The concrete crushing and loss of bond cause the bar to slip in the direction of the tensile force.

2.11 Current Standards for NSM Titanium-alloy Bars

There are two standards for NSM TiABs. The design standard is the AASHTO Guide for Design and Construction of Near-Surface Mounted Titanium-alloy Bars for Strengthening Concrete (AASHTO Guide) (AASHTO, 2020), and the material standard for TiAB is ASTM B-1009: Standard Specification for Titanium-alloy Bars for Near Surface Mounts in Civil Structures (2020).

2.11.1 AASHTO Guide (2020)

The AASHTO Guide (AASHTO, 2020) provides guidance on both shear and flexural strengthening of RC members using NSM TiABs. The suggested installation method requires the use of standard 90-degree hooks at both ends of the bars to provide adequate anchorage. A

minimum concrete compressive strength of 3000 psi is required so the concrete substrate can effectively transmit bond stresses along the length of the TiABs.

In accordance with the AASHTO Guide, the nominal flexural capacity *(M$_n$)* for the case in which both reinforcing steel and TiABs are yielding can be computed as indicated in Equation 2.2. This expression is based on assuming that the flexural tensile strength of the concrete is negligible; the reinforcing steel and TiABs have idealized elastic-plastic behavior; there is no relative slip between the concrete and steel or TiABs; and the use of the equivalent rectangular concrete stress block (Whitney stress block).

$$M_n = A_s f_y \left(d_s - \frac{\beta_1 c}{2} \right) + A_{Ti} \alpha_E f^*_{yTi} \left(d_{Ti} - \frac{\beta_1 c}{2} \right) \qquad \textbf{Equation 2.2}$$

where

A_s = the area of flexural tension steel reinforcement.

f_y = the minimum specified yield stress of steel.

d_s = the distance from the extreme compression fiber to the centroid of the flexural steel.

A_{Ti} = the area of flexural tension TiAB.

α_E = the environmental sensitivity factor for the bonding material (taken as 0.85 for routine exposure environments and 1.00 for insensitive exposure environments).

f^*_{yTi} = the minimum specified yield stress for TiAB.

d_{Ti} = the distance from the extreme compression fiber to the centroid of the flexural TiABs.

$\beta_1 c$ = the height of the rectangular stress block including the effects of the NSM TiAB, determined from Equation 2.3.

$$\beta 1_c = \frac{A_s f_y + A_{Ti} \alpha_E f^*_{yTi}}{0.85 f'_c b_f} \qquad \textbf{Equation 2.3}$$

where

f'_c = the concrete compressive strength.

31

b_f = the effective width of the compression block.

The nominal bond stress specified to determine the development length is calculated in accordance with the AASHTO Guide. The development length (l_{dTi}) of the TiABs with hooks can be determined with Equation 2.4:

$$l_{dTi} = \frac{D_{Ti}}{4} \frac{\alpha_E f_{yTi}^*}{\overline{\mu_u}}$$ **Equation 2.4**

where

D_{Ti} = the diameter of TiAB.

$\overline{\mu_u}$ = the average bond strength when the TiAB yields (taken as 1.0 ksi. for hooked-bonded specimen).

α_E = the environmental sensitivity factor (taken as 1.0 in this study due to the laboratory conditions).

The average bond strength is the focus of this study for the hooked-bonded and straight-bonded bars. The expected average bond strength of 1.0 ksi is referenced from ACI440.R2 (2017) regarding FRP. As discussed in section 2.9, this value was calibrated using the maximum debonding strain for CFRP as the concrete-epoxy interface is typically the limiting factor in NSM reinforcement (Amneus, 2014). Straight-bonded bars that do not have hooked anchorage are not considered in the AASHTO guide and therefore do not have a design average bond strength in AASHTO (2020).

For the design of NSM TiAB the AASHTO Guide provides a flexural resistance factor (Φ_b). This resistance factor depends on the strain distribution in the section when the extreme concrete fiber reaches the assumed crushing strain of 0.003. When the strain in the extreme fiber of the steel is 0.005 then the design is classified as ductile and Φ_b is 0.9. Φ_b is 0.75 when the strain in the extreme fiber is below 0.002. Interpolation is used whenever the strain in the steel is

in-between 0.002 and 0.005. Equations 2.5, 2.5-a, and 2.5-b represent the flexural resistance factor.

$$\Phi_b Mn \geq Mu \qquad \text{Equation 2.5}$$

$$if\ 0.005 > \varepsilon t \geq 0.002\ then\ \Phi_b = 0.75 + \frac{0.15(\varepsilon t - 0.002)}{0.003} \qquad \text{Equation 2.5-a}$$

$$if\ \varepsilon t < 0.002\ then\ \Phi_b = 0.75 \qquad \text{Equation 2.5-b}$$

The AASHTO Guide provides hook diameter and overall tail length recommendations based on the diameter of TiAB. This study follows the recommendations for the hooked-bonded and hooked-unbonded specimens. These values are provided in Table 2.2.

Table 2.2 - Pin Diameters and Overall Tail lengths (obtained from AASHTO (2020))

Bar Designation	Pin Diameter (in.)	Overall Tail Length (in.)
#2	2.00	5
#3	2.75	5
#4	3.00	6
#5	3.75	6
#6	4.50	12

The AASHTO Guide also provides groove dimensions and spacing requirements. The groove width and depth are required to be 1.5 times the D_{Ti}. The minimum clear groove spacing must be twice the groove depth and the minimum edge distance must be four times the depth of the groove. The required groove dimensions and spacing according to bar specifications can be seen in Table 2.3.

Table 2.3 - Groove Dimensions and Spacing Requirements (adapted from AASHTO, 2020)

Bar Designation	Square Groove Dimension (in.)	Minimum Clear Spacing (in.)	Minimum Edge Spacing (in.)
#2	3/8	3/4	1 - 1/2
#3	9/16	1 - 1/8	2 - 1/4
#4	3/4	1 - 1/2	3
#5	15/16	1 - 7/8	3 - 3/4
#6	1 - 1/8	2 - 1/4	4 - 1/2

2.11.2 ASTM B1009 (2022)

This specification covers titanium-alloy bars with surface deformations and 90-degree anchorage hooks for use as near-surface mount reinforcement for flexural strengthening of concrete beams. The titanium-alloy bars specified to be used in these applications are Ti-6Al-4V (Grade 5). This alloy is mainly composed of titanium but also includes small amounts of other elements such as aluminum and vanadium. The detailed chemical composition ranges are provided in Table 2.4.

Table 2.4 - Ti-6Al-4V Chemical Composition (obtained from ASTM Committee B10 2020)

Composition By Weight Percentage	
Grade	5
Carbon (max)	0.080
Oxygen (max)	0.200
Nitrogen (max)	0.050
Hydrogen (max)	0.015
Iron (max)	0.400
Aluminum	5.500-6.750
Vanadium	3.500-4.500
Other Elements (max each)	0.100
Other Elements (max total)	0.400
Titanium	Balance

Two material grades recognized for the titanium-alloy bars in ASTM B1009 (2022) are class 120 and class 130. The minimum yield stress corresponds to 120 ksi and 130 ksi for each class, respectively. The specification requires that all bars should achieve a minimum elongation

of 2 inches or 10% at break. Dimensions, weight, permissible variations, bending requirements, and other restrictions are also provided in ASTM B1009 (2022).

CHAPTER 3: BRIDGE STRENGHTENING CANDIDATE

ALDOT Maintenance Bureau engineers identified a three-span, continuous reinforced-concrete

bridge built in 1962 to be a potential candidate for strengthening with NSM TiABs. The bridge

(NBI ID: 7755) is in Cullman, Alabama on US Route 278 (State Route 74) that is part of the

main street (3rd St.). The exact location is shown in Figure 3.1.
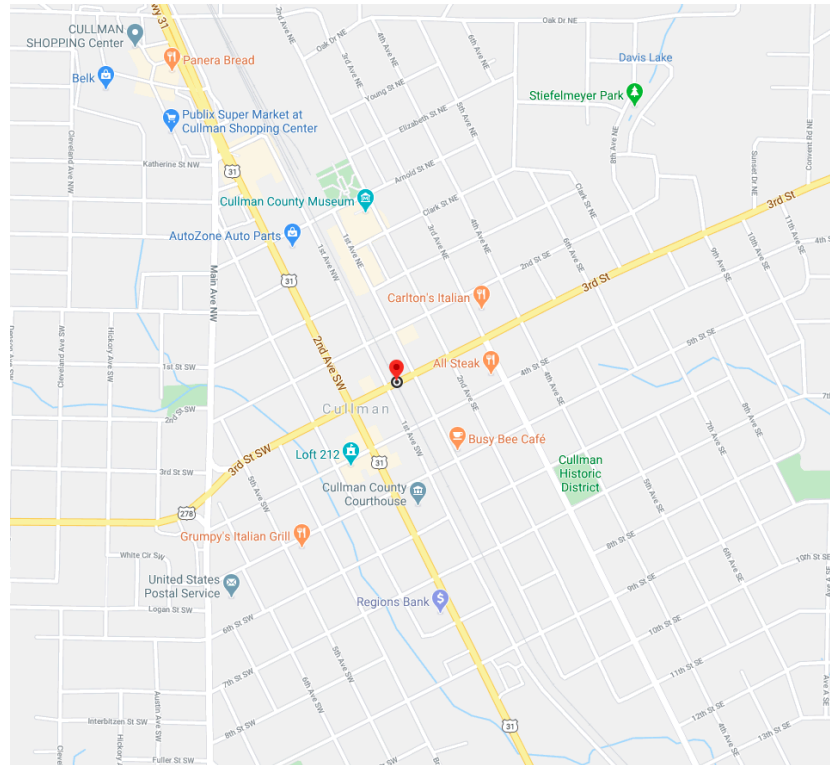
Figure 3.1 - Location of Cullman Bridge (Google Maps 2021)

This bridge is an overpass over the South and North Alabama subdivision railroad line of

CSX Transportation. The bridge has been weight-restricted due to both positive and negative

flexural strength deficiencies for several different truck types, as shown in Figure 3.2.

Figure 3.2 - Cullman Bridge and Posted Weight Limit Sign

Table 3.1 summarizes the locations with insufficient flexural strength for the Emergency

Vehicle (EV3) loading case obtained from the AASHTOWare Bridge Rating (BrR) software.

Load rating factors (LRF) calculated at these critical locations indicate flexural strength

deficiencies in the range of 20%, highlighted in Table 3.1: Span 1, section at 19 ft, LRF = 0.791

(positive moment in yellow), and section at 21.29 ft, LRF = 0.821 (negative moment in orange).

These critical locations coincide with reinforcement cutoff locations at the ends of the haunch

regions where the section depth parabolically decreases from 3'-0" to 1'-8", as shown in Figure

3.3.

Table 3.1 - Locations with Flexural Strength Deficiencies Based on EV3 Load Case

Location (ft)	Percent	Limit State	Units	Capacity	DL + Adj -LL*	LL	Operating Rating Factor	Operating Load Rating (Ton)
Span 1								
15.42	51.4	Flexure	kip-ft	328.46	23.66	211.99	1.080	46.45
18.00	60.0	Flexure	kip-ft	-163.77	8.68	-143.05	0.941	40.48
19.00	63.3	Flexure	kip-ft	185.31	1.21	178.72	0.791	34.01
21.00	70.0	Flexure	kip-ft	-205.50	-16.26	-166.89	0.850	36.54
21.29	71.0	Flexure	kip-ft	-205.50	-19.11	-169.21	0.821	35.32
21.49	71.6	Flexure	kip-ft	-211.19	-21.04	-170.79	0.828	35.60
21.50	71.7	Flexure	kip-ft	-211.44	-21.15	-170.87	0.828	35.61
Span 2								
10.83	25.8	Flexure	kip-ft	185.31	7.08	154.41	0.877	37.73
11.00	26.2	Flexure	kip-ft	192.85	8.67	157.82	0.885	38.05
31.00	73.8	Flexure	kip-ft	192.85	6.93	153.20	0.923	39.69

Table 3.1 and Figure 3.3 confirmed that both positive and negative flexural strengthening is required at the reinforcement cutoff locations in the two end spans (e.g., Section A-A in Figure 3.3). Since the bridge passes over the railroad line, there was also limited clearance and access to perform any work under the bridge (positive moment strengthening). Therefore, this bridge was selected as the representative case to demonstrate the use of NSM TiABs for the strengthening method to address both negative- and positive-moment deficiencies.
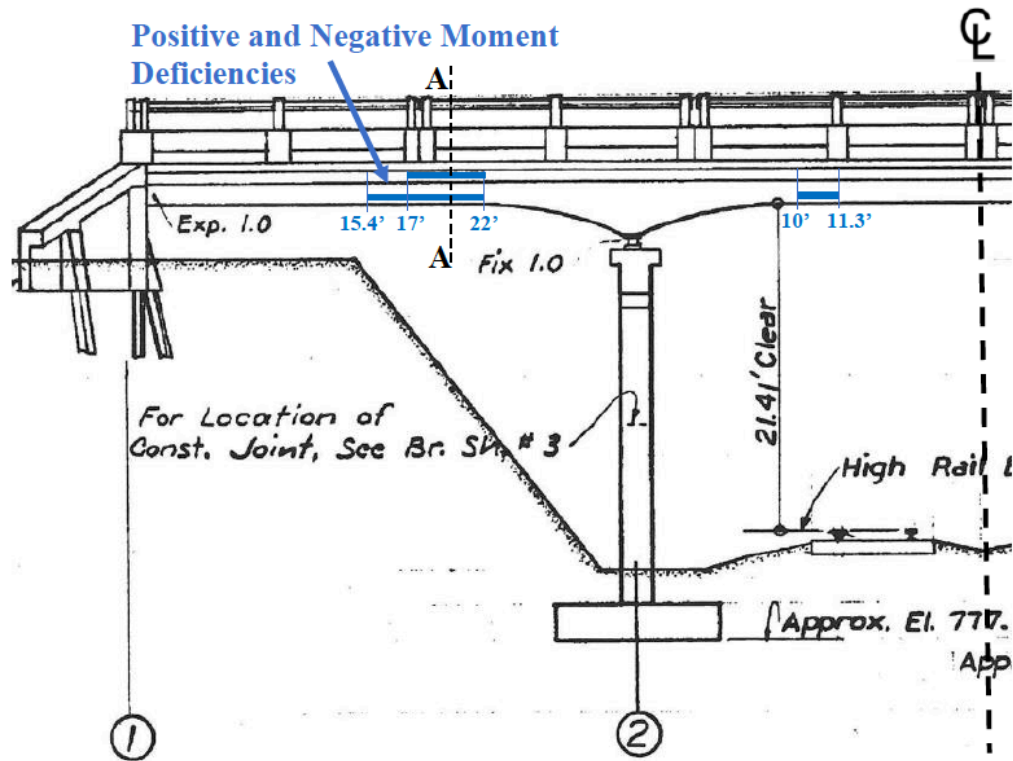
Figure 3.3 - Cullman Bridge Schematic with Critical Sections Highlighted

Other potential anchorage methods besides the hooked-bonded anchorage method mentioned in the AASHTO Guide could be used to strengthen the Cullman bridge. The bridge has a shallow 6-inch deck that could potentially not accommodate the required hook length. Another characteristic of the bridge that discourages the use of hooks is potentially coinciding with the existing reinforcement. For this reason, the experimental investigations also considered straight-bonded bars. Straight-bonded bars require longer embedment lengths to achieve desired performance but will minimize the possibility of colliding with the existing reinforcement. The AASHTO Guide groove is required to be 3/4 inch thick for #4 TiAB and the clear cover of the bridge in Cullman is 1 inch.

The railroad underneath the Cullman bridge poses additional challenges. The closure of the railroad line for the strengthening work will be inconvenient from economical and traffic

disruption standpoints. Therefore, using hooked-unbonded TiABs could be a viable option. This anchorage method would significantly reduce the time to close the railroad line because it is not necessary to cut a groove. Cutting the groove for NSM with TiAB is a lengthy process that requires specialized saw and other equipment and generates a slurry. The unbonded anchorage, if effective, could completely by-pass the groove cutting process and be an efficient method that is quick and economical.

4.1 Specimen Name Specification

Fifteen test specimens comprised of five hooked-bonded, five straight-bonded, four hooked-unbonded, and one control specimen were tested in this study. The following naming configuration was used.

$$\overline{R/T} \cdot \overline{H/S} \quad \overline{B/U} \cdot \overline{2 \times l_d}$$

where

R = (Rectangular) - Rectangular Beam.

T = (T – Beam) - T- Shaped Beam.*

H = (Hooked) – Hooked TiAB end anchorage method.

S = (Straight) - The TiAB has straight end anchorage.

B = (Bonded) - The TiAB is bonded to the concrete inside a groove along the length of the bar.

U = (Unbonded) - The TiAB is unbonded along the length of the bar.

l_d = (development length) – TiAB development length based on 130 ksi yield stress.

*Represents Task 2 test specimens which are not discussed in this thesis.

For example, R.HB.40 represents a rectangular beam with hooked anchorages and bonded along the length (hooked-bonded) with 40 inches of bonded length, which is twice the tested development length because of the loading configuration used for the studies. Figure 4.1 is a visual representation of R.HB.40.
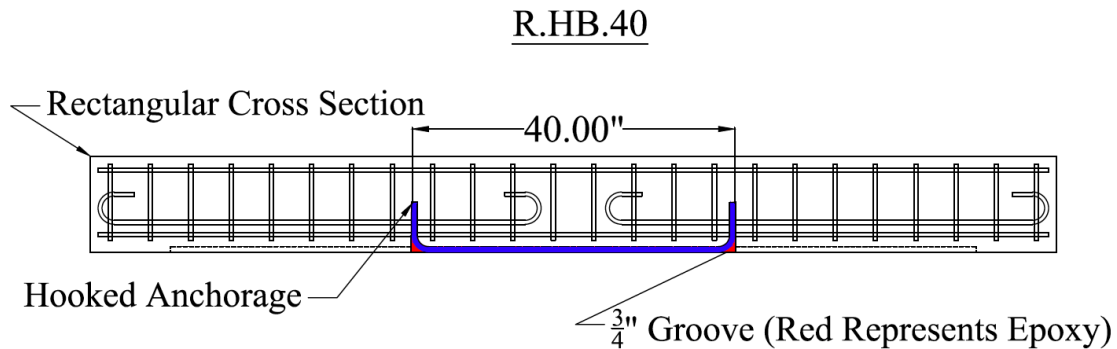
R.HB.40

Figure 4.1 - R.HB.40 Drawing

4.2 Critical Test Parameters

The main objective of the hooked-bonded (HB) and straight-bonded (SB) tests were to determine the effective bond strength that the epoxy-titanium-concrete interaction was capable of sustaining through the yielding of the TiAB in the composite mechanism. Figure 2.14 demonstrates that as bonded length increases, the CFRP strain increases until the bond strength of the NSM reinforcement equals or exceeds the bond demand.

To generate a similar curve as developed for CFRP reinforcement, the testing conducted in this thesis used Equation 2.4 from the AASHTO Guide to back-calculate varying bonded (or development) lengths based on corresponding assumed average bond strengths. The associated average bond strength to the smallest bonded length that successfully yielded the titanium can be considered the effective bond strength for the respective anchorage method.

The only variable to change for each anchorage method was the length of the TiAB. #4 bars were used for all tests making D_{Ti} a constant at 0.5 inches, and f^*_{yTi} was initially assumed to be 120 ksi for all bars. Later, the f^*_{yTi} was measured to be 131 ksi from testing (see Figure 5.4), and the average bond strengths were revised accordingly.

4.2.1 Hooked-Bonded TiAB Test Matrix

Based on the recommendations in the AASHTO Guide, 1.0 ksi was the assumed effective bond strength for designing the hooked-bonded tests. This bond strength was associated with achieving titanium yielding in the AASHTO Guide, which is highlighted in Table 4.1. An assumed average bond strength of 1.0 ksi corresponds to 15 inches of development length for a hooked-bonded TiAB with a 0.5 in. diameter. The three-point loading test setup used for this study requires the TiAB to develop on both sides of the midspan load point. This results in the overall bonded length being 30 inches from outside to outside of the hook, considering a 15-inch development length from each side. With the 30-inch specimen established, two embedment lengths longer than 30 in. and shorter than 30 in. were chosen to ensure that the behavior of NSM TiAB with higher bond demands as well as lower bond demand could be evaluated. The assumed average bond strengths were 0.50, 0.75, 1.00, 1.50, and 2.00 ksi corresponding to bonded lengths of 60, 40, 30, 20, and 15 inches, respectively. Table 4.1 displays the hooked-bonded test matrix and expected TiAB performance.

Table 4.1 - Hooked-Bonded TiAB Test Matrix

Specimen Name	l_d (in.)	Bonded Length (in.)	Assumed Average Bond Strength (ksi)	Expected TiAB Performance
R.HB.15	7.5	15	2.00	Bond Failure
R.HB.20	10.0	20	1.50	Bond Failure
R.HB.30	15.0	30	1.00	Yield
R.HB.40	20.0	40	0.75	Yield
R.HB.60	30.0	60	0.50	Yield

The test matrix shown in Table 4.1, and the specimen design were based on the nominal strength properties of the TiAB. The measured yield strength of the TiAB (f_{yTi}) was 131 ksi for the TiABs, as mentioned in Section 4.2. Since the specimen design and bonded lengths were

determined prior to the measuring the TiAB yield strength, the assumed bond strenths were

revised based on the measured yield strength of the TiAB according to Equation 2.4 and

presented in Table 4.2. The remainder of the thesis will refer to the average bond strenths

calculated based on the measured $f_{yTi.}$

Table 4.2 - Hooked-Bonded TiAB Assumed Average Bond Strengths using Measured f_{yTi}

Specimen	Using Measured f_{yTi} (ksi)	Expected TiAB Performance
R.HB.15	2.18	Bond Failure
R.HB.20	1.64	Bond Failure
R.HB.30	1.09	Bond Failure
R.HB.40	0.82	Yield
R.HB.60	0.55	Yield

4.2.2 Straight-Bonded TiAB Test Matrix

A similar approach was taken for the straight-bonded specimen with the 0.5 ksi being the

assumed average bond strength to achieve the TiAB yielding. This was decided based on the

straight-bonded tests that Vavra (2016) conducted (discussed in Section 2.7.3). Equation 2.4 was

used to design specimens with bonded lengths based on various assumed average bond strengths.

For the straight-bonded bars, the assumed average bond strengths used were 0.31, 0.38, 0.50,

0.75, and 1.00 ksi which is associated with bonded lengths of 96, 80, 60, 40, and 30 inches

respectively. Table 4.3 displays the straight-bonded test matrix.

Table 4.3 – Straight-Bonded TiAB Test Matrix

Specimen Name	l_d (in.)	Bonded Length (in.)	Assumed Average Bond Strength (ksi)
R.SB.30	15	30	1.00
R.SB.40	20	40	0.75
R.SB.60	30	60	0.50
R.SB.80	40	80	0.38
R.SB.96	48	96	0.31

The values of the assumed bond strengths were obtained based on a nominal yield stress of 120. A revised test matrix was developed for the bond stresses based on the measured TiAB yield strength of 131 ksi. Table 4.4 presents the updated table with average bond strength based on the measured value of the TiAB yielding. The remainder of the thesis refer to the average bond strengths calculated based on the measured f_{yTi}.

Table 4.4 - Straight-Bonded TiAB Assumed Average Bond Strengths using Measured f_{yTi}

Specimen	Using Measured f_{yTi} (ksi)
R.SB.30	1.09
R.SB.40	0.82
R.SB.60	0.55
R.SB.80	0.41
R.SB.96	0.34

4.2.3 Hooked-Unbonded TiAB Test Matrix

The specimen design for the unbonded bars were different that Equation 2.4 was not used to determine the lengths. Since the bars were not bonded along the length, the strain in the bar was the same along the whole length until the hook region. That strain in the bar is dependent upon the tension strain variation (moment diagram) in between the two anchor points. With a triangular moment diagram associated with the simply supported three-point loading that was used as the test set-up, the variation in the moment diagram in between the anchor point needed to be accounted for when obtaining the TiAB stress. Figure 4.2 depicts the moment diagram for the hooked-unbonded anchorage method.
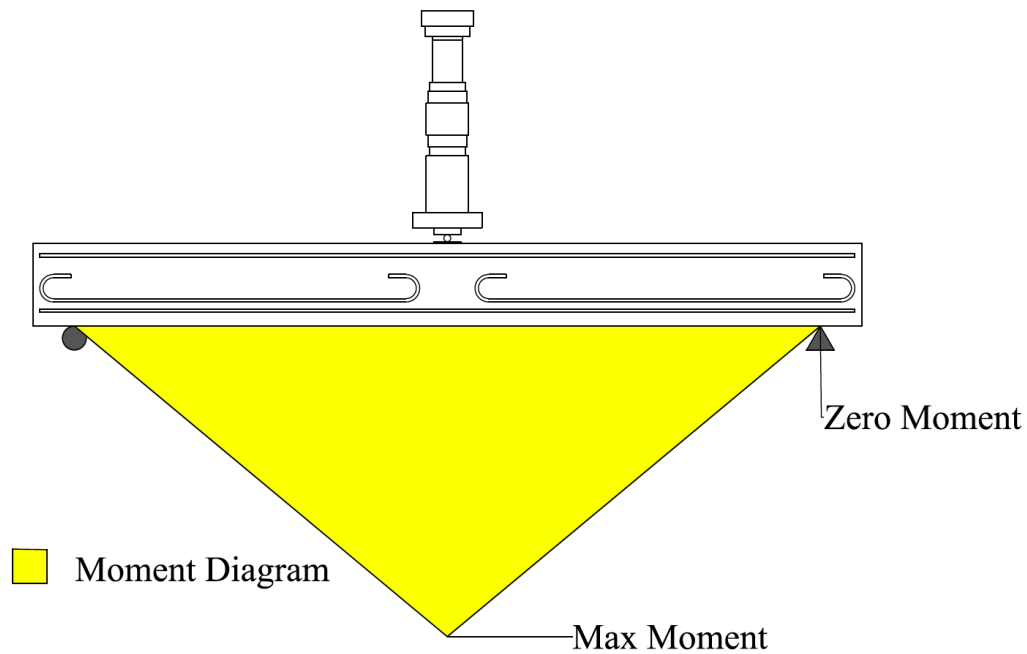
Figure 4.2 - Three-Point Test Moment Diagram

The effectiveness of the unbonded anchorage method diminishes with longer bar lengths, therefore the bar lengths were aimed to be minimized for increased efficiency of the method. For this reason, the test matrix had TiAB bars with hook distances ranging from 10, 30, 40, and 60-inch lengths, also to observe the progression of performance as the length increased. The selected hook distances also corresponded to bonded lengths used in the hooked-bonded and straight-bonded test programs which allowed comparisons between the different anchorage methods. The test matrix for the hooked-unbonded bars is presented in Table 4.5.

Table 4.5 - Hooked-Unbonded TiAB Test Matrix

Specimen Name	L(in.)	2L (in.)
R.HU.10	5	10
R.HU.30	15	30
R.HU.40	20	40
R.HU.60	30	60

4.3 Specimen Design

Fifteen specimens were tested in this study, including a control specimen (conventional RC without strengthening). The specimens were 9 in. wide, 12 in. deep, and 10 ft long, with 6 in. overhangs beyond the supports on either end. The beam specimens were simply supported with a span of 9 ft and loaded using a three-point loading arrangement. The 9-foot span was chosen because it was the shortest span that could encompass all practical ranges of bonded lengths needed to be tested for the TiABs (i.e., 96 inches).

The specimen geometries were selected to minimize the possibility of shear failure therefore a shear span-to-depth ratio of 4.5 was selected. The beam cross-section was designed so that the shear strength contribution by the concrete (V_c) was sufficient to resist the expected loading without the contributions from the stirrups, but shear reinforcement was still provided with reasonably tight stirrup spacing.

The representative bridge in Cullman, Alabama (discussed in Chapter 3), was built in 1962 which had lower concrete design strengths than in typical construction nowadays. Thus, the concrete properties developed for this study were specifically selected to represent this bridge built in the 1960's. Section 5.1.3 provides more details regarding the properties of the concrete.

The bridge in Cullman used Grade 40 reinforcing steel which is not readily available for use in the construction market nowadays. All specimens were reinforced with six #4 ASTM

A615 Grade 60 longitudinal bars located in three layers (one top layer and two bottom layers, as shown in Figure 4.3). The specimens were built with an 8 in. long segment in the mid-span region, where half of the longitudinal reinforcement (the second layer from the bottom) was terminated with 180° hooks to create a weak region. This bar termination was to ensure that the beam would fail in a predictable manner in the mid-span region as well as to simulate a beam that required flexural strengthening. A similar three-point-loading test with a weak region in the center of the beam was previously used by Hassan and Rizkalla (2003) to investigate the effectiveness of NSM CFRP strips, as discussed in Section 2.8.1. The flexural reinforcement and beam cross-sections are shown in Figure 4.3.

Elevation View

Overall Dimensions   Cross Section AA   Cross Section BB
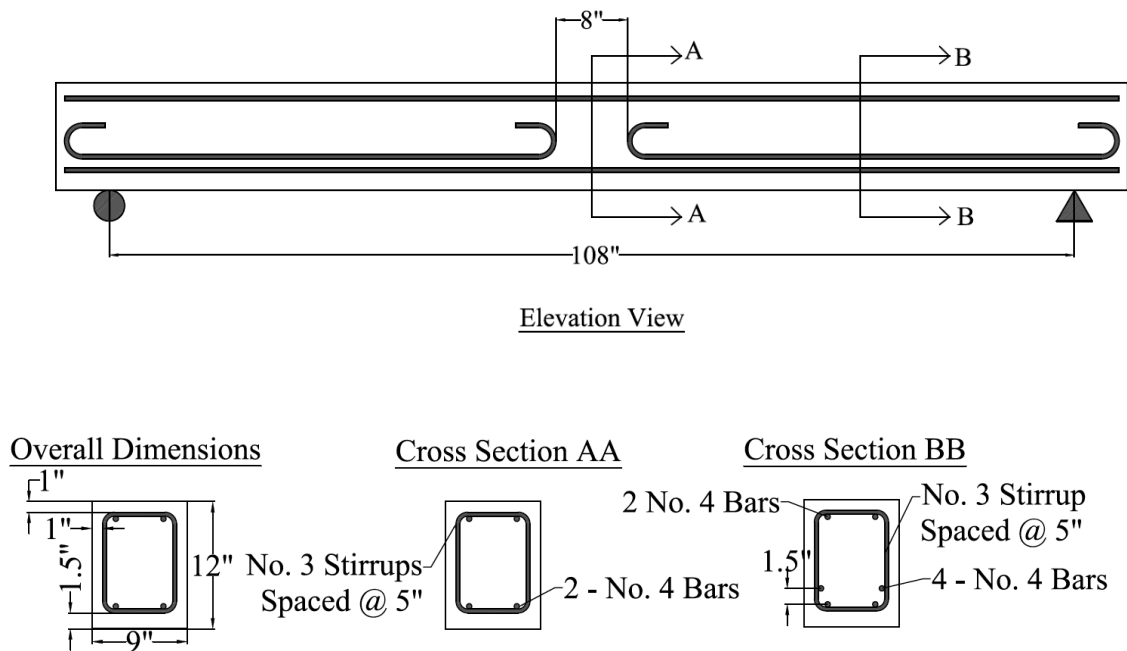
Figure 4.3 - Beam Flexural Reinforcement and Cross Sections

For stirrups, #3 ASTM A615 Grade. 60 bars were used that were spaced 5 in. on center. The stirrup spacing was arranged so that the hooks for the NSM TiAB would be positioned in the center of the two stirrups. Figure 4.3 displays the elevation view and several cross-sections of the

beam. Stirrups were not included in the elevation view of this figure to clearly indicate the flexural reinforcement. The stirrup layout is presented in Figure 4.4.
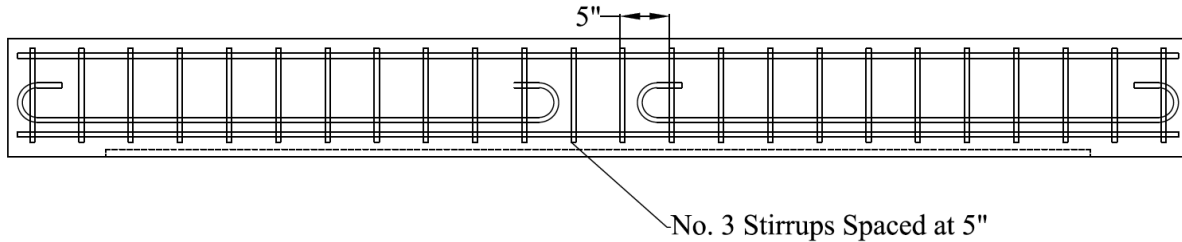
Figure 4.4 - Stirrup Layout

The hook bend and tail geometries, groove size, and reinforcement spacing complied with requirements presented in the AASHTO Guide. #4 TiABs were used in this study which required a 3-inch bend diameter and the overall tail length to be 6 inches. The square groove dimension was 0.75 inches for both hooked-bonded and straight-bonded TiAB installation. The hooked-unbonded specimen did not require a groove because epoxy was not used to bond the TiAB along the length. Two tensile steel reinforcement layers of two #4 longitudinal steel bars were required to create the hinge in the middle of the beam. One layer was terminated near the midspan of the beam the other layer was continuous to achieve the targeted strength of 10 kips. #3 bars were used for transverse reinforcement because the 5-inch spacing that would allow for the hooked TiABs to be placed directly between two stirrups for all but R.HB.15. #4 TiABs were chosen because the 3/4-inch square groove required by the AASHTO Guide would not interfere with the internal reinforcing steel.

The predicted strengths of the beam (P_{pred}) before failure using both the yield strain and ultimate strain material measured properties can be seen in Table 4.6. The control specimen was designed (R.CON) to resist approximately 10 kips and the strengthened members to double the capacity to approximately 20 kips using the measured yield stresses. These values were determined

using Equation 2.2. R.CON was expected to yield the steel at 9.1 kips based on Equation 4.1.

Figure 4.5 presents the moment-curvature response plot from a numerical fiber-model that

analyzed the strength based on the <u>strengthened</u> specimen's cross-section and material properties.

The model assumed constant curvature through the cross-section and assumes strain compatibility

in the section. The response curve indicated concrete cracking at 100 kip-in (3.7 kips), the first

softening in the response due to steel yielding to occur at 350 kip-in (13 kips), and a second

softening due to TiAB yielding to occur at 530 kip-in (19.7 kips). The fiber model predicted the

maximum moment to be 552 kip-in (20.4 kips) and the maximum curvature to be 0.0027 in^{-1} for

the strengthened members before concrete crushing.

Table 4.6 – Strength Predictions

Cross-Section	Model	Material Property Values Used	P_{pred} (k)
R.CON	Equation 2.2	Measured Yield	9.6
	Numerical Fiber Model	Measured Yield	10.7
	Equation 2.2	Measured Ultimate	14.8
NSM TiAB Specimens	Equation 2.2	Measured Yield	19.8
	Numerical Fiber Model	Measured Yield	20.4
	Equation 2.2	Measured Ultimate	25.5
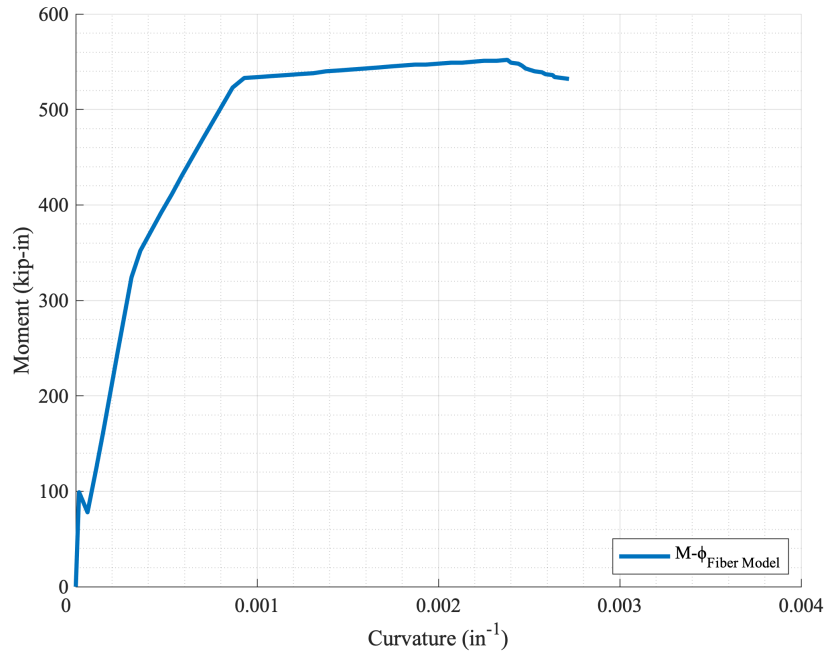
Figure 4.5 – Strengthened Beam Moment vs Curvature using Fiber Model

The steel in R.CON was expected to yield at 246 k-in. (9.1 kips) based on Equation 4.1 which uses the same assumptions as Equation 2.2. As mentioned, the fiber model expected the steel in strengthened model to yield at 350 kip-in (13 kips) and the titanium to yield at 530 kip-in (19.7 kips). The yield resistance values (P_y) shown in Table 4.7 were calculated using the measured yield values.

Table 4.7 – Predicted Strengths at Reinforcement Yielding

Cross-Section	Model	Material	Py (k)
R.CON	Equation 4.1	Steel	9.6
NSM TiAB Specimens	Numerical Fiber Model	Steel	19.8
	Numerical Fiber Model	TiAB	20.4

$$M_y = \frac{f_y}{n} * \frac{I_{cr}}{(d_s - C_{cr})}$$

Equation 4.1

where

M_y = the moment (k-in.) when the steel yields.

n = the modulus of elasticity transformation coefficient for steel to concrete.

I_{cr} = the cracked moment of inertia of a multi-material section transformed to one material and neglecting the area of concrete in tension.

C_{cr} = depth of the Whitney stress block in a cracked beam.

4.3.1 Hooked-Bonded TiAB Specimens

The hooked-bonded TiAB specimens mounted the TiAB inside the groove and had hooks that penetrated into the concrete substrate. Figure 4.6 depicts the elevation view of the hooked-bonded specimens' flexural reinforcement, the mid-span cross-section, and cross-section dimensions.
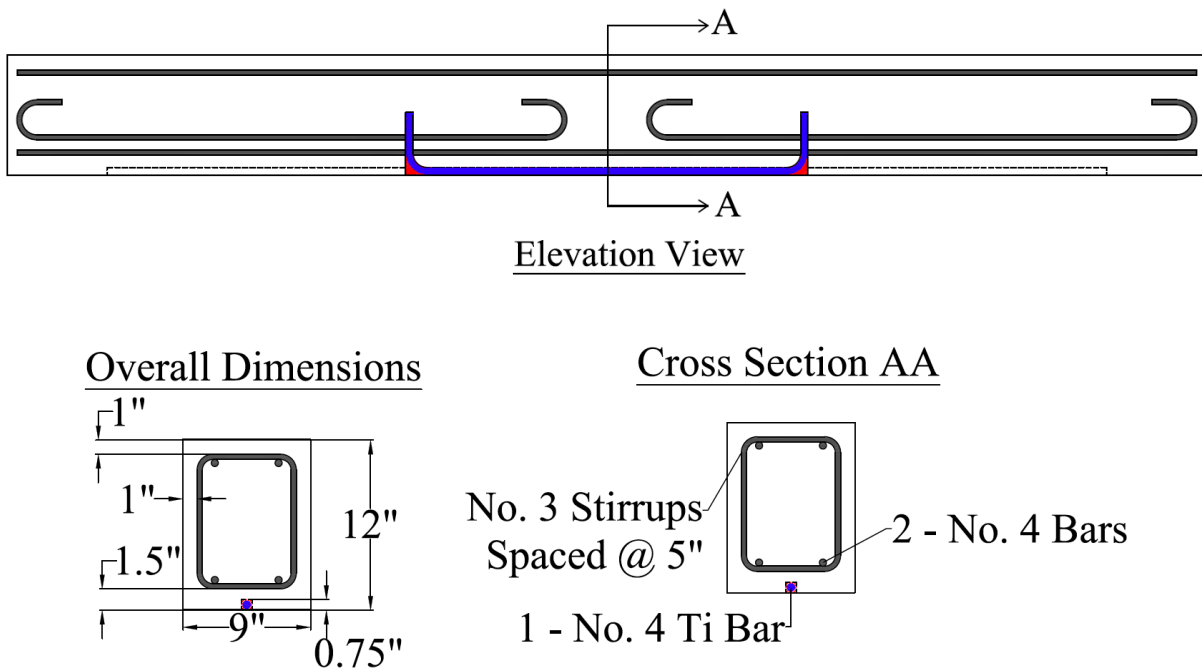
Figure 4.6 - Hooked-Bonded Specimen Design

52

R.HB.15 required a different stirrup spacing to accommodate the hooks of the 15-inch

TiAB embedment. The hook ends were placed 7.5 inches from the center on either side by

having the stirrups shifted over 2.5 inches. The spacing of 5 inches was kept the same as the

other specimens but allowing the 7.5 in hook for RHB.15 to be positioned in between two

stirrups. The stirrup layout for R.HB.15 is presented in Figure 4.7.

No. 3 Stirrups Spaced at 5" with a stirrup at Midspan.
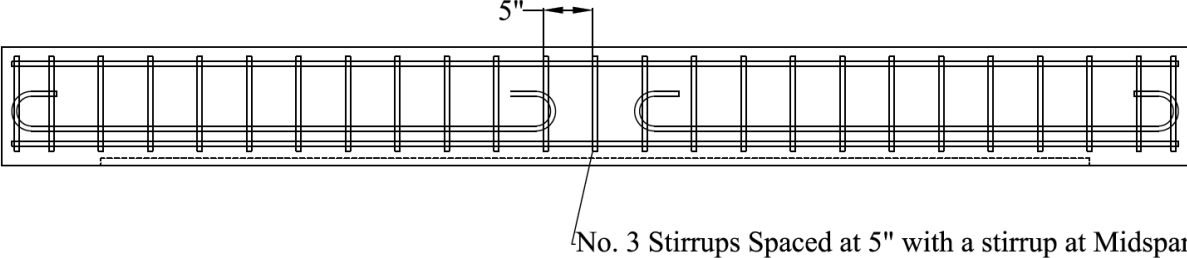
Figure 4.7 - R.HB.15 Stirrup Spacing

4.3.2 Straight-Bonded TiAB Specimens

The straight-bonded TiAB specimens had the TiAB bonded inside the groove and had straight end

anchorages. Figure 4.8 depicts the elevation view of the straight-bonded specimens' flexural

reinforcement, the mid-span cross-section, and cross-section dimensions.

$\frac{3}{4}$" Groove (Red Represents Epoxy)

→A

Elevation View

Overall Dimensions

1"

1"

1.5"

12"

9"

0.75"

Cross Section AA

No. 3 Stirrups
Spaced @ 5"

2 - No. 4 Bars

1 - No. 4 Ti Bar
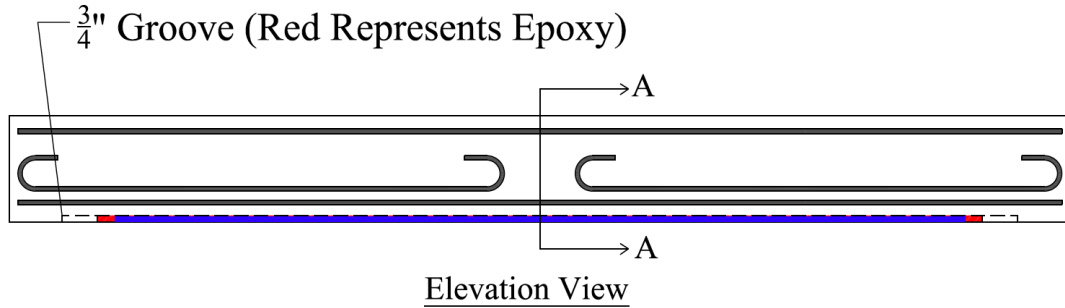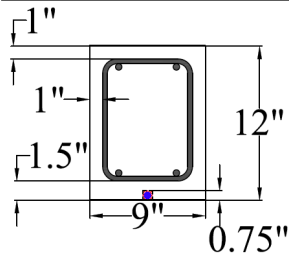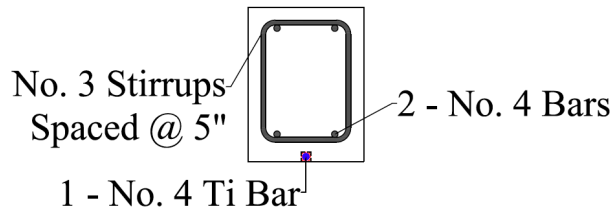
Figure 4.8 – Straight-Bonded TiAB Specimen Design

4.3.3 Hooked-Unbonded TiAB Specimens

Hooked-unbonded TiAB specimens did not have a groove and the TiABs were flush with the bottom face of the beam with penetrating hooks epoxied into the concrete. Figure 4.9 depicts the elevation view of the hooked-unbonded specimens' flexural reinforcement, the mid-span cross-section, and cross-section dimensions.
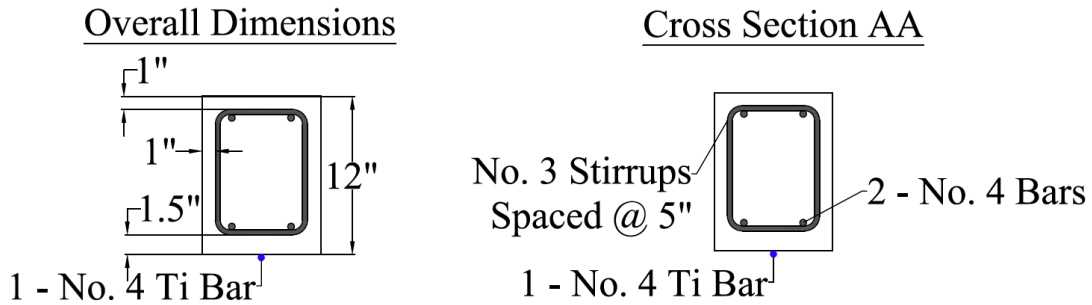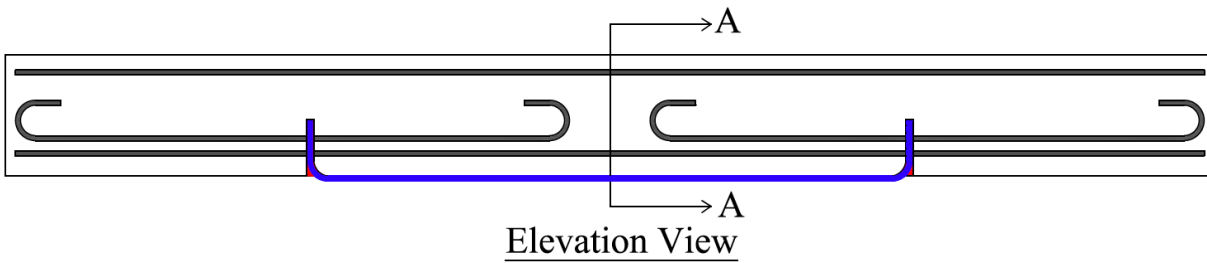
Figure 4.9 - Hooked-Unbonded TiAB Specimen Design

R.HU.60 was a unique specimen because it was tested in a flipped orientation resulting in different concrete clear covers and reinforcement configuration. An illustration of the midspan cross-section is shown in Figure 4.10. Due to the flipped orientation, the steel rebar in R.HU.60 had a structural depth of 10.38 inches rather than 9.88 inches. This was done because the beam was repurposed from its original intention as another hooked-bonded TiAB specimen. The hook bending diameter was also changed for R.HU.60 to mitigate the anchorage failure mode observed in other specimens with the same anchorage method. A larger hook bending diameter of 6 inches and tail length of 6 incehs was used for this specimen to increases the bearing area against the concrete and to reduce the potential of anchorage slippage. The bending diameter for all the other hooks was 3 inches with a consistent tail length of 6 inches, as mentioned in Section 2.10.1.
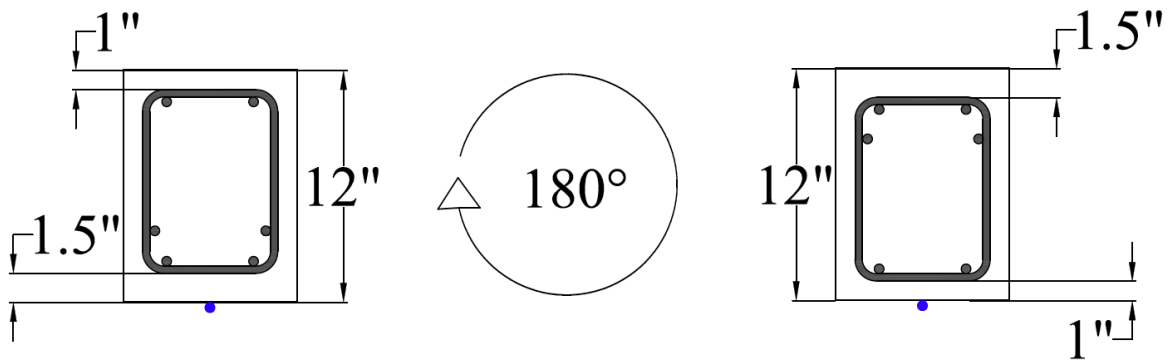
Figure 4.10 – Normal Hooked-Unbonded (Left) and R.HU.60 (Right) Cross Sections

CHAPTER 5: SPECIMEN MATERIALS AND FABRICATION

The experimental portion of this study started in August '21 and was completed in a year with the following timeline outlining the major lab activities. The construction of the concrete formwork started in the beginning of August and finished at the end of September '21. The steel and TiAB arrived at the end of August and tensile test were conducted in September '21. The reinforcing cages were built in October and placed inside the forms in early November '21. The concrete was poured in mid-November '21. Testing of the beams started in June and was completed in August '22.

5.1 Materials

Details regarding the material properties for the steel, TiABs, concrete, and epoxy are discussed in this section. The values determined from testing using the applicable ASTM standards were later used for theoretical analysis and calculations.

5.1.1 Steel Material Test

As discussed in the specimen design, Grade 60 reinforcing bars were used in this study. Uniaxial tension tests were conducted to determine the yield stress, tensile strength, and elongation at fracture of the steel rebars. The tests conformed to ASTM E8 (2022) and were conducted in a universal testing machine (UTM) as shown in Figure 5.1. The measurements were made using both strain gauges and clip-in extensometers. To investigate the sensitivity of the strength due to grinding the surface to attach strain gauges, three regular bars and three grounded bars were tested in the UTM all from the same production run (mill certificates provided in Appendix B). The testing indicated negligible difference in the behavior of grounded bars with the necking and rupture even occurring outside the ground locations. The strength values measured during the

test and the mill certified test report (MCTR) values can be seen in Table 5.1. Figure 5.2 shows a

typical stress-strain curve obtained from the tension tests.
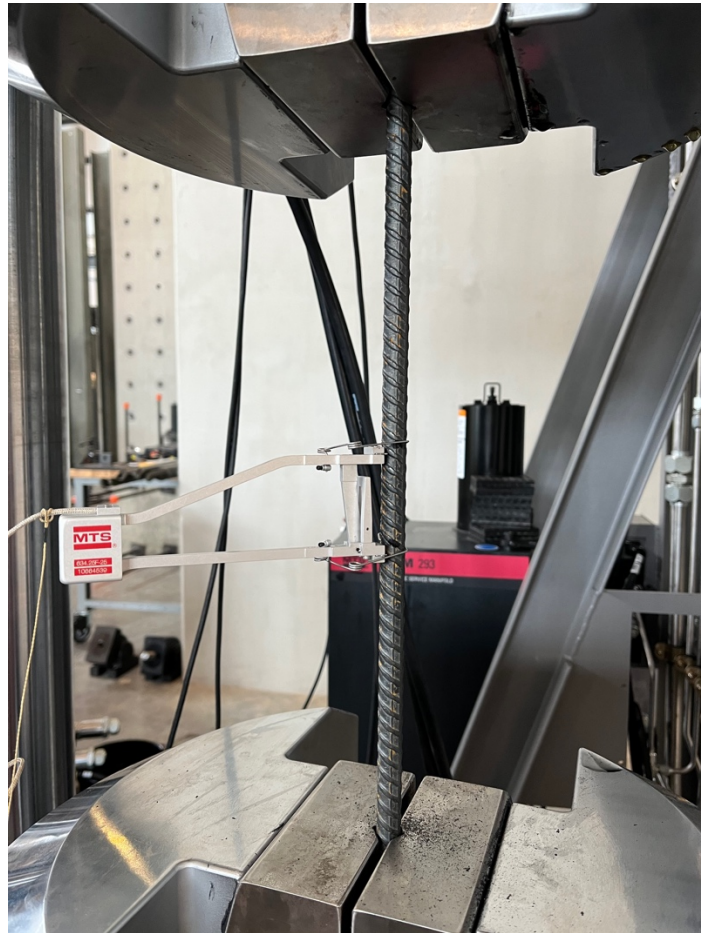
Figure 5.1 – Reinforcing Steel Tensile Test

Table 5.1–- Reinforcing Rebar Tension Tests

Bar Designation	Test	Yield Stress (ksi)	Ultimate Stress (ksi)	Elongation at Fracture (%)
Regular	1	67	105	9
	2	70	109	5
	3	69	107	6
	Average	**69**	**107**	**7**
Ground	1	65	104	16
	2	68	106	8
	3	70	108	10
	Average	**68**	**106**	**11**
MCTR	1	74	107	12
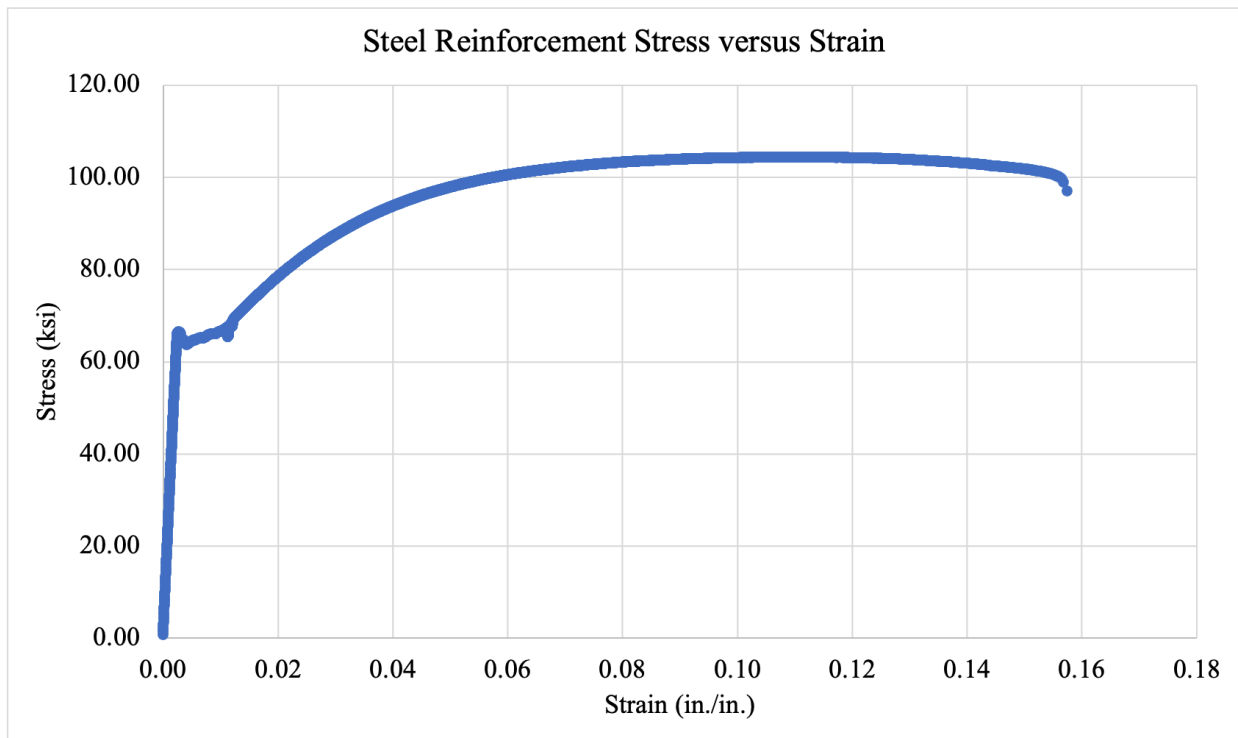
Figure 5.2–- Steel Reinforcement Measured Response

5.1.2 Titanium Material Test

The titanium-alloy bars used in this study were class 130 Ti-6Al-4V (Grade 5). The TiAB were

supplied by Perryman Company with an in-house classification of textured infrastructure bar.

The surface pattern on the TiABs resembled threads on a threaded rod, and the peaks and valleys of the threaded pattern were slightly rounded to minimize stress concentrations (Amneus, 2014). The mill certification obtained from the manufacturer conformed to the requirements of ASTM B1009-(2022). Tensile testing was performed in the laboratory to verify the reported material properties and provide strength properties to be used for calculations and analysis. All the titanium bars were rolled from the same production run (mill certification provided in Appendix B), and tension tests were completed on samples taken from several bars. Figure 5.3 depicts a TiAB bar prior to tension testing using the UTM.

Figure 5.3-- TiAB Tensile Test

These tests conformed to ASTM E8 (2022). Similar to the steel samples, three regular bars and three ground bars were tested for a total of six bars. Despite being a negligible difference for the steel, the TiABs had a noticeable decrease in performance because of the surface grinding, specifically regarding the elongation at fracture. The measured yield stress, tensile strength, and elongation at fracture obtained for the TiAB sample bars and the MCTR values can be seen in Table 5.2. Figure 5.4 shows a typical stress-strain curve from the tension testing of TiAB and demonstration of how the yield stress was obtained.

Table 5.2— TiAB Material Property Averages

Bar Designation	Test	Yield Stress (ksi)	Ultimate Stress (ksi)	Elongation at Fracture (%)
Regular	1	132	146	8
	2	132	145	9
	3	133	145	10
	Average	**132**	**145**	**9**
Ground	1	133	143	7
	2	130	143	5
	3	131	144	5
	Average	**131**	**143**	**6**
MCTR	1	137	152	11
	2	136	154	13
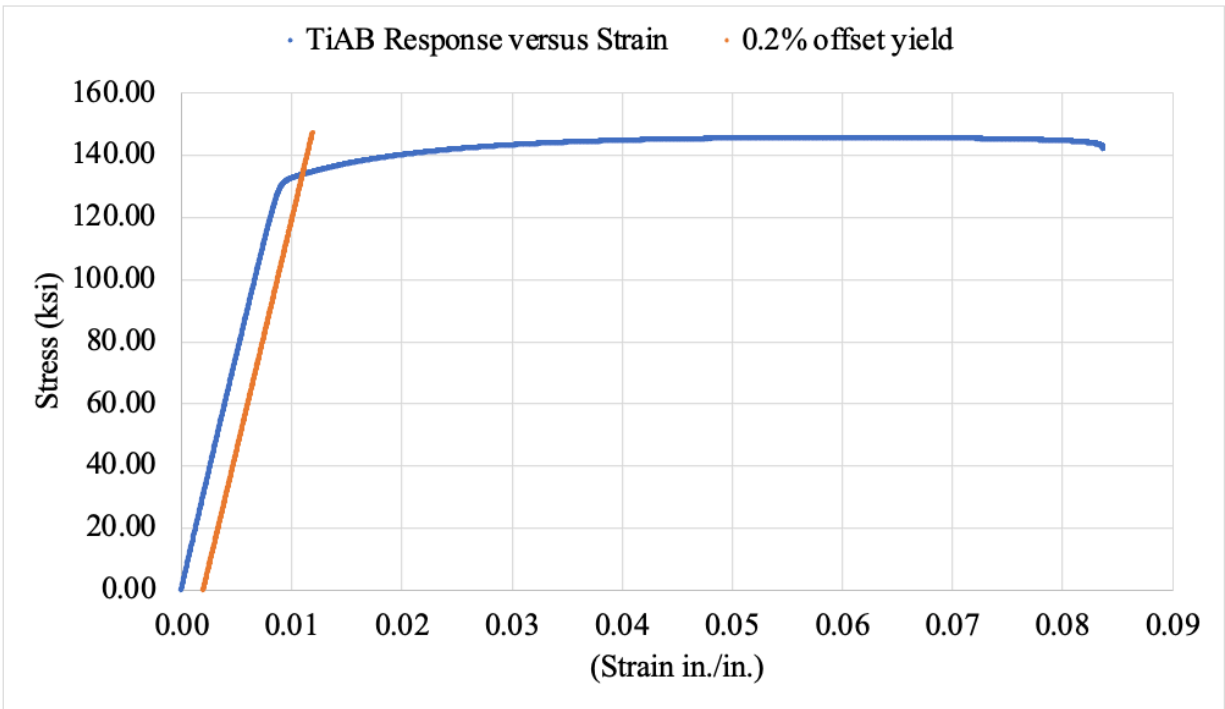
Figure 5.4–- TiAB Measured Response

The tension test results highlighted the impact of the grinding process on the tensile properties of the TiAB. The tensile test measured values reported in Table 5.2 were lower than the MCTR values, therefore the measured values were used for all calculations and analysis.

5.1.3 Concrete Properties

The concrete used in the beam tests was intended to mimic the low strength concrete used in older bridges; most bridges built around the 1960s and earlier could be potential candidates for strengthening using this method. The Cullman bridge that is the focus of this study, was built in 1962 had a reported compressive strength of 4500 psi. The concrete core strengths are provided in Appendix F. Concrete proportions, presented in Table 5.3, were prepared to specifically to capture comparable strength to the Cullman bridge.

Table 5.3 – Concrete Mixture Proportions

Item	Value	
Water Content (34 Gallons)	284	lbs/yd^3
Cement Content	535	lbs/yd^3
Coarse Aggregate (SSD)	1,792	lbs/yd^3
Fine Aggregate (SSD)	1,260	lbs/yd^3
Total Air Content (4%)	0.0	lbs/yd^3
Air Entrained Admixture (0.8 oz/cwt)	4.3	oz/yd^3
Water-to-Cement-Ratio	0.53	

The 15 beam specimens tested in this study were cast at the same time from the same ready-mixed concrete truck. A total of twelve 6"x12" cylinders were made to evaluate the strength of the concrete as it matured. The cylinders were moist cured for seven days then demolded and air cured. The same process was applied to the beam specimens. Three cylinders were tested at 7, 28, 91, and 287 days in accordance with the ASTM C39-(2021) concrete compressive strength testing standard. The 28 – day compressive strength was 4,380 psi which is similar to the target strength of 4500 psi. Table 4.4 provides the 7, 28, 91, and 287 day strengths, where the 287 days correlated with testing the last beam. Equation 4.1 from ACI 209R (1992) was used to develop a predictive curve of the concrete strength.

$$f_c(t) = f_c(28) * \left(\frac{t}{a+Bt}\right)$$

Equation 4.1

where

$f_c(t)$ = the concrete strength as a function of time.

t = time.

α = 4.000 and 3.768 in the original ACI 209 and best-fit ACI 209 functions respectively.

B = 0.850 and 0.857 in the original ACI 209 and best-fit ACI 209 functions respectively.

$f_c(28)$ = the 28-day concrete compressive strength.

The values reported in Table 5.4 were used to generate a strengthening curve to determine the strength gain over time using the ACI 209R (1992) recommendations. This strength development plot and the points used to generate the curve are provided in Figure 5.5.

Table 5.4 – Concrete Strength Test Results

Age (days)	Measured Strength (psi)
7	3140
28	4381
91	4990
287	4950
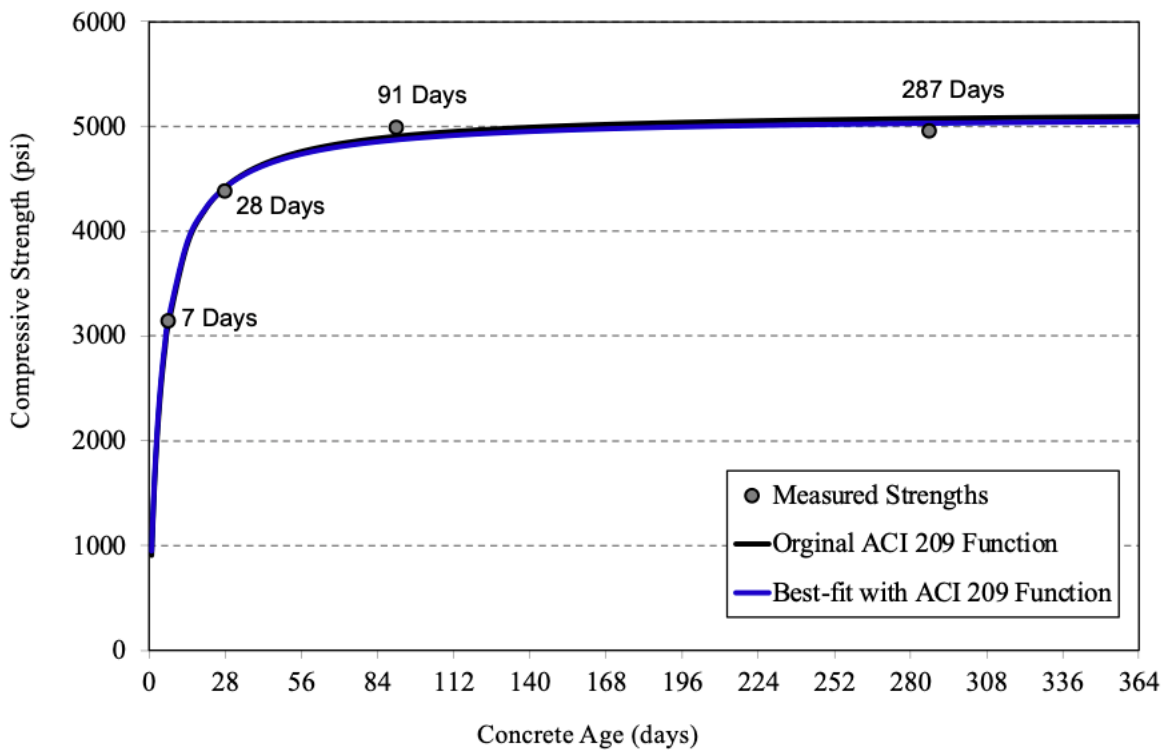
Figure 5.5–- Compressive Strength Gain of Concrete over Time

5.1.4 Epoxy Properties

The epoxy used to achieve bond between the TiAB and reinforced concrete member was Hilti's HIT-RE 500 V3 epoxy anchor. This epoxy is classified as an ultimate-performance injectable epoxy mortar that is commonly used for rebar connections and heavy-duty anchoring. The fully cured material properties can be seen in Table 5.5. At 72 degrees Fahrenheit it takes 7 hours to achieve full cure. See Appendix D for HIT-RE 500 V3 material properties and cure times.

Table 5.5–- Fully Cured Epoxy Properties Adapted from (Hilti, 2021)

HIT-RE 500 V3 Full Cure Properties	
Bond Strength (psi)	1690
Compressive Strength (psi)	12000
Tensile Strength (psi)	7150
Elongation at Break (%)	1.1

5.2 Steel Reinforcement Cages

The reinforcing steel was obtained from a single batch from a local supplier. All bars, including stirrups, were cut and bent by the local supplier and were ready upon delivery. The cages were erected and tied together on wooden lifts as can be seen in Figure 5.6. Once cast, the beams would need to be lifted and flipped several times for groove cutting, cracking, and for mounting of the TiAB. Lifting hardware was placed on both sides of the beam for the purpose of handling the beams, as shown in Figure 5.6. The hardware created a hole with an inverted thread pattern and reinforcement around the hole. A bolt with a D-ring for crane attachment could then be placed inside the hole with the threaded pattern.

Figure 5.6–- Rebar Cage (left) and Lifting Hardware (Right)

5.3 Concrete Placement

Formwork for the 15 specimens were constructed in the Advanced Structural Engineering Lab (ASEL) at Auburn University. A timber frame was constructed on the ground with a 3/4-inch plywood surface to serve as platform for all the forms. All 15 forms were rectangular in shape and polyurethane sealed to provide a smooth surface for the faces of the beam. The seams and corners were caulked with silicone to keep any concrete paste from exiting. Figure 5.7 shows a picture of the completed formwork with the steel cages resting inside. On the far left of Figure 5.7, a wooden apparatus with handles can be seen on top of one of the forms. This was used as a sliding funnel during casting. The forms were made to resist the hydrostatic forces of the wet concrete. The beams were oriented right-side-up and 1.5-inch chairs were used to create the proper cover between the bottom of the beam and the stirrups. Small holes were drilled in the

bottom of the forms for the strain gauge wires to exit and then the holes were caulked appropriately. On casting day, form-oil was used to lubricate the bottom and sides of the form to ensure that the forms would be easy to remove after casting.

Figure 5.7–- Concrete Forms and Sliding Funnel

The concrete was delivered in a single ready mixed concrete truck from a local supplier. The beams and cylinders for material properties were all cast within a two-hour period. The concrete's slump, air content, unit weight, and fresh temperature were all tested to ensure that the concrete was adequate. Those values are reported in Table 5.6.

Table 5.6-- Concrete Fresh Properties

Date and Fresh Properties	
Placement Date	11/16/21
Slump (in.)	4.0
Total Air Content (%)	4.0
Unit Weight (pcf)	142.7
Fresh Concrete Temperature (°F)	71.0

The concrete truck was able to back straight into the high-bay area where the beams were ready to be cast. Figure 5.8 shows the test cylinders being made for strength evaluation. The sliding funnel mentioned in earlier in this seciton can be seen in Figure 5.9. This was to avoid concrete spilling over the sides of the forms due to the narrow width of the beams. The concrete was consolidated with a mechanical vibrator as can be seen in the far left of Figure 5.9. Excess concrete was struck off using a 2 x 4 piece of dimensional lumber. A metal trowel was then used to finish the concrete which can also be seen in Figure 5.9.
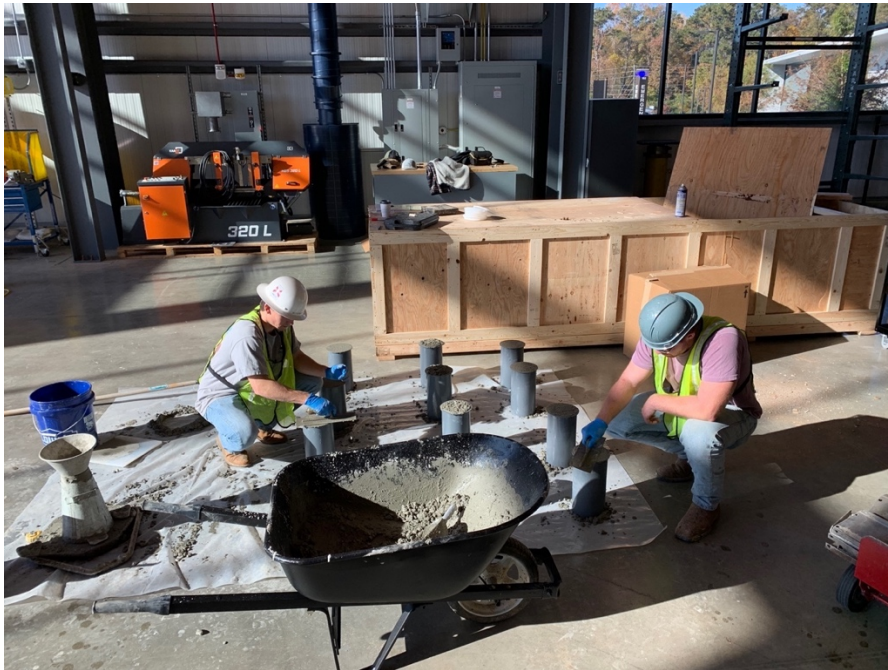
Figure 5.8-- Test Cylinders for Strength Evaluation

Figure 5.9-- Concrete Casting, Vibrating, and Finishing

Once all the beams had been finished, they were covered with wet burlap and a plastic sheet to keep the moisture in. The concrete was wet cured for 7 days with wetting every other day to ensure that the burlap stayed wet, and a moist curing environment was maintained. Once removed from the forms, the beams were kept inside the lab until full 28-day compressive strength was achieved. Figure 5.10 shows all the beams after they had been finished and during curing.

Figure 5.10 – Beams after Placement (Left) and During Curing (Right)

6.1 Test Set Up

Three-point loading configuration was used in these tests to minimize specimen lengths. The beam was simply supported with a roller on one side and a pin on the other with 6 inches of overhang beyond the supports as illustrated in Figure 6.1 creating a 9-foot span. The beams were elevated to 4 feet from the strong floor to conveniently observe the underside of the beam during testing, where the NSM TiABs were mounted. An 82-kip actuator was used to load the specimens monotonically on a 4-inch-wide bearing plate placed at the center of the beam.
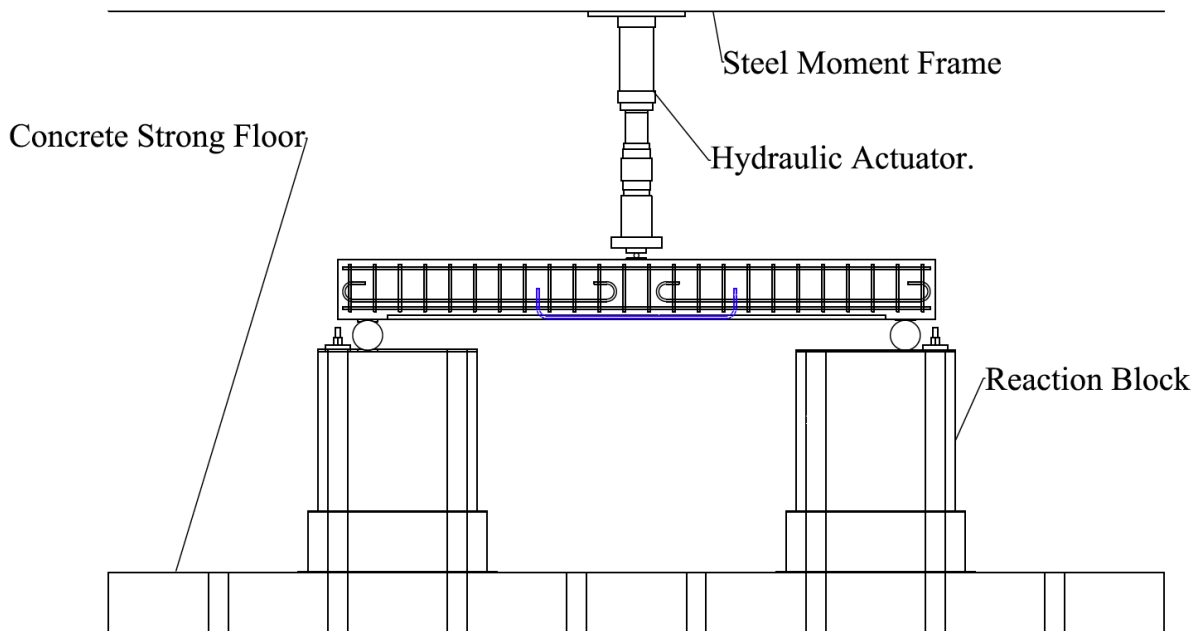
Figure 6.1–- Test Set Up for NSM TiAB Bond Test

The pin support was created using a steel cylinder cradled between two steel plates that had a curve in them that matched the circumference of the cylinder. The roller support was created on the other side by using a steel cylinder resting on a steel plate. The supports are shown in Figure 6.2.

Figure 6.2–- Pin Support (left) and Roller Support (Right)

6.2 Instrumentation

Data was collected using internal and external sensors with GI.Bench software and Gantner

hardware as the data acquisition system and recorded at a rate of 2 hertz. Each reinforcing rebar

was instrumented with one strain gauge at the mid-span cross-section. The strains in the TiABs

were monitored during the tests with several strain gauges along the length. The strain gauges

were placed at the midspan (center) section and consistently spaced towards either side of the

bars. The first set was attached at 4 in. on either side of the center, and then spaced at 6 in. until

the end of the TiAB as shown in Figure 6.3. Linear position transducers (LPTs) were used to

measure the displacement at the center and in the shear span of the beam. Two 10 in. stroke

LPTs were attached at the center of the beam, and one 5 in. stroke LPT was attached in each

shear span. The average of the two LPTs at the center of the beam were used to record the

displacement of the specimens. The two LPTs in the shear span were used to confirm that the

single point loading resulted in symmetric beam deformation. Two inclinometers were mounted

to one side face of the specimen to measure the rotation at the cross sections 4 in. from the center

of the specimens. Figure 6.3 and Figure 6.4 show the instrumentation layout.

71
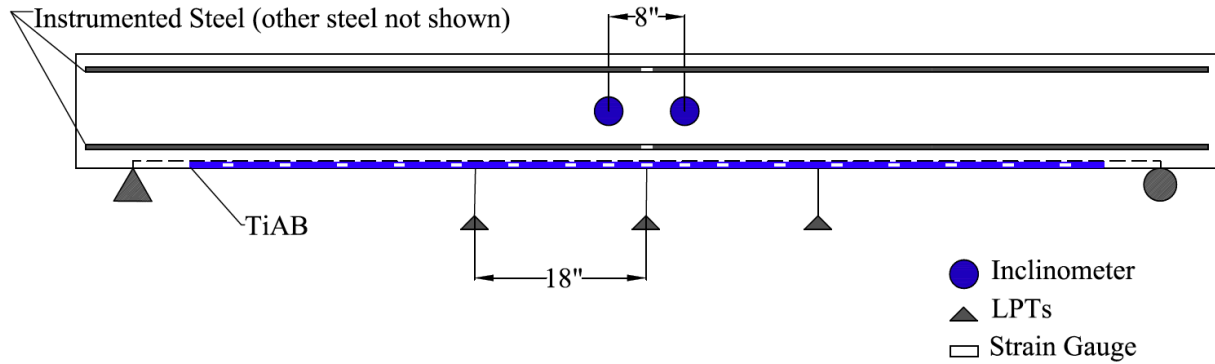
Figure 6.3–- Instrumentation Layout – Elevation View
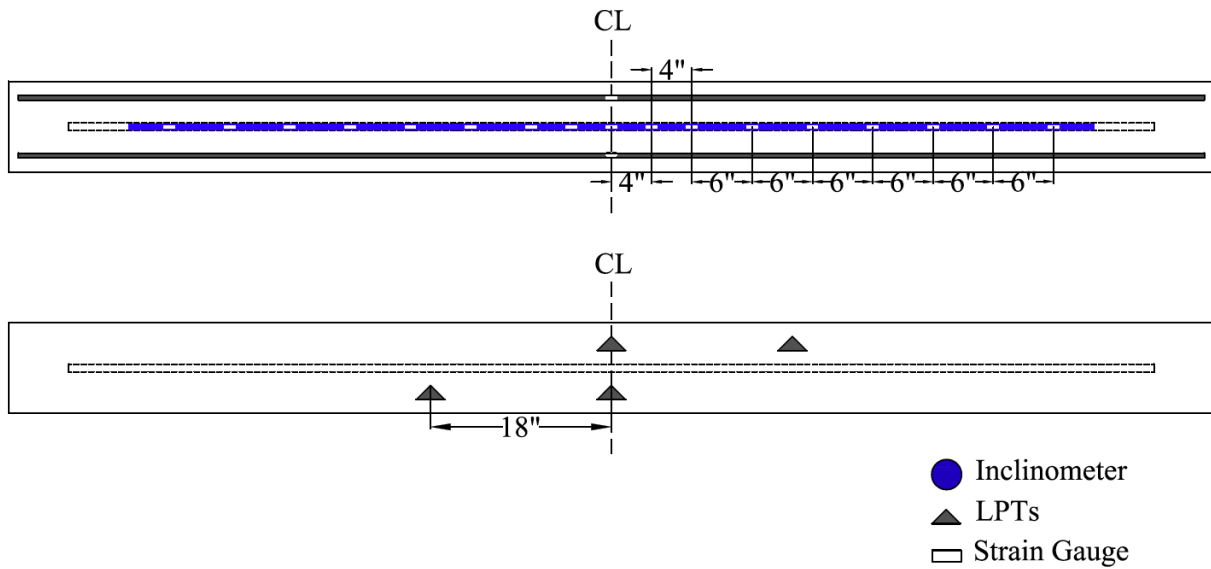
Figure 6.4–- Bottom View of Strain Gauges (Top) and LPTs (Bottom)

The curvature of the beams during the final loading was measured using the strain gauges and inclinometer. The strain-based moment-curvature response was obtained by calculating the curvature between the strain measurements on the top and bottom steel rebars at the midspan using Equation 5.1. This method did not always produce a curve representative of the test in its entirety because the data acquisition system was limited to 20,000 με. For tests that exceeded

20,000 με in the tensile steel, the moment-curvature graphs were only partially reported. Typically, the first softening of the beam could still be captured in these curves.

$$\phi = \frac{|C|+|T|}{7.25} * 1000000 \qquad \text{Equation 5.1}$$

where

ϕ = Curvature (in^{-1}).

C is the strain in the compression steel at midspan.

T is the strain in the tensile steel at midspan.

7.25 is the vertical distance between the two gauges in inches.

The equation is multiplied by 1000000 because the strain values were measured in microstrain ($\mu\varepsilon$).

The rotation-based moment-curvature response was obtained by calculating the average curvature using the rotation measurements at 4 inches from the midspan on either side (8-inch near the mid-span region) as calculated form Equation 5.2.

$$\phi = \frac{(|Inc.R|+|Inc.P|)}{8} * \frac{\pi}{180} \qquad \text{Equation 5.2}$$

where

ϕ = Curvature (in^{-1}).

Inc.R is the inclinometer reading on the roller side in degrees.

Inc.P is the inclinometer reading on the pin side in degrees.

8 is the distance between the two inclinometers in inches.

The TiAB strain gauge spacing was modified for two specimens to prevent the edge strain gauges from being near the end of the bar. The 30-inch bonded TiABs (i.e., R.HB.30 and R.SB.30) had three strain gauges placed at 4 inches. For the hooked-unbonded bars, one gauge

was placed at the center of the TiAB and one was placed at the quarter length on each side of the TiAB for a total of three strain gauges due to the expectation of constant stress along the bar.

It was observed during the testing that the TiAB strain gauges for the bonded specimens malfunctioned during testing. The strain gauge malfunctioning typically occurred around 6000 microstrains, which is prior to capturing the TiAB yielding and (yielding of the TiAB occurs around 8500 microstrains). The strain gauges would adhere to the epoxy once the TiAB was mounted into the groove. The epoxy has a lower tensile strength than the TiAB and whenever the cracks formed the gauges would stop reporting values indicative of the TiAB. Figure 6.5 depicts stain gauges attached to the epoxy rather than the TiAB post-test.

Figure 6.5 – Strain Gauges and Epoxy Post-Test

6.3 Strain Gauge Installation

To give the strain gauges a smooth surface to adhere to, a 1.5-inch section of the bar surface where a strain gauge was to be placed was smoothened using an angle grinding tool. CSM-3

degreaser was used to remove any grease or oil from the smooth surface. The surface was then wet-sanded with 220-grit sandpaper followed by 320-grit with a mild phosphoric-acid conditioner. An ammonia-based neutralizer was then used to chemically neutralize the surface and clean any contaminants. The strain gauge was then attached to the bar using a cyanoacrylate adhesive. Figure 6.6 displays strain gauges attached to reinforcing bars.

Figure 6.6–- Strain Gauge on Tension Steel

The strain gauges placed on the internal reinforcement had to withstand being covered by concrete, so a polysulfide coating was used for protection. This coating also protected the strain gauges from damage that might occur during concrete casting. A picture of the two strain gauges with the polysulfide coating on them can be seen in Figure 6.7.

Figure 6.7–- Strain Gauges with Polysulfide Coating

The same process was used to apply the strain gauges to the TiAB. Instead of an angle grinding tool, a bench grinder was used for convenience. The TiAB was not covered in coating to not disrupt the bond with the epoxy. Figure 6.8 shows a TiAB with strain gauges attached.

Figure 6.8-- Strain Gauge attached to TiAB

6.4 Load Protocol

The specimens were pre-cracked to simulate in-service conditions, next the TiABs were installed and then subjected to final loading. The final loading was a monotonic load that pushed the beam to its capacity until it failed. The final load commenced in force control (1 kip/min) until the steel yielded and then the loading switched to displacement control. The displacement control started at 0.02 in/min and was increased to 0.05 in/min once the beam's resistance plateaued. The displacement-control loading is suitable for capturing the behavior in the plateau and post-peak region of the beam response. During the force-controlled portion of the testing, the loading was paused every 2 kips to mark cracks with a black permanent marker (pre-cracking cracks were marked in red) until steel yielding (based on strain gauge readings). After steel yielding, cracks were marked upon propagation until the failure of the beams.

7.1 Pre-Cracking of the Specimens

NSM TiAB strengthening is an application targeted for bridges that are in service. To accurately represent/simulate the in-service bridge condition, all the beam specimens were pre-cracked prior to mounting the TiAB. The beams were taken to 85% of steel yielding (this equated to about 2,000 microstrains in the longitudinal steel which yields around 2,350 microstrains). Eighty-five percent of yielding was chosen because the beams would be stressed beyond typical service load conditions but remain in the linear-elastic region. This was done using the same monotonic three-point loading configuration that was also used for the failure tests as shown in Figure 6.1. The strains were monitored using the strain gauges that were attached to the tensile longitudinal reinforcement at the center of the beams. The cracks were marked with red permanent markers to distinguish from the failure load cycle, and crack widths were measured at 1-kip intervals. Figure 7.1 show the typical tensile strain and displacement variation plots during the cracking of the beams prior to installing the TiAB.
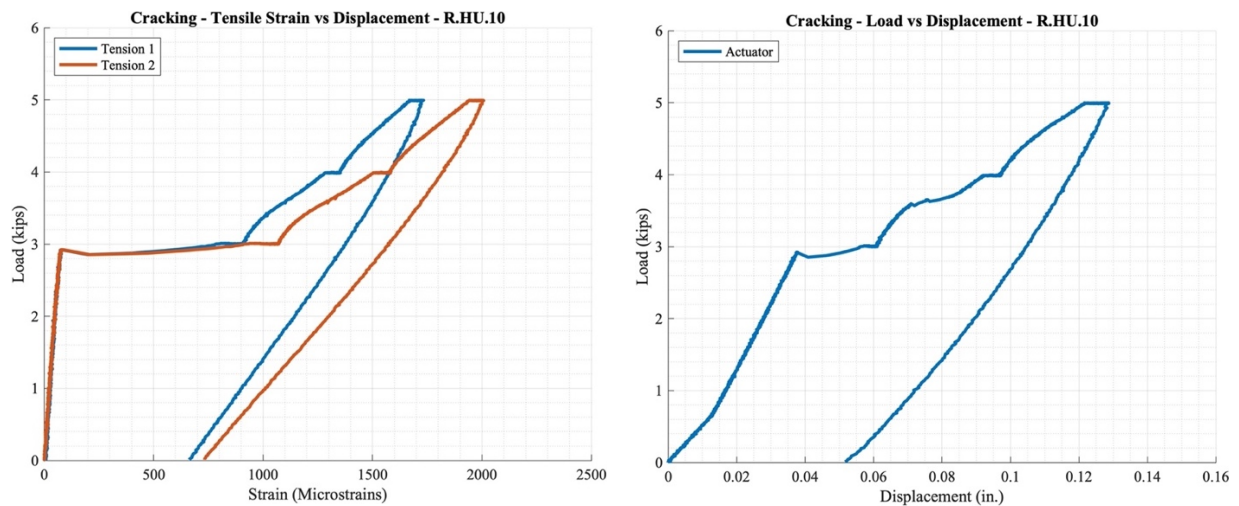
Figure 7.1-- Example Tensile Strain vs Displacement (Left) Load vs Displacement (Right)

It has been consistently observed during the cracking process that the first crack would appear around 3 kips near the midspan on either side of center where stirrups were located. This crack was typically classified as a narrow (hairline) crack with a width of 0.003 inches. An example of crack initiation in a beam can be seen in Figure 7.2. As the load increased, the crack propagated towards the load point, and more cracks were initiated away from the center of the beam. When the steel reached 2000 micro strains, usually between 5 to 6 kips, the largest crack width for each beam varied from 0.008 inches to 0.012 inches. At the end of the pre-cracking stage, there were numerous cracks under the load point and in the shear span, as shown in Figure 7.3.

Figure 7.2–- Crack initiation during Pre-Cracking

Figure 7.3–– Typical Crack Pattern at end of Pre-Cracking

Upon completion of cracking there was residual strain in the longitudinal reinforcement and permanent deformation of the beam. The strain gauges and LPTs had to be disconnected from the data acquisition system after each beam's cracking cycle to incorporate the next beam. The residual strains ranged from 500-800 microstrain and the residual displacement were in the range of 0.05 inches. The recorded residual strains and beam deformations obtained at the end of the cracking cycles were manually added to the plots of the final (failure) loading cycles.

7.2 Preparing the TiAB for Installation

There were several steps that needed to be taken for NSM TiAB to be ready for mounting. These steps included; (i) cutting to length, (ii) heating and bending appropriately to form the anchorage hooks, (iii) grinding down the strain gauge locations, (iv) putting the wedges in place to keep the TiAB from falling out of the groove, (v) attaching strain gauges along the bar length. The straight-bonded bars were cut to the representative length directly, while the hooked bars (both bonded and unbonded) had cut lengths that was calculated using the Bar Bending Work

Instructions provided by the TiAB supplier, Perryman Company, to ensure that the TiAB were the proper length once bent (Appendix C).

The bars cut and bent to desired lengths using the bending and cutting machine at ASEL. For the hooked bars, the bar bending work instructions required that the bars be heated to approximately 1200°F and then placed in the bar bending machine at that temperature. TiAB naturally turns blue when heated to 1200°F making this process convenient. An acetenyl-oxygen torch with a rosebud tip was used to heat the TiAB. Figure 7.4 displays the TiAB being heated and bent.
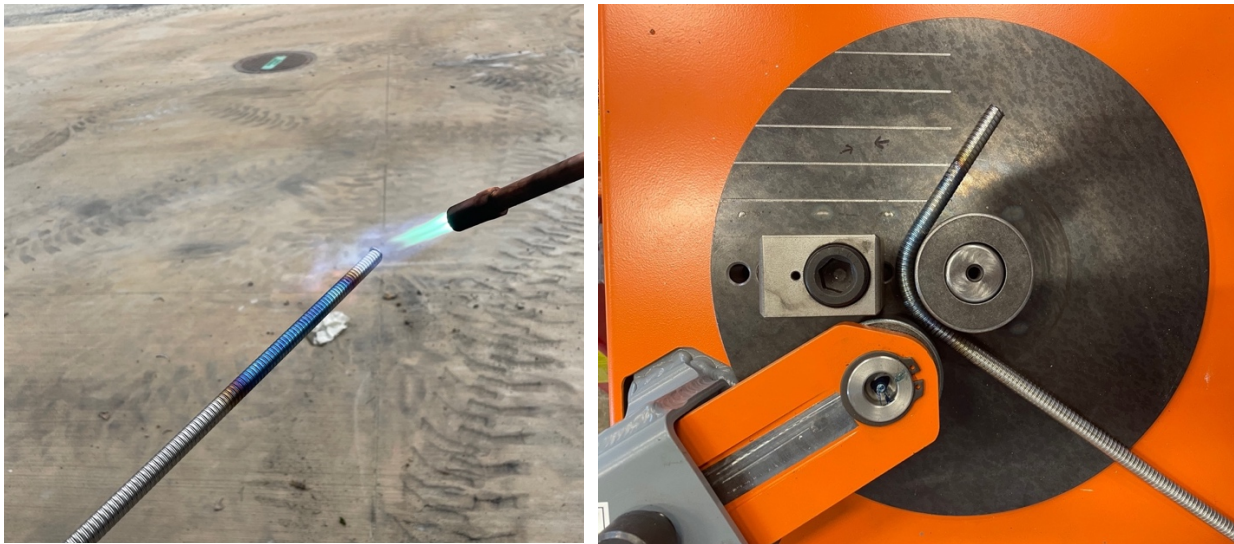
Figure 7.4 – TiAB Heating (Left) and Bending (Right)

To keep the bars in place inside the cut grooves, a rubber hose with an inside diameter of 0.5 inches and an outside diameter of 0.75 inches was cut into half-inch segments to act as wedges. These wedges were slid onto the bar about every 18 inches to ensure the longest bar could be kept in place. For some cases, a small layer of electrical tape was added on the outside of the wedges for the TiAB to fit better with the walls of the groove.

The last step to prepare the TiAB for installation was to add the strain gauges. The process for attaching the strain gauges is outlined in Section 5.3. Figure 7.5 depicts one of the wedges as well as two strain gauges attached on either side of the wedge.
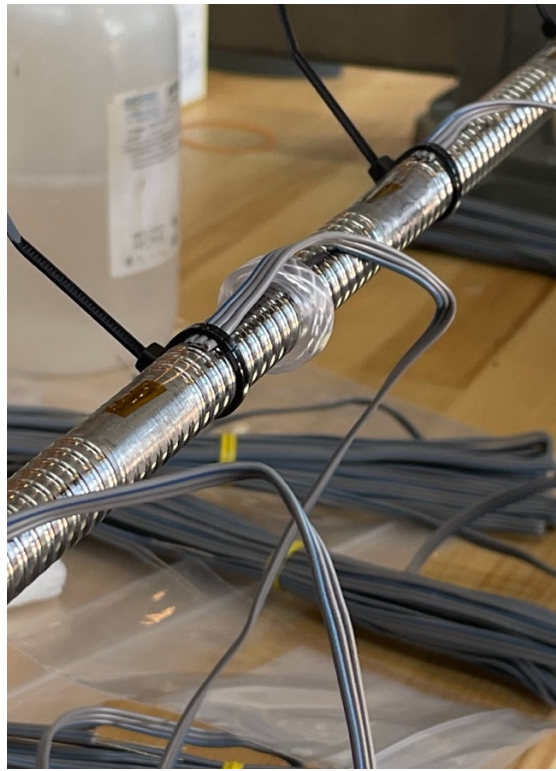
Figure 7.5–- TiAB with Wedge and Strain Gauges

7.3 Preparing the Concrete Specimen for NSM Strengthening

The concrete beams were prepared for NSM TiABs by; (i) cutting a 0.75 in. square groove in the soffit of the beams, (ii) drilling holes and chiseling the concrete to accommodate the bend radius of the hooked TiABs, (iii) low-pressure water blasting with abrasives for cleaning and achieving optimal bond performance. The hooked-unbonded specimens only required drilling of the holes and chiseling to accommodate the bending diameter due to not needing to be placed in a groove.

Conversely, the straight-bonded specimens only required groove cutting because there were no hooks to penetrate into the concrete.

Cutting the grooves into the beams was performed by concrete cutting professionals. As mentioned, the groove was a 0.75-inch square groove based on the 0.5-inch bar diameter used in this research, as prescribed by the AASHTO Guide. A single blade with 0.75-inch thickness was acquired to ensure the proper groove width was maintained along the length as shown in Figure 7.6. For the cutting process, the beams were flipped to where the soffit of the beam was facing up and put on heavy-duty sawhorses, as shown in Figure 7.7. All hooked-bonded and straight-bonded beams were cut to a length of 104 inches which accounted for the full 96 in. length and an additional 8 in. to accommodate for the tapering of the blade. Cutting all the beams to the maximum length was convenient and provided flexibility in terms of revising the embedment length in the test matrix, if deemed necessary.

Figure 7.6–- Custom 0.75 in. wide blade and Corresponding Groove

Figure 7.7-- Track Saw Mounted on Beam

The holes that were drilled to incorporate the TiAB hooks were also 0.75 inches in diameter to maintain continuity with the groove. The holes were drilled 6 inches deep using a hammer drill, as shown in Figure 7.8. To incorporate the bend diameter of the hook, a jig was made from plywood to guide the hammer drill out of the hole and bevel the concrete substrate at the same radius as the TiAB hook. After the work with the hammer drill was finished, a hammer and chisel were used to refine the bevel between the groove and the hole, as shown in Figure 7.9. The hole and bevel radius were refined until the TiAB was in continuous contact with the beveled concrete surface on both ends.

Figure 7.8–- Hammer drill used for Hole (Left) and Bevel (Right)

Figure 7.9–- Chiseling to Refine Bevel

The groove cutting and the drilling of the holes created slurry and dust/powder that left debris inside the grooves. The walls of the grooves also had damaged concrete from the cutting process. Therefore, the grooves were cleaned before the TiAB was mounted to the concrete using low-pressure water blasting with abrasive, as prescribed in ACI 546R (2014). This method was chosen because it is a precise method that selectively removes defective concrete and produces minimal damage to remaining concrete. Low-pressure water blasting with abrasives shoots a combination of water and masonry sand out of a nozzle at 4000 psi, as shown in Figure 7.10. The result is a clean and porous surface suitable for good bonding without further damaging the concrete surface, as Figure 7.11 shows a before and after sequence.

Figure 7.10–- Low-Pressure Water Blasting with Abrasives

Figure 7.11-- Before (Left) and After (Right) Water Blasting with Abrasives

7.4 Near-Surface Mounting of the TiAB

This section discusses the specific process of mounting the TiAB to the beams. Appendix A

provides the specific installation procedure used in this study. This appendix includes guidance

for the installation process starting with the preparation of the concrete and TiABs as well as

guidance for the near-surface mounting of the TiABs. The TiABs were installed from the

underside of the beam to be representative of the worst practical strengthening case. A wooden

trowel fitted with a custom-made triangular tip to penetrate 2/3 of the groove volume was used to

push the epoxy into the corners of the groove. This ensured that the epoxy was adequately

packed in the corners and that there were no air bubbles to disrupt the bond, as shown in Figure

7.12. Once placed in the groove, a putty knife was used to consolidate the epoxy around the

TiAB and smooth the epoxy over the surface of the bars. Figure 7.13 shows a straight-bonded

bar after being completely installed into the beam. After the TiAB had been completely installed,

the beams were left to cure for at least 7 days, according to the epoxy manufacturer's

documentation which is provided in Appendix D.

Figure 7.12–- First Lift of Epoxy application

Figure 7.13–- Installed TiAB after Final Epoxy Lift

CHAPTER 8: EXPERIMENTAL BEHAVIOUR, RESPONSE, AND DISCUSSION

This chapter presents the experimental behavior, response and post-test discussion from the failure load application of the beam specimens strengthened with NSM TiABs. The beams failed in various modes, including TiAB rupture, epoxy rupture, debonding, and anchorage slip, as each failure mode described in Section 2.9. Upon data analysis, the failure of each specimen was defined as a peak load reduction of 5%. The peak and failure displacements were considered as the displacements that occurred at the peak and failure loads respectively. The predicted AASHTO capacity using experimental values of the concrete, steel, and TiAB was used to indicate when the TiAB yielded. The TiAB strain gauges that were not embedded in epoxy (i.e., the hooked-unbonded specimens) were capable of capturing TiAB in which case those values were used for determining TiAB yielding.

8.1 Experimental Behavior and Responses

The following sections discuss the experimental responses of each beam. The load versus displacement graphs are marked with "X" markers that indicate major milestones that occurred during the test and associated pictures of the beams are provided for each test. Each section discusses the failure mode attributed to each beam's strength loss as well as the displacement, rotation, and strain responses observed pre- and post-failure.

8.1.1 R.CON

This specimen was the control beam test that did not include any strengthening using TiAB and was tested to provide the baseline performance to compare against the strengthened beams. The specimen was pre-cracked as explained in Section 7.1 (initial loading cracks marked with red). The load versus displacement graph is shown in Figure 8.1 and the pictures corresponding to the

points on the plot are provided in Figure 8.2. The load-displacement response figure includes the pre-crack load cycle and the initial displacement for the failure load cycle was shifted to match the residual displacement from the earlier load cycle (plotted as R.CON$_{cracking}$). As the applied force increased, pre-cracks propagated, and existing crack extensions and new cracks were marked in black. An almost linear response was observed at around an applied actuator load of 8 kips, where nonlinearity in the load-displacement behavior was observed beyond this load level.

Several flexural cracks were observed at this load level with almost constant spacing between the cracks. The test was transitioned into displacement-controlled loading as the force response entered a plateau behavior. The peak load occurred at 14.5 kips at a mid-span deflection of 2.89 inches. The flexural cracks propagated toward the load point near the peak load and widened extensively (in excess of 0.25 inches of crack width). Local concrete crushing was also observed under the load point in the post-steel yielding response. In the post-peak portion of the beam's behavior, the load was mostly maintained, and the beam was eventually unloaded at 3.39 inches due to excessive damage in the specimen. The load never dropped below 5% but local concrete crushing was observed under the load point and excessive tensile cracking in the beam was observed, therefore concrete crushing/excessive tensile cracking is the designated failure mode of the control beam. The load and displacement at failure were assigned to be the load and displacement at unloading, which was 14.5 kips and 3.39 inches.

The strains measured in the steel reinforcing bars and TiAB are presented in Figure 8.3. Similar to the displacement plots, the pre-crack load cycle is shown for the bottom reinforcing bar, and the strains are initiated from the residual strain that resulted from the pre-cracking load cycle. The bottom reinforcing rebars exceeded the steel yield strain of 2345 microstrain ($\mu\varepsilon$) at 6.6 kips at the mid-span section. The bottom reinforcement strains (T1 and T2) exhibited a yield

plateau response at around 9 kips. The difference between the initiation of rebar yielding and the yield plateau response is credited to the formation of the plastic hinge at the midspan and the load increase necessary to extend the yielded portion. The data acquisition system was capable of recording strains up to 2% strain (20,000 με), but the test continued beyond the force levels that achieved this strain limit.

The moment-curvature responses obtained from the strain and beam rotation measurements are provided in Figure 8.4 and with an abbreviated x-axis in Figure 8.5. The strain-based moment-curvature response (M-$\phi_{R.CON\ Strn1}$) and M-$\phi_{R.CON\ Strn2}$) was obtained by calculating the curvature between the strain measurements on the top and bottom steel rebars at the midspan. These curves are not representative of the full test due to the 20,000 με limitation of the data acquisition system. The responses indicated that a transition into non-linear response at around 250 kip-in and 0.0005 in^{-1} of curvature, consistent with the load displacement behavior. The beam softened from the yielding of the tensile steel. The peak moment for R.CON was 392 kip-in. The control beam was not instrumented with inclinometers, therefore a rotation-based moment curvature representing the entire test was not plotted.
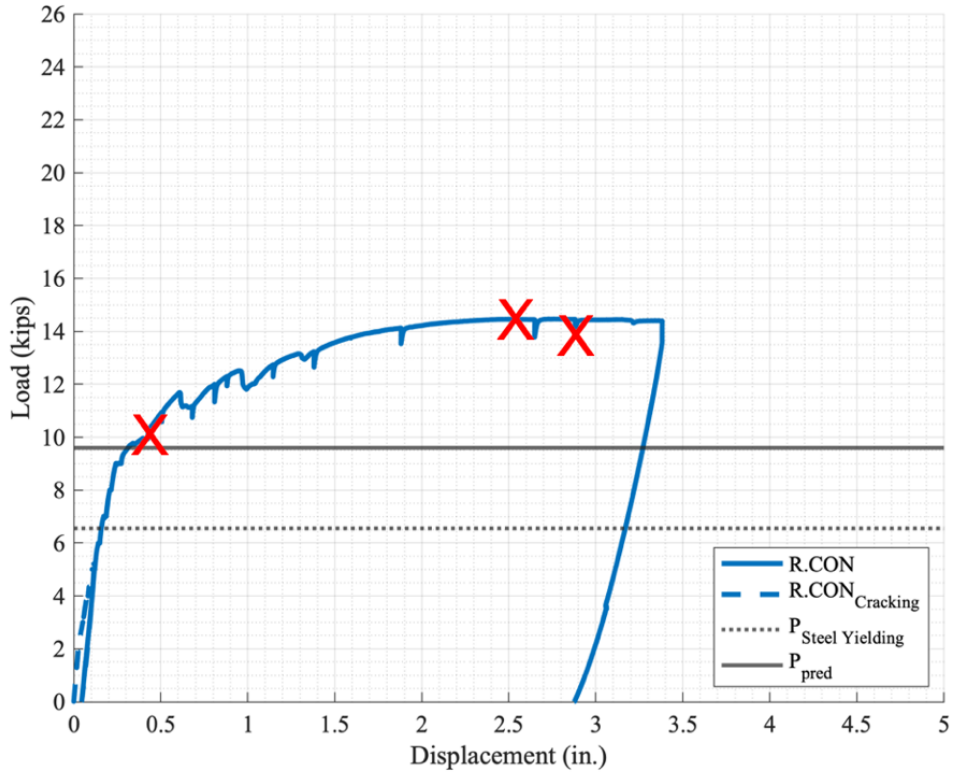
Figure 8.1-- R.CON Load versus Displacement

10.0 kips
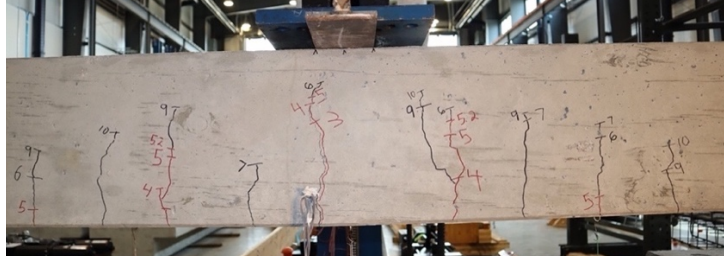
14.5 kips
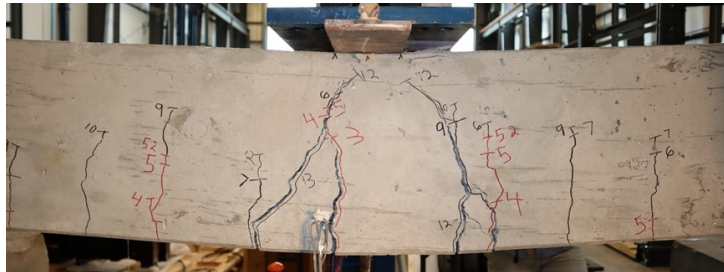
13.9 kips
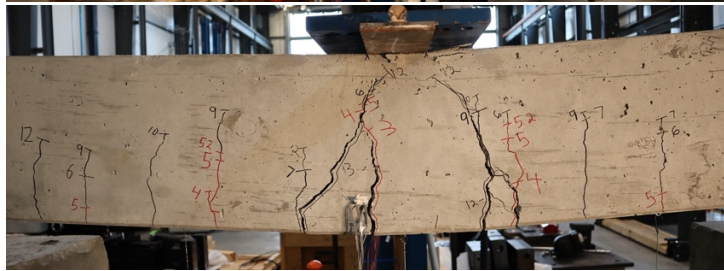
Figure 8.2–- R.CON Progression
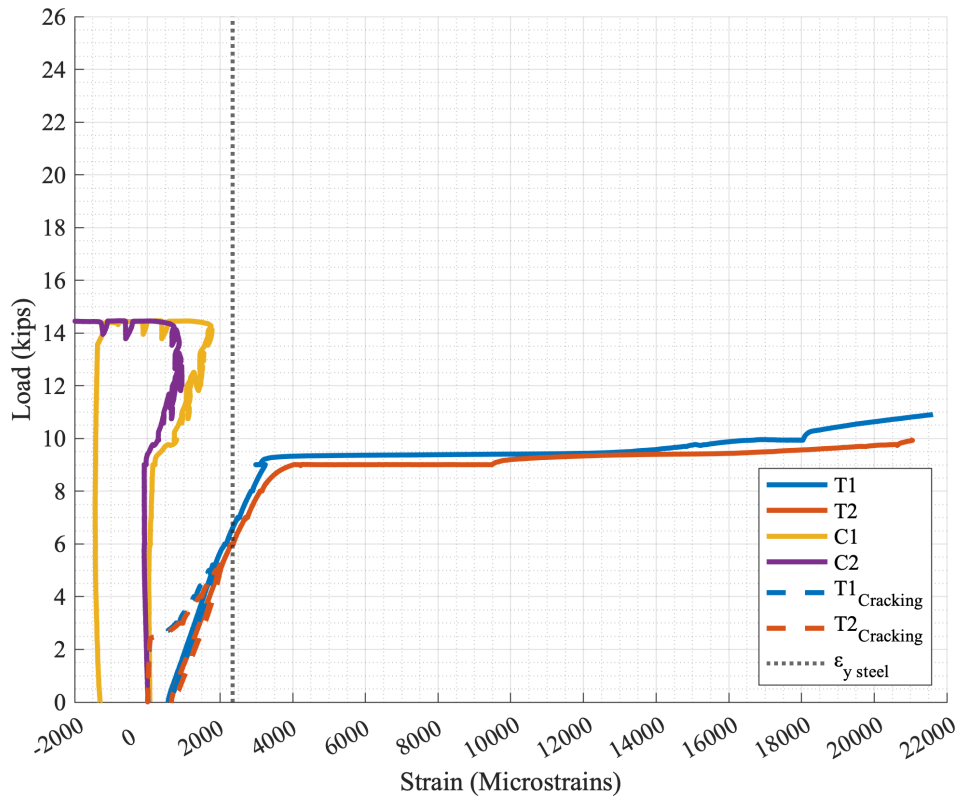
Figure 8.3 – R.CON Load versus Strain
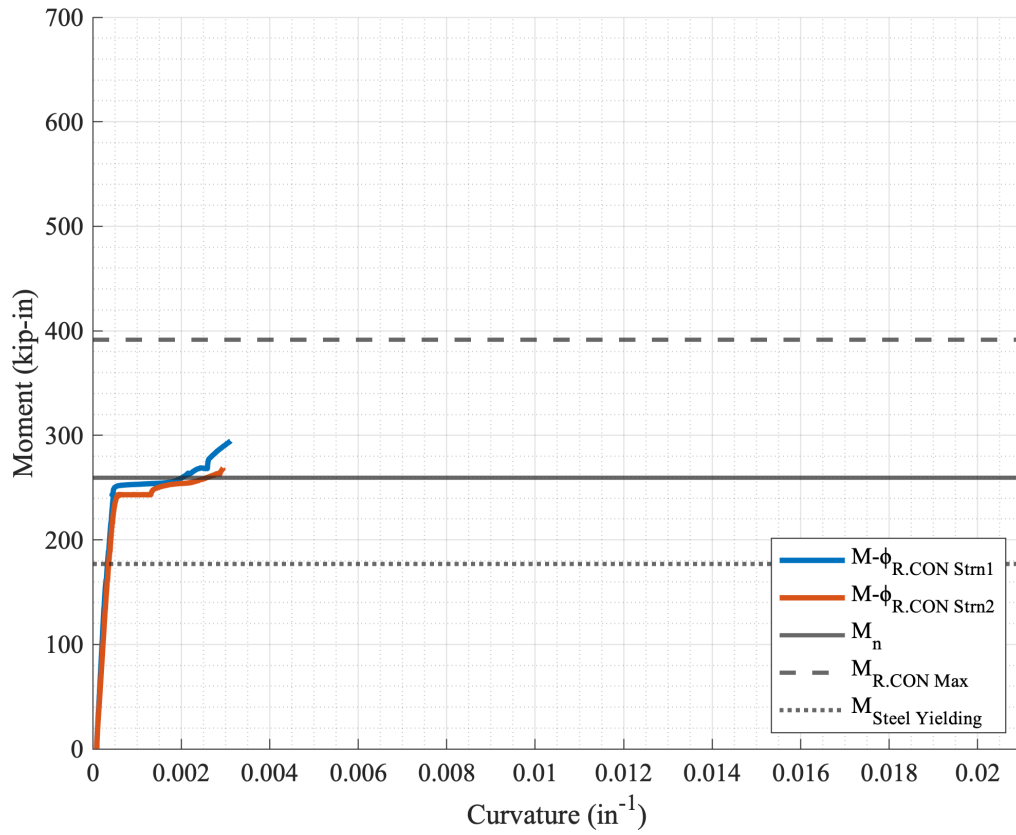
Figure 8.4 – R.CON Moment versus Curvature Response
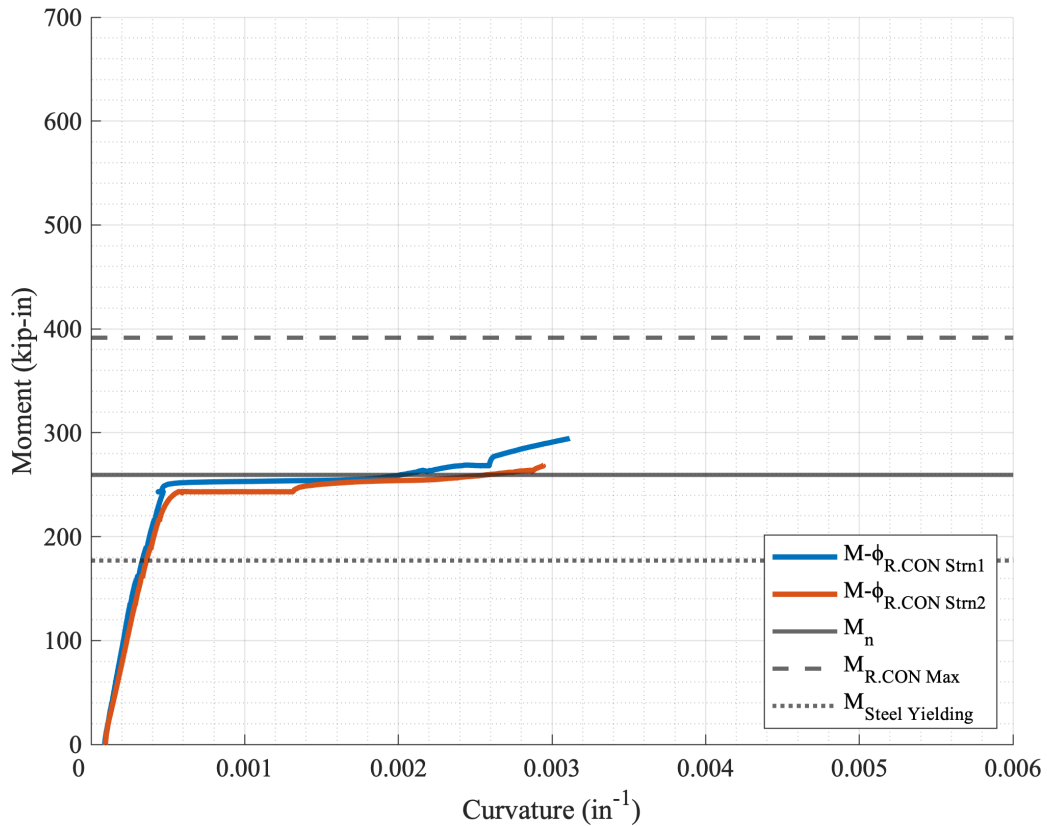
Figure 8.5–- R.CON Moment versus Curvature Response with Shorter Axis Limit

8.2 Hooked-Bonded Tests

This section discusses the experimental responses of the beams with hooked-bonded NSM TiAB.

8.2.1 R.HB.15

This specimen was strengthened with a 15-inch-long hooked-bonded TiAB (length measured from outside-to-outside of the hooks). The specimen was pre-cracked as explained in Section 7.1 (initial loading cracks marked with red). The complete load versus displacement graph is shown in Figure 8.6, and the pictures corresponding to the points on the plot are provided in Figure 8.7. Similar to the control specimen, the load-displacement response figure includes the pre-crack load cycle and the initial displacement for the failure load cycle was shifted to match the residual displacement from the earlier load cycle (plotted as R.HB.15$_{cracking}$). As the applied load

increased, pre-cracks widened and propagated, and existing crack extensions and new cracks were marked in black. An almost linear response was observed up to an applied force of about 13 kips, where nonlinearity in the load-displacement behavior was observed beyond this force level. The test was then transitioned into displacement-controlled loading. Similar to the control specimen, flexural cracks were observed with almost constant spacing between the cracks.

In addition to the flexural cracks, tensile cracking was observed near the TiAB hook anchorage zone. The peak load occurred at 15.5 kips at a mid-span deflection of 1.31 inches. The cracks observed near the TiAB hook anchorage zone widened extensively and extended toward the load point. Local concrete crushing was also observed under the load point in the post steel-yielding response. After excessive cracking near the hook anchorage zone, the strength gradually reduced to the force levels observed for the strength of the control beam (R.CON). In the post-peak portion of the beam's behavior, the load was mostly maintained, and the beam was eventually unloaded due to excessive damage in the specimen.

The beam was unloaded when the force dropped to 13.8 kips at 4.21 inches of mid-span displacement. The peak load observed for the test was marginally larger than the control specimen (15.5 versus 14.5 kips) and was not near the calculated capacity that corresponded to TiAB yielding (19.8 kips, as discussed in Section 3.3). Based on the failure definition of 5% force drop from the peak load, the specimen had a failure force of 14.7 kips at 1.69 inches of mid-span displacement. The observed failure mode was classified as hook debonding due to excessive cracking in the hook anchorage zone. Figure 8.8 includes a post-test photo that illustrates the anchorage zone failure.

The strains measured in the steel reinforcing bars and TiAB are presented in Figure 8.9. The bottom reinforcing bar strains initiated from the residual strain that resulted from the pre-

cracking load cycle. The bottom reinforcing rebars exceeded the steel yield strain of 2345

microstrain ($\mu\varepsilon$) at 8.9 kips at the mid-span section. The bottom reinforcement strains (T1 and

T2) exhibited a yield plateau response at around 13 kips. The difference between the initiation of

rebar yielding and the yield plateau response is credited to the formation of the plastic hinge at

the midspan and the load increase necessary to extend the yielding portion. The data acquisition

system was capable of recording strains up to 2% strain (20,000 $\mu\varepsilon$), but the tests continued

beyond the force levels that achieved this strain limit. Several of the strain gauges on the TiAB

malfunctioned prior to the test, and the ones that functioned in the test (strain gauges C, T1)

stopped reporting values at around 3000 $\mu\varepsilon$. The reason for TiAB strain gauges malfunctioning

prior to the TiAB yielding was credited to the cracks that occurred in the epoxy as explained in

more detail in Section 6.2.

The moment-curvature responses obtained from the strain and beam rotation

measurements are provided in Figure 8.10 and with an abbreviated x-axis in Figure 8.11. The

strain-based moment-curvature response (M-$\phi_{\text{R.HB.15 Strn}}$) was obtained by calculating the

curvature between the strain measurements on the top and bottom steel rebars at the midspan.

These curves are not representative of the full test due to the 20,000 $\mu\varepsilon$ limitation. The rotation-

based moment-curvature response (M-$\phi_{\text{R.HB-15 Inc}}$) was obtained by calculating the average

curvature using the rotation measurements at 4 inches from the midspan on either side (8-inch

central region) as mentioned in Section 6.2. The moment-curvature response indicates consistent

behavior with the one obtained from the 2D fiber model (M-$\phi_{\text{Fiber Model}}$) mentioned in Section 3.3

until the yielding of the steel rebars and deviating from the prediction. The responses indicated

that a transition into non-linear response at around 350 kip-in and 0.001 in^{-1} of curvature,

consistent with the load displacement behavior. The peak moment of 418 kip-in was achieved at

0.004 in^{-1} of curvature and the moment capacity gradually dropped with increasing curvature.
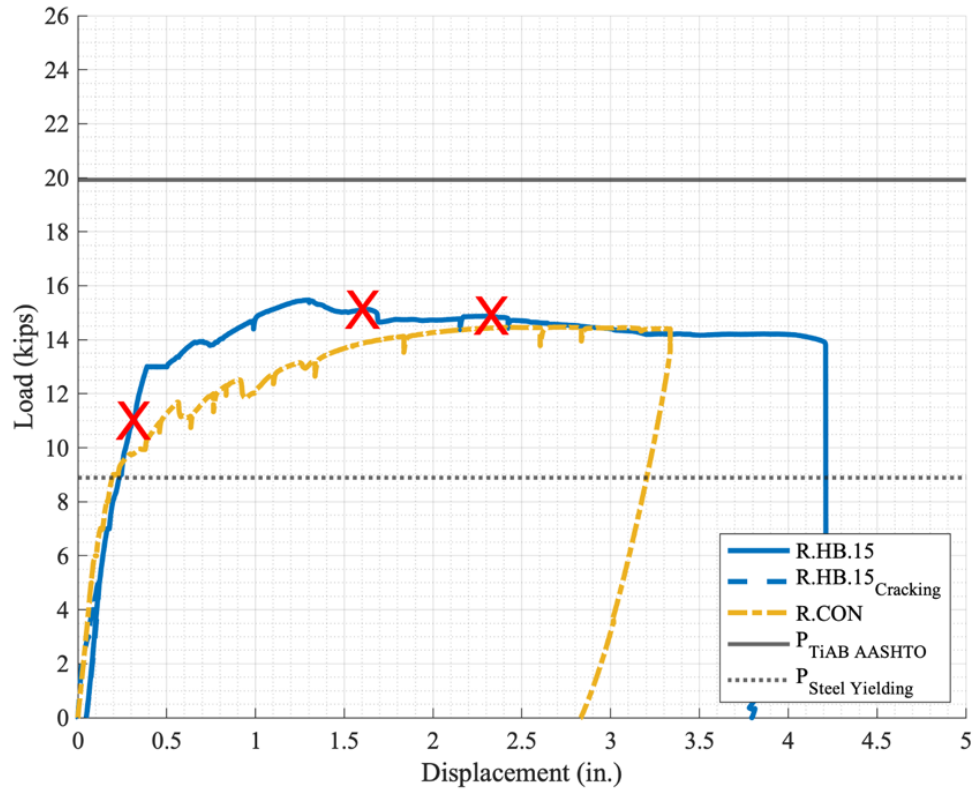
Figure 8.6–- R.HB.15 Load versus Displacement

11.0 kips

15.1 kips

14.9 kips

End Debonding Crack

End Debonding Crack
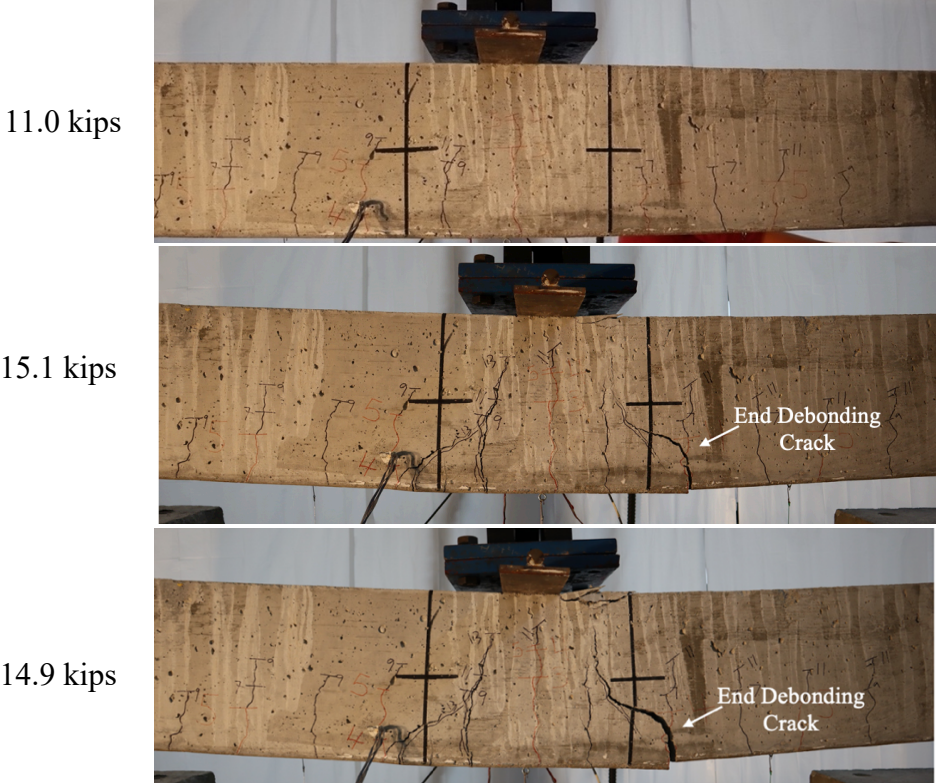
Figure 8.7-- R.HB.15 Progression

Figure 8.8–- R.HB.15 Post-Test
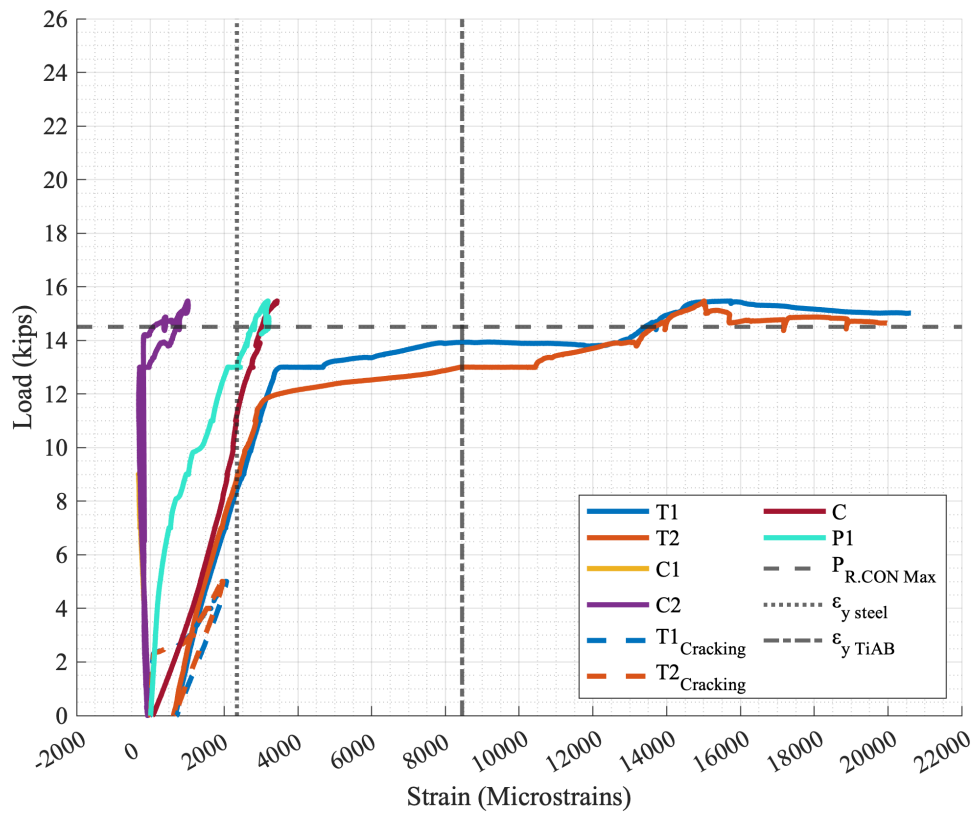
Figure 8.9 – R.HB.15 Load versus Strain Response
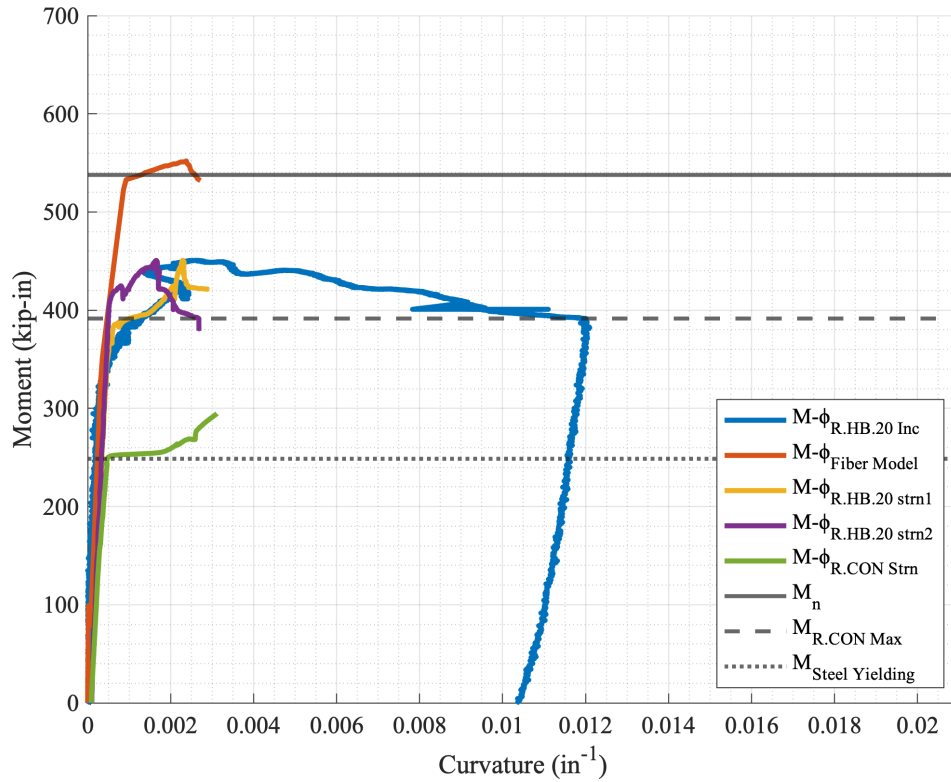
Figure 8.10 – R.HB.15 Moment versus Curvature Response
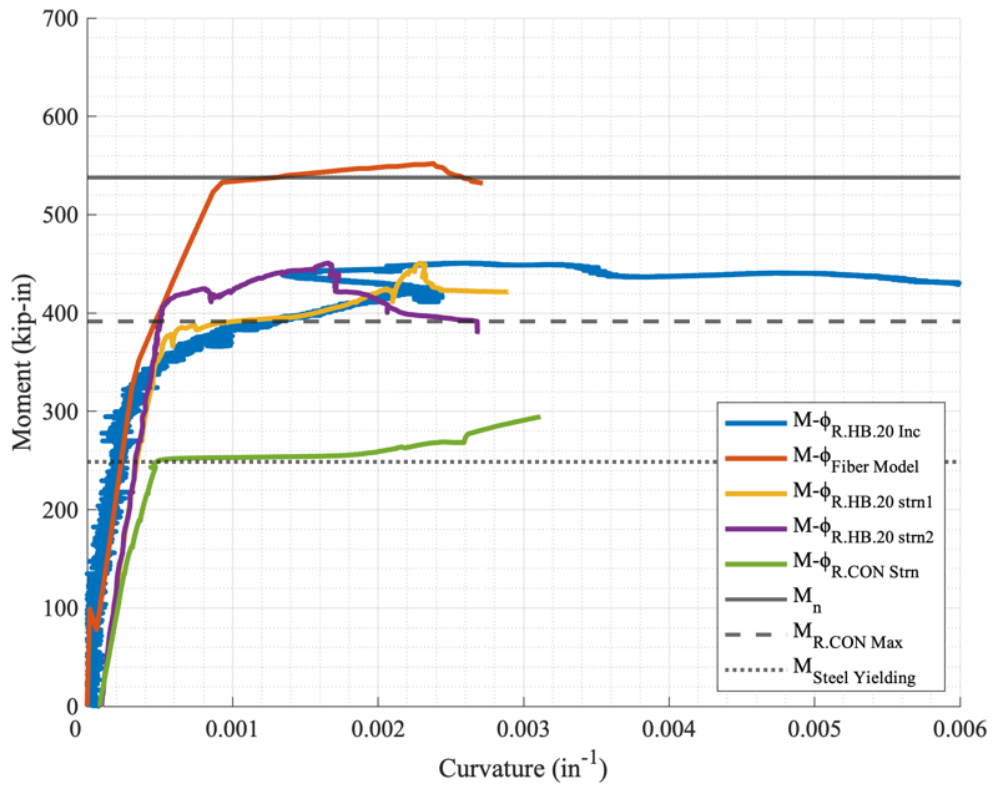
Figure 8.11–- R.HB.15 Moment versus Curvature Response with Shorter Axis Limit

8.2.2 R.HB.20

This specimen was strengthened with a 20-inch-long hooked-bonded TiAB (length measured from outside-to-outside of the hooks). The specimen was pre-cracked as explained in Section 7.1 (initial loading cracks marked with red). The complete load versus displacement graph is shown in Figure 8.12, and the pictures corresponding to the points on the plot are provided in Figure 8.13. As the applied load increased, pre-cracks widened and propagated, and existing crack extensions and new cracks were marked in black. An almost linear response was observed up to an applied force of about 13 kips, where nonlinearity in the load-displacement behavior became more visible beyond this force level. Similar to the earlier specimens, flexural cracks were observed at almost constant spacing between the cracks until the yielding of the steel rebars.

A considerably wide crack began to open and propagate towards the load point before TiAB hook on the right side of the central portion of the beam. Local concrete crushing was also observed under the load point in the post steel-yielding response. The peak load occurred at 16.7 kips at a mid-span deflection of 1.48 inches. The significant crack on the right side of the central portion of the beam continued to widen and the load response gradually reduced as the beam midspan continued to increase.

The peak load observed for the test was larger than the control specimen (16.7 versus 14.5 kips) but did not achieve the calculated strength that corresponds to the TiAB yielding (16.7 versus 19.8 kips). Based on the failure definition of 5% force drop from the peak load, the specimen had a failure load of 15.9 kips at 2.04 inches of mid-span displacement. The observed failure mode was classified as Intermediate Crack (IC) debonding, as Figure 8.14 illustrates the epoxy-concrete interface failure propagating from the IC.

The strains measured in the steel reinforcing bars and TiAB are presented in Figure 8.15. The bottom reinforcing bar strains were offset from the origin as they initiated from the residual strain that resulted from the pre-cracking load cycle. The bottom reinforcing rebars exceeded the steel yield strain of 2345 microstrain ($\mu\varepsilon$) at 9.2 kips at the mid-span section. The bottom reinforcement strains (T1 and T2) exhibited a yield plateau response at around 15 kips. The difference between the initiation of rebar yielding and the yield plateau response is credited to the formation of the plastic hinge at the midspan, and the load increase necessary to extend the yielding portion. Several of the strain gauges on the TiAB malfunctioned prior to the test, and the ones that functioned during the test (C, R1, P1, and P2) recorded values until about 4000 $\mu\varepsilon$.

The moment-curvature responses obtained from the strain and beam rotation measurements are provided in Figure 8.16 and with an abbreviated x-axis in Figure 8.17. The moment-curvature response indicates consistent behavior with the one obtained from the 2D fiber model (M-$\phi_{\text{Fiber Model}}$) up to high load levels. The responses indicated a transition into non-linear response at around 350 kip-in and 0.001 in^{-1} of curvature, consistent with the load-displacement behavior. The peak moment of 451 kip-in was achieved at 0.003 in^{-1} of curvature and the moment capacity gradually dropped with increasing curvature until unloaded at 0.012 in^{-1} of curvature.
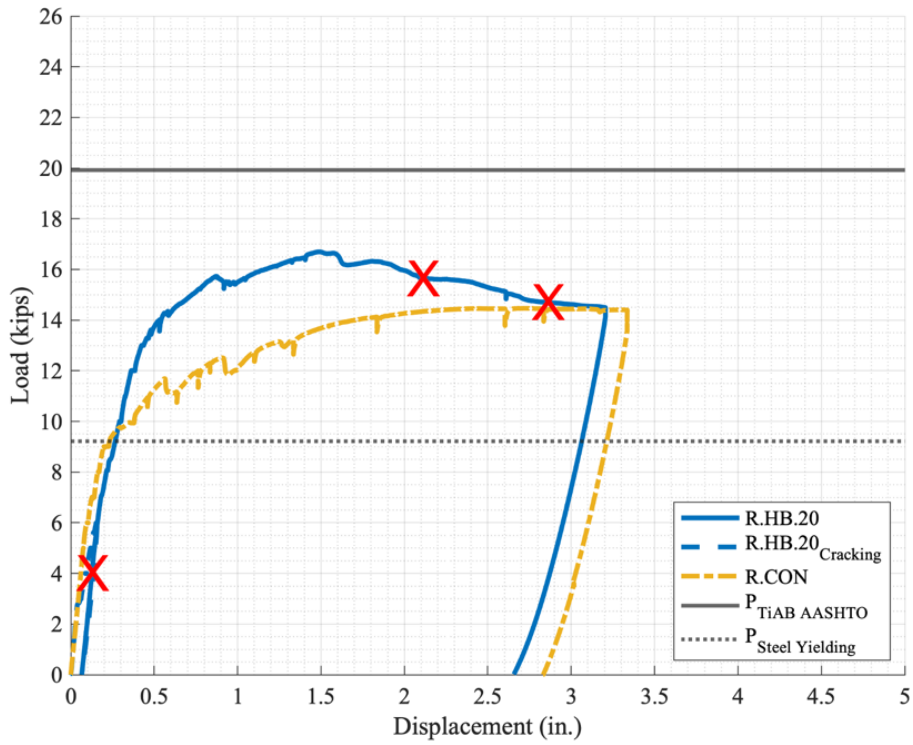
Figure 8.12–- R.HB.20 Load versus Displacement Response

4.0 kips

15.7 kips

14.6 kips
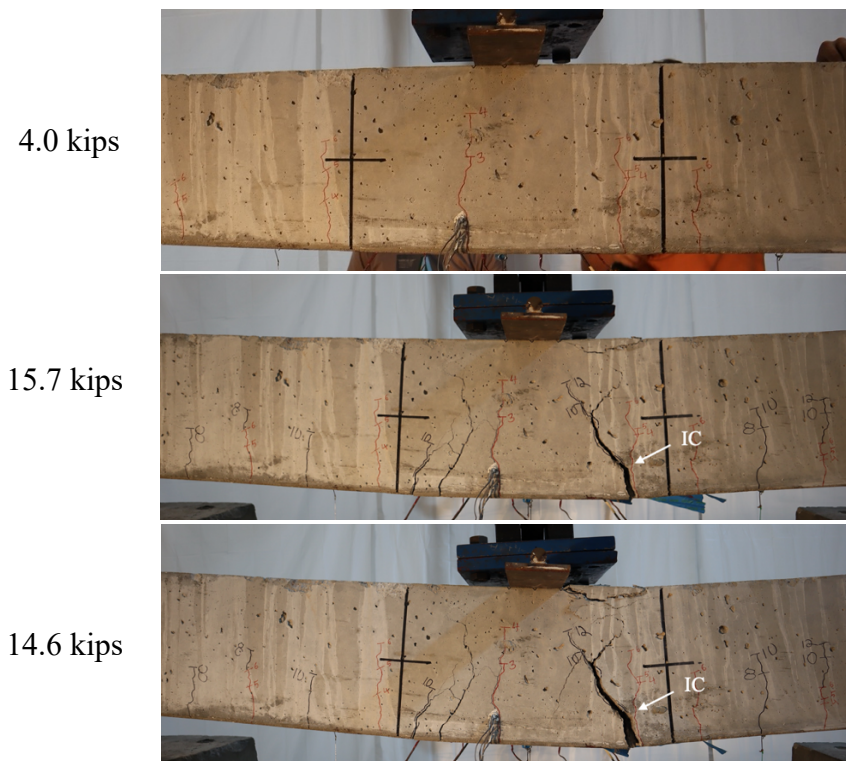
Figure 8.13–- R.HB.20 Progression

Figure 8.14–- R.HB.20 Post-Test
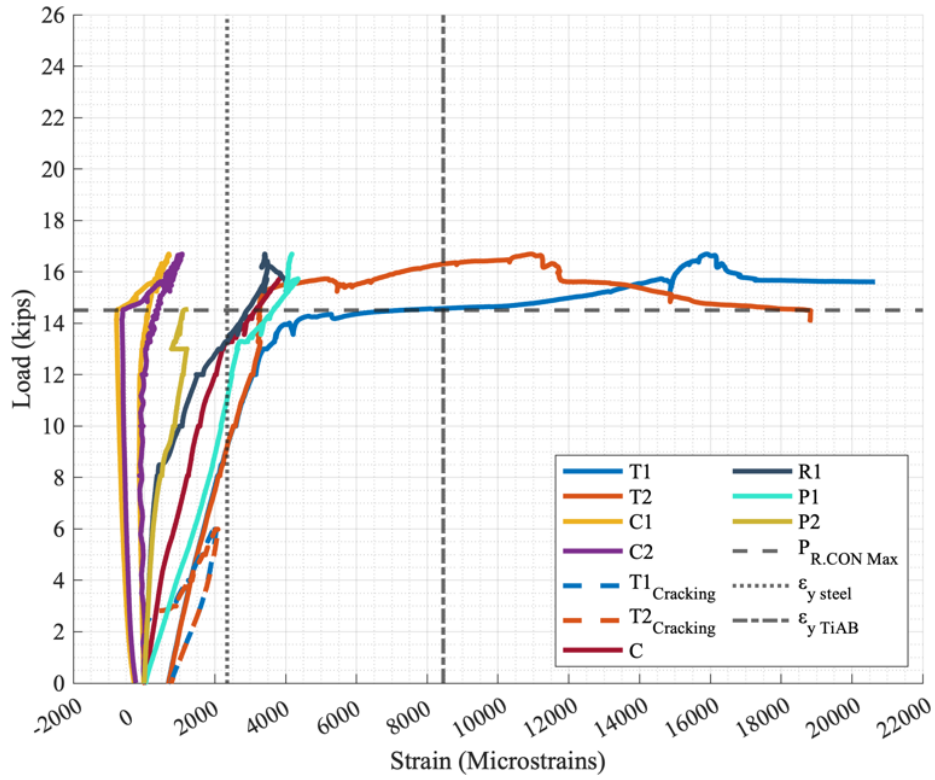
Figure 8.15 – R.HB.20 Load versus Strain Response
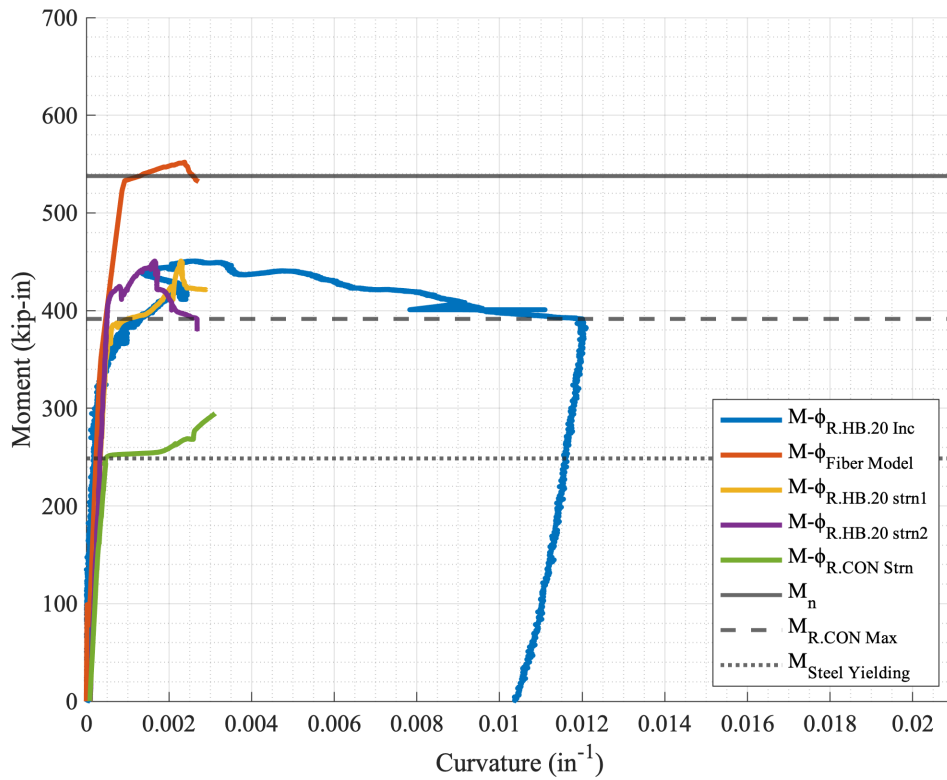
Figure 8.16 – R.HB.20 Moment versus Curvature Response

107
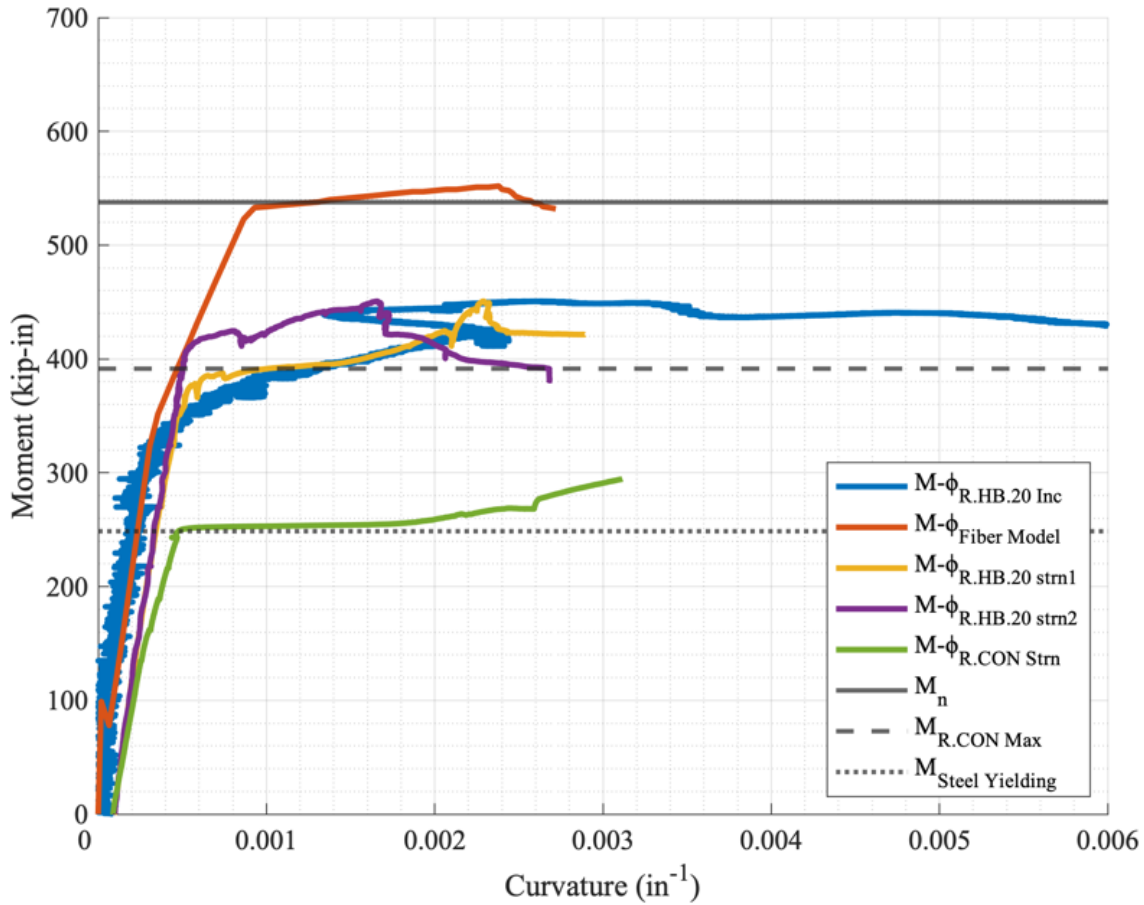
Figure 8.17— R.HB.20 Moment versus Curvature Response with Shorter Axis Limit

8.2.3 R.HB.30

This specimen was strengthened with a 30-inch-long hooked-bonded TiAB (length measured

from outside-to-outside of the hooks). The specimen was pre-cracked as explained in Section 7.1

(initial loading cracks marked with red). The complete load versus displacement graph is shown

in Figure 8.18, and the pictures corresponding to the points on the plot are provided in Figure

8.19. As the applied load increased, pre-cracks widened and propagated, and existing crack

extensions and new cracks were marked in black. An almost linear response was observed up to

an applied force of about 13 kips, where nonlinearity in the load-displacement behavior became

more visible beyond this force level. Similar to the earlier specimens, flexural cracks were observed at almost constant spacing between the cracks until the yielding of the steel rebars.

Four central cracks propagated towards the load point but with a maximum width of 0.03 inches at 21 kips. The peak load occurred at 21.9 kips at a mid-span deflection of 1.80 inches. After the peak load, the cracks doubled in width from 0.03 inches just before the peak to 0.06 inches just after the peak at 21.7 kips. The two cracks in the central-right portion of the beam representing the widest crack widths. The beam did not exhibit a plateau and the resistance dropped till unloaded at 17.05 kips and 2.94 inches of midspan displacement.

The strength observed for the test was larger than the control specimen (21.9 versus 14.5 kips) and larger than the calculated strength that corresponding to the TiAB and steel rebar yielding (21.9 versus 19.8 kips). Based on the failure definition of 5% force drop from the peak load, the specimen had a failure load of 20.8 kips at 2.15 inches of mid-span displacement. The observed failure mode was classified as IC debonding, as Figure 8.20 illustrates the epoxy-concrete interface failure propagating from the iCs that were on the central-right portion of the beam.

The strains measured in the steel reinforcing bars and TiAB are presented in Figure 8.21. The bottom reinforcing bar strains were offset from the origin as they initiated from the residual strain that resulted from the pre-cracking load cycle. The bottom reinforcing rebars exceeded the steel yield strain of 2345 microstrain ($\mu\varepsilon$) at 9.4 kips at the mid-span section. The bottom reinforcement strains (T1 and T2) exhibited a yield plateau response at around 13 kips. The difference between the initiation of rebar yielding and the yield plateau response is credited to the formation of the plastic hinge. Several of the strain gauges on the TiAB malfunctioned prior to the test, and the ones that functioned during the test (C, R1, R2, R3, P1, P2, and P3) recorded

values until about 5000-6000 $\mu\varepsilon$, which could not capture the yielding of the TiAB that was expected to occur around 8450 $\mu\varepsilon$. The epoxy cracking was credited as the reason for TiAB strain gauges malfunctioning as explained in Section 6.2.

The moment-curvature responses obtained from the strain and beam rotation measurements are provided in Figure 8.22 and with an abbreviated x-axis in Figure 8.23. The moment-curvature response indicates consistent behavior with the one obtained from the 2D fiber model (M-$\phi_{\text{Fiber Model}}$) up to a mid-span moment of 350 kip-in where the first softening occurred in both the model and measured response. The response deviated from the 2D fiber model response and indicated a gradually reducing slope (stiffness) until the peak moment, with a second softening occurring at 0.0035 in^{-1}. The gradually reducing stiffness is credited to the cracking occurring in the epoxy that might have caused slip of the TiAB and the second softening is likely a result of the TiAB yielding. The peak moment of 591 kip-in was achieved at 0.005 in^{-1} of curvature and the maximum curvature was recorded to be just beyond 0.08 in^{-1}. The curves quick descent after the peak indicates that even though the beam could achieve the capacity associated with TiAB yielding, it was not able to undergo large deformations at the peak load level.
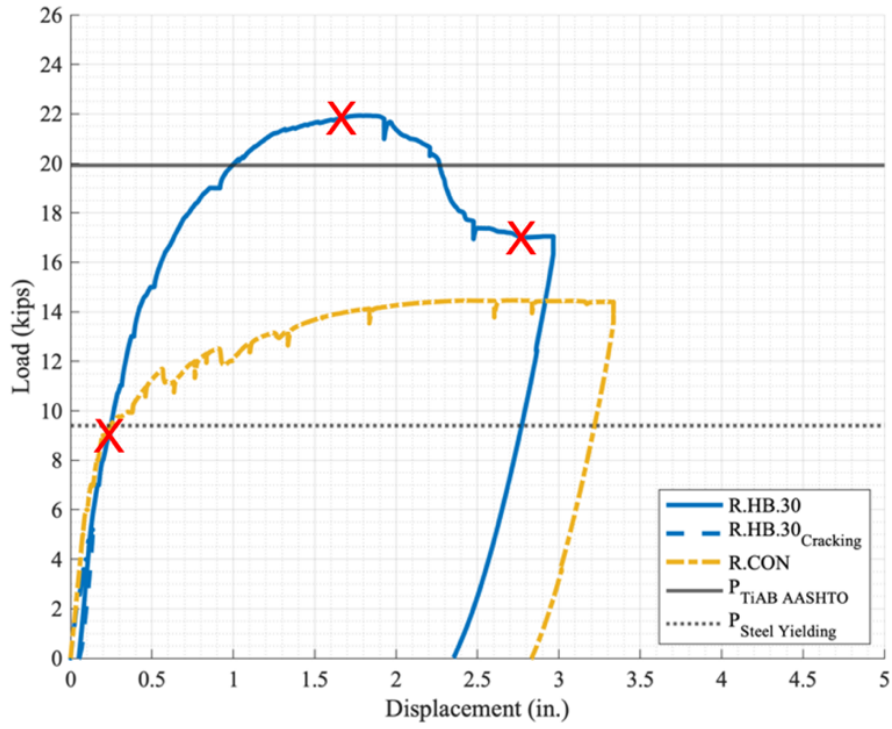
Figure 8.18–- R.HB.30 Load versus Displacement Response
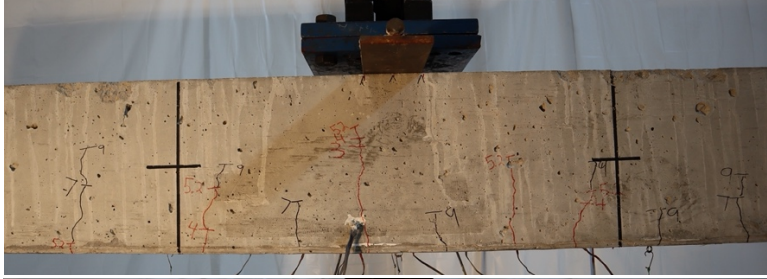
9.0 kips

21.9 kips
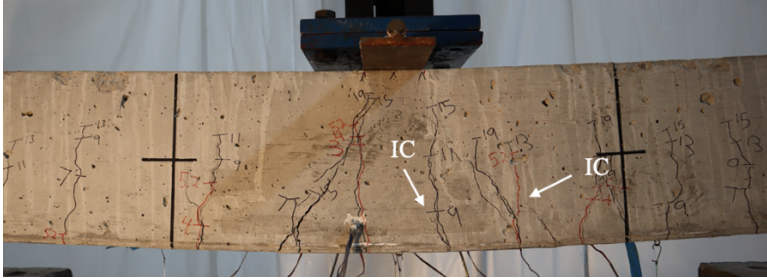
17.0 kips

Figure 8.19–- R.HB.30 Progression

Figure 8.20–- R.HB.30 Post-Test
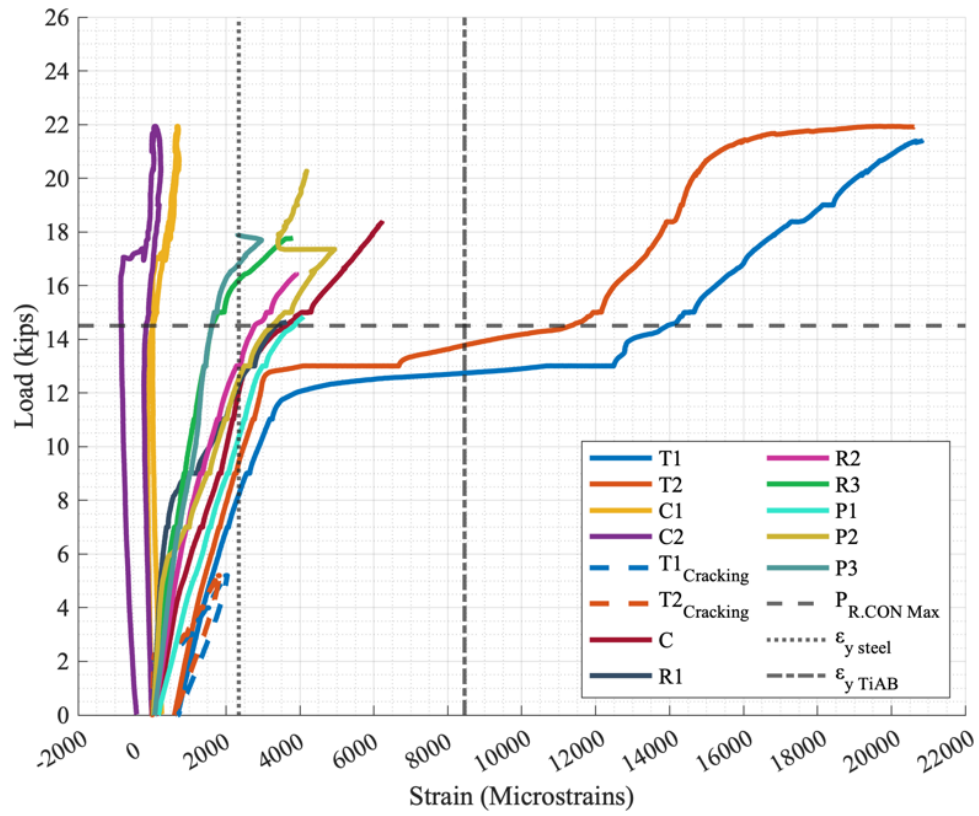
Figure 8.21 – R.HB.30 Load versus Strain Response
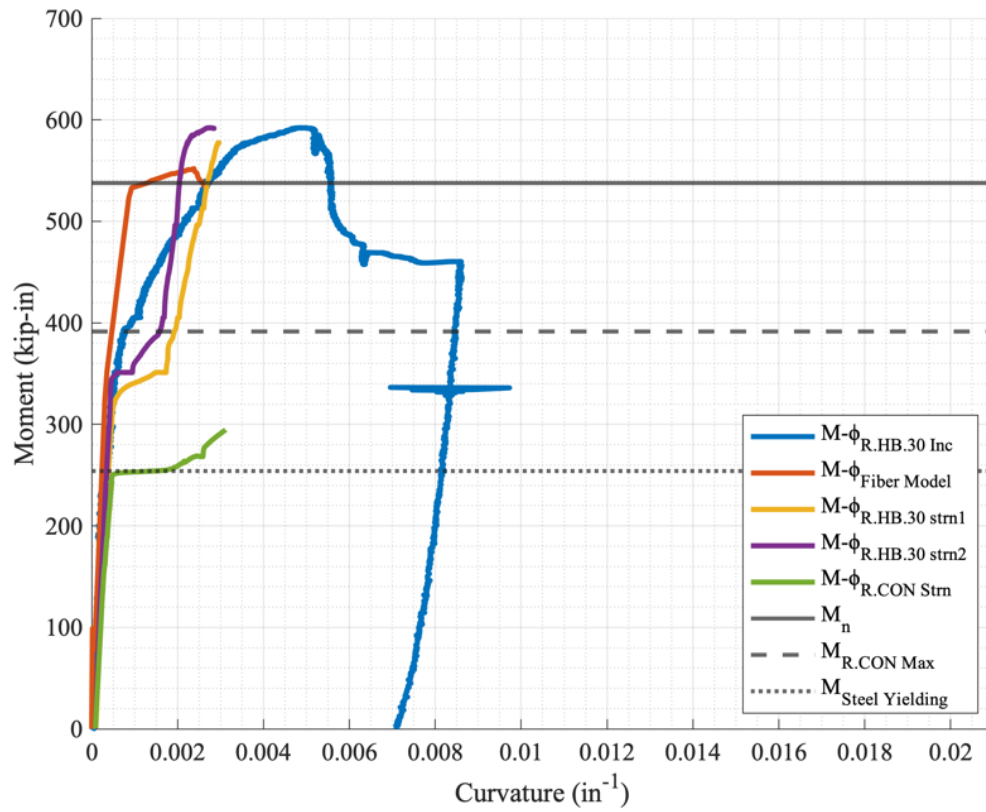
Figure 8.22 – R.HB.30 Moment versus Curvature Response
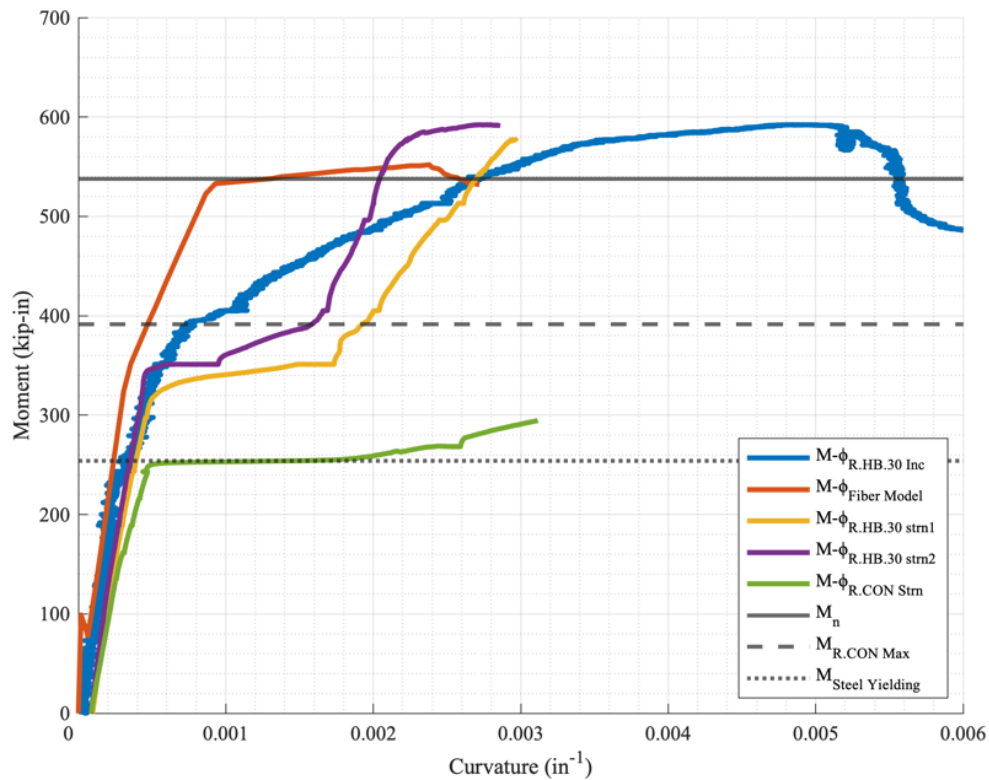
Figure 8.23–- R.HB.30 Moment versus Curvature Response with Shorter Axis Limit

8.2.4 R.HB.40

This specimen was strengthened with a 40-inch-long hooked-bonded TiAB (length measured from outside-to-outside of the hooks). The specimen was pre-cracked as explained in Section 7.1 (initial loading cracks marked with red). The complete load versus displacement graph is shown in Figure 8.24, and the pictures corresponding to the points on the plot are provided in Figure 8.25. As the applied load increased, pre-cracks widened and propagated, and existing crack extensions and new cracks were marked in black. An almost linear response was observed up to an applied force of about 13 kips, where nonlinearity in the load-displacement behavior became more visible beyond this force level. Similar to the earlier specimens, flexural cracks were observed at almost constant spacing between the cracks until the yielding of the steel rebars.

A large diagonal crack appeared in the central-left portion of the beam that initiated from a flexural crack between 11 kps and the peak load. The peak load occurred at 23.3 kips at a mid-span deflection of 2.01 inches. The load plateaued around 23 kips with increasing midspan displacement. A horizontal crack initiated from a flexural crack close to the left hook and propagated towards the diagonal crack. Local concrete crushing was also observed under the load point in the post steel-yielding response. The beam began to gradually lose resistance and a section of concrete from the diagonal crack fell at which point the beam was unloaded at 21.7 kips and 4.00 inches of midspan deflection.

The strength observed for the test was significantly larger than the control specimen (23.3 versus 14.5 kips) and exceeded the calculated strength that corresponded to the TiAB and steel rebar yielding (23.3 versus 19.8 kips). Based on the failure definition of 5% force drop from the peak load, the specimen had a failure load of 22.1 kips at 3.91 inches of mid-span displacement. The observed failure mode was classified as critical diagonal crack (CDC) debonding, as Figure 8.26 illustrates the failed epoxy-concrete interface along the groove where a concrete portion fell and wide cracks extended parallel the groove in both directions.

The strains measured in the steel reinforcing bars and TiAB are presented in Figure 8.27. The bottom reinforcing bar strains were offset from the origin as they initiated from the residual strain that resulted from the pre-cracking load cycle. The bottom reinforcing rebars exceeded the steel yield strain of 2345 microstrain ($\mu\varepsilon$) at 9.0 kips at the mid-span section. The bottom reinforcement strains (T1 and T2) exhibited a yield plateau response at around 14 kips The difference between the initiation of rebar yielding and the yield plateau response is credited to the formation of the plastic hinge. Several of the strain gauges on the TiAB malfunctioned prior to the test, and the ones that functioned during the test (R1, R2, P1, P2, and P3) recorded values

until about 4000 $\mu\varepsilon$, which could not capture the yielding of the TiAB that was expected to occur around 8450 $\mu\varepsilon$. The epoxy cracking was credited as the reason for TiAB strain gauges malfunctioning as explained in Section 6.2.

The moment-curvature responses obtained from the strain and beam rotation measurements are provided in Figure 8.28 and with an abbreviated x-axis in Figure 8.29. The moment-curvature response indicates consistent behavior with the one obtained from the 2D fiber model (M-$\phi_{\text{Fiber Model}}$) up to a mid-span moment of 400 kip-in. The response deviated from the 2D fiber model response and indicated a gradually reducing slope (stiffness) until the peak moment. The gradually reducing stiffness is credited to the cracking occurring in the epoxy that might have caused slip of the TiAB. The peak moment of 629 kip-in was achieved at 0.006 in^{-1} of curvature and the maximum curvature was recorded to be nearly 0.014 in^{-1}. The curve indicates a ductile response by sustaining the high force at large deformations, and also large energy dissipation under the curve.
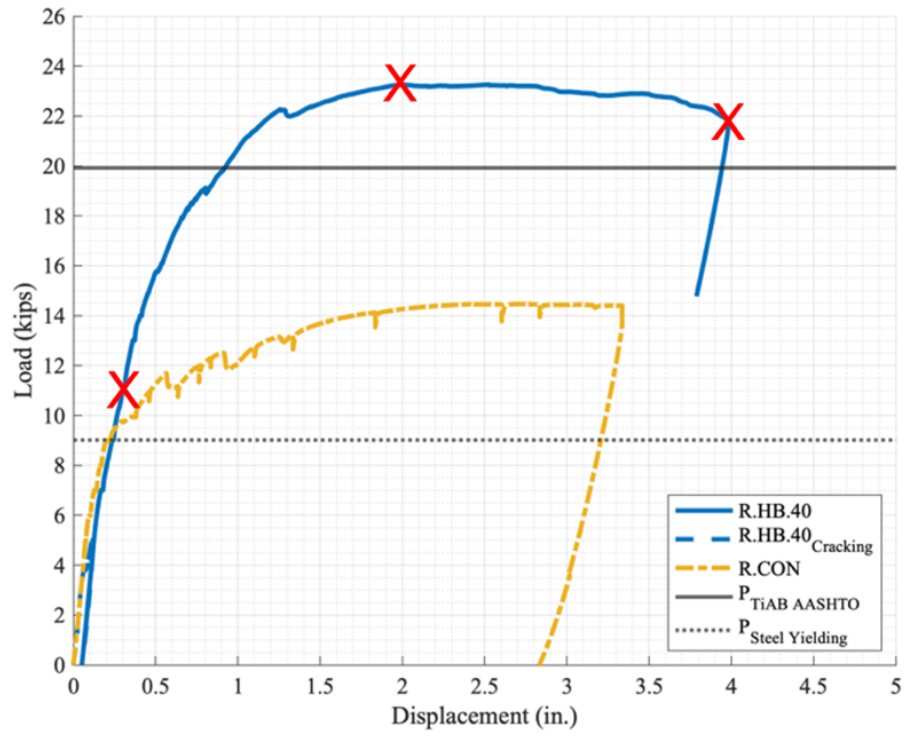
Figure 8.24–- R.HB.40 Load versus Displacement Response

11.0 kips
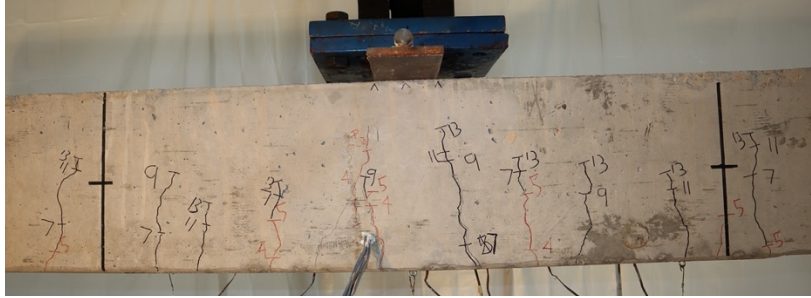
23.2 kips
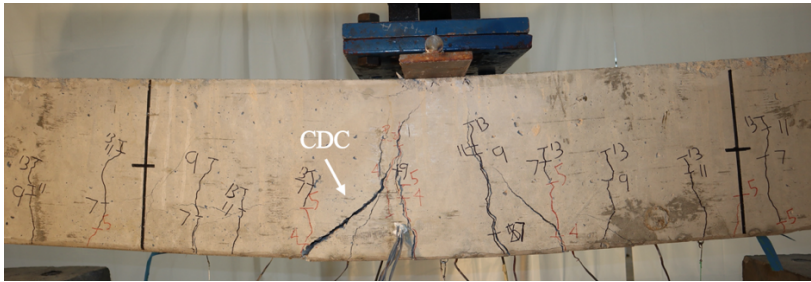
21.6 kips

Figure 8.25–- R.HB.40 Progression

Figure 8.26–- R.HB.40 Post-Test
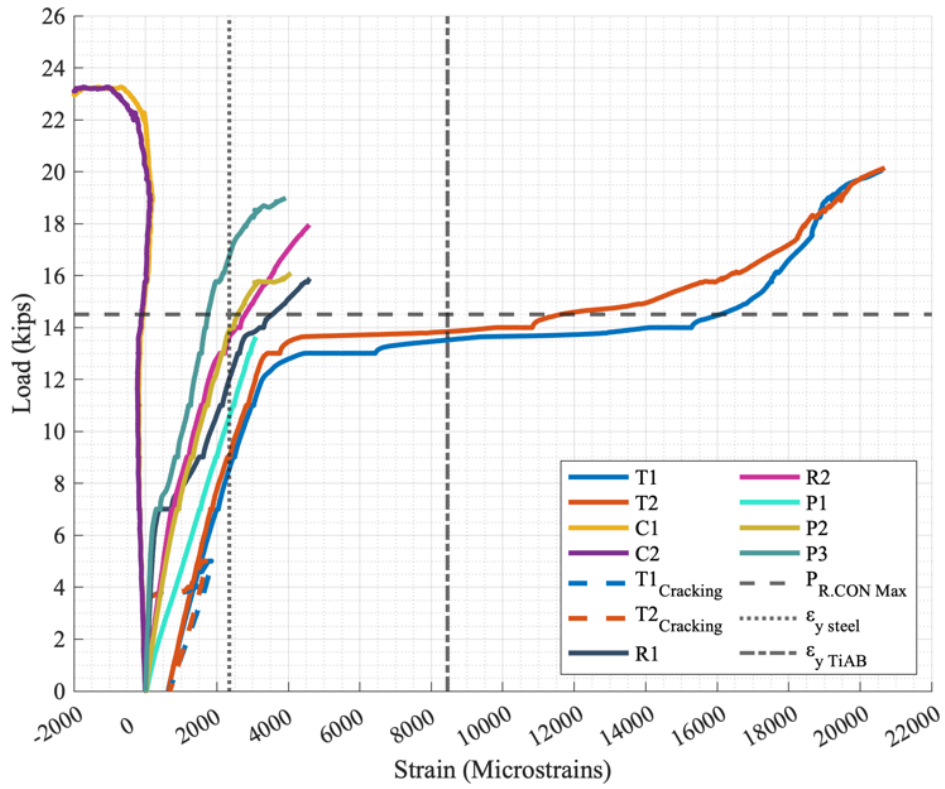
Figure 8.27 – R.HB.40 Load versus Strain Response
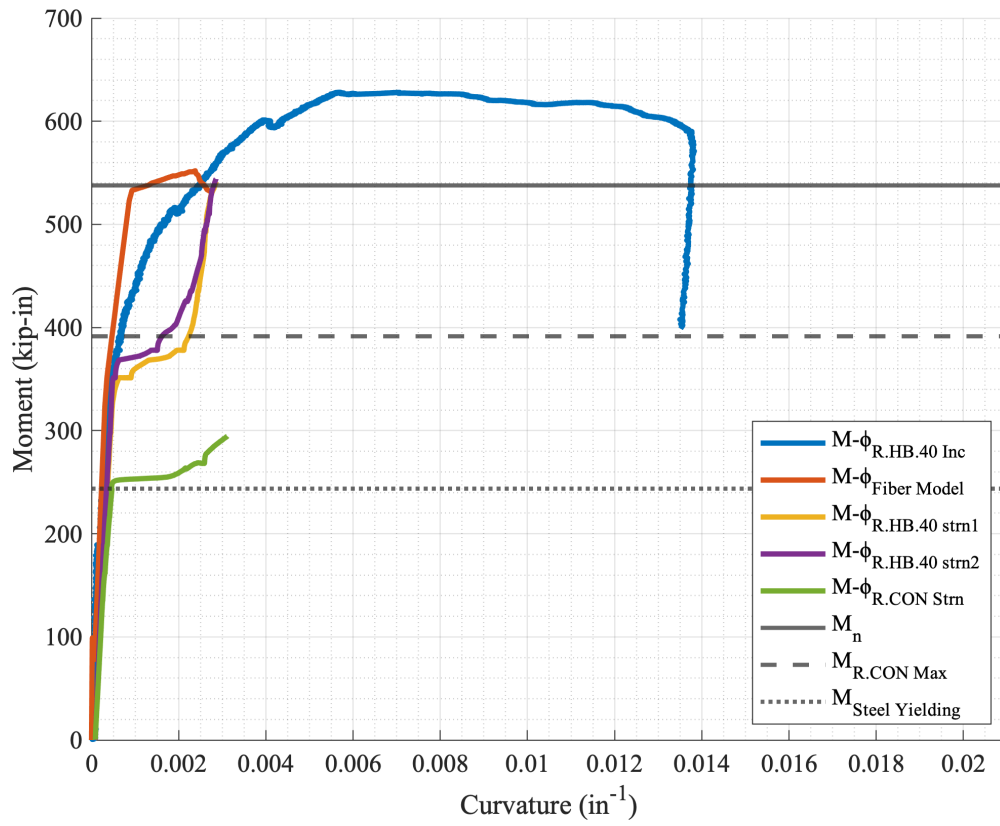
Figure 8.28 – R.HB.40 Moment versus Curvature Response
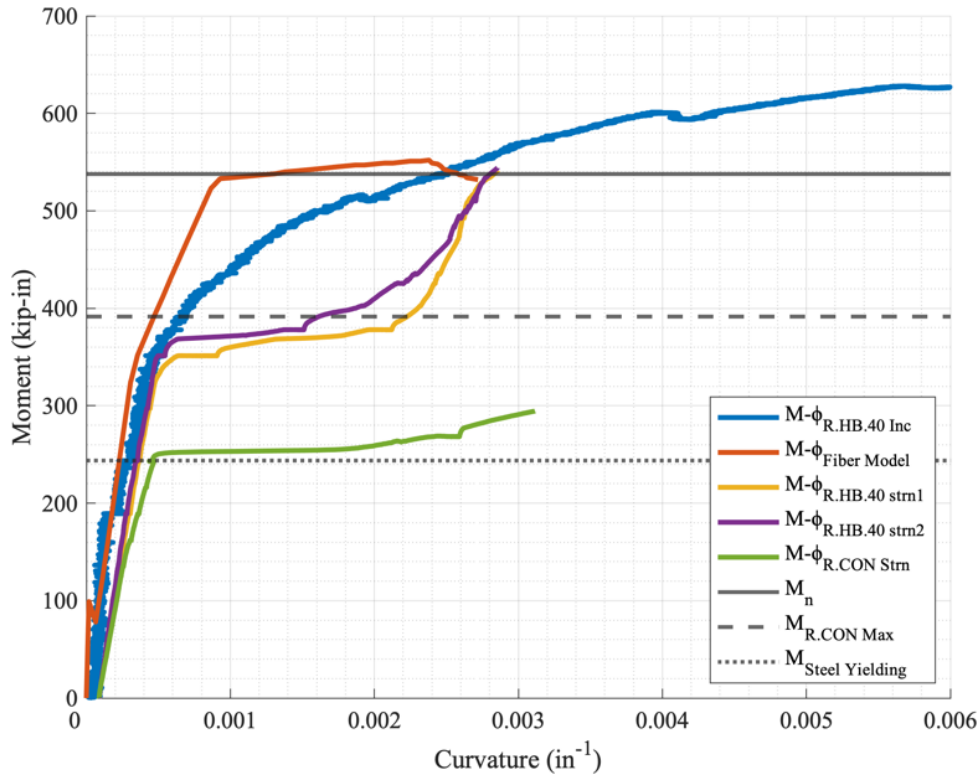
Figure 8.29-- R.HB.40 Moment versus Curvature Response with Shorter Axis Limit

8.2.5 R.HB.60

This specimen was strengthened with a 60-inch-long hooked-bonded TiAB (length measured
from outside-to-outside of the hooks). The specimen was pre-cracked as explained in Section 7.1
(initial loading cracks marked with red). The complete load versus displacement graph is shown
in Figure 8.30, and the pictures corresponding to the points on the plot are provided in Figure
8.31. As the applied load increased, pre-cracks widened and propagated, and existing crack
extensions and new cracks were marked in black. An almost linear response was observed up to
an applied force of about 13 kips, where nonlinearity in the load-displacement behavior became
more visible beyond this force level. Similar to the earlier specimens, flexural cracks were
observed at almost constant spacing between the cracks until the yielding of the steel rebars.

The flexural crack in the central region of the beam widened to 0.06 inches at 21 kips from 0.012 inches at 13 kips and propagated towards the load point. The peak load occurred at 24.2 kips at a mid-span deflection of 2.54 inches. Local concrete crushing was also observed under the load point in the post steel-yielding response. The load plateaued around 24 kips with increasing midspan displacement until the TiAB ruptured in the central portion of the beam at 23.6 kips and 4.65 inches of midspan displacement. The TiAB rupture occurred in a sudden manner.

The strength observed for the test was significantly larger than the control specimen (24.2 versus 14.5 kips) and exceeded the calculated strength that corresponding to the TiAB and steel rebar yielding (24.2 versus 19.8 kips). Based on the failure definition of 5% force drop from the peak load, the specimen had a failure load of 23.6 kips at 4.65 inches of mid-span displacement. The observed failure mode was classified as TiAB rupture, as Figure 8.32 illustrates the bar rupture occurred near the midspan.

The strains measured in the steel reinforcing bars and TiAB are presented in Figure 8.33. T2 and C1 malfunctioned for unknown reasons and did not report values for the R.HB.60 test. The bottom reinforcing bar strain was offset from the origin as it initiated from the residual strain that resulted from the pre-cracking load cycle. The bottom reinforcing rebars exceeded the steel yield strain of 2345 $\mu\varepsilon$ at 7.3 kips at the mid-span section. The bottom reinforcement strain (T1) exhibited a yield plateau response at around 13 kips. The difference between the initiation of rebar yielding and the yield plateau response is credited to the formation of the plastic hinge. Several of the strain gauges on the TiAB malfunctioned prior to the test, and the ones that functioned during the test (C, R1, R2, R3, R4, R5, P1, P2, P3, P4, and P5) recorded values until

just under the excepted TiAB yield strain of 8450 $\mu\varepsilon$. The epoxy cracking was credited as the reason for TiAB strain gauges malfunctioning as explained in Section 6.2.

The moment-curvature responses obtained from the strain and beam rotation measurements are provided in Figure 8.34 and with an abbreviated x-axis in Figure 8.35. The strain-based moment-curvature response could not be captured because the two working strain gauges were on opposite sides of the beam. The rotation-based moment-curvature response was obtained by calculating the average curvature using the rotation measurements at 4 inches from the midspan on either side (8-inch central region) as mentioned in Section 6.2. The moment-curvature response indicates consistent behavior with the one obtained from the 2D fiber model (M-$\phi_{\text{Fiber Model}}$) up to a mid-span moment of 400 kip-in. The response deviated from the 2D fiber model response around the peak moment level of control specimen capacity and indicated a gradually reducing slope (stiffness) until the peak moment. The gradually reducing stiffness is credited to the cracking occurring in the epoxy that might have caused slip of the TiAB. The peak moment of 653 kip-in was achieved at 0.01 in^{-1} of curvature and the maximum curvature was recorded to be beyond 0.02 in^{-1}. The curve indicates a ductile response by sustaining the high force at large deformations, and also large energy dissipation under the curve.
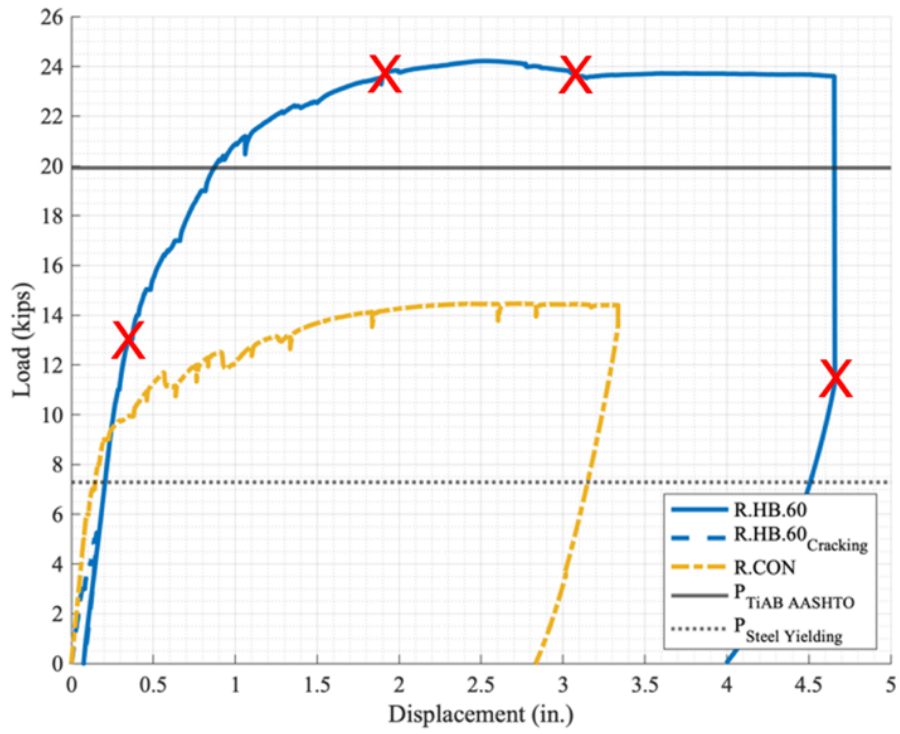
Figure 8.30–- R.HB.60 Load versus Displacement Response

13.0 kips
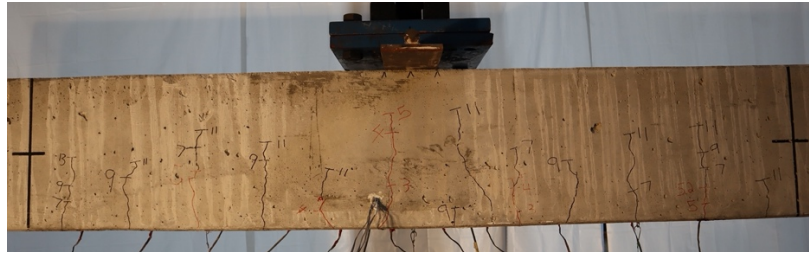
23.8 kips

23.7 kips

11.4 kips

Figure 8.31–- R.HB.60 Progression
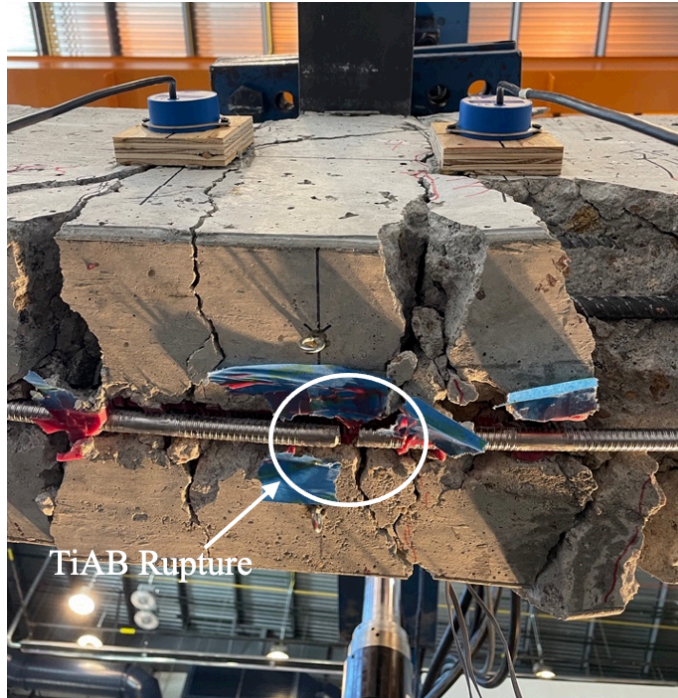
Figure 8.32–- R.HB.60 Post Failure
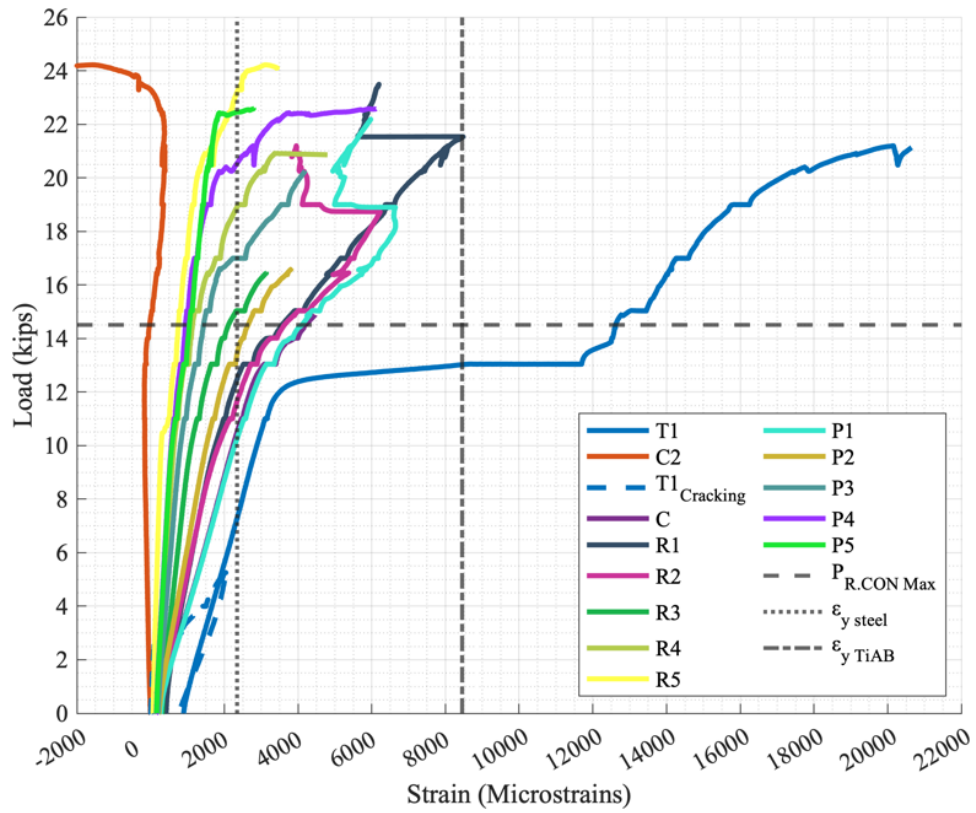
Figure 8.33 – R.HB.60 Load versus Strain Response
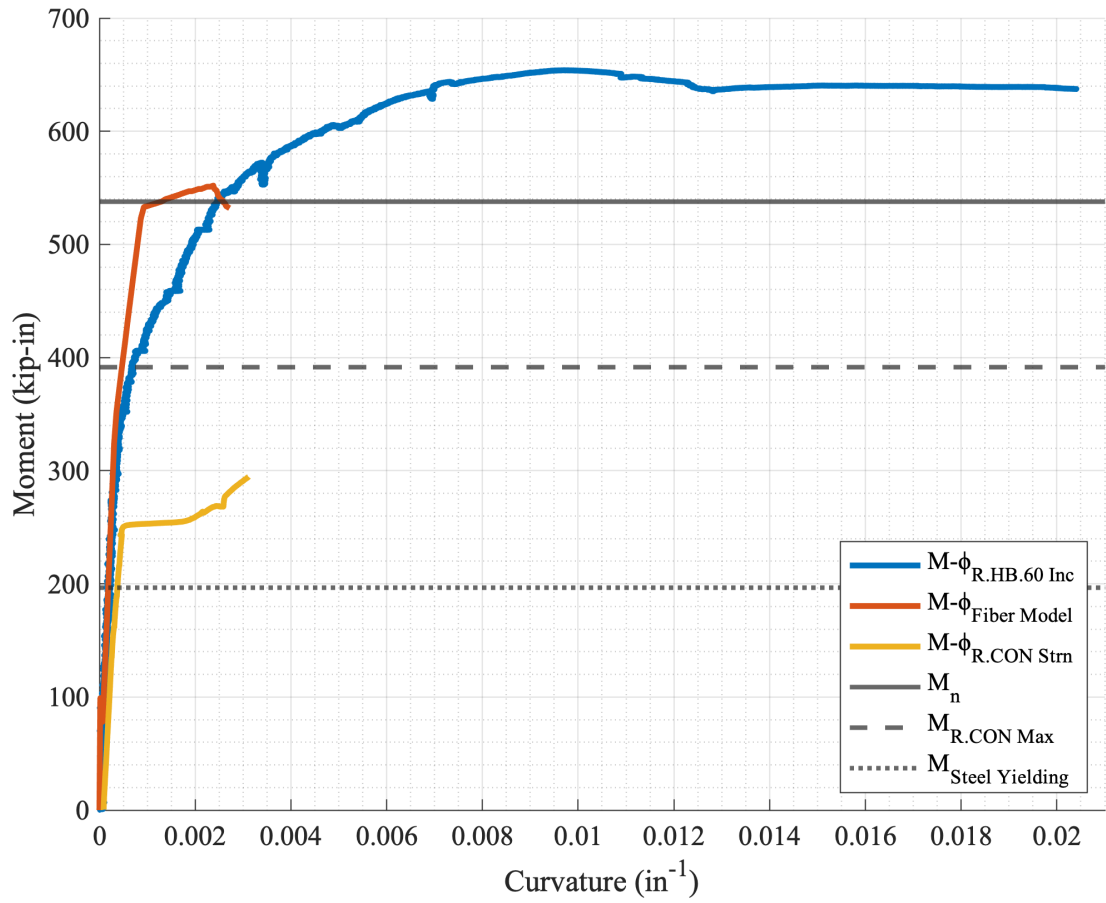
Figure 8.34 – R.HB.60 Moment versus Curvature Response
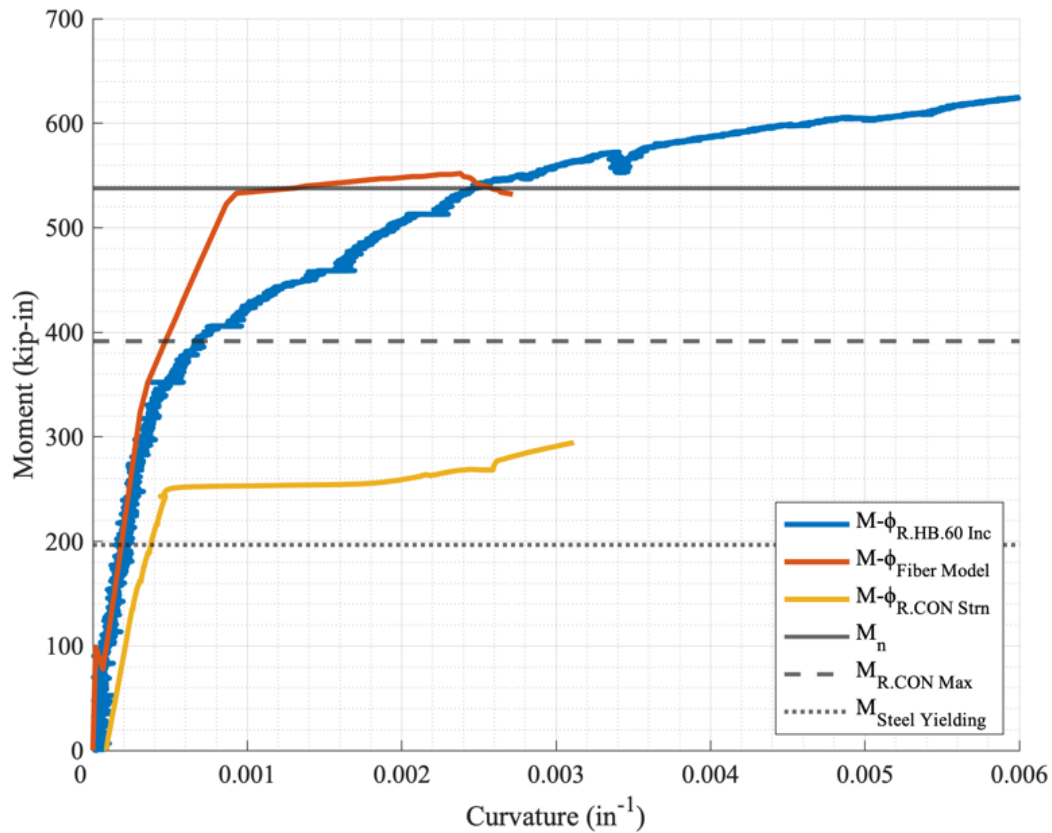
Figure 8.35–- R.HB.60 Moment versus Curvature Response with Shorter Axis Limit

8.3 Straight-Bonded Tests

This section discusses the experimental responses of the beams with straight-bonded NSM TiAB.

8.3.1 R.SB.30

This specimen was strengthened with a 30-inch straight-bonded TiAB. The specimen was pre-cracked as explained in Section 7.1 (initial loading cracks marked with red). The complete load versus displacement graph is shown in Figure 8.36, and the pictures corresponding to the points on the plot are provided in Figure 8.37. As the applied load increased, pre-cracks widened and propagated, and existing crack extensions and new cracks were marked in black. An almost linear response was observed up to an applied force of about 13 kips, where nonlinearity in the

load-displacement behavior became more visible beyond this force level. After the steel yielded, the actuator was in force-control and when the load exceeded the resistance capacity of the beam the actuator head pushed the R.SB.30 for its full stroke and ruptured the bottom steel abruptly. The peak load occurred at 14.8 kips and 0.47 inches of displacement before the large deformation was induced by the actuator head.

The strength observed for the test was negligibly higher than the control specimen (14.8 versus 14.5 kips) and considerably lower than the calculated strength that corresponding to the TiAB and steel rebar yielding (14.8 versus 19.8 kips). The specimen had a failure load of 14.8 kips at 0.47 inches of mid-span displacement. The observed failure mode was unclear due to not switching to a slower load rate (displacement-controlled loading) before the specimen failure, but the crack curving in from the outside of the TiAB as seen in Figure 8.38 suggest that the failure mode could have been debonding of the bar ends.

The strains measured in the steel reinforcing bars and TiAB are presented in Figure 8.39. The bottom reinforcing bar strains were offset from the origin as they initiated from the residual strain that resulted from the pre-cracking load cycle. The bottom reinforcing rebars exceeded the steel yield strain of 2345 microstrain ($\mu\varepsilon$) at 8.9 kips at the mid-span section. The bottom reinforcement strains (T1 and T2) exhibited a yield plateau response at around 13 kips. The difference between the initiation of rebar yielding and the yield plateau response is credited to the formation of the plastic hinge at the midspan and the load increase necessary to extend the yielding portion. Several of the strain gauges on the TiAB malfunctioned prior to the test, and the ones that functioned during the test (R1, R2, R3, and P1) reached values of about 4000 $\mu\varepsilon$ before the beam failed, and not reaching to the TiAB yield strain of 8450 $\mu\varepsilon$.

The moment-curvature responses obtained from the strain and beam rotation measurements are provided in Figure 8.40 and with an abbreviated x-axis in Figure 8.41. The moment-curvature response indicates consistent behavior with the one obtained from the 2D fiber model (M-$\phi_{Fiber\ Model}$) up to a mid-span moment of 400 kip-in at which point the failure occurred. The peak moment of 400 kip-in was achieved at 0.001 in^{-1} of curvature. The curve indicates that the beam's maximum capacity was nearly identical to the control specimen.
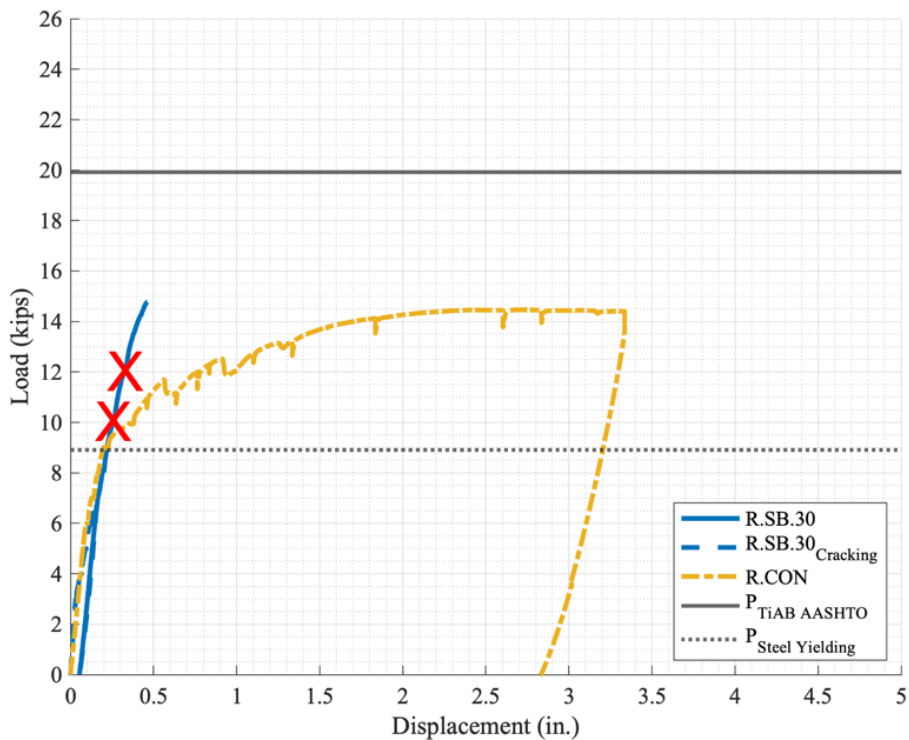
Figure 8.36–- R.SB.30 Load versus Displacement Response

10.0 kips

12.0 kips

Figure 8.37–- R.SB.30 Progression

Figure 8.38–- R.SB.30 Post-Test
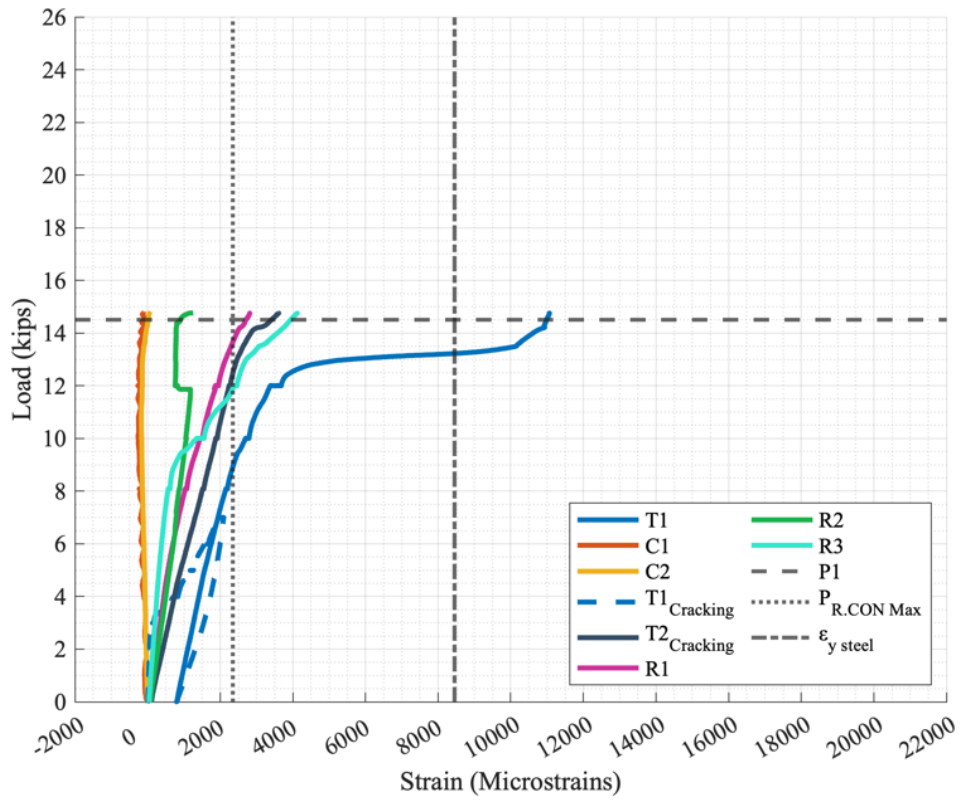
Figure 8.39 – R.SB.30 Load Strain Response
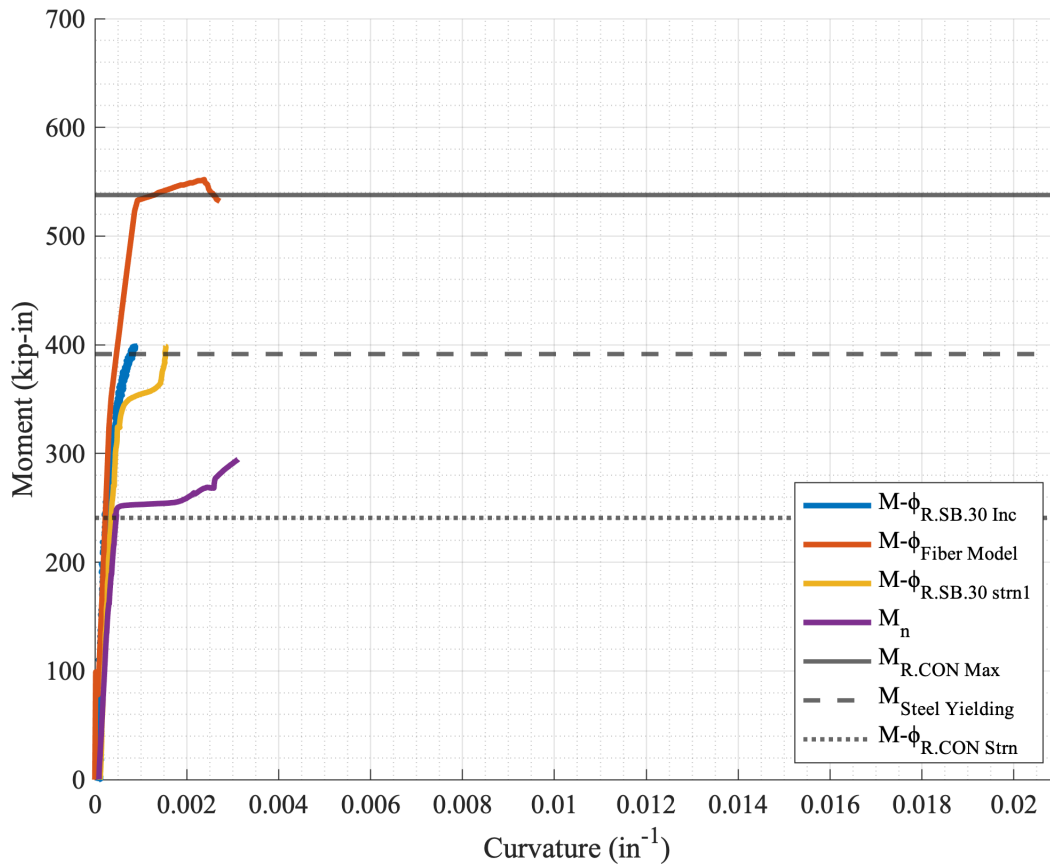
Figure 8.40 – R.SB.30 Moment versus Curvature Response
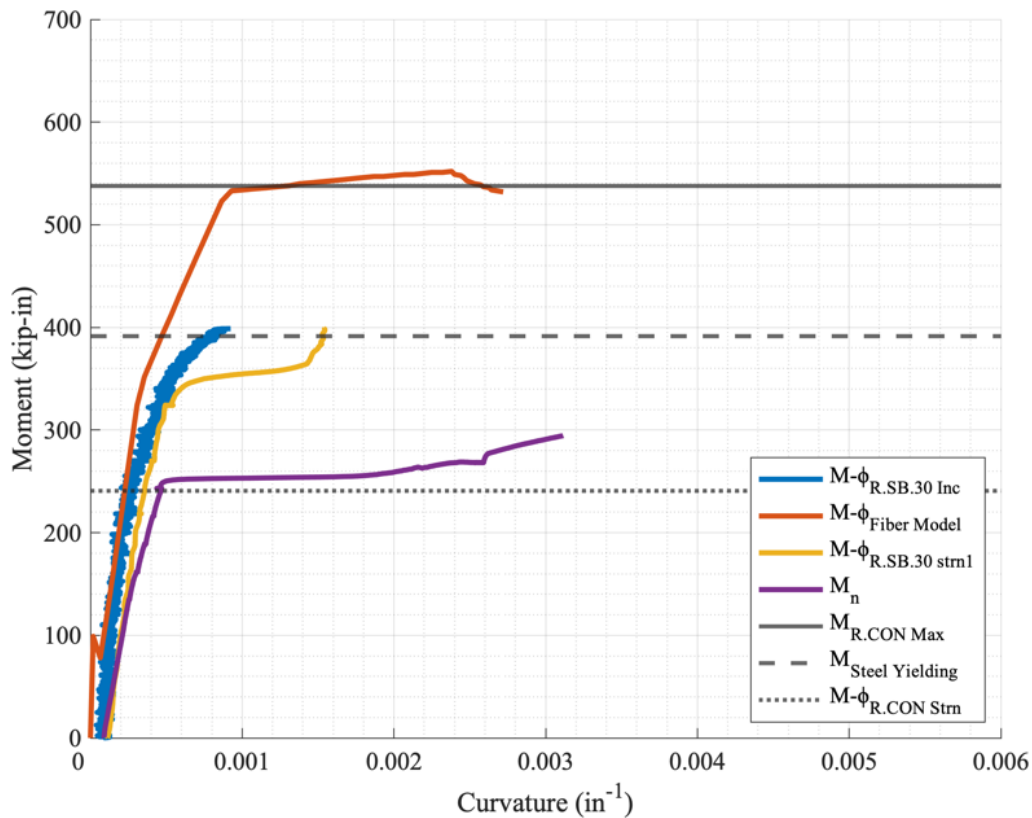
Figure 8.41— R.SB.30 Moment versus Curvature Response with Shorter Axis Limit

8.3.2 R.SB.40

This specimen was strengthened with a 40-inch straight-bonded TiAB. The specimen was pre-cracked as explained in Section 7.1 (initial loading cracks marked with red). The complete load versus displacement graph is shown in Figure 8.42, and the pictures corresponding to the points on the plot are provided in Figure 8.43. As the applied load increased, pre-cracks widened and propagated, and existing crack extensions and new cracks were marked in black. An almost linear response was observed up to an applied force of about 13 kips, where nonlinearity in the load-displacement behavior became more visible beyond this force level. Similar to the earlier specimens, flexural cracks were observed at almost constant spacing between the cracks until the yielding of the steel rebars.

At 14 kips the cracks were 0.02 inches wide, and the cracks continued to represent flexural behavior. The peak load occurred at 18.3 kips at a mid-span deflection of 0.67 inches. A diagonal crack formed in the left-central portion of the beam and the load dropped suddenly to 11 kips where the beam was then unloaded.

The strength observed for the test was larger than the control specimen (18.3 versus 14.5 kips) but lower than the calculated strength that corresponding to the TiAB and steel rebar yielding (18.3 versus 19.8 kips). Based on the failure definition of 5% force drop from the peak load, the specimen had a failure load of 17.4 kips at 0.68 inches of mid-span displacement. The observed failure mode was classified as CDC debonding, as Figure 8.44 illustrates a wide diagonal crack that extended to the end of the groove.

The strains measured in the steel reinforcing bars and TiAb are presented in Figure 8.45. The bottom reinforcing bar strains were offset from the origin as they initiated from the residual strain that resulted from the pre-cracking load cycle. The bottom reinforcing rebars exceeded the steel yield strain of 2345 microstrain ($\mu\varepsilon$) at 9.6 kips at the mid-span section. The bottom reinforcement strain T1 malfunctioned at 3000 $\mu\varepsilon$ and T2 exhibited a yield plateau response at around 17 kips. The difference between the initiation of rebar yielding and the yield plateau response is credited to the formation of the plastic hinge at the midspan and the load increase necessary to extend the yielding portion. Several of the strain gauges on the TiAB malfunctioned prior to the test, and the ones that functioned during the test (C, R1, and P2) recorded values until about 6000 $\mu\varepsilon$ before the beam failed, shy of the 8450 $\mu\varepsilon$ TiAB yield strain. The epoxy cracking was credited as the reason for TiAB strain gauges malfunctioning as explained in Section 6.2.

The moment-curvature responses obtained from the strain and beam rotation measurements are provided in Figure 8.46 and with an abbreviated x-axis in Figure 8.47. The

moment-curvature response indicates consistent behavior with the one obtained from the 2D

fiber model (M-$\phi_{\text{Fiber Model}}$) until the failure prior to reaching 500 kip-in. The peak moment of 494

kip-in was achieved at 0.001 in^{-1}. The curve indicates that the beam failed in a sudden manner

with a brittle response.
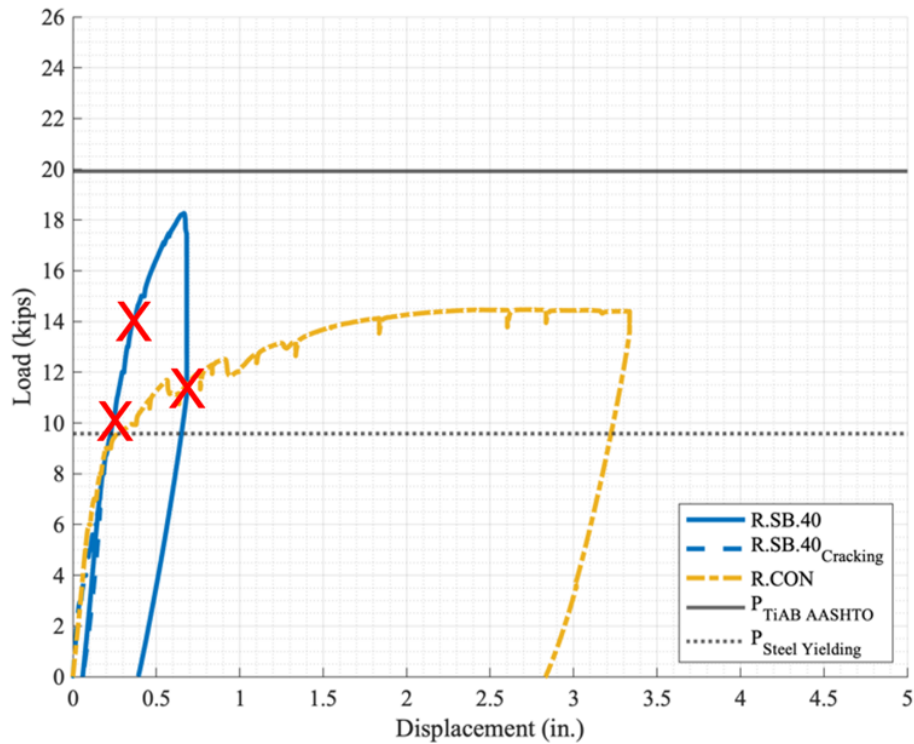
Figure 8.42–- R.SB.40 Load versus Displacement Response
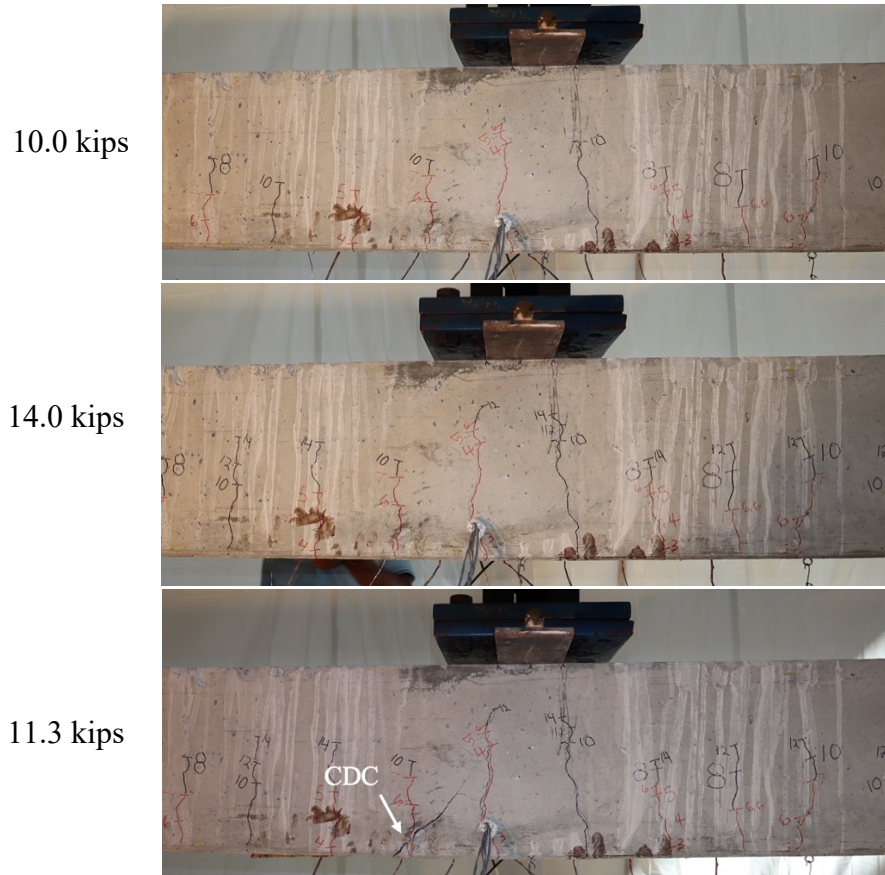
Figure 8.43–- R.SB.40 Progression
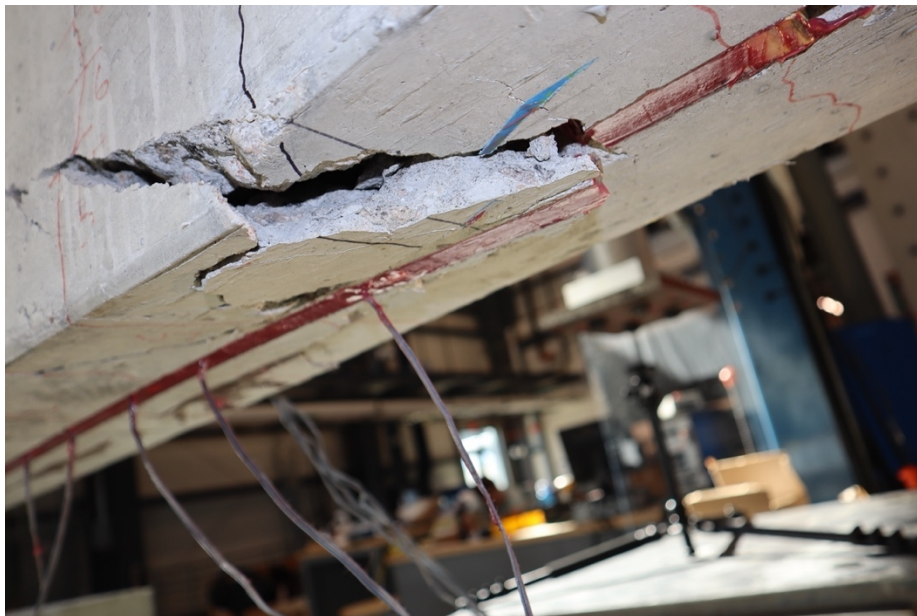
Figure 8.44–- R.SB.40 Post-Test

138
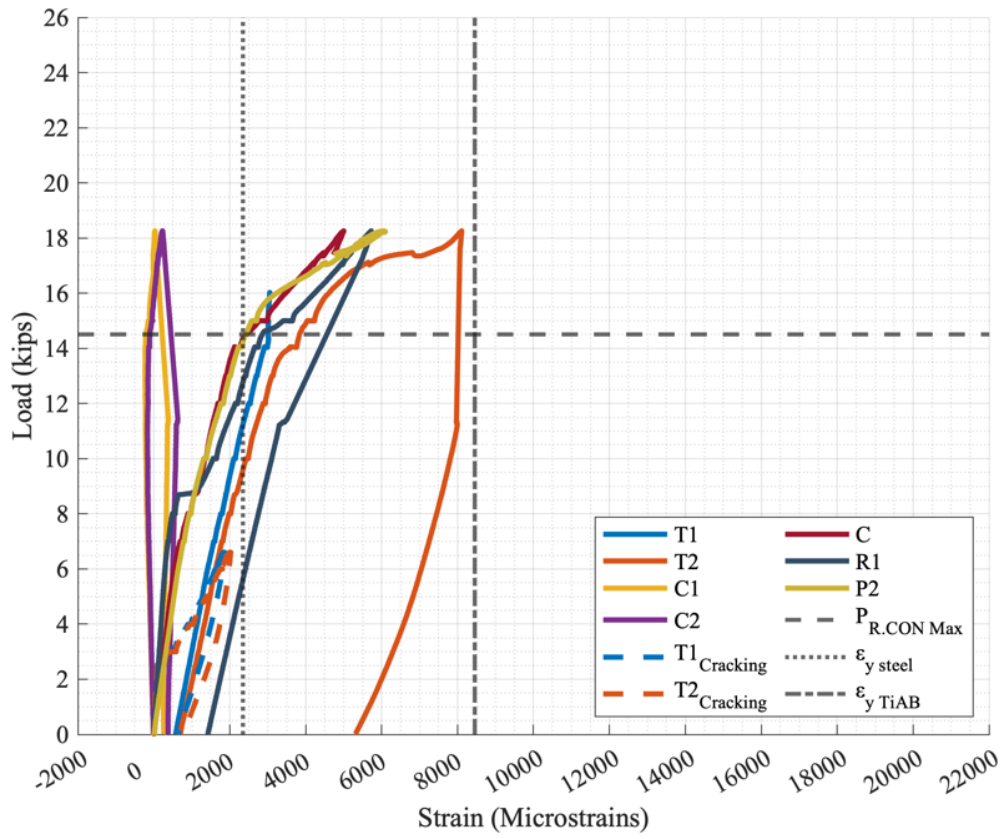
Figure 8.45 – R.SB.40 Load versus Strain Response
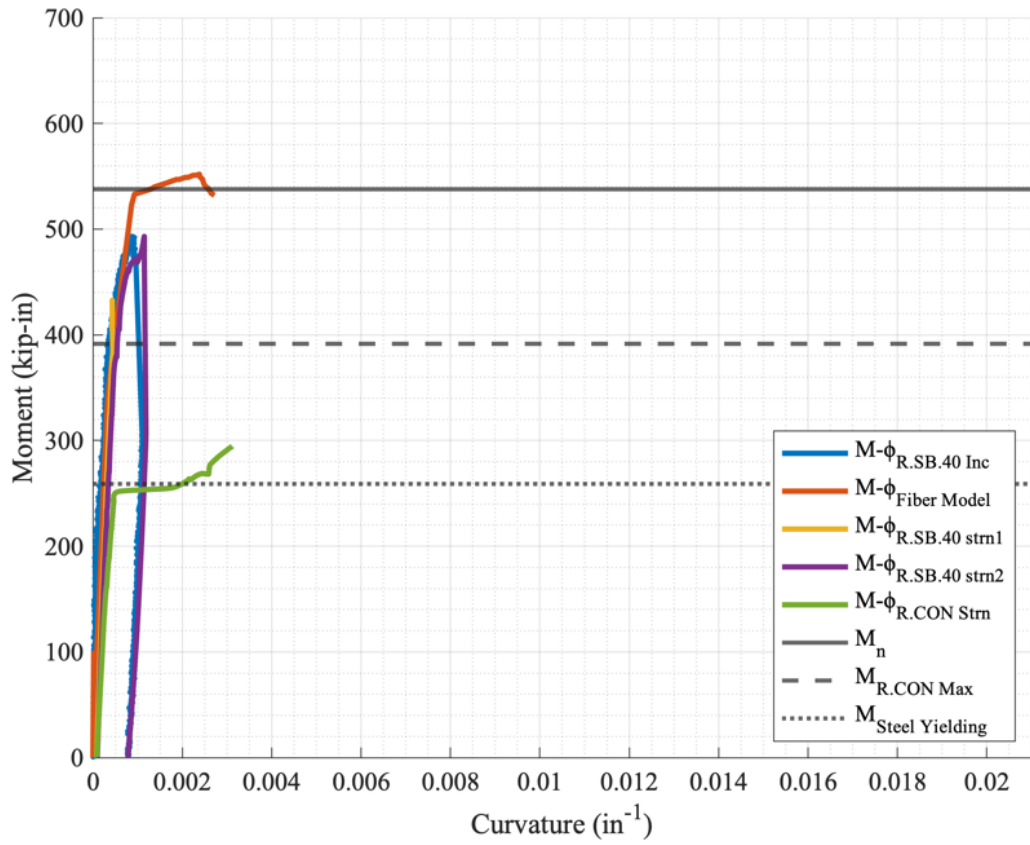
Figure 8.46 – R.SB.40 Moment versus Curvature Response
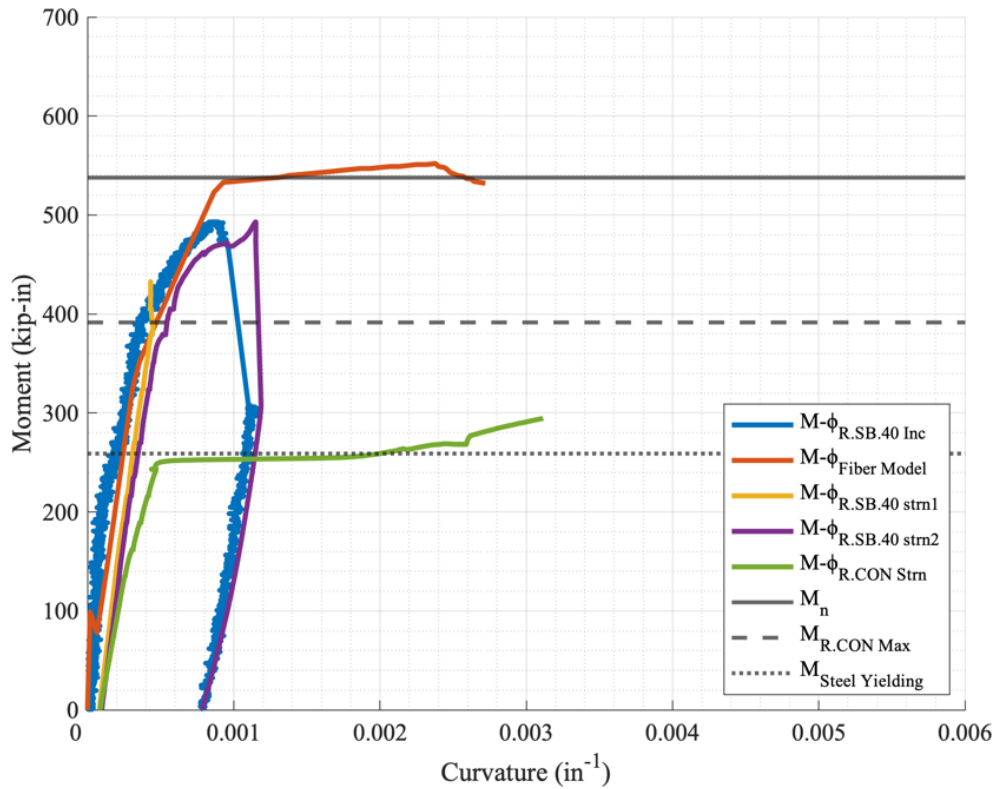
Figure 8.47— R.SB.40 Moment versus Curvature Response with Shorter Axis Limit

8.3.4 R.SB.60

This specimen was strengthened with a 60-inch straight-bonded TiAB. The specimen was pre-cracked as explained in Section 7.1 (initial loading cracks marked with red). The complete load versus displacement graph is shown Figure 8.48, and the pictures corresponding to the points on the plot are provided Figure 8.49. As the applied load increased, pre-cracks widened and propagated, and existing crack extensions and new cracks were marked in black. An almost linear response was observed up to an applied force of about 13 kips, where nonlinearity in the load-displacement behavior became more visible beyond this force level.

The cracks propagated towards the load point, the widest being 0.05 inches in width at 20 kips. The peak load occurred at 22.8 kips at a mid-span deflection of 1.33 inches which is when the epoxy in the central portion of the beam fractured in a sudden manner.

The strength observed for the test was significantly larger than the control specimen (22.8 versus 14.5 kips) and exceeded the calculated strength that corresponding to the TiAB and steel rebar yielding (22.8 versus 19.8 kips). Based on the failure definition of 5% force drop from the peak load, the specimen had a failure load of 22.7 kips at 1.33 inches of mid-span displacement. The observed failure mode was classified as epoxy rupture, as Figure 8.50 illustrates fractured pieces of epoxy and no rupture of the TiAB.

The strains measured in the steel reinforcing bars and TiAB are presented in Figure 8.51. The bottom reinforcing bar strains were offset from the origin as they initiated from the residual strain that resulted from the pre-cracking load cycle. The bottom reinforcing rebars exceeded the steel yield strain of 2345 microstrain ($\mu\varepsilon$) at 9.8 kips at the mid-span section. The bottom reinforcement strains (T1 and T2) exhibited a yield plateau response at around 13 kips. The difference between the initiation of rebar yielding and the yield plateau response is credited to the formation of the plastic hinge. Several of the strain gauges on the TiAB malfunctioned prior to the test, and the ones that functioned during the test (P1 and P5) recorded values until about 4500 $\mu\varepsilon$, which could not capture the yielding of the TiAB that was expected to occur around 8450 $\mu\varepsilon$. The epoxy cracking was credited as the reason for TiAB strain gauges malfunctioning as explained in Section 6.2.

The moment-curvature responses obtained from the strain and beam rotation measurements are provided in Figure 8.52 and with an abbreviated x-axis in Figure 8.53. The moment-curvature response indicates consistent behavior with the one obtained from the 2D fiber model (M-$\phi_{Fiber\ Model}$) up to a mid-span moment of 400 kip-in. The response deviated from the 2D fiber model response and indicated a gradually reducing slope (stiffness) and then a second softening before the peak moment. The gradually reducing stiffness is credited to the

cracking occurring in the epoxy that might have caused slip of the TiAB and the further softened, potentially due to the TiAB yielding. The peak moment of 616 kip-in was achieved at 0.0035 in^{-1} of curvature. The curve indicates a ductile response by sustaining the high force at large deformations, and also large energy dissipation under the curve.
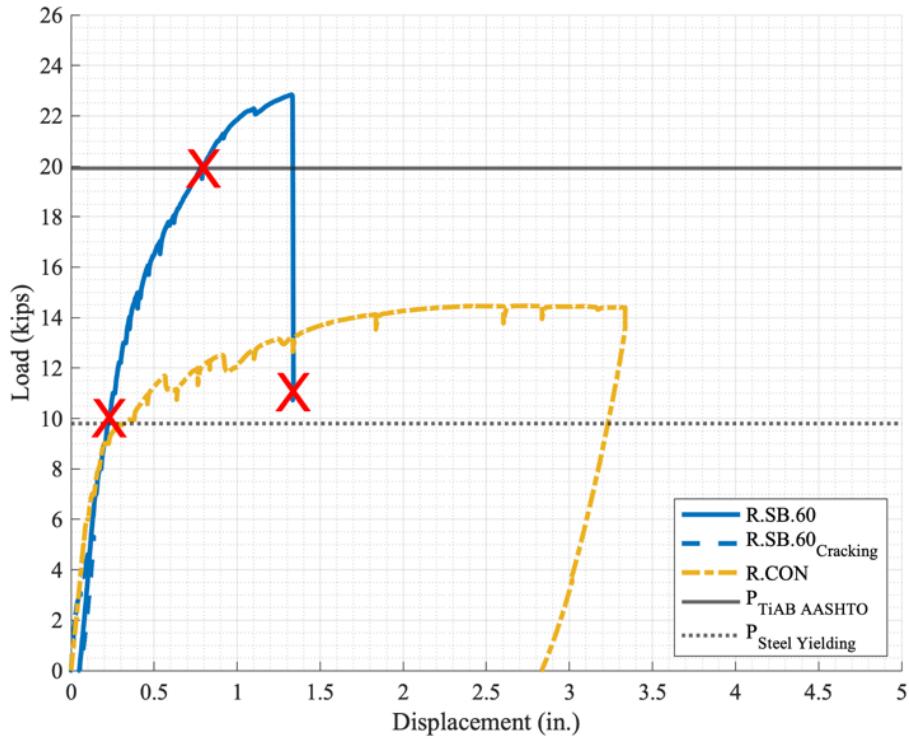
Figure 8.48–- R.SB.60 Load versus Displacement Response

10.0 kips

20.0 kips

11.0 kips

Figure 8.49–- R.SB.60 Progression

Figure 8.50–- R.SB.60 Post-Test
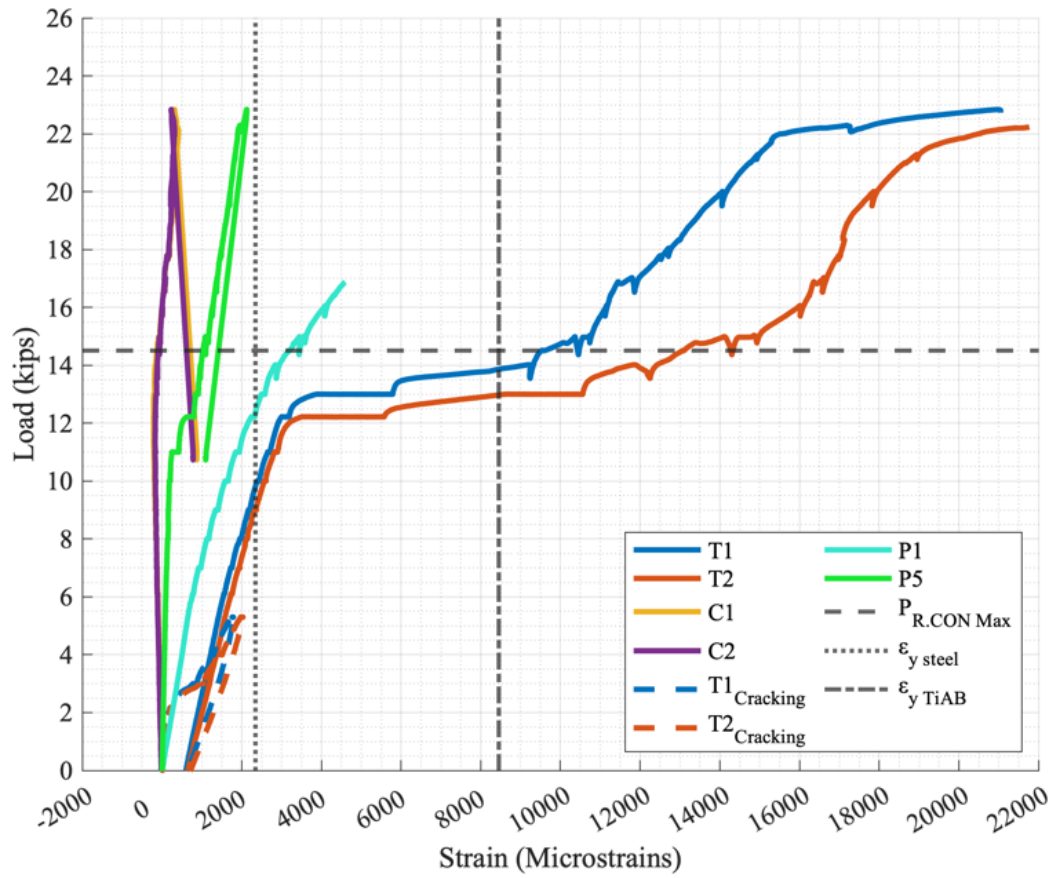
Figure 8.51 – R.SB.60 Load versus Strain Response
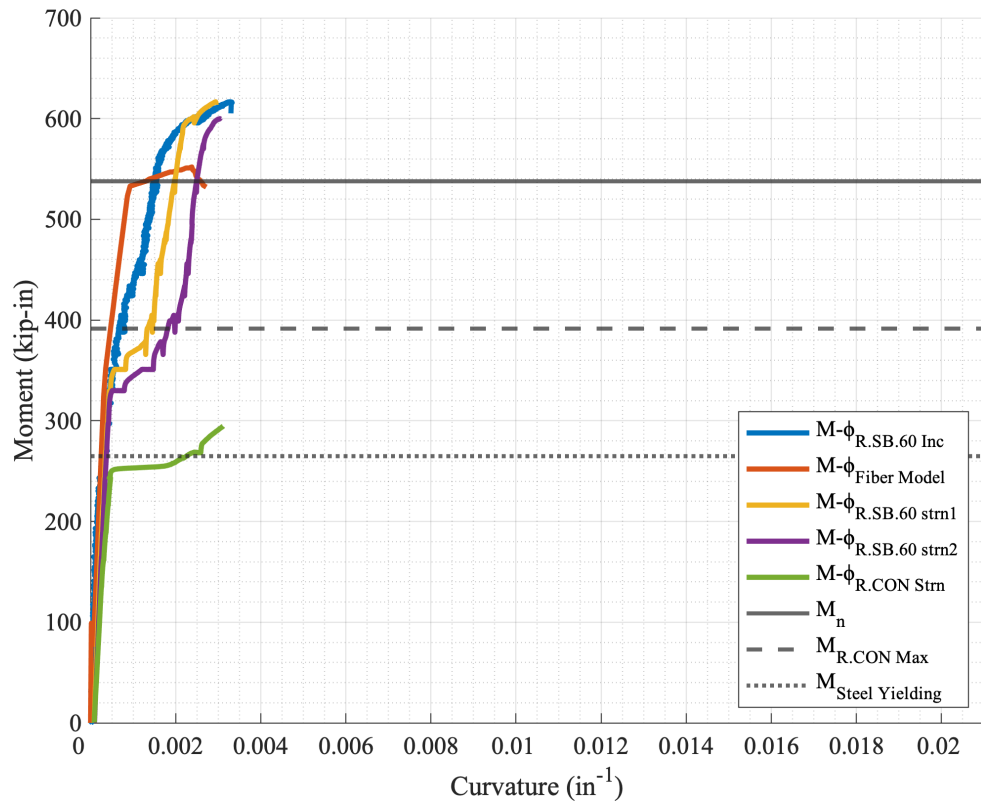
Figure 8.52 – R.SB.60 Moment versus Curvature Response
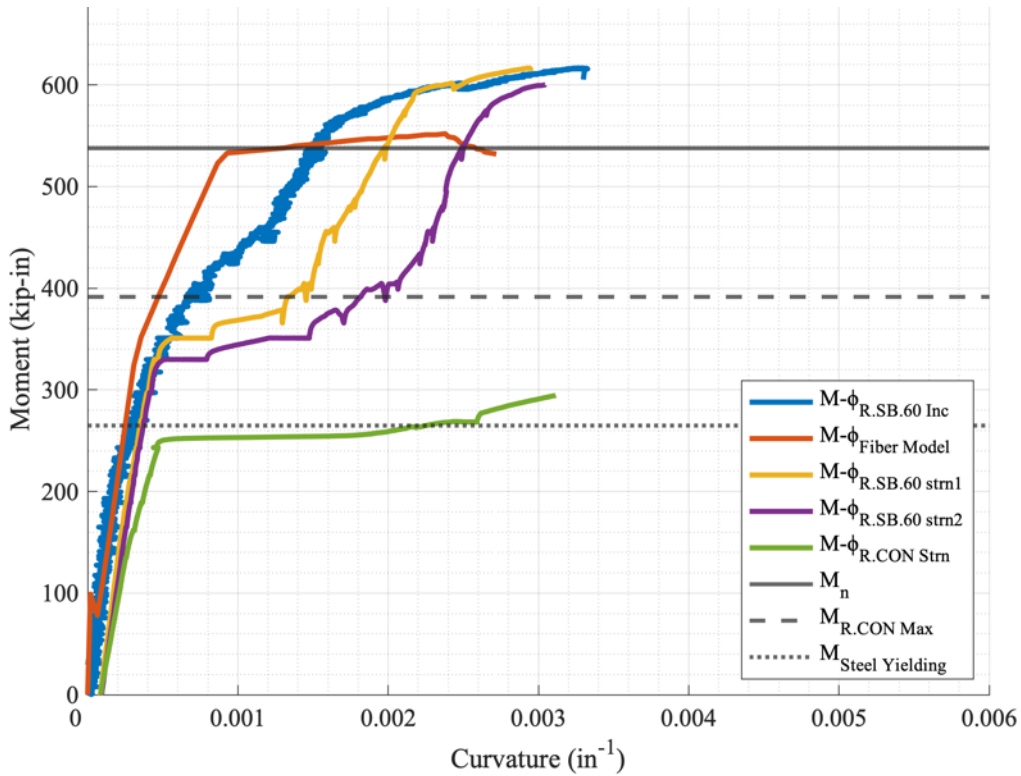
Figure 8.53— R.SB.60 Moment versus Curvature Response with Shorter Axis Limit

8.3.5 R.SB.80

This specimen was strengthened with an 80-inch straight-bonded TiAB. The specimen was pre-cracked as explained in Section 7.1 (initial loading cracks marked with red). The complete load versus displacement graph is shown in Figure 8.54 and the pictures corresponding to the points on the plot are provided in Figure 8.55. As the applied load increased, pre-cracks widened and propagated, and existing crack extensions and new cracks were marked in black. An almost linear response was observed up to an applied force of about 13 kips, where nonlinearity in the load-displacement behavior became more visible beyond this force level.

Two major cracks on either side of the load point widened excessively for loads beyond the steel rebar yielding. A diagonal crack was observed on the left side of the beam and local concrete crushing was observed under the load point in the post steel-yielding response. The

147

peak load occurred at 24.1 kips at a mid-span deflection of 2.31 inches. The load plateaued around 24 kips with increasing midspan displacement until the TiAB ruptured at 23.4 kips and 3.11 inches of displacement. The rupture occurred in a sudden manner.

The strength observed for the test was significantly larger than the control specimen (24.1 versus 14.5 kips) and exceeded the calculated strength that corresponded to the TiAB and steel rebar yielding (24.1 versus 19.8 kips). Based on the failure definition of 5% force drop from the peak load, the specimen had a failure load of 23.4 kips at 3.11 inches of mid-span displacement. The observed failure mode was classified as TiAB rupture, as Figure 8.56 illustrates the bar rupture occurred near the midspan.

The strains measured in the steel reinforcing bars and TiAB are presented in Figure 8.57. The bottom reinforcing bar strains were offset from the origin as they initiated from the residual strain that resulted from the pre-cracking load cycle. The bottom reinforcing rebars exceeded the steel yield strain of 2345 microstrain ($\mu\varepsilon$) at 8.8 kips at the mid-span section. The bottom reinforcement strains (T1 and T2) exhibited a yield plateau response at around 13 kips. The difference between the initiation of rebar yielding and the yield plateau response is credited to the formation of the plastic hinge. Several of the strain gauges on the TiAB malfunctioned prior to the test, and the ones that functioned during the test (R1, R2, R3, R4, R5, R6, P1, P2, P3, P5, P6) recorded values until about 6000 $\mu\varepsilon$, which could not capture the yielding of the TiAB that was expected to occur around 8450 $\mu\varepsilon$. The epoxy cracking was credited as the reason for TiAB strain gauges malfunctioning as explained in Section 6.2.

The moment-curvature responses obtained from the strain and beam rotation measurements are provided in Figure 8.58 and with an abbreviated x-axis in Figure 8.59. The moment-curvature response indicates consistent behavior with the one obtained from the 2D

fiber model (M-$\phi_{\text{Fiber Model}}$) up to a mid-span moment of 400 kip-in. The response deviated from the 2D fiber model response and indicated a gradually reducing slope (stiffness) until the peak moment. The gradually reducing stiffness is credited to the cracking occurring in the epoxy that might have caused slip of the TiAB. The peak moment of 650 kip-in was achieved at 0.008 in^{-1} of curvature and the maximum curvature was recorded to be beyond 0.01 in^{-1}. The moment-curvature response indicated a ductile response by sustaining the high force at large deformations, and also large energy dissipation under the curve.
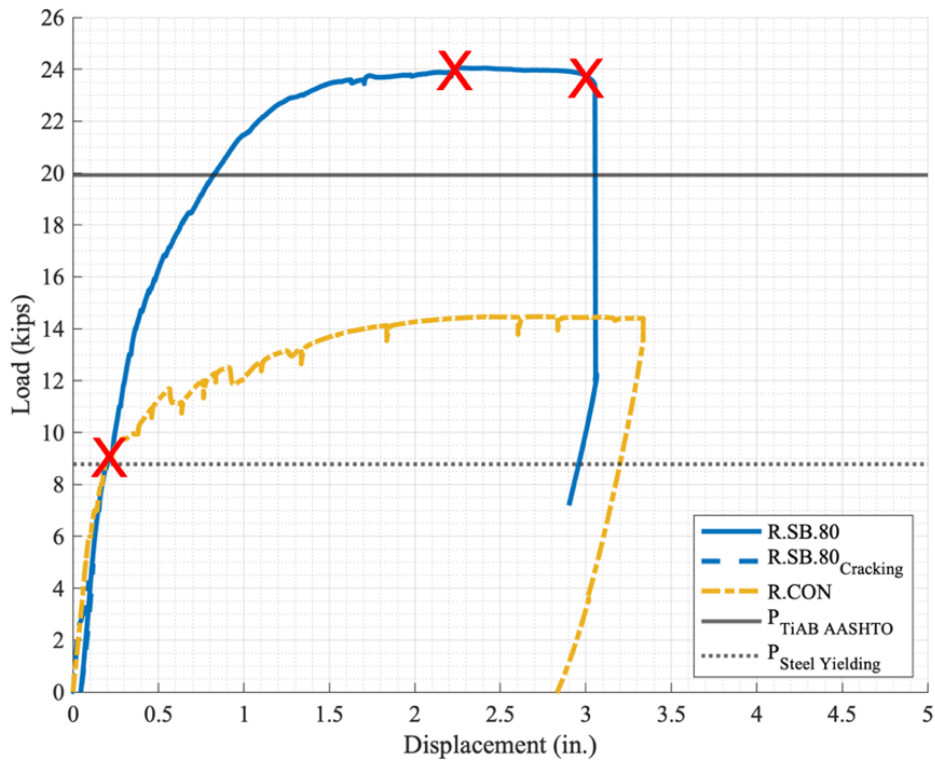
Figure 8.54–- R.SB.80 Load versus Displacement Response

9.0 kips

24.0 kips

23.9 kips
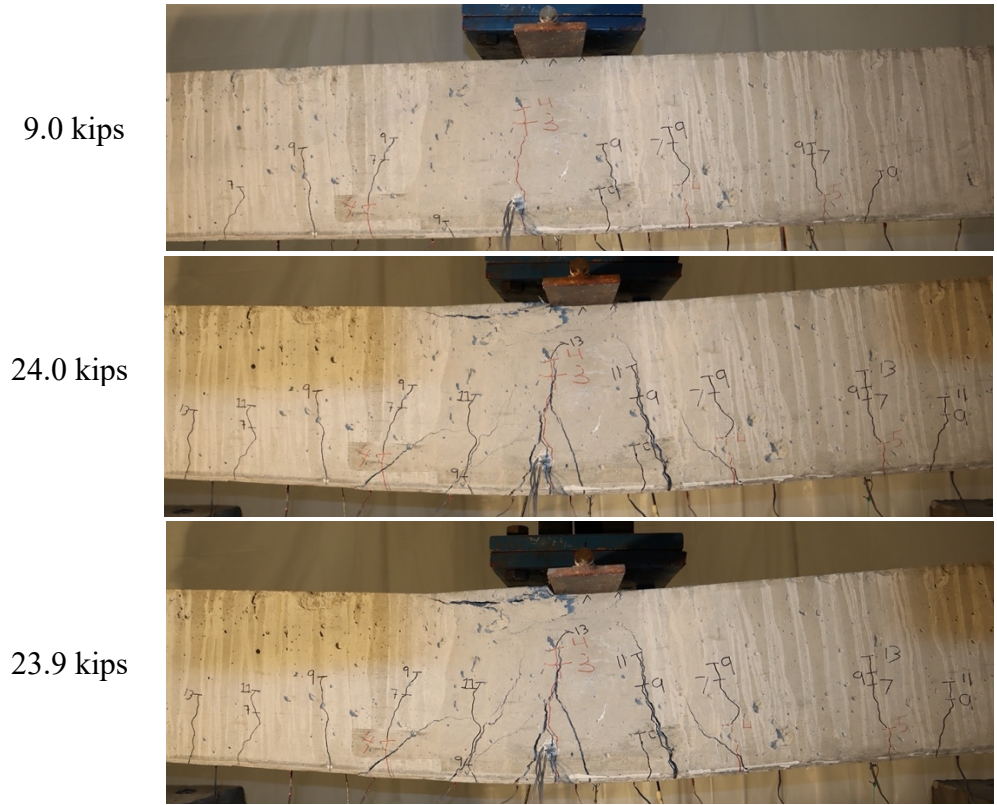
Figure 8.55–- R.SB.80 Progression

TiAB Rupture
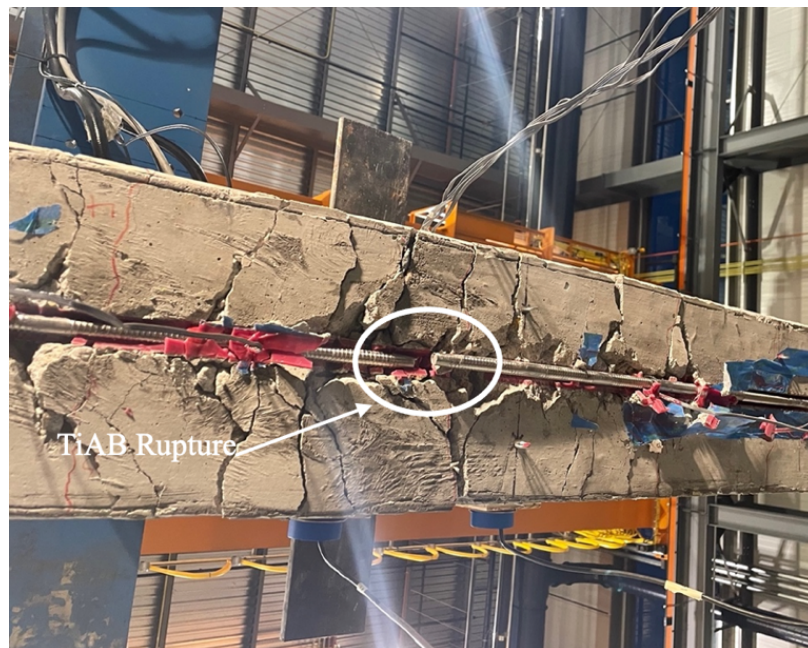
Figure 8.56–- R.SB.80 Post-Test
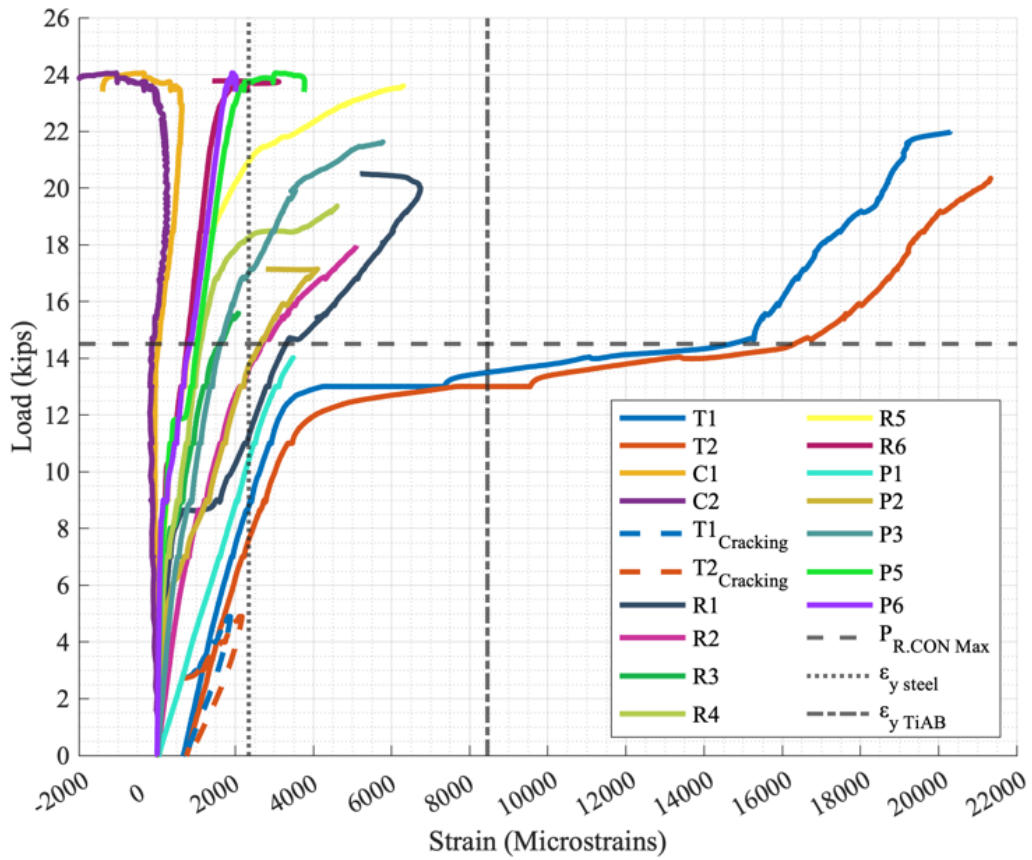
Figure 8.57 – R.SB.80 Load versus Strain Response
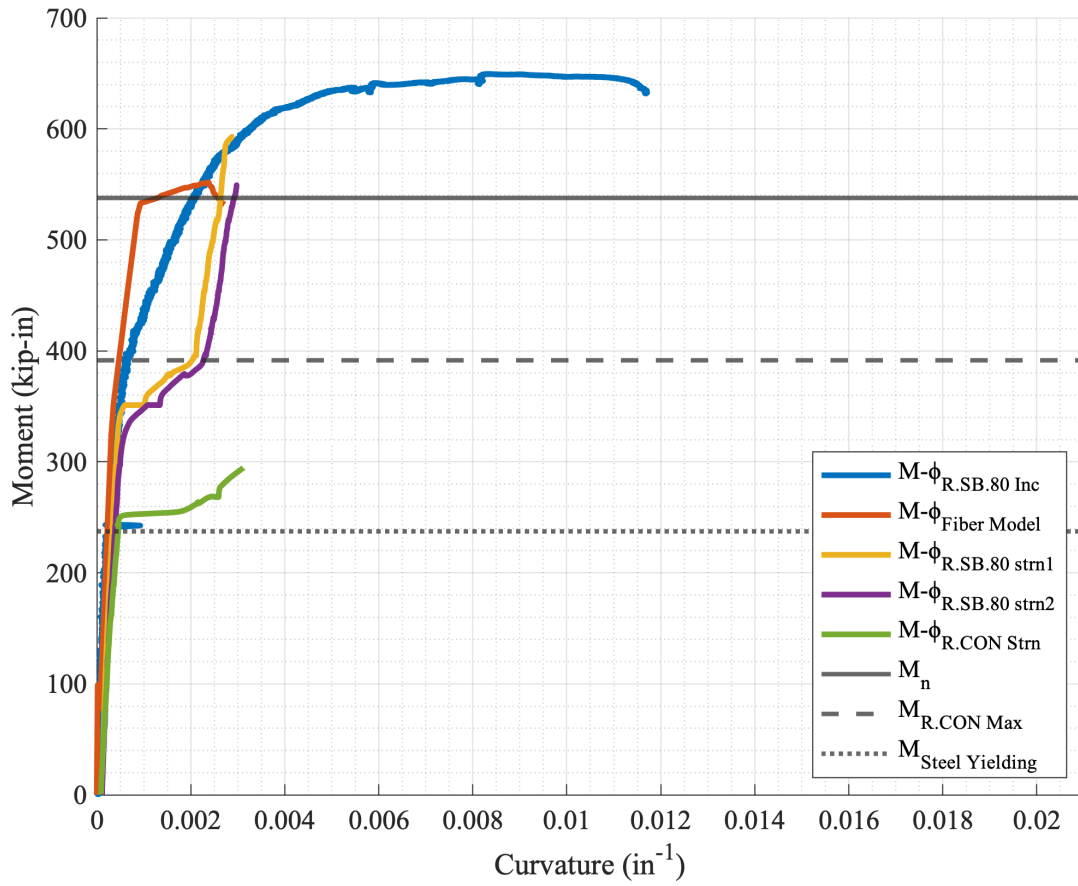
Figure 8.58 – R.SB.80 Moment versus Curvature Response
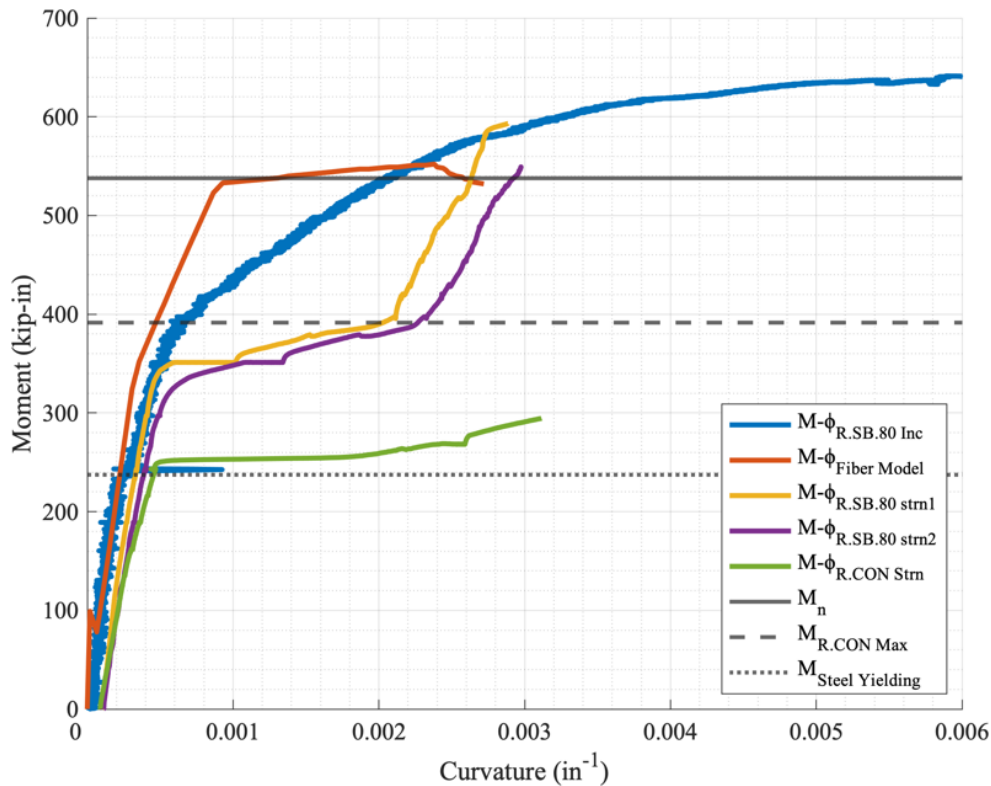
Figure 8.59—- R.SB.80 Moment versus Curvature Response with Shorter Axis Limit

8.3.6 R.SB.96

This specimen was strengthened with an 96-inch straight-bonded TiAB. The specimen was pre-cracked as explained in Section 7.1 (initial loading cracks marked with red). The complete load versus displacement graph is shown in Figure 8.60, and the pictures corresponding to the points on the plot are provided in Figure 8.61. As the applied load increased, pre-cracks widened and propagated, and existing crack extensions and new cracks were marked in black. An almost linear response was observed up to an applied force of about 13 kips, where nonlinearity in the load-displacement behavior became more visible beyond this force level.

Flexural cracks widened and propagated towards the load point and two diagonal cracks appeared on each side initiating from a flexural crack and propagated towards the center of the beam. The peak load occurred at 23.6 kips at a mid-span deflection of 1.86 inches. Signs of local

concrete crushing were visible at 23.6 kips. The load plateaued around the peak load with increasing midspan displacement. A horizontal crack traveled along the length of the beam starting on the left side. The central cracks severely widened in excess of 0.25 inches. The beams failure occurred whenever the horizontal crack curved to the end of the TiAB and separated it from the beam and the epoxy in the central area of the beam shattered simultaneously.

The strength observed for the test was significantly larger than the control specimen (23.6 versus 14.5 kips) and considerably larger than the calculated strength that corresponding to the TiAB and steel rebar yielding (23.6 versus 19.8 kips). Based on the failure definition of 5% force drop from the peak load, the specimen had a failure load of 23.4 kips at 4.65 inches of mid-span displacement. The observed failure mode was classified as both end debonding and epoxy rupture due to the seemingly simultaneous occurrence of the two. Figure 8.62 illustrates the epoxy fragments in the central portion of the beam as well as the end section that separated from the concrete beam.

The strains measured in the steel reinforcing bars and TiAB are presented in Figure 8.63. The bottom reinforcing bar strains were offset from the origin as they initiated from the residual strain that resulted from the pre-cracking load cycle. The bottom reinforcing rebars exceeded the steel yield strain of 2345 microstrain ($\mu\varepsilon$) at 9.4 kips at the mid-span section. The bottom reinforcement strains (T1 and T2) exhibited a yield plateau response at around 13 kips. The difference between the initiation of rebar yielding and the yield plateau response is credited to the formation of the plastic hinge. Several of the strain gauges on the TiAB malfunctioned prior to the test, and the ones that functioned during the test (C, R4, R5, R7, P2, P3, P4, and P6) recorded values until about 6000 $\mu\varepsilon$, which could not capture the yielding of the TiAB that was

expected to occur around 8450 $\mu\varepsilon$. The epoxy cracking was credited as the reason for TiAB strain gauges malfunctioning as explained in Section 6.2.

The moment-curvature responses obtained from the strain and beam rotation measurements are provided in Figure 8.64 and with an abbreviated x-axis in Figure 8.65. The moment-curvature response indicates consistent behavior with the one obtained from the 2D fiber model (M-$\phi_{Fiber\ Model}$) up to a mid-span moment of 400 kip-in. The response deviated from the 2D fiber model response and indicated a gradually reducing slope (stiffness) until the peak moment. The gradually reducing stiffness is credited to the cracking occurring in the epoxy and concrete that would cause slip between the concrete substrate and epoxy and the TiAB. The peak moment of 637 kip-in was achieved at 0.008 in^{-1} of curvature and the maximum curvature was recorded to be nearly 0.016 in^{-1}. The moment-curvature response indicated a ductile response with large energy dissipation under the curve.
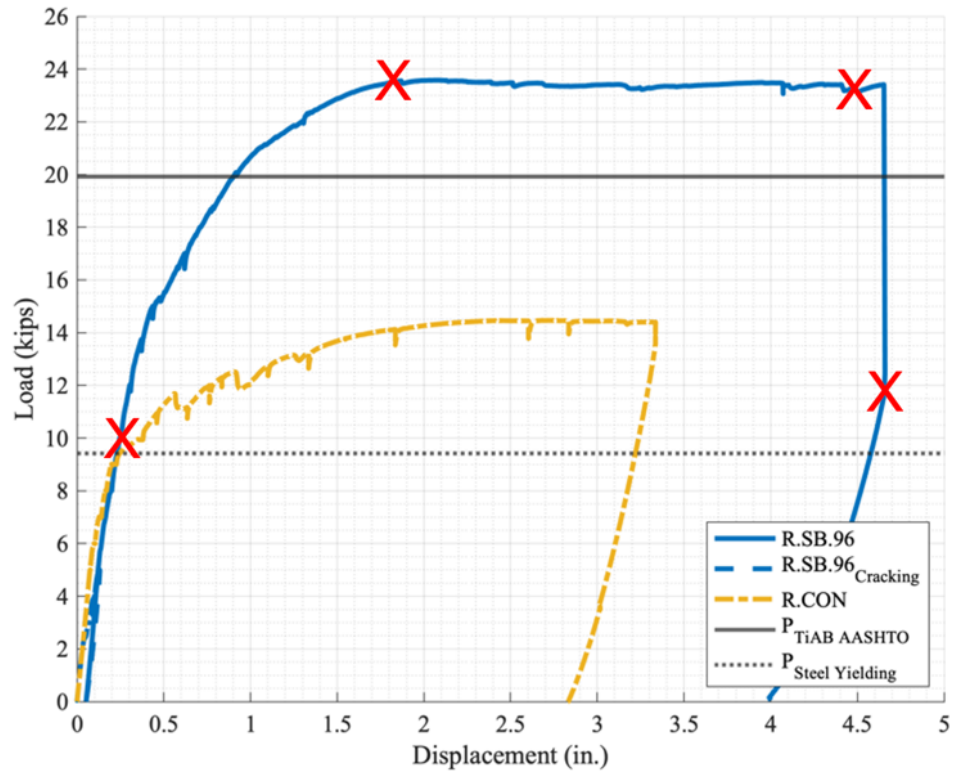
Figure 8.60 – R.SB.96 Load versus Displacement Response

10.0 kips

23.6 kips

23.2 kips

11.8 kips
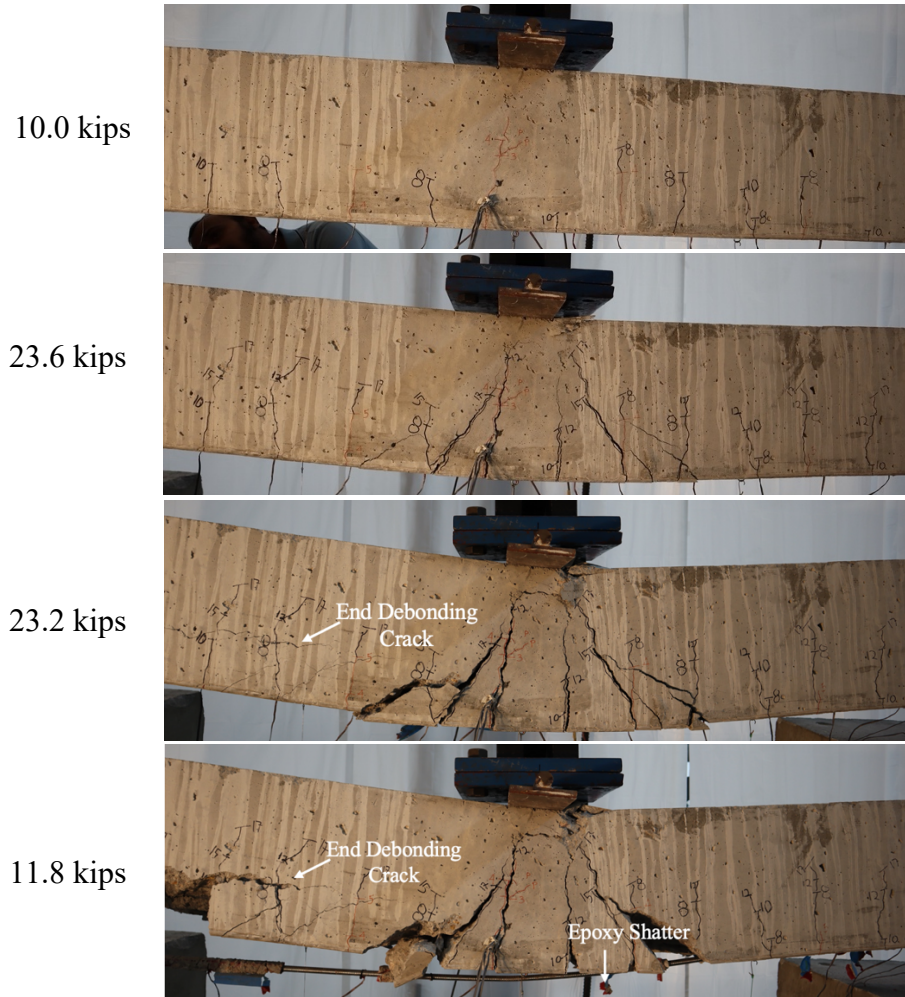
Figure 8.61 – R.SB.96 Progression

Figure 8.62 – R.SB.96 Post-Test
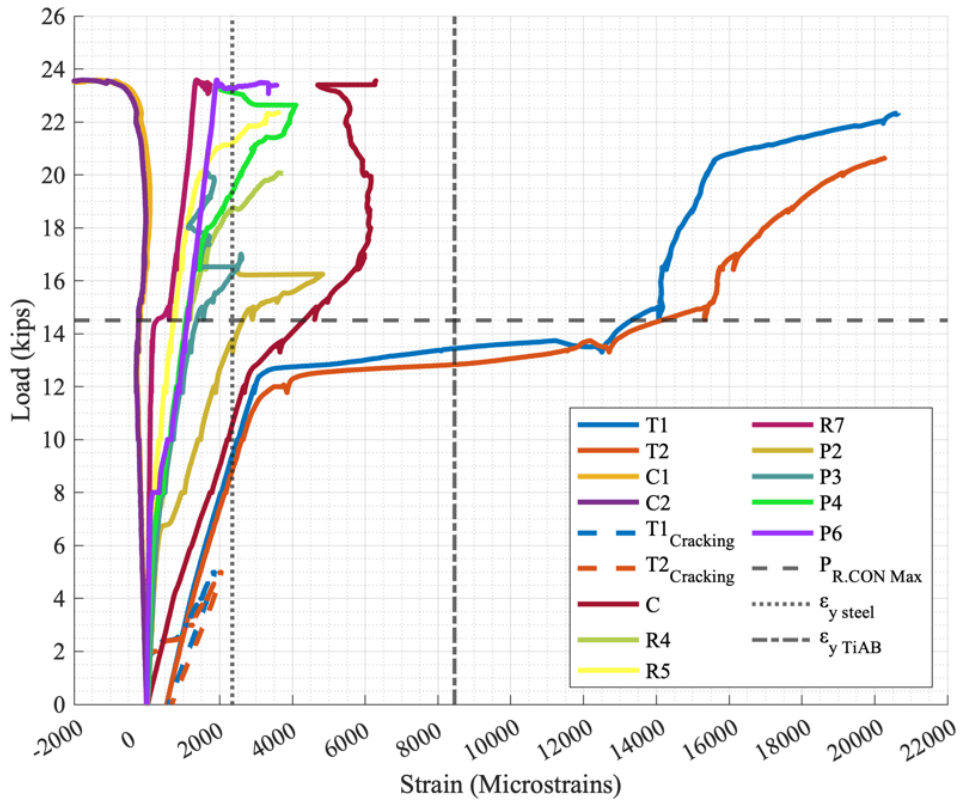
Figure 8.63 – R.SB.96 Load versus Strain Response
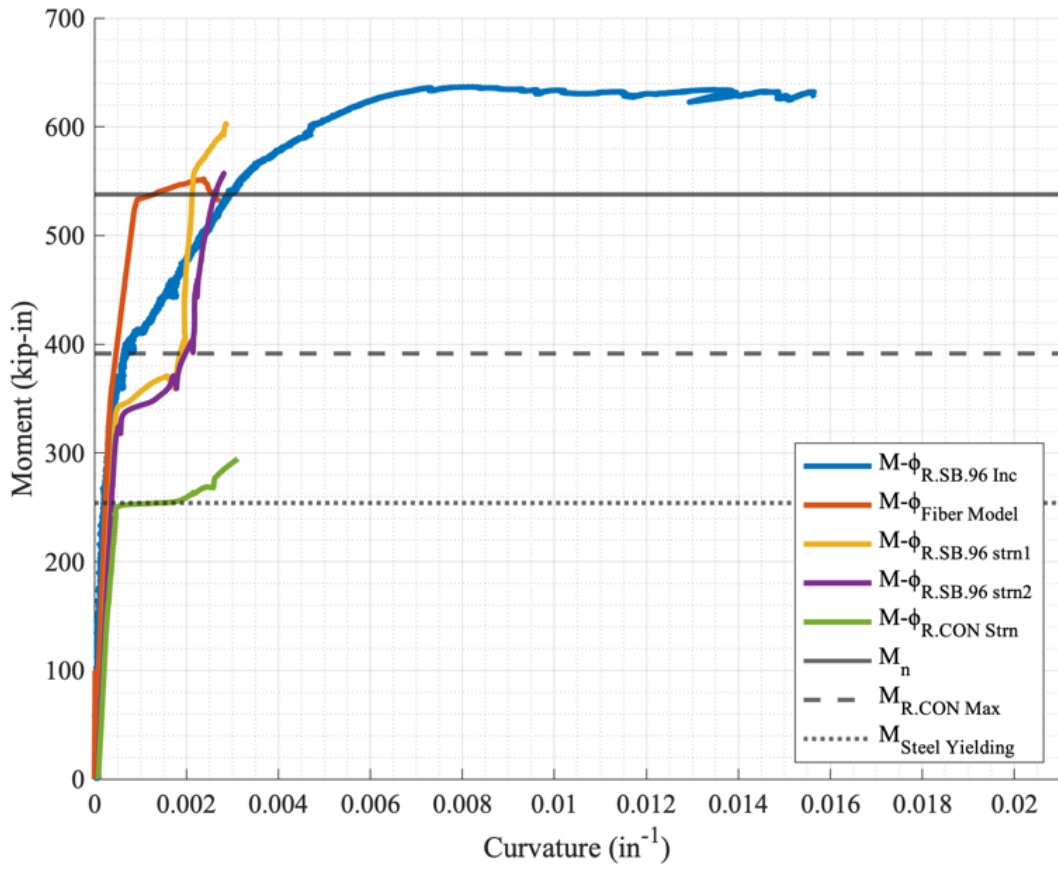
Figure 8.64 – R.SB.96 Moment versus Curvature Response
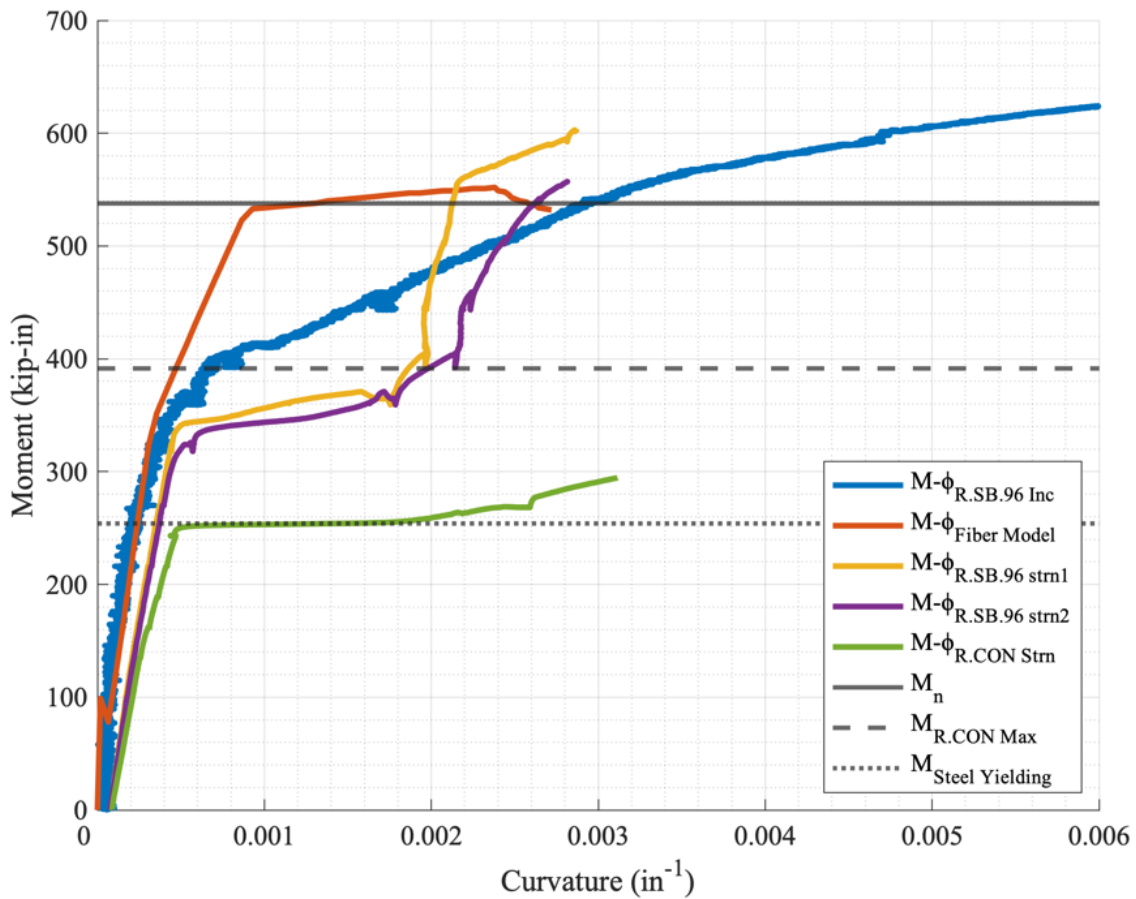
Figure 8.65 – R.SB.96 Moment versus Curvature Response with Shorter Axis Limit

8.4 Hooked-Unbonded Tests

This section discusses the experimental responses of the beams with hooked-unbonded NSM TiAB.

8.4.1 R.HU.10

This specimen was strengthened with a 10-inch hooked-unbonded TiAB. The specimen was pre-cracked as explained in Section 7.1 (initial loading cracks marked with red). The complete load versus displacement graph is shown in Figure 8.66, and the pictures corresponding to the points on the plot are provided in Figure 8.67. As the applied load increased, pre-cracks widened and propagated, and existing crack extensions and new cracks were marked in black. An almost linear response was observed up to an applied force of about 11 kips, where nonlinearity in the

160

load-displacement behaviour became more visible beyond this force level. Similar to the earlier specimens, flexural cracks were observed at almost constant spacing between the cracks until the yielding of the steel rebars. After yielding, cracks quickly formed outside the hooks and propagated towards the load point.

The peak load occurred at 13.8 kips at a mid-span deflection of 2.29 inches. The load response briefly descended after 11 kips and then rose again till it plateaued around the peak load. There was excessive cracking across the hooks and the beam behaved similar to R.CON after the load dip at 11 kips. The beam was eventually unloaded after it was clear that the TiAB was not contributing to any strength gain at 13.2 kips and 4.05 inches of midspan deflection.

The strength observed for the test was marginally smaller than the control specimen (13.8 versus 14.5 kips) and significantly lower than the calculated strength that corresponding to the TiAB and steel rebar yielding (13.8 versus 19.8 kips). Based on the failure definition of 5% force drop from the peak load, the specimen had a failure load of 13.05 kips at 4.03 inches of mid-span displacement. The observed failure mode was classified as hooked end debonding, as Figure 8.68 illustrates the cracks crossing the hooks and separating the section of concrete with the TiAB.

The strains measured in the steel reinforcing bars and TiAB are presented in Figure 8.69. The bottom reinforcing bar strains were offset from the origin as they initiated from the residual strain that resulted from the pre-cracking load cycle. The bottom reinforcing rebars exceeded the steel yield strain of 2345 microstrain ($\mu\varepsilon$) at 7.3 kips at the mid-span section. The bottom reinforcement strains (T1 and T2) exhibited a yield plateau response at around 12 kips. The difference between the initiation of rebar yielding and the yield plateau response is credited to the formation of the plastic hinge at the midspan and the load increase necessary to extend the yielding portion. The data acquisition system was capable of recording strains up to 2% strain

(20,000 $\mu\varepsilon$), but the test continued beyond the force levels that achieved this strain limit. The TiAB Strain gauges (C, R1, and P1) reached 2000 $\mu\varepsilon$ and did not reach the expected TiAB yield strength of 8450 $\mu\varepsilon$.

The moment-curvature responses obtained from the strain and beam rotation measurements are provided in Figure 8.70 and with an abbreviated x-axis in Figure 8.71. The strain-based moment-curvature response was obtained by calculating the curvature between the strain measurements on the top and bottom steel rebars at the midspan. The rotation-based moment-curvature response was obtained by calculating the average curvature using the rotation measurements at 4 inches from the midspan on either side (8-inch central region) as mentioned in Section 6.2. The moment-curvature response indicates consistent behavior with the one obtained from the 2D fiber model (M-$\phi_{\text{Fiber Model}}$) up to a mid-span moment of 300 kip-in. The response deviated from the 2D fiber model response and indicated a gradually reducing slope (stiffness) until the peak moment. The peak moment of 373 kip-in was achieved just before 0.012 in^{-1} of curvature and the maximum curvature was recorded to be beyond 0.018 in^{-1}. The curve indicates the performance of the 10-inch hooked-unbonded TiAB did not increase the strength of the beam.
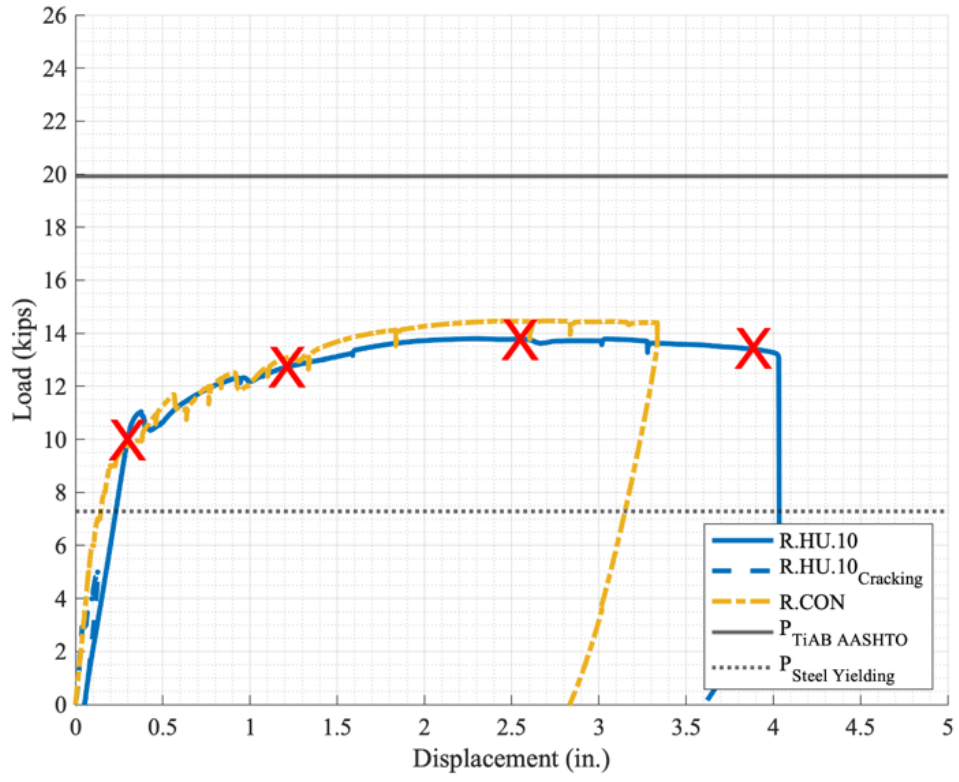
Figure 8.66–- R.HU.10 Load versus Displacement

10.0 kips

12.7 kips
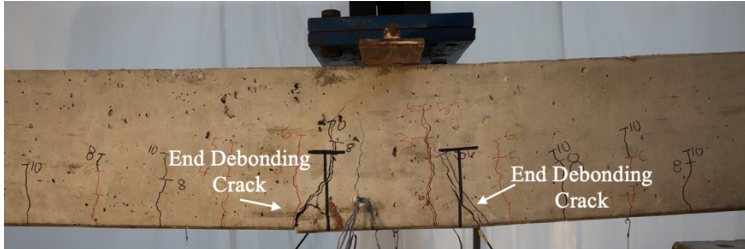
13.8 kips
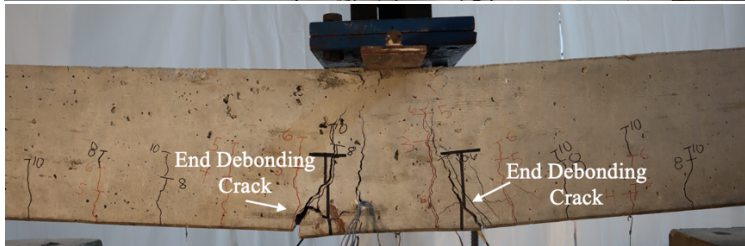
13.4 kips
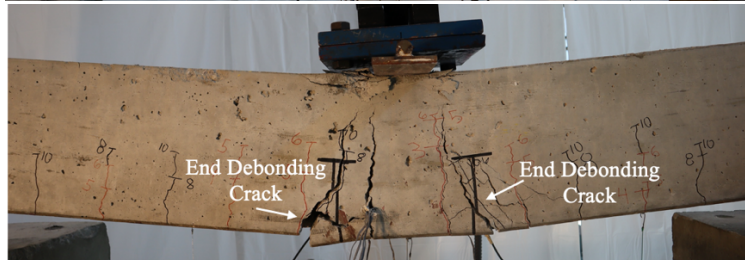
Figure 8.67–- R.HU.10 Progression

Figure 8.68–- R.HU.10 Post-Test
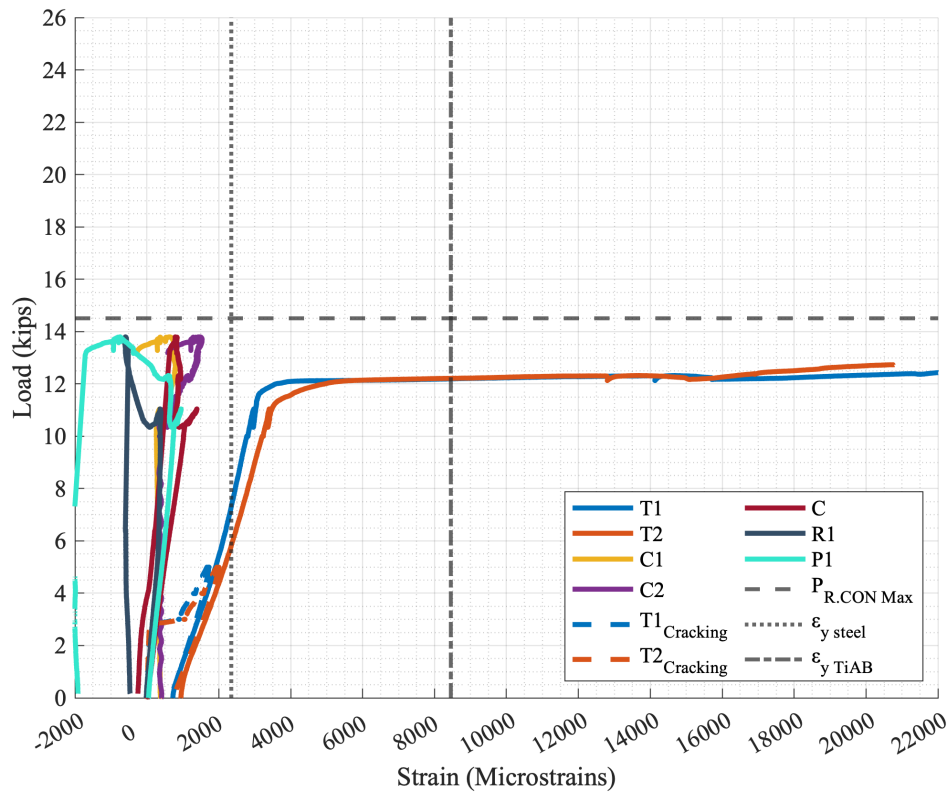
Figure 8.69 – R.HU.10 Load versus Strain
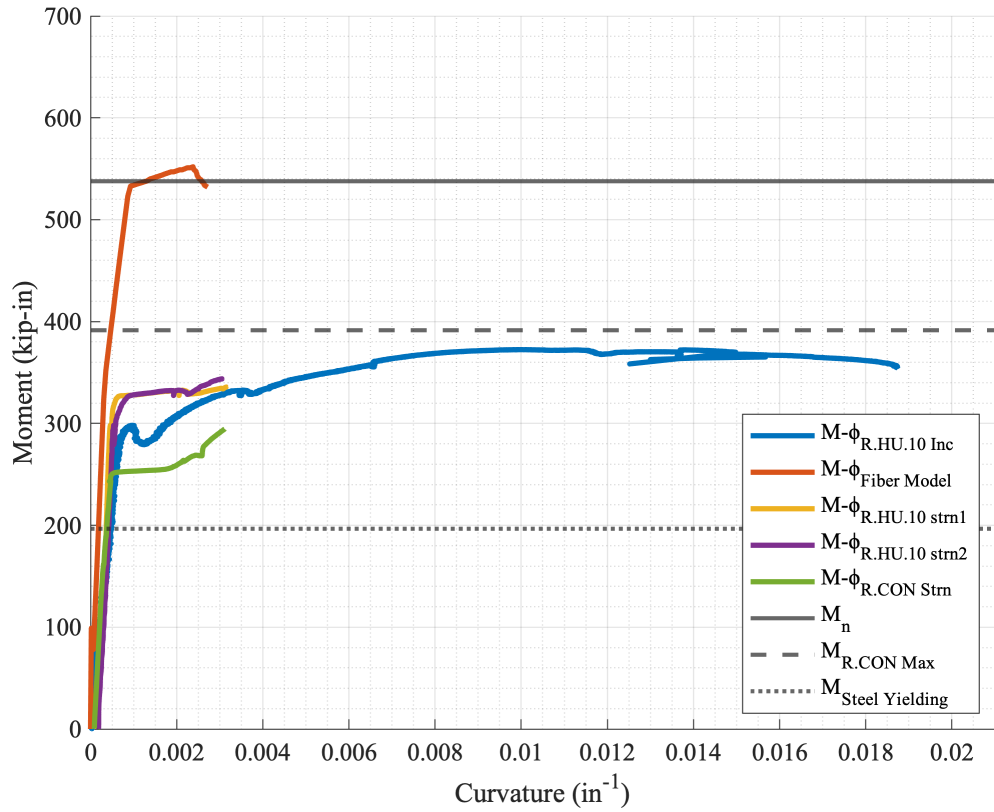
Figure 8.70 – R.HU.10 Moment versus Curvature Response
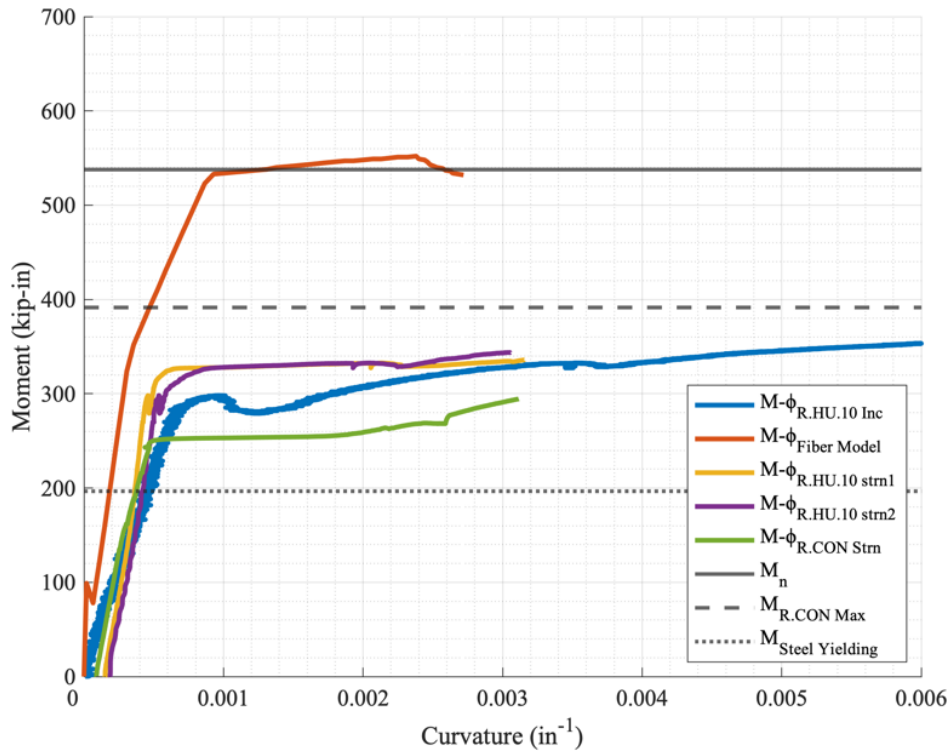
Figure 8.71–- R.HU.10 Moment versus Curvature Response with Shorter Axis Limit

8.4.2 R.HU.30

This specimen was strengthened with a 30-inch hooked-unbonded TiAB. The specimen was pre-cracked as explained in Section 7.1 (initial loading cracks marked with red). The complete load versus displacement graph is shown in Figure 8.72, and the pictures corresponding to the points on the plot are provided in Figure 8.73. In those figures the TiAB is not labeled as they were in the other tests. As the applied load increased, pre-cracks widened and propagated, and existing crack extensions and new cracks were marked in black. An almost linear response was observed up to an applied force of about 12 kips, where nonlinearity in the load-displacement behavior became more visible beyond this force level. Similar to the earlier specimens, flexural cracks were observed at almost constant spacing between the cracks until the yielding of the steel rebars.

After steel yielding the cracks propagated but maintained the nearly constant spacing. At 12 kips the largest crack width was 0.03 inches. The peak load occurred at 18.0 kips at a mid-span deflection of 0.83 inches. A diagonal crack formed suddenly on the outside of the right TiAB hook and the load dropped to 13 kips.

The strength observed for the test was larger than the control specimen (18.0 versus 14.5 kips) and lower than the calculated strength that corresponding to the TiAB and steel rebar yielding (18.0 versus 19.8 kips). Based on the failure definition of 5% force drop from the peak load, the specimen had a failure load of 17.5 kips at 0.85 inches of mid-span displacement. The observed failure mode was classified as hooked end debonding, as Figure 8.74 illustrates the crack starting outside the TiAB hook and then crossing over it.

The strains measured in the steel reinforcing bars and TiAB are presented in Figure 8.75. The bottom reinforcing bar strains were offset from the origin as they initiated from the residual

strain that resulted from the pre-cracking load cycle. The bottom reinforcing rebars exceeded the steel yield strain of 2345 microstrain (με) at 7.9 kips at the mid-span section. The bottom reinforcement strains (T1 and T2) exhibited a yield plateau response at around 13 kips. The difference between the initiation of rebar yielding and the yield plateau response is credited to the formation of the plastic hinge at the midspan and the load increase necessary to extend the yielding portion. The TiAB Strain gauges (C, R1, and P2) reached 6000 με and did not reach the expected TiAB yield strength of 8450 με.

The moment-curvature responses obtained from the strain and beam rotation measurements are provided in Figure 8.76 and with an abbreviated x-axis in Figure 8.77. The moment-curvature response indicates consistent behavior with the one obtained from the 2D fiber model (M-$\phi_{\text{Fiber Model}}$) up to a mid-span moment of 320 kip-in. The response deviated from the 2D fiber model response and indicated a softening that occurred potentially form the steel yielding. The peak moment of 486 kip-in was achieved at 0.002 in^{-1} which was also the max curvature. The moment-curvature response indicated sudden drop without much softening indicates that the debonding occurred before the full capacity of the beam was achieved.
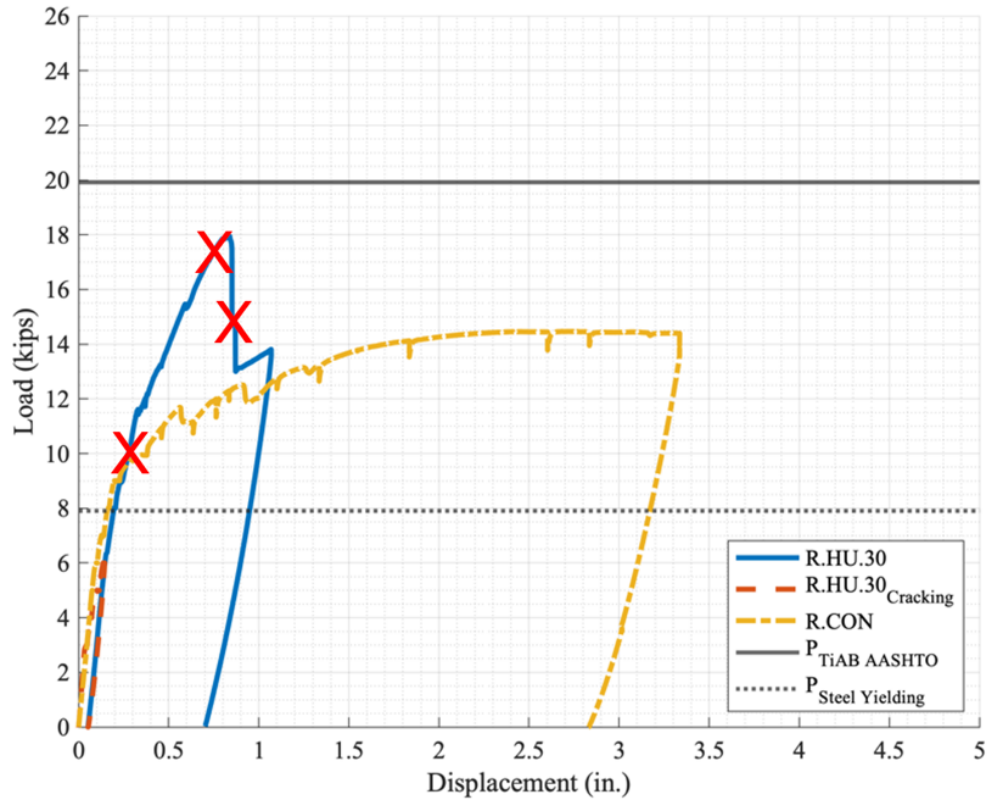
Figure 8.72–- R.HU.30 Load versus Displacement Response

10.0 kips

17.7 kips

14.7 kips

End Debonding
Crack
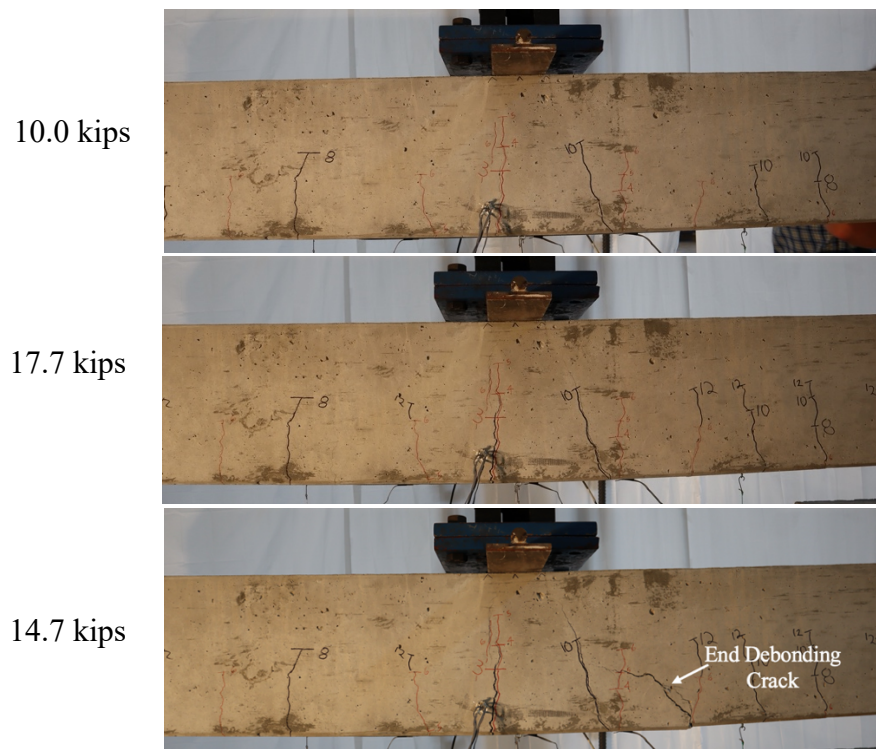
Figure 8.73–- R.HU.30 Progression
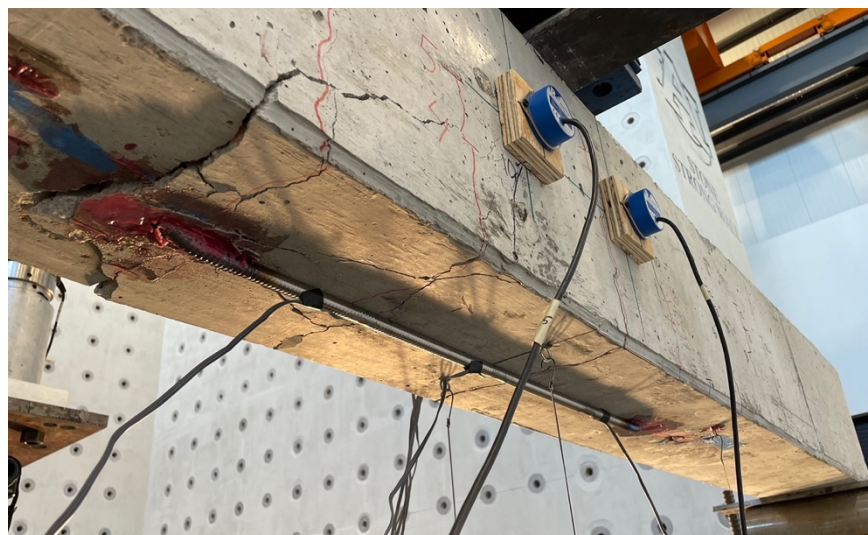
Figure 8.74–- R.HU.30 Post-Test
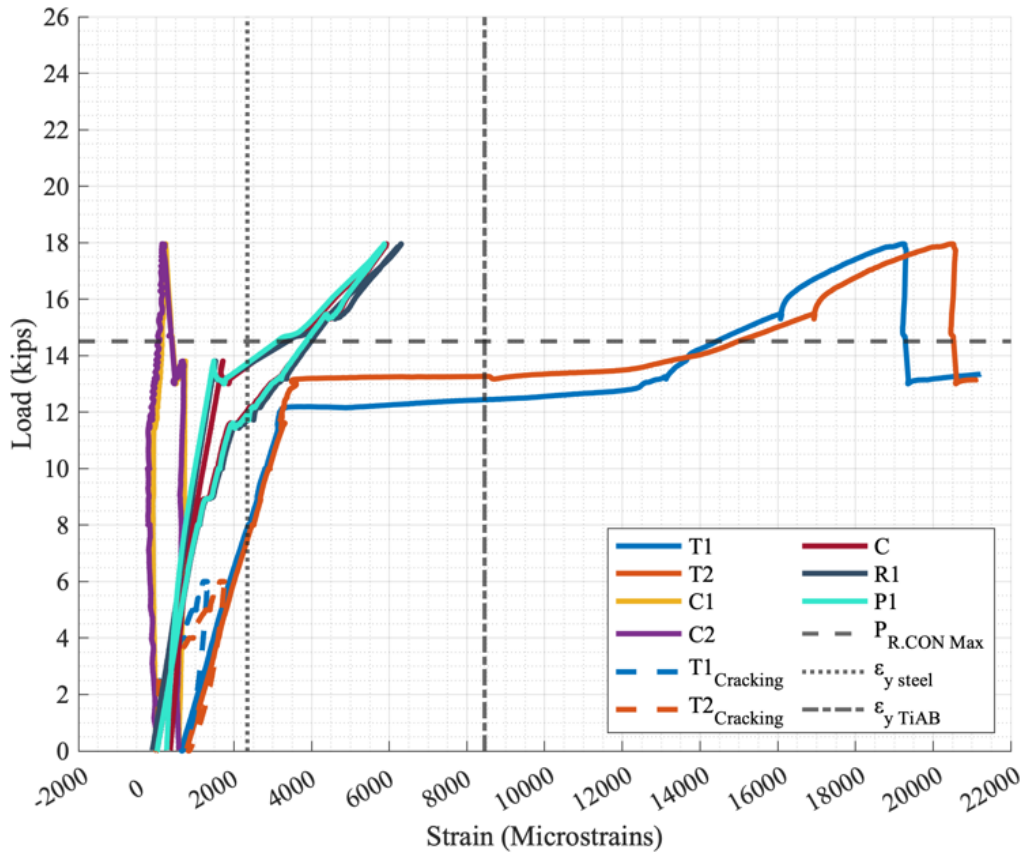
Figure 8.75 – R.HU.30 Load versus Strain Response
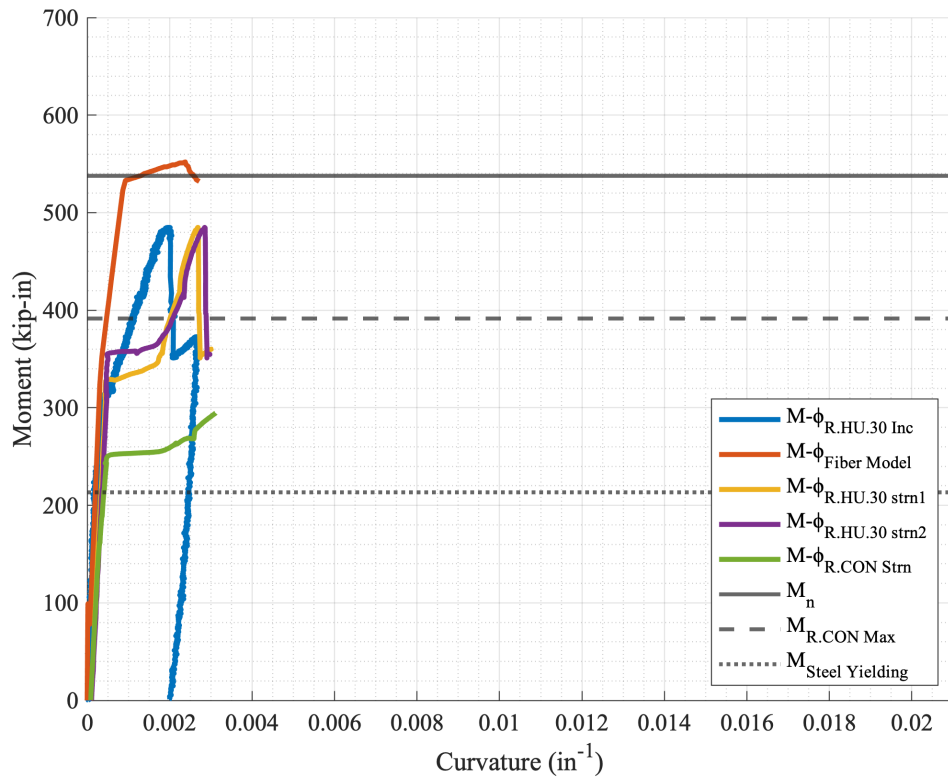
Figure 8.76 – R.HU.30 Moment versus Curvature Response
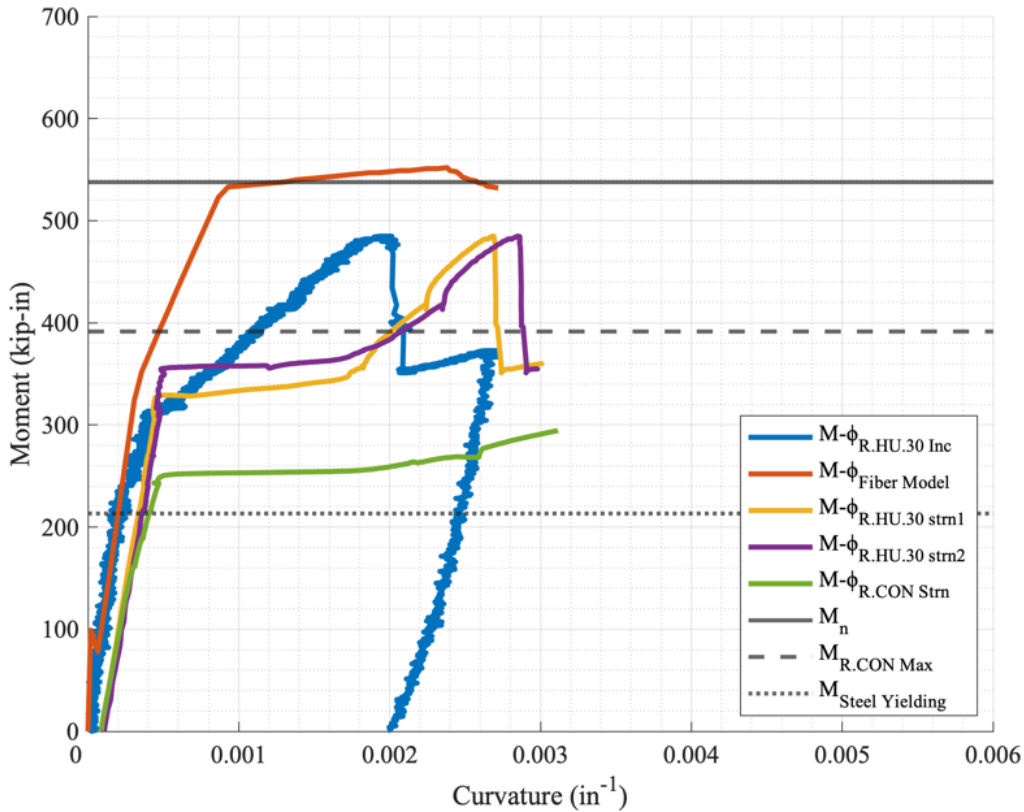
Figure 8.77–- R.HU.30 Moment versus Curvature Response with Shorter Axis Limit

8.4.3 R.HU.40

This specimen was strengthened with a 40-inch hooked-unbonded TiAB. The specimen was pre-cracked as explained in Section 7.1 (initial loading cracks marked with red). The complete load versus displacement graph is shown in Figure 8.78, and the pictures corresponding to the points on the plot are provided in Figure 8.79. As the applied load increased, pre-cracks widened and propagated, and existing crack extensions and new cracks were marked in black. An almost linear response was observed up to an applied force of about 13 kips, where nonlinearity in the load-displacement behavior became more visible beyond this force level. Similar to the earlier specimens, flexural cracks were observed at almost constant spacing between the cracks until the yielding of the steel rebars.

After the initiation of steel yielding the cracks widened and propagated towards the load point. The central crack was the widest. The peak load occurred at 22.9 kips at a mid-span deflection of 1.44 inches. At the peak load the left-central crack was excessively wide and hairline cracks around the left TiAB hook indicated signs of distress. The load gradually dropped with increasing midspan displacement and eventually plateaued around 18 kips. The beam was unloaded when the load dropped to 17.7 kips and 3.90 inches of displacement.

The strength observed for the test was significantly larger than the control specimen (22.9 versus 14.5 kips) and larger than the calculated strength that corresponding to the TiAB and steel rebar yielding (22.9 versus 19.8 kips). Based on the failure definition of 5% force drop from the peak load, the specimen had a failure load of 21.8 kips at 1.66 inches of mid-span displacement. The observed failure mode was classified as anchorage slip, as Figure 8.80 illustrates the back of the TiAB hook was separated from the concrete/epoxy and visible distress was observed in the hook-bearing area of the concrete.

The strains measured in the steel reinforcing bars and TiAB are presented in Figure 8.81. The bottom reinforcing bar strains were offset from the origin as they initiated from the residual strain that resulted from the pre-cracking load cycle. The bottom reinforcing rebars exceeded the steel yield strain of 2345 microstrain ($\mu\varepsilon$) at 7.7 kips at the mid-span section. The bottom reinforcement strains (T1 and T2) exhibited a yield plateau response at around 11 kips. The difference between the initiation of rebar yielding and the yield plateau response is credited to the formation of the plastic hinge at the midspan and the load increase necessary to extend the yielding portion. The TiAB Strain gauges (C, R1, and P2) reached 10000 $\mu\varepsilon$ which is beyond the 8450 $\mu\varepsilon$ expected TiAB yield strain.

The moment-curvature responses obtained from the strain and beam rotation measurements are provided in Figure 8.82 and with an abbreviated x-axis in Figure 8.83. The moment-curvature response indicates consistent behavior with the one obtained from the 2D fiber model (M-$\phi_{\text{Fiber Model}}$) up to a mid-span moment of 300 kip-in. The response deviated from the 2D fiber model response and indicated a softening that occurred potentially form the steel yielding. The peak moment of 353 kip-in was achieved at 0.003 in^{-1}. The max curvature was captured to be 0.001 in^{-1}.
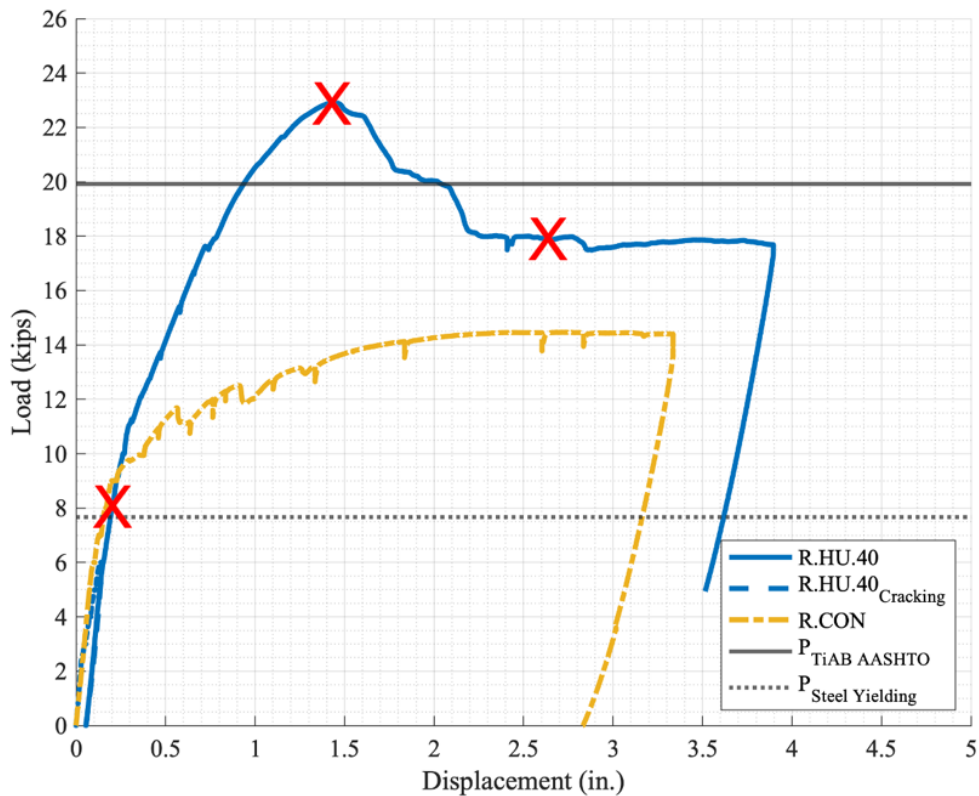
Figure 8.78-- R.HU.40 Load versus Displacement
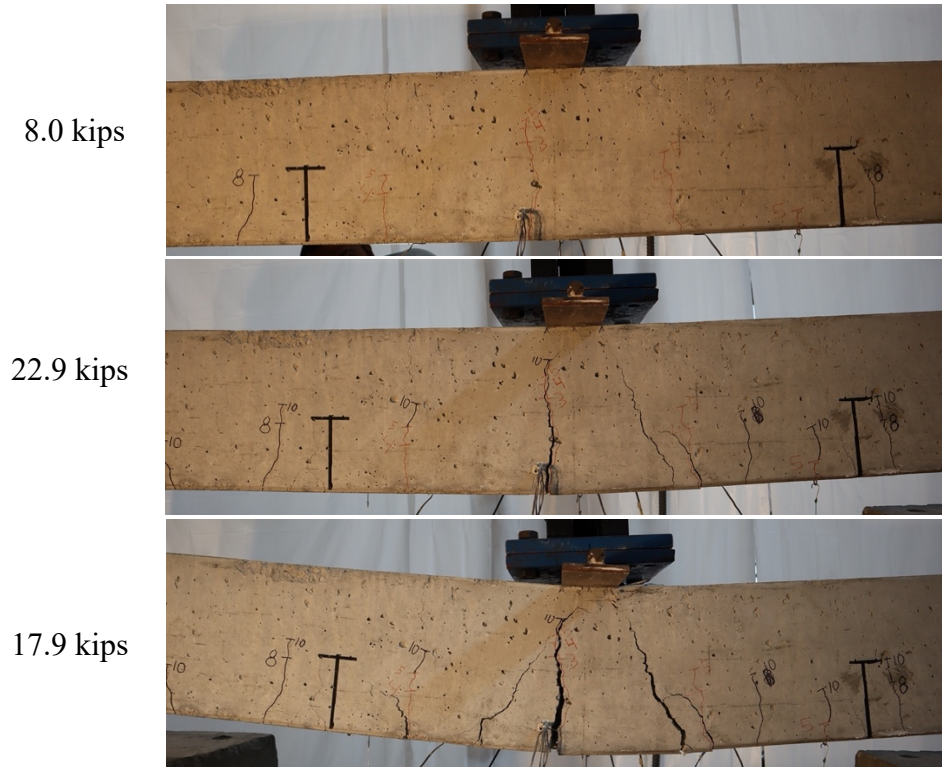
Figure 8.79–- R.HU.40 Progression

Figure 8.80–- R.HU.40 Post-Test

176
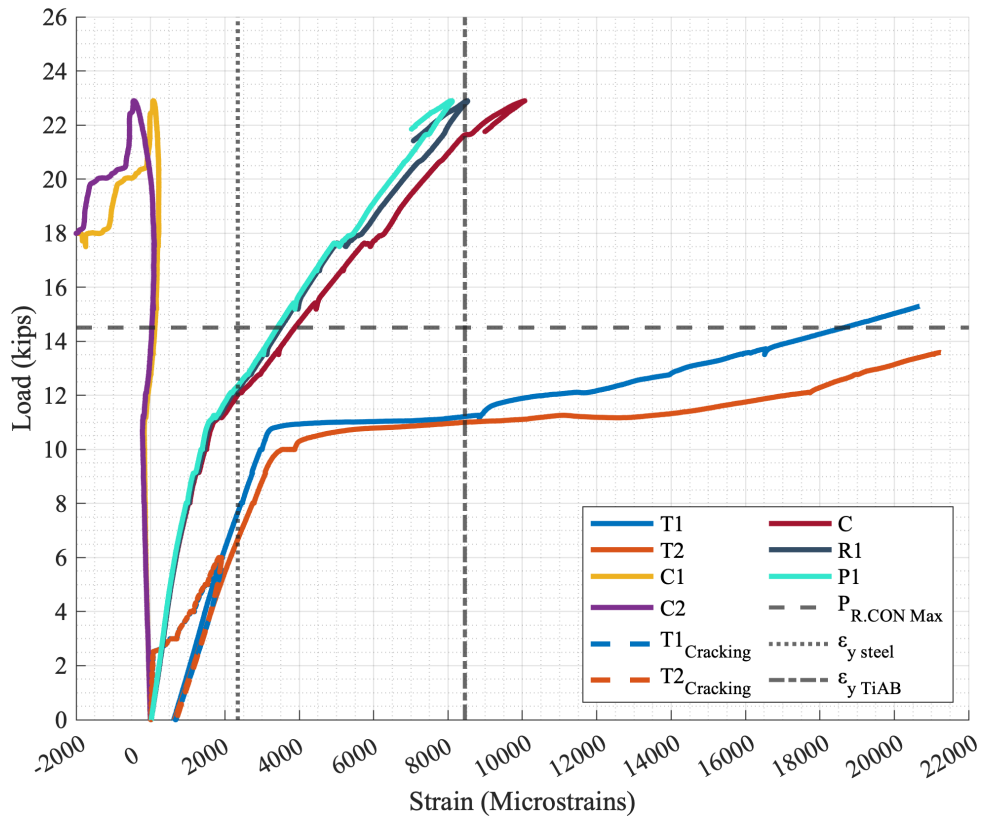
Figure 8.81 – R.HU.40 Load versus Strain Response
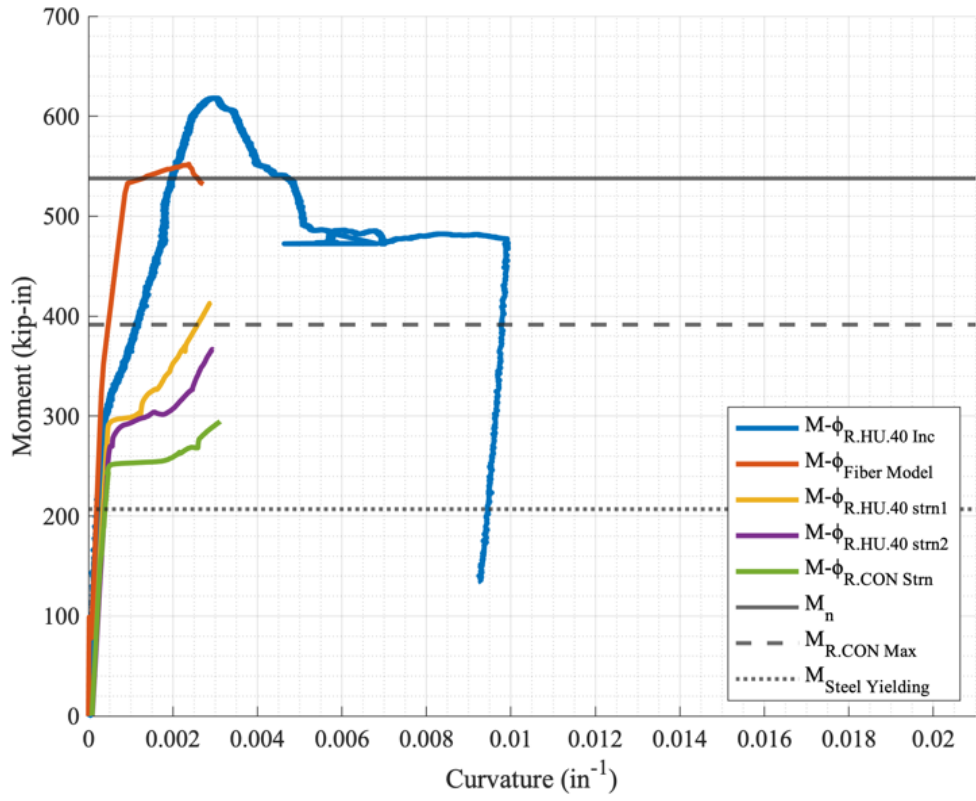
Figure 8.82 – R.HU.40 Moment versus Curvature Response
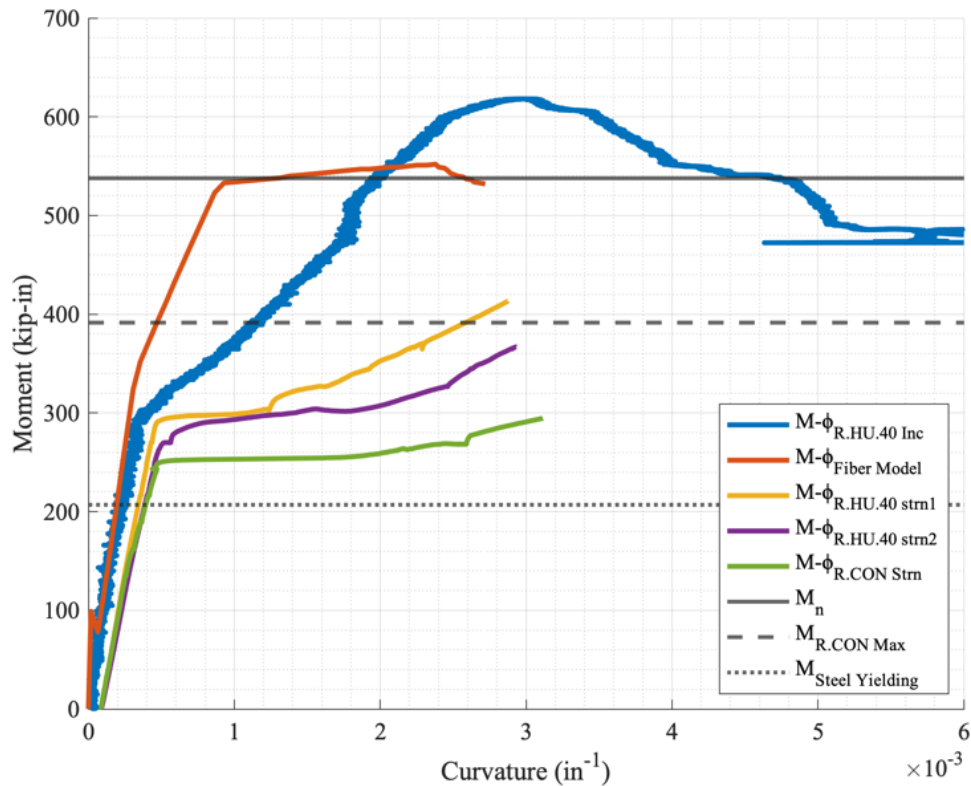
Figure 8.83-- R.HU.40 Moment versus Curvature Response with Shorter Axis Limit

8.4.4 R.HU.60

This specimen was strengthened with a 60-inch hooked-unbonded TiAB that used a larger bend

diameter of 6-in. rather than 3-in. (the tail length remained a constant 6 inches as was provided in

the other specimens). R.HU.60 was also rotated 180 degrees providing a 1 in. clear cover rather

than 1.5 inches. The specimen was pre-cracked as explained in Section 7.1 (initial loading cracks

marked with red). The complete load versus displacement graph is shown in Figure 8.84, and the

pictures corresponding to the points on the plot are provided in Figure 8.85. As the applied load

increased, pre-cracks widened and propagated, and existing crack extensions and new cracks

were marked in black. An almost linear response was observed up to an applied force of about 11

kips, where nonlinearity in the load-displacement behavior became more visible beyond this

force level. Similar to the earlier specimens, flexural cracks were observed at almost constant spacing between the cracks until the yielding of the steel rebars.

After the initiation of steel yielding the cracks widened and propagated towards the load point. The left-central crack was the widest. Diagonal cracks also formed near both hooks. The peak load occurred at 23.1 kips at a mid-span deflection of 1.79 inches. The load suddenly dropped to 17 kips without any noticeable change in the crack pattern on the sides of the beam. The load drop might have been due to a sudden slip in the anchorage. The test continued and the load leveled out close to 19 kips where it continued to displace until unloaded at 17.3 kips and a midspan deflection of 1.83 inches.

The strength observed for the test was significantly larger than the control specimen (23.1 versus 14.5 kips) and larger than the calculated strength that corresponding to the TiAB and steel rebar yielding (23.1 versus 19.8 kips). Based on the failure definition of 5% force drop from the peak load, the specimen had a failure load of 22.8 kips at 1.83 inches of mid-span displacement. The observed failure mode was classified as anchorage slip, as Figure 8.86, illustrates the 1- and 1/8-inch difference in the line on the beam and the line on the TiAB that started in the same location.

The strains measured in the steel reinforcing bars and TiAB are presented in Figure 8.87. The bottom reinforcing bar strains were offset from the origin as they initiated from the residual strain that resulted from the pre-cracking load cycle. The bottom reinforcing rebars exceeded the steel yield strain of 2345 microstrain ($\mu\varepsilon$) at 7.0 kips at the mid-span section. The bottom reinforcement strains (T1 and T2) exhibited a yield plateau response at around 11 kips. The difference between the initiation of rebar yielding and the yield plateau response is credited to the formation of the plastic hinge at the midspan and the load increase necessary to extend the

yielding portion. The TiAB Strain gauges (C, R1, and P2) reached 8450 $\mu\varepsilon$ which is the expected

TiAB yield strain.

The moment-curvature responses obtained from the strain and beam rotation

measurements are provided in Figure 8.88 and with an abbreviated x-axis in Figure 8.89. The

moment-curvature response indicates consistent behavior with the one obtained from the 2D

fiber model (M-$\phi_{\text{Fiber Model}}$) up to a mid-span moment of 300 kip-in. The response deviated from

the 2D fiber model response and indicated a softening that occurred potentially form the steel

yielding. The peak moment of 623 kip-in was achieved at 0.004 in^{-1}. The max curvature was

captured to be 0.008 in^{-1}.
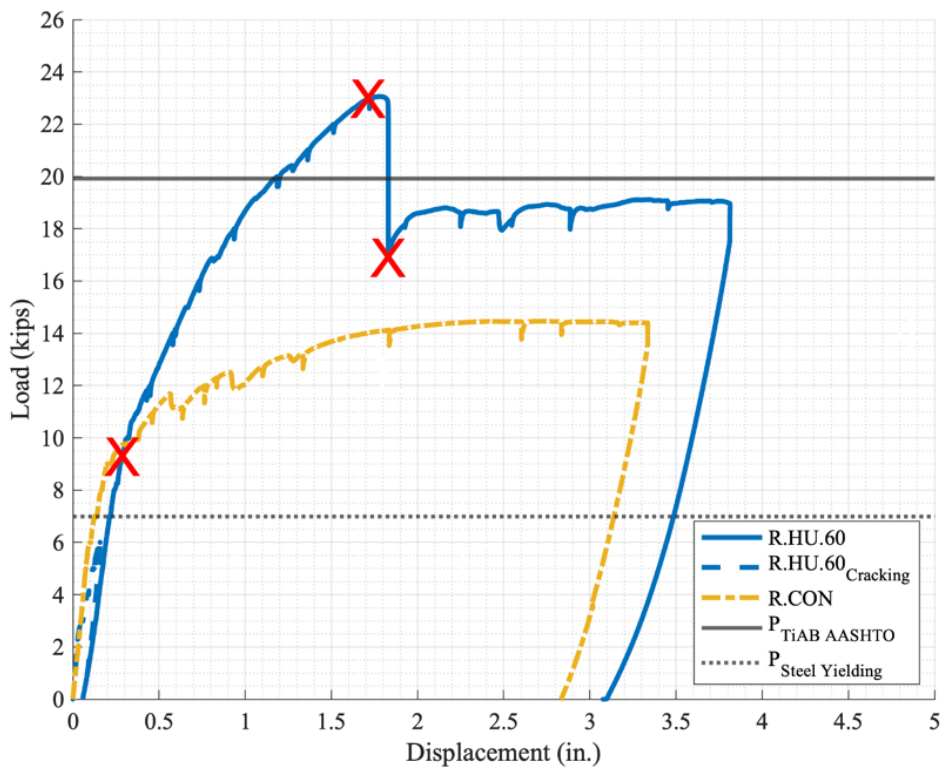
Figure 8.84 - R.HU.60 Load versus Displacement Response

Figure 8.85 - R.HU.60 Progression

Figure 8.86 - R.HU.60 Post-Test
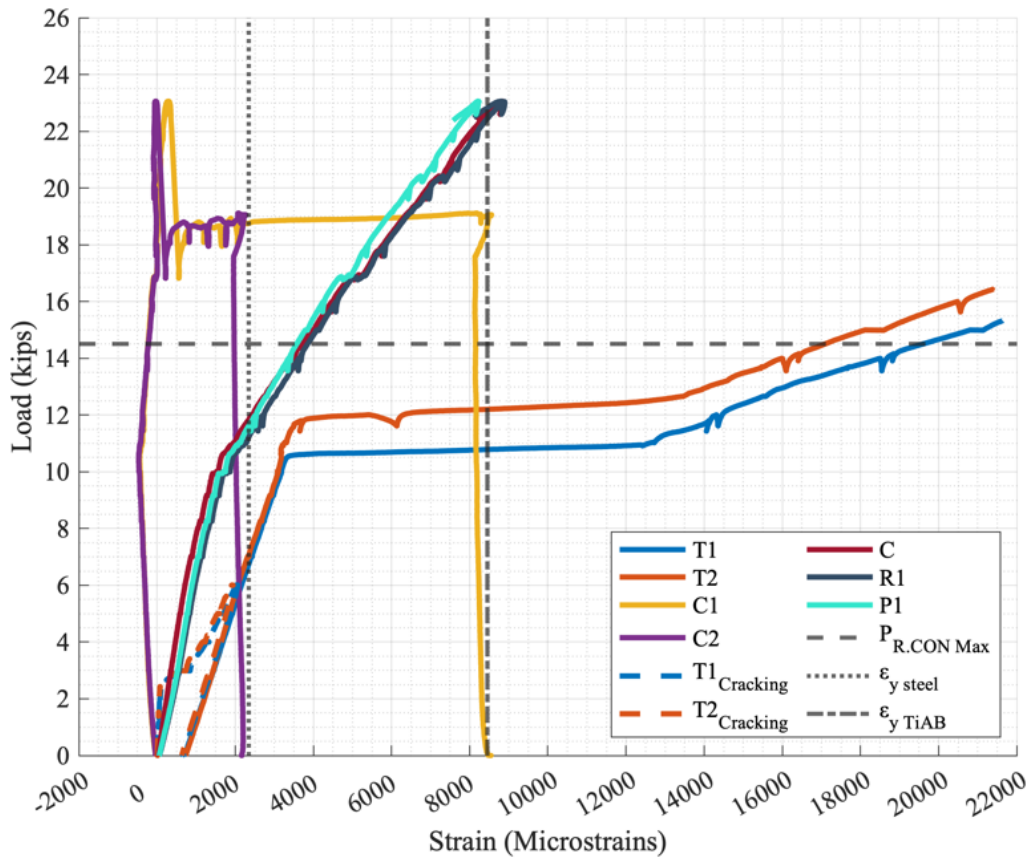
Figure 8.87 – R.HU.60 Load versus Strain Response
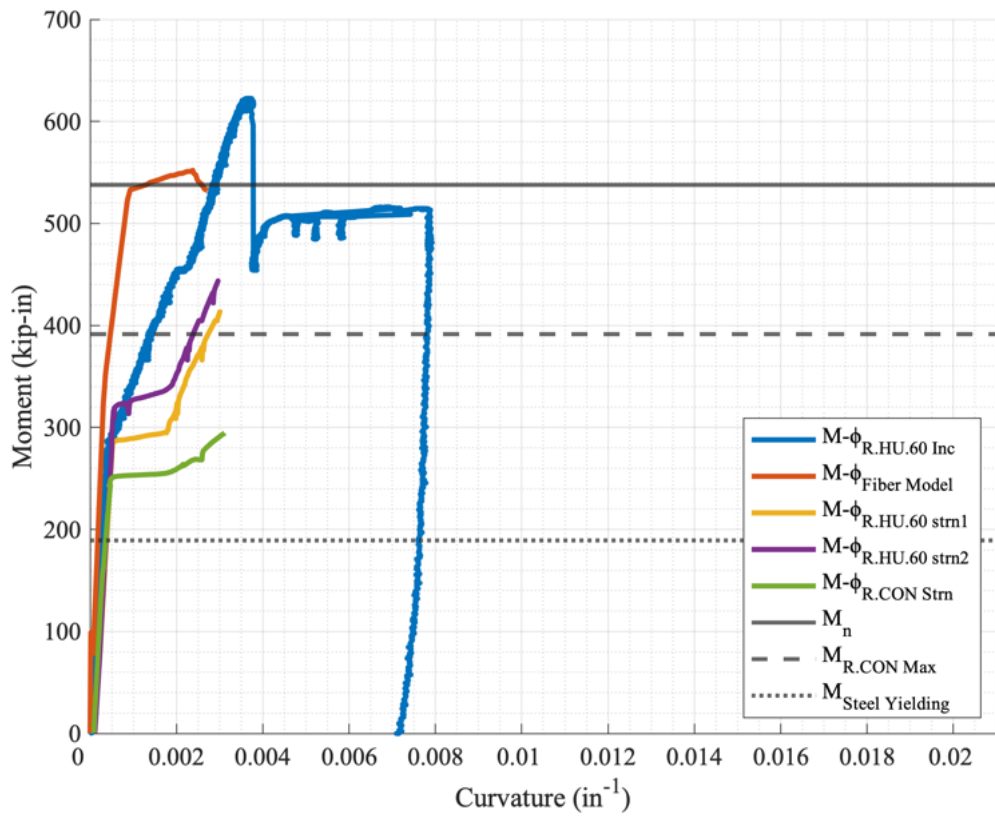
Figure 8.88 – R.HU.60 Moment versus Curvature Response
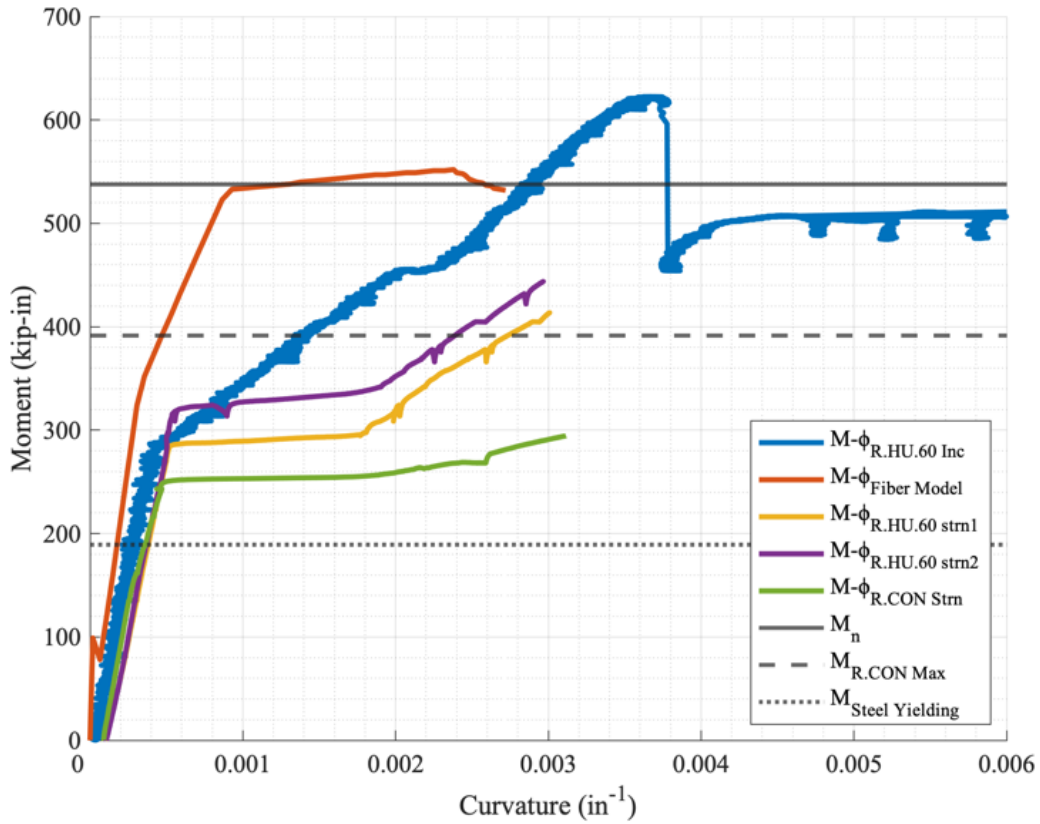
Figure 8.89 - R.HU.60 Moment versus Curvature Response with Shorter Axis Limit

8.5 Summary of Tested Specimens

Figure 8.90 illustrates the load versus displacement of all the specimens. This figure indicates the consistent behavior before the initial softening for all beams.
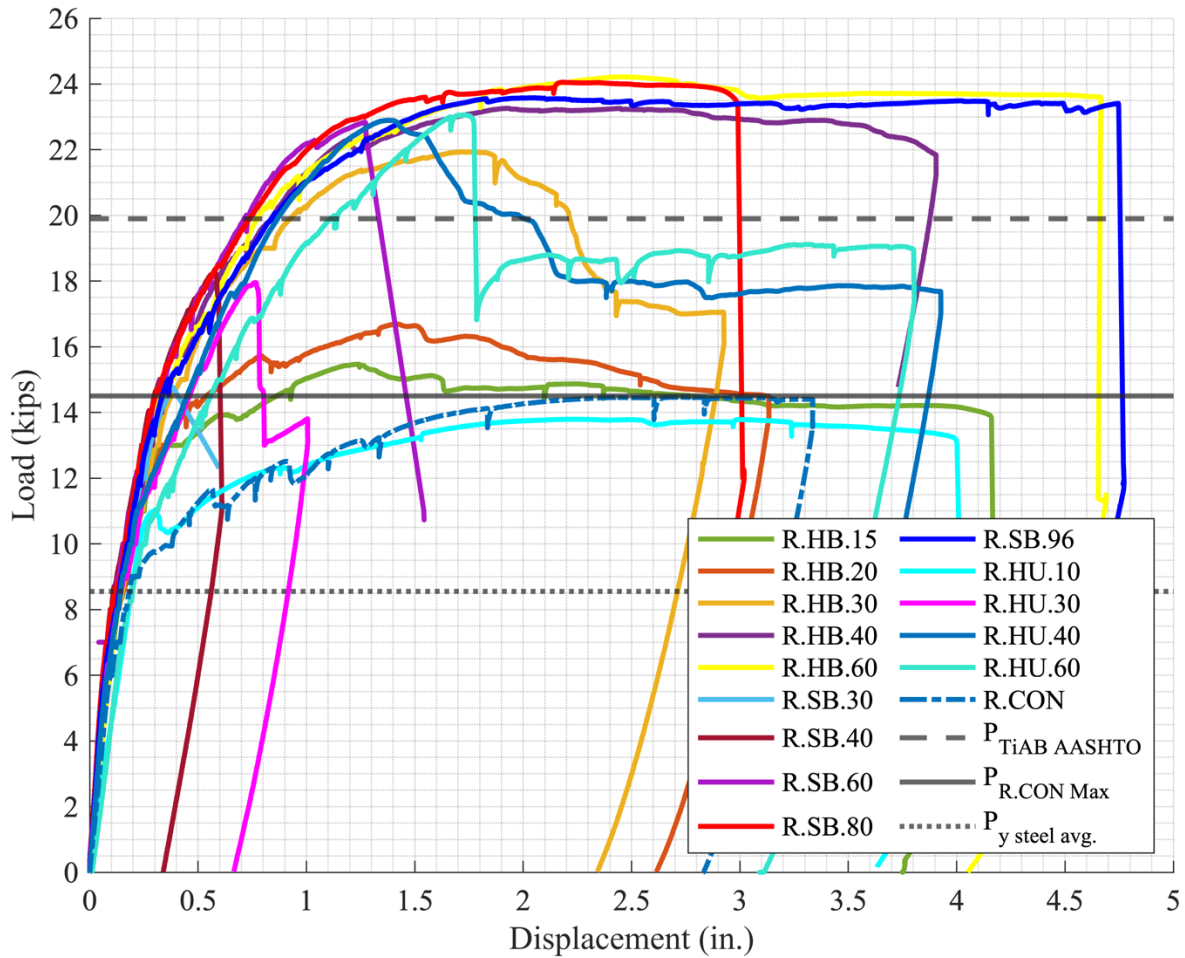
Figure 8.90 – All Specimens Load versus Displacement Response

The hooked-bonded specimens that had a TiAB development length of 15 in. (1.09 ksi of bond strength) and longer (bond strength < 1.09 ksi) exhibited desirable responses by achieving yielding and AASHTO's nominal strength and sustaining large deformations at peak load levels after the yielding of both steel and TiAB. After undergoing significant deformation beyond the yielding of the bars, the specimens eventually failed with titanium or epoxy rupture, which were sudden failure modes. Having the hooked ends significantly reduced the bonded length required to achieve the yielding of the TiAB.

Similarly, the straight-bonded specimens that had a TiAB development length of 30 in. (0.55 ksi of bond strength) and longer (bond strength < 0.55 ksi) exhibited desirable responses by

186

achieving yielding and AASHTO's nominal strength and sustaining large deformations at peak load levels after the yielding of both steel and TiAB. The R.SB.80 failed due to TiAB rupture, indicating that the straight-bonded anchorage method can be utilized to achieve the full-strength from the TiAB, if sufficient embedment length is provided.

The hooked-unbonded specimens were capable of achieving the plastic capacities similar to the bonded tests. R.HU.40 and R.HU.60 achieved the capacity calculated from Equation 2.2. Despite being able to achieve high resistance, the loads were not sustained through large displacements and indicated wide cracking that would be excessive for crack controlling limits.

R.HB.30, R.SB.60, R.HU.40, and R.HU.60 all exhibited TiAB yielding, but without a post-peak plateau. R.HB.40, R.HB.60, R.SB.80. and R.SB.96 exhibited TiAB yielding with a post-peak plateau. Equation 2.2 in the AASHTO Guide uses the yield stress when calculating the strength contribution from titanium-alloy in tensions for nominal moment strength. Therfore, the TiAB was considered to have yielded when the specimen achieved the strength predicted from AASHTO. Figure 8.91 illustrates each anchorage methods' peak load versus TiAB length and Figure 8.92 depicts the displacement at failure for each beam where the TiAB yielded.

Peak Load vs TiAB Length
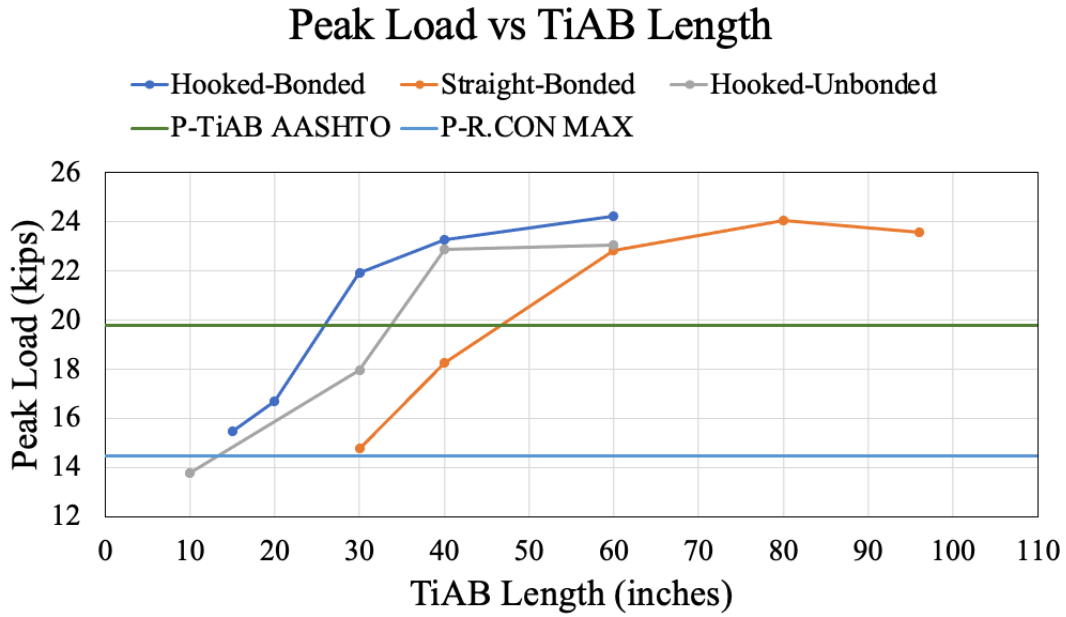
Figure 8.91 - Peak Load versus TiAB Length for all Anchorage Methods

Deflections at Failure
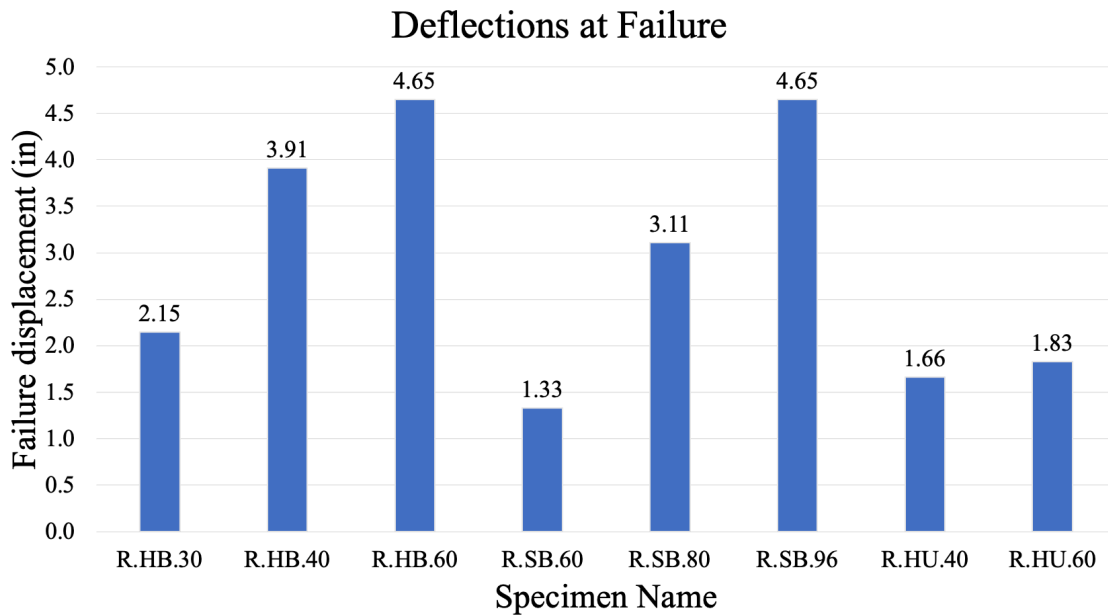
Figure 8.92 - Deflections at Failure for Specimens that reached TiAB Yielding

These figures indicate that the bonded bars achieved larger deflections prior to failure with increasing embedment length. The loads achieved during these tests exceeded the predicted

strengths. Table 8.1 displays the predicted strengths, the strengths of the control specimen, and the strengths of the beams that exceeded the AASHTO predicted capacity.

Table 8.1 – Strength Comparison to Control

Beam	Nominal Strength Based on Eq. 2.2 (k)	Measured Strength (k)	Strength Increase from R.CON
R.CON	9.6	14.5	N/A
R.HB.30	19.8	21.9	7.4
R.HB.40	19.8	23.3	8.8
R.HB.60	19.8	24.2	9.7
R.SB.60	19.8	22.8	8.3
R.SB.80	19.8	24.1	9.6
R.SB.96	19.8	23.6	9.1
R.HU.40	19.8	22.9	8.4
R.HU.60	19.8	23.1	8.6

The measured strength of the control beam (R.CON) was 4.9 kips greater than the nominal flexural strength calculated based only on yielding of the steel reinforcing bars and assuming a rectangular stress block for concrete in compression. Similarly, R.HB.60 was the specimen with the greatest flexural capacity after strengthening and achieved 4.4 kips greater than the AASHTO prediction of yielding of both steel reinforcing bar and TiAB along with an assumed rectangular stress block for concrete in compression.

The reason for the increased measured strengths from the calculated capacities is uncertain but could have been due to support restraint (pin-pin type support versus pin-roller), strut and tie action, or the concentrated load nature of the three-point loading test. Regardless, the larger measured strengths than predicted values potentially discredit the AASHTO predicted capacity as an indicator of TiAB yield. The strength increase due to the addition of the TiAB was calculated to be 10.2 kips. As shown in Table 7.1, this expected strength increase was consistent with the increase in strength observed for the strengthened specimens from the control specimen.

8.6 Hooked-Bonded Results

The hooked-bonded specimens had increasing peak loads and failure displacements as the embedded/bonded length increased. This indicates better composite interaction and therefore bond performance as the bonded length increased. R.HB.30, R.HB.40, and R.HB.60 achieved yielding of the TiAB and exceeded the AASHTO nominal moment capacity. The predicted capacities, peak and failure loads, peak and failure displacements, peak moments, and the maximum curvatures observed for each specimen are presented in Table 8.2. The peak load variation against the TiAB embedded length is plotted in Figure 8.91.

Table 8.2 - Hooked-Bonded Load and Displacements

Specimen	AASHTO Capacity (k)	Peak Load (k)	Deflection at Peak (in)	Load at Failure (k)	Deflection at Failure (in)	Peak Moment (k-in)	Maximum Curvature (in^{-1})
R.CON	9.6	14.47	2.89	14.40	3.39	391	-
R.HB.15	19.8	15.47	1.31	14.69	1.69	418	0.012
R.HB.20	19.8	16.69	1.48	15.85	2.04	451	0.012
R.HB.30	19.8	21.93	1.80	20.84	2.15	592	0.009
R.HB.40	19.8	23.26	2.01	22.10	3.91	628	0.014
R.HB.60	19.8	24.22	2.54	23.60	4.65	654	0.025

The AASHTO Guide uses 1.0 ksi of average bond strength to determine the minimum length to yield TiABs (development length) for bonded TiAB with hooked anchorages. R.HB.30 was intended to represent approximately 1.0 ksi of average bond strength with a 15 in. development length. Using Equation 2.4 and the measured TiAB yield strength obtained from testing (131 ksi), R.HB.30 was associated with 1.09 ksi of average bond strength. Even at this slightly higher average bond strength (shorted bonded length), the AASHTO calculated capacity of the beam was exceeded which indicated yielding of the TiAB. This proves that the AASHTO recommended effective bond strength of 1.0 ksi to reach the member capacity with TiAB

yielding is conservative. However, the ductile response that makes NSM TiAB advantageous over other strengthening methods (e.g., FRP strengthening) was better exhibited in the longer embedment lengths that corresponded to lower assumed average bond stresses (l_d = 20 [R.HB.40], $\bar{\mu}$ = 0.82 ksi and l_d = 30 [R.HB.60], $\bar{\mu}$ = 0.55 ksi). Table 8.3 provides the failure mode, average bond strengths, development lengths using Equation 2.4, and the TiAB yielding based on the tests results. R.HB.15 and R.HB.20did not reach to the AASHTO moment capacity, and therefore the associated bond strengths of 2.18 and 1.64 ksi, respectively, were not achieved. Figure 8.93 displays the load versus displacement response curves for the hooked-bonded TiAB test specimens.

Table 8.3 – Summary of Hooked-Bonded TiAB Results

Specimen	Failure Mode	Assumed Average Bond Strength (ksi)	l_d (in.)	TiAB Yield
R.HB.15	Excessive Damage	2.18*	7.5	No
R.HB.20	IC Debonding	1.64*	10.0	No
R.HB.30	IC debonding	1.09	15.0	Yes
R.HB.40	CDC Debonding	0.82	20.0	Yes
R.HB.60	TiAB Rupture	0.55	30.0	Yes
	Note: * These values were not achieved.			
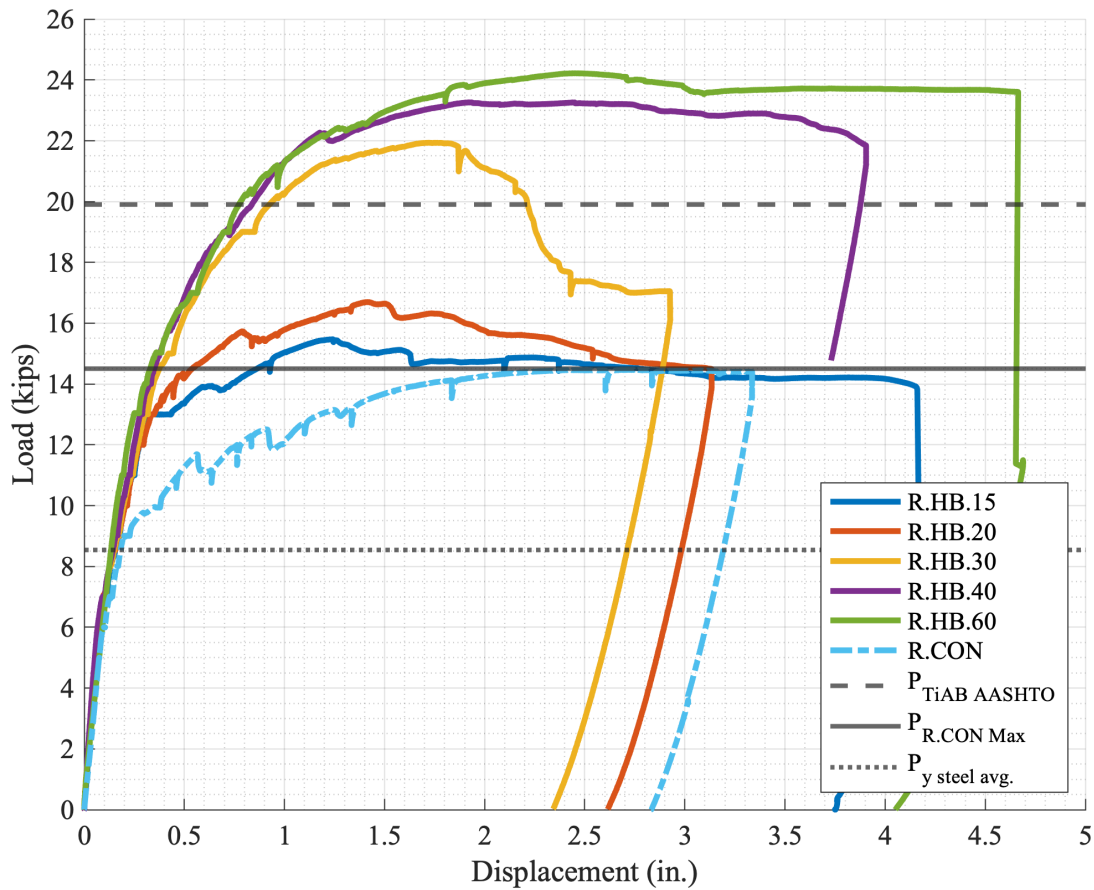
Figure 8.93 - Hooked-Bonded TiAB Load versus Displacement

8.7 Straight-Bonded Results

The straight-bonded specimens had increasing failure load and displacements as the embedded length increased. R.SB.60, R.SB.80, and R.SB.96 achieved yielding of the TiAB by exceeding the calculated AASHTO load capacity. The peak and failure loads and displacements are presented in Table 8.4. The peak load variation against the TiAB embedded length is plotted in Figure 8.91.

Table 8.4 - Straight-Bonded Loads and Displacements

Specimen	AASHTO Capacity (k)	Peak Load (k)	Deflection at Peak (in)	Load at Failure (k)	Deflection at Failure (in)	Peak Moment (k-in)	Maximum Curvature (in⁻¹)
R.CON	9.6	14.47	2.89	14.40	3.39	361	-
R.SB.30	19.8	14.77	0.47	14.77	0.47	399	0.001
R.SB.40	19.8	18.26	0.67	17.44	0.68	493	0.001
R.SB.60	19.8	22.84	1.33	22.73	1.33	617	0.003
R.SB.80	19.8	24.06	2.31	23.40	3.11	650	0.012
R.SB.96	19.8	23.60	1.86	23.40	4.65	637	0.016

Table 8.5 provides the failure mode, average bond strengths, development lengths using Equation 2.4, and the TiAB yielding based on the tests results. As mentioned in Section 4.2.2, 0.5 ksi was expected to be the required bond strength to achieve yielding of the TiAB. R.SB.60 demonstrated that an average bond strength of 0.55 ksi for straight-bonded TiAB would reach the nominal AASHTO flexural capacity given in Equation 2.2. This proves that 0.5 ksi can be considered as a reasonable effective bond strength to reach the member capacity and yield the TiAB. However, the ductile response that makes NSM TiAB advantageous over other strengthening methods (e.g., FRP strengthening) was better exhibited in the longer embedment lengths/lower bond strengths (l_d = 40 [R.SB.80], $\bar{\mu}$ = 0.41 ksi and l_d = 48 [R.SB.96], $\bar{\mu}$ = 0.34 ksi). R.SB.30 and R.SB.40 did not achieve the expected capacity and therefore the associated calculated bond strengths of 1.09 ksi and 0.82 ksi, respectively, were not achieved. Figure 8.94 displays the load versus displacement response curves for all the straight-bonded specimen.

Table 8.5 - Straight-Bonded Yield Results

Specimen	Failure Mode	Assumed Average Bond Strength (ksi)	l_d (in.)	TiAB Yield
R.SB.30	Indeterminate	1.09*	15	No
R.SB.40	CDC Debonding	0.82*	20	No
R.SB.60	Epoxy Rupture	0.55	30	Yes
R.SB.80	TiAB Rupture	0.41	40	Yes
R.SB.96	Concrete Failure/Epoxy Shatter	0.34	48	Yes
Note: * These values were not achieved.				
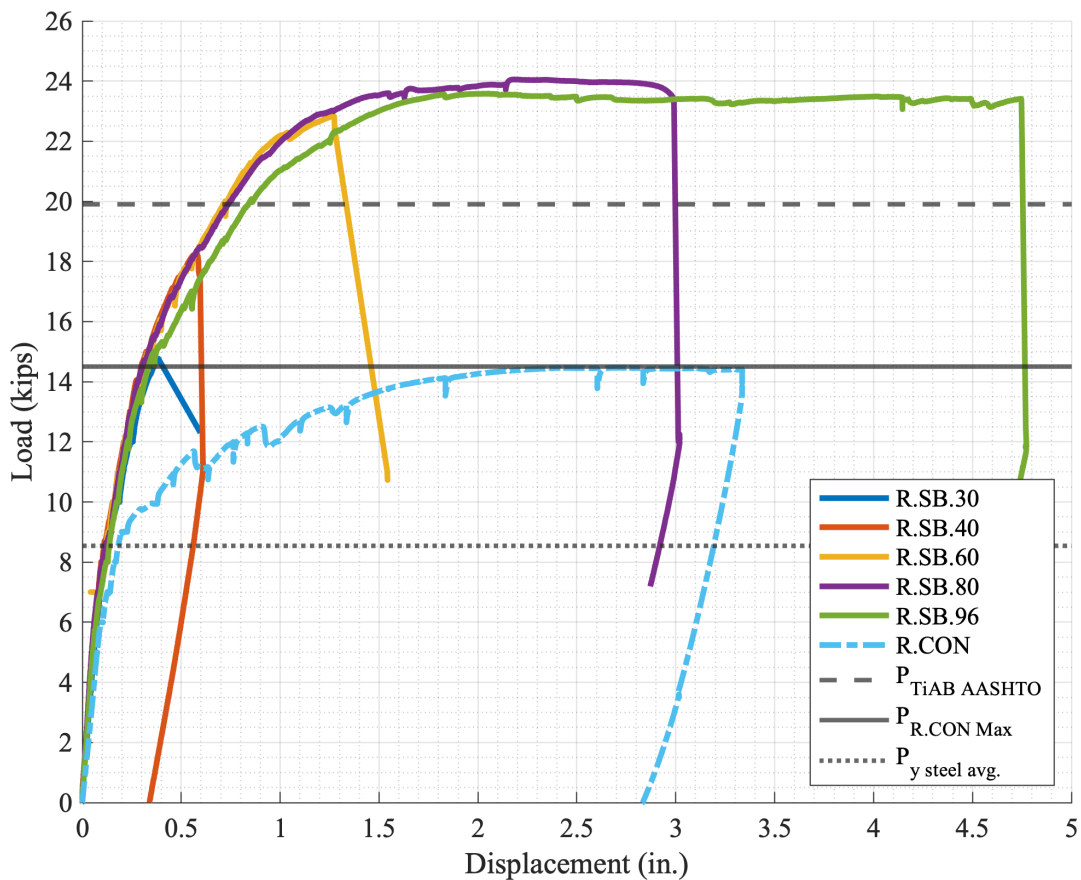
Figure 8.94 - Straight-Bonded Load versus Displacement

8.8 Hooked-Unbonded Results

R.HU.40 and R.HU.60 achieved TiAB yielding and exceeded the AASHTO predicted capacity

of the beam. The peak and failure loads and displacements, maximum curvature, and yield of the

TiAB are presented in Table 8.6. The peak load variation against the TiAB length is plotted in

Figure 8.91. The trend indicates that the longer lengths achieved greater capacity.

Table 8.6 - Hooked-Unbonded Loads and Displacements

Specimen	AASHTO Capacity (k)	Peak Load (k)	Deflection at Peak (in)	Load at Failure (k)	Deflection at Failure (in)	Peak Moment (k-in)	Maximum Curvature (in^{-1})	TiAB Yield
R.CON	9.6	14.47	2.89	14.40	3.39	391	-	N/A
R.HU.10	19.8	13.80	2.29	13.05	4.03	373	0.019	No
R.HU.30	19.8	17.96	0.83	17.49	0.85	485	0.003	No
R.HU.40	19.8	22.89	1.44	21.75	1.66	618	0.010	Yes
R.HU.60	19.8	23.06	1.79	22.81	1.83	623	0.008	Yes

It is also notable that R.HU.60 achieved about the same capacity with the longer length

and larger hook bend diameter of 4.5 inches compared to the standard 3-inch hooked bend

diameter of R.HU.40. The hooked unbonded specimens displayed larger cracks at lower

displacements than the bonded specimens and exhibited lower stiffness. This is concurrent with

the research observed by Eric Vavra (2016) discussed in Section 2.6.6. Figure 8.95 displays the

load versus displacement response curves for all the hooked-unbonded specimens.
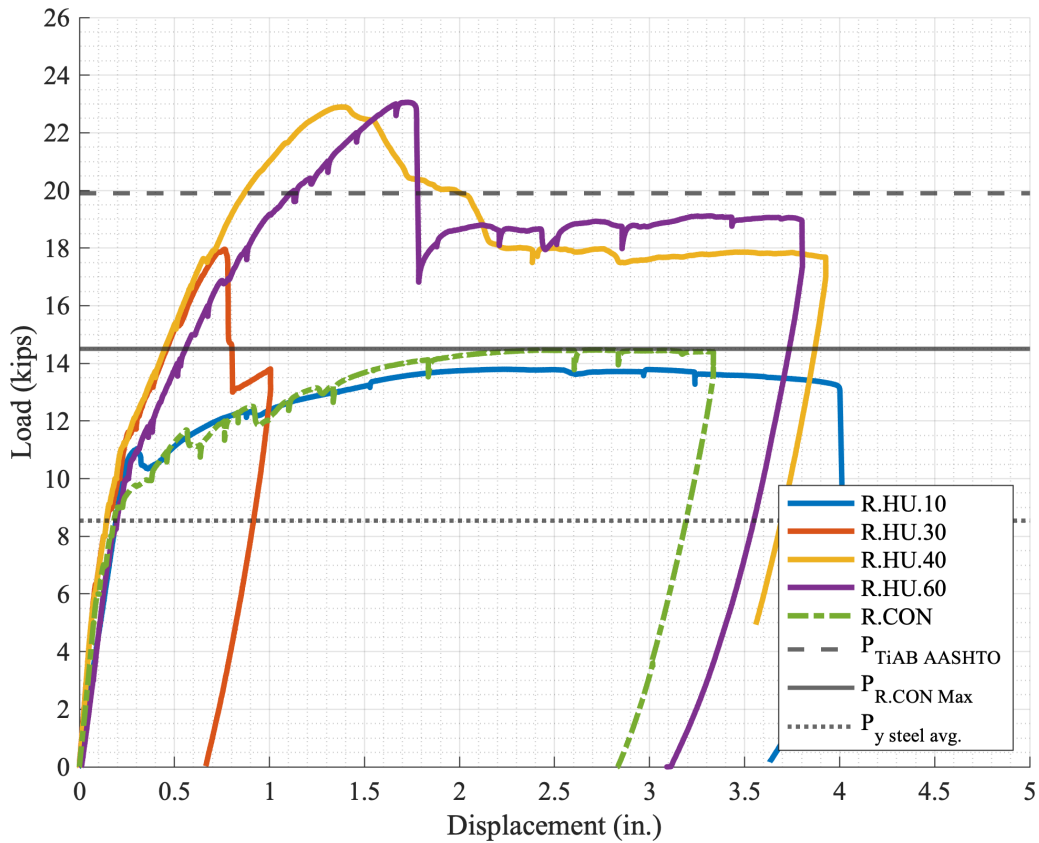
Figure 8.95 - Hooked-Unbonded Load versus Displacement

8.9 Ductility

Ductility is the ability of a structural member to sustain large inelastic deformations in comparison with elastic deformation before collapse or significant loss in resistance according to the definition provided by the Report on Fiber-Reinforced Polymer (FRP) Reinforcement for Concrete Structures by ACI Committee 440 (2007) Figure 8.96 presents the ductility ratio obtained by normalizing the failure displacement to the initiation of steel yielding for the specimens that achieved the predicted AASHTO capacity. These ductility ratios do not properly represent the true nature of the beams' ductility since the TiAB was in the elastic range during the steel reinforcement initiated yielding and exhibited an ascending load-displacement response

196

with a slightly softened response. Figure 8.97 depicts the ductility for the specimens that achieved the predicted AASHTO capacity, by normalizing the failure displacement by the displacement at which TiAB yielding was observed. The specimens that achieved the AASHTO Guide expected capacity indicated ductility ratios in the range of 5.0.
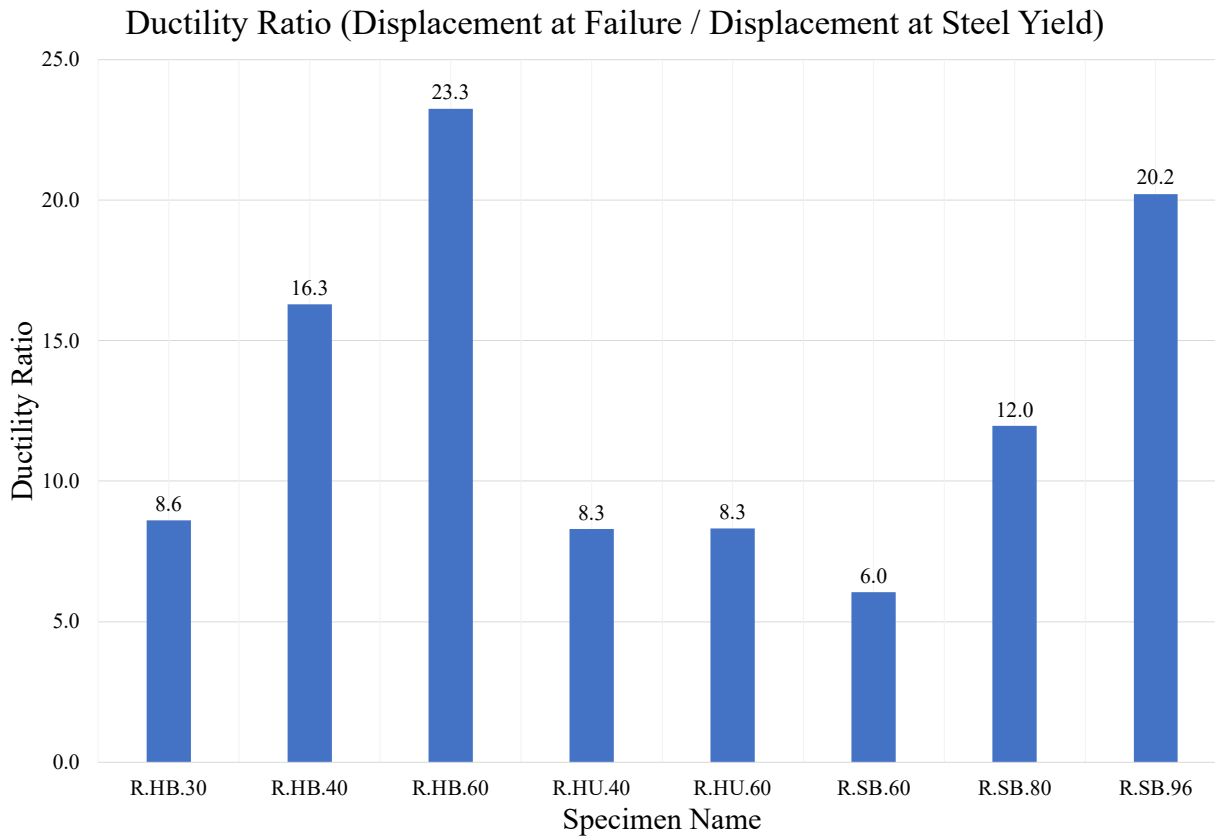
Figure 8.96 – Ductility Ratios using Steel Yield
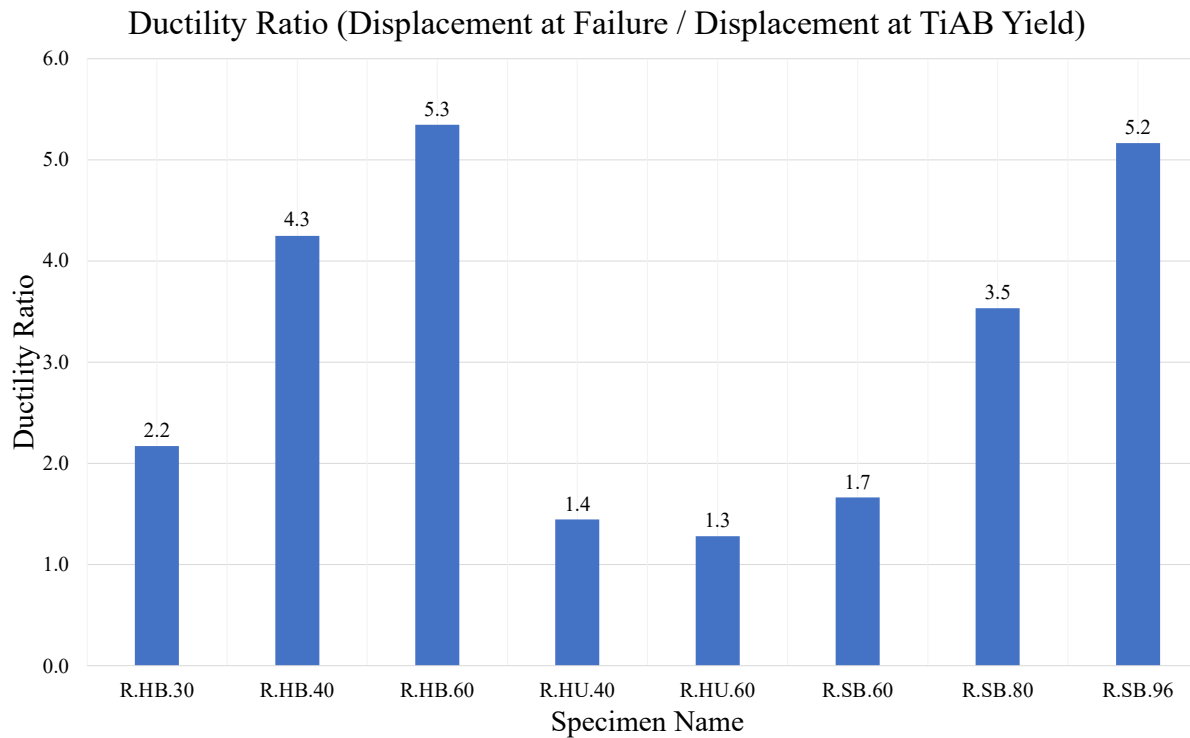
Figure 8.97 - Ductility Ratios using TiAB Yield

The AASHTO Guide provides strain requirements in the extreme layer of tension steel for the resistance factor used in flexural design, as mentioned in Section 2.11.1. The requirements for a strength reduction factor (Φ_b) of 0.9 is obtained for a strain of 0.005 or greater in the extreme layer of longitudinal steel. The longitudinal steel strain was greater than 0.005 for all tests that achieved the predicted AASHTO capacity. Therefore, the design criteria in the AASHTO Guide for a tension-controlled flexural failure was satisfied in these specimens.

CHAPTER 9: SUMMARY AND CONCLUSIONS

9.1 Summary

The repair and strengthening of existing structures have become active research areas in civil engineering with the objective of developing efficient means to extend the service life of bridges to avoid the high cost of replacing transportation infrastructure. Several bridge repair/strengthening methods, including NSM FRP, have been used to extend the service life of aging bridges. The use of NSM TiABs has emerged as another strengthening method because of titanium's corrosive resistance and ductile stress-strain response. AASHTO created the Guide for Design and Construction of Near-Surface Mounted Titanium-Alloy Bars for Strengthening Concrete Structures released in 2020. This guide only designates an average bond strength value (1.0 ksi) for NSM TiAB with hooked anchorages. Factors such as shallow decks, location of original mild steel, and time of installation have led to the consideration of straight-bonded and hooked-unbonded anchorage methods for NSM TiABs. This project investigated: (i) the effective bond strength for bonded TiAB with hooked anchorage (hooked-bonded) to achieve yielding and the assumed 1 ksi of bond strength, (ii) the effective bond strength for bonded TiAB with no hooked anchorage at the bar ends (straight-bonded) to achieve yielding, and (iii) the flexural behavior of TiAB that are unbonded along the length of the bar with hooked anchorage (hooked-unbonded).

Fifteen test specimens, including one control, with varying TiAB strengthening anchorage types and lengths were tested. There were three anchorage types that were used - five hooked-bonded specimens, five straight-bonded specimens, and five hooked-unbonded specimens. The reinforced concrete beams strengthened with different NSM methods had identical overall geometries (length and cross-section), internal steel reinforcement layout (with the exception of

RHU.60 that was rotated 180°), and concrete. The test specimens were pre-cracked and then strengthened with NSM TiABs and loaded until failure.

9.2 Hooked-Bonded Conclusions

Average bond strengths of 1.09 ksi, 0.82 ksi, and 0.55 ksi yielded a hooked-bonded #4 TiAB in a NSM flexural bending application. The specimen that exhibited 1.09 ksi of average bond strength achieved the expected strength expected from the AASHTO Guide's nominal moment equation adapted for the use of NSM TiAB. However, improved ductility was observed with longer bonded lengths that represent a lower average bond strength such as 0.82 ksi. The AASHTO Guide average bond strength recommendation of 1.0 ksi for hooked-bonded anchorage method appears to be a reasonable effective bond strength designation based on the testing conducted in this research, but large-scale testing is recommended to gain greater confidence for use in design documents

9.3 Straight-Bonded Conclusions

 Average bond strengths of 0.55 ksi, 0.41 ksi, and 0.34 ksi yielded a straight-bonded #4 TiABs in a NSM flexural bending application. The specimen that exhibited the 0.55 ksi of average bond strength achieved the expected strength expected from the AASHTO Guide's nominal moment equation adapted for the use of NSM TiAB for hooked-bonded anchorage. However, more ductile behavior was observed in development lengths that represent a lower average bond strength such as 0.41 ksi. 0.5 ksi for straight-bonded anchorage methods appears to be a reasonable effective bond strength designation based on the testing conducted in this research, but large-scale testing is recommended to gain greater confidence for use in design documents.

9.4 Hooked-Unbonded Conclusions

Specimens mounted with hooked-unbonded TiAB achieved yielding and similar capacities as the hooked-bonded and straight-bonded strengthening methods with larger crack widths and a lower stiffness. The observed low stiffness and large crack widths supports Eriv Vavra's (2016) recommendations to use hooked-unbonded TiAB for temporary operations.

9.5 Remarks on Member Ductility

Two of the main advantages of using NSM TiAB as a near-surface-mounting option are the steel-like stress versus strain behavior and the mechanical ability to form hooks. The conventional definition of ductility considers inelastic deformations to start at the initiation of steel yielding. However, for NSM TiAB applications, considering the inelastic deformations to start after the TiAB yielding is a better reference point to quantify ductility. This is due to TiAB being in the elastic region when the steel reinforcement enters yielding, and the force capacity increases significantly beyond this point. When measuring the ductility from TiAB yielding, the specimens that achieved the AASHTO Guide expected capacity indicated ductility factors in the range of 5.0, which is significantly higher than specimens strengthened using NSM-FRP.

9.6 Research Needs

To further investigate the effective bond stress and development length of NSM TiAB the following research is needed (i) The performance of varying sizes of NSM TiABs (ii) The effects of varying the details of the hooked anchorage (i.e., pin diameter and tail length) (iii) large-scale tests that demonstrate full-scale bridge members with more dominant flexure behavior (iv) Asses the effect of cyclic loads on NSM TiAB straight-bonded and hooked-unbonded strengthening methods.

REFERENCES

AASHTO. (2020). *AASHTO Guide for Design and Construction of Near-Surface Mounted Titanium Alloy Bars for Strengthening Concrete Structures* (2020th ed.).

ACI Committee 440. (2007). *Report on fiber-reinforced polymer (FRP) reinforcement for concrete structures* (3. print). American Concrete Inst.

ACI Committee 440. (2017). *Guide for the design and construction of externally bonded FRP systems for strengthening concrete structures*. American Concrete Institute.

ACI Committee 546. (2014). *Guide to concrete repair*. American Concrete Institute.

Al-Mahmoud, F., Castel, A., François, R., & Tourneur, C. (2009). Strengthening of RC members with near-surface mounted CFRP rods. *Composite Structures*, *91*(2), 138–147. https://doi.org/10.1016/j.compstruct.2009.04.040

Amneus, D. (2014). *Methods for Strengthening Flexural Steel Details In Reinforced Concrete Bridge Girders using a Near-Surface Mounted Retrofitting Technique*. Oregan State University.

ASTM B1009 (2020) *Standard Specification for Titanium Alloy Bars for Near Surface Mounts in Civil Structures*. ASTM International. https://doi.org/10.1520/B1009-20

ASTM C0039/C0039M. (2021). *Test Method for Compressive Strength of Cylindrical Concrete Specimens*. ASTM International. https://doi.org/10.1520/C0039_C0039M-21

ASTM D638. 2022. *Standard Test Method for Tensile Properties of Plastics*. ASTM International. https://doi.org/10.1520/D0638-22

ASTM E000/E0008M (2022). *Test Methods for Tension Testing of Metallic Materials*. ASTM International. https://doi.org/10.1520/E0008_E0008M-22

Barker, L. (2014). *Flexural Anchorage Performance and Strenghtening on Negative Moment Regions Using Near-Surface Mounted Retrofitting in Reinforced Concrete Bridge Girders*. Oregan State University.

Bertolotti, E. (2012). *Near-Surface-Mounted Fiber-Reinforced Polymer Strips for Strengthening of Reinforced Concrete Girders*. Auburn University.

Bomberger, H. B., Cambourelis, P. J., and Hutchinson, G. E. (1954). Corrosion Properties of Titanium in Marine Environments. *Journal of The Electrochemical Society*, *101*(9), 442. https://doi.org/10.1149/1.2781297

Choi, K.-S., Lee, D., You, Y.-C., & Whan Han, S. (2022). Long-term performance of 15-year-old full-scale RC beams strengthened with EB FRP composites. *Composite Structures*, *299*, 116055. https://doi.org/10.1016/j.compstruct.2022.116055

Coelho, M. R. F., Sena-Cruz, J. M., and Neves, L. A. C. (2015). A review on the bond behavior of FRP NSM systems in concrete. *Construction and Building Materials*, *93*, 1157–1169. https://doi.org/10.1016/j.conbuildmat.2015.05.010

Hadi, S., kazeminezhad, E., and safakhah, S. (2022). Full-scale experimental evaluation of flexural strength and ductility of reinforced concrete beams strengthened with various FRP mechanisms. *Structures*, *43*, 1160–1176. https://doi.org/10.1016/j.istruc.2022.07.011

Hassan, T., and Rizkalla, S. (2003). Investigation of Bond in Concrete Structures Strengthened with Near Surface Mounted Carbon Fiber Reinforced Polymer Strips. *Journal of Composites for Construction*, *7*(3), 248–257. https://doi.org/10.1061/(ASCE)1090-0268(2003)7:3(248)

Higgins, C., Amneus, D., & Barker, L. (2015a). *Methods for Strengthening Reinforced Concrete Bridge Girders Containing Poorly Detailed Flexural Steel Using Near-Surface Mounted Metallics* (Final Report SPR 750; p. 138). Oregant State University.

Higgins, C., Amneus, D., & Barker, L. (2015b). Titanium alloy bars for strengthening a reinforced concrete bridge. In *Sustainable Bridge Structures: Proceedings of the 8th New York City Bridge.* (p. CH. 20 225-234). CRC PRESS.

Higgins, C., Knudtsen, J., Amneus, D., & Barker, L. (2017, April). *Shear and Flexural Strengthening of Reinforced Concrete Beams with Titanium Alloy Bars*. The 2nd World Congress on Civil, Structural, and Environmental Engineering. https://doi.org/10.11159/icsenm17.141

Hilti. (2021). *Hilti North American Product Technical Guide*.

Jill Adkins and Warren George. (2017). Titanium Finds a Home in Civil Engineering. *Concrete International*, *39*(12).

Maheswaran, J., Chellapandian, M., & Arunachelam, N. (2022). Retrofitting of severely damaged reinforced concrete members using fiber reinforced polymers: A comprehensive review. *Structures*, *38*, 1257–1276. https://doi.org/10.1016/j.istruc.2022.02.059

Nowak, A., and Latsko, O. (2018). Are Our Bridges Safe? *The Bridge*, *48*(2), 27–30.

Nurbaiah, M. N., Hanizah, A. H., Nursafarina, A., & Nur Ashikin, M. (2010). Flexural behaviour of RC beams strengthened With externally bonded (EB) FRP sheets or Near Surface Mounted (NSM) FRP rods method. *2010 International Conference on Science and Social Research (CSSR 2010)*, 1232–1237. https://doi.org/10.1109/CSSR.2010.5773725

Perryman Company. (2021). *Bridge Bar Bending Work Instructions*. Perryman Company.

Platt, S., and Harries, K. A. (2018). Study of galvanic corrosion potential of NSM titanium

reinforcing bars. *Case Studies in Construction Materials*, *9*, e00175.

https://doi.org/10.1016/j.cscm.2018.e00175

Platt, S. L., Harries, K. A., & McCabe, M. J. (2019). Reinforced Concrete Bridge Deck Repair

with Titanium NSM. In R. Dissanayake & P. Mendis (Eds.), *ICSBE 2018* (Vol. 44, pp.

447–457). Springer Singapore. https://doi.org/10.1007/978-981-13-9749-3_39

Prediction of creep, shrinkage, and temperature effects in concrete structures. (2009). American

Concrete Institute.

Subagia, I. D. G. A., and Kim, Y. (2014). Tensile behavior of hybrid epoxy composite laminate

containing carbon and basalt fibers. *Science and Engineering of Composite Materials*,

21(2), 211–217. https://doi.org/10.1515/secm-2013-0003

Vavra, E. (2016). *Application of Titanium Alloy Bars For Strengthening Reinforced Concrete

Bridge Girders in Flexure*. Oregan State University.

Zhang, S. S., Yu, T., and Chen, G. M. (2017). Reinforced concrete beams strengthened in flexure

with near-surface mounted (NSM) CFRP strips: Current status and research needs.

Composites Part B: Engineering, *131*, 30–42.

https://doi.org/10.1016/j.compositesb.2017.07.072

APPENDIX A: FIELD INSTALLATION PROCEDURE

Based on the experience gained during laboratory testing regarding the Near Surface mounting (NSM) of Titanium-alloy Bars (TiAB) as well as the current guidelines found in the AASHTO Guide for Design and Construction of Near-Surface Mounted Titanium-alloy Bars for Strengthening Concrete Structures (2020) the following field installation procedure has been recommended:

A.1 – Hooked-Bonded Bars

1. Cut grooves in the concrete using a wet track saw with a circular diamond blade. The width and the depth of the groove must be at least 1.5 times the diameter of the TiAB used for strengthening. The minimum edge distance must be at least 6 times the diameter of the TiAB and the minimum clear spacing between grooves must be at least 3 times the diameter of the TiAB. The tolerance for these dimensions and clearance requirements must fall within 1/4 in. If a single blade wide enough to create a groove to the dimensions required, stacking blades is permitted.

2. Ensure that the slurry that is created from the wet-cutting can be sucked up using an industrial wet-dry vacuum or has a designated run-off area that complies with the local authority's rules and regulations.

3. Confirm existing steel reinforcement will not be cut or damaged during the groove cutting using non-destructive means such as a ground-penetrating radar.

4. Create the TiAB hooks using an industrial grade rebar cutter/bender and an acetylene-oxygen torch by following the these (iv) steps. To create the desired results is typically an

iterative process and using scrap metal for these iii steps is advised before moving on to bending TiABs.

    i. Cut the TiAB using the industrial grade rebar cutting equipment. The cut length can be determined using the following equation provided by the TiAB supplier:

$$L=(W-D-2R) + (H-R-D/2)2 + \pi R$$

    Where:

        L = Bar length prior to bending (Cut Length)

        W = Straight Length (Outside to Outside of hook)

        D = TiAB Diameter

        H = Total Hook Length (the distance from the tip of the hook to the tangent line that runs parallel to the main portion of the TiAB)

        R = Mandrel radius

    ii. Heat the TiAB bend area using an acetylene-oxygen torch with a rosebud torch tip to 1200°F. At 900°F it will turn a straw color and at 1200°F it will turn a blue color. If a red tinge develops, the anneal temperature has been exceeded and the bar should be disposed of and not used for reinforced concrete strengthening.

    iii. While the TiAB is still hot (1200°F) place it in the bar bending machine equipped with the mandrel radius matching the desired radius of the TiAB. Be sure to make the hook at the other end in the same plane as the first

hook. This can be accomplished by placing the already made hook on a table the same height as the bar bending machine.

5. Use a hammer drill with the same size bit as the width of the groove to drill holes the same depth as the total hook length. Since the bars will be resting in the groove, drilling the holes the same depth as the total hook length will provide excess depth the diameter of the TiAB.

6. The hooked TiAB will not be able to fit into the groove and hole without beveling the concrete substrate to match the radius of the bar. This can be achieved with a hammer and chisel. Periodically check to ensure that the bevel is the correct radius and that too much concrete is not being taken off because the bearing area between the concrete and the TiAB is critical for the positive behavior of the NSM reinforcement. If time and resources allow it a jig can be created to guide the hammer drill out of the hole at the same curvature as the radius of the TiAB. The bevel can then be refined using the hammer and chisel.

7. The groove and holes can then be prepared and cleaned by using low-pressure water blasting with adhesive. This can be done by using a 1500-5000 psi pressure washer with a nozzle attachment that feeds sand (abrasive) into the high-pressure stream. Masonry sand is a suitable abrasive. 5-7 passes or until the pores of the concrete are openly exposed is adequate. A final pass with only the high-pressure water stream and no abrasives is recommended to clear the groove and holes of any residual sand. After this step, wait to continue with step 8 until the entirety of the groove is dry to the touch.

8. Find a rubber hose/tube with the outside diameter that is the same as the width of the groove and an inside diameter the same as the diameter of the TiAB. Cut the hose/tube

into half-inch segments and slide them onto the TiAB to act as wedges. This is a good method because it simultaneously keeps the TiAB from falling out and centers the TiAB inside of the groove. Place the wedges at whatever spacing will keep the TiAB from falling out. Spacing them at 18 inches is typically sufficient. If extra friction is required, increase the diameter of the wedge by wrapping it in electrical tape cut to the same width as the wedge. Test to make sure the TiAB will stay before applying any epoxy.

9. If placing the epoxy in the groove on a hot day, keep the epoxy refrigerated at its lowest allowed storage temperature (i.e., 41°F for Hilti Hit-RE-500 V3). This will keep the viscosity of the epoxy high enough to stay inside the groove.

10. Before applying any TiABs place inch-long wooden blocks the same width and depth of the groove two inches past the ends of the TiAB to give the epoxy a stopping point. If they are sliding out, use tape to increase the thickness of the wooden blocks similarly to what was done in step 8.

11. Start the first lift of epoxy application by completely filling the holes for the hooks. Holding a rag around the end of the epoxy gun and against the concrete closes the hole allowing the epoxy to completely fill it without any falling/dripping out.

12. The next step of the installation is to place the nipple of the epoxy gun at one of the stops and start applying the first lift. The first lift of epoxy application is intended to fill the groove two-thirds of the way. The epoxy must be consolidated, and air bubbles removed. The best way to do this is to follow immediately behind the nipple of the epoxy gun with a consolidating tool. A custom wooden trowel with a triangular prism that has the same base width as the groove and height that is two-thirds of the groove depth has proven to work effectively.

13. After the first lift of epoxy, the TiABs are ready to be installed. Gently place the bars, that have been properly fitted with wedges, into the groove applying even pressure along the whole length of the bar. Continue to apply pressure until it is completely seated into the center of the groove and holding on its own.

14. At this point the final lift of epoxy can be applied. Again, start by placing the nipple of the epoxy gun at one of the stops and work towards the other end with the putty knife immediately following. Once the rest of the TiAB is covered, use the putty knife to smooth the surface of the epoxy and remove excess epoxy from the outside of the groove.

15. Steps 11- 14 should be completed within the working time of the epoxy. Depending on the epoxy and outside temperature, this working time can vary anywhere from 10 minutes to 2 hours. See the technical information describing the epoxy being used and plan accordingly.

16. Allow the epoxy to achieve full cure according to the technical information provided before re-opening the newly reinforced area. The full cure time can vary from 4 hours to 7 days based on the epoxy and ambient conditions.

A.2 – Straight-Bonded Bars

Follow steps from Section A.1 but skip steps 4-6 and 11.

A.3 – Hooked Bonded Bars

Follow steps from Section A.1 but skip steps 1,2,8,10,12 and 14.

phase -1

NUCOR

Mill Certification
01/13/2021

MTR#:590440-2
Lot #:380001667620
3630 Fourth Street
Flowood, MS 39232 US
601 939-1623
Fax: 601 936-6202

Sold To: SABEL STEEL SERVICE INC
PO BOX 4747
MONTGOMERY, AL 36103 US

Ship To: SABEL STEEL SERVICES INC
704 LAFAYETTE ST
MONTGOMERY, AL 36104 US

Customer PO	06-2020-087		Sales Order #	37014179 - 9.1
Product Group	Rebar		Product #	1053861
Grade	A615 Gr 60/AASHTO M31		Lot #	380001667620
Size	#3		Heat #	3800016676
BOL #	BOL-667443		Load #	590440
Description	Rebar #3/10mm A615 Gr 60/AASHTO M31 40' 0" [480"] 2001-6000 lbs		Customer Part #	
Production Date	12/18/2020		Qty Shipped LBS	25265
Product Country Of Origin	United States		Qty Shipped EA	1680
Original Item Description			Original Item Number	

I hereby certify that the material described herein has been manufactured in accordance with the specifications and standards listed above and that it satisfies those requirements.

Melt Country of Origin : United States

Melting Date: 12/11/2020

C (%)	Mn (%)	P (%)	S (%)	Si (%)	Ni (%)	Cr (%)	Mo (%)	Cu (%)	V (%)	Nb (%)
0.39	0.82	0.011	0.026	0.210	0.10	0.10	0.03	0.25	0.029	0.001

Other Test Results

Yield (PSI) : 73400

Tensile (PSI) : 100000

Average Deformation Height (IN)   0.031

Elongation in 8" (%) : 18.8

Bend Test . Pass

Weight Percent Variance (%) : -3.09

Comments:

Nucor Steel Jackson. Inc. is ISO 9001:2015, 14001:2015, and ABS certified. All manufacturing processes of the steel materials in this product. including melting. have occurred within the United States. Mercury, in any form has not been used in the production or testing of this material Manufactured in the US and complies with the Buy American Act. No weld repair was performed.

Nolan Guess. Quality Supervisor

Page 1 of 1

Perryman company

213 Vandale Drive Houston, PA 15342   USA
phone: 724-746-9390   fax: 724-746-9392

Certified Test Report

Customer:	Auburn University 311 Ingram Hall Auburn, AL 36849	Heat No:	PVD7162	Date:	8/9/2021	
		Melting Source:	Perryman Company, USA	Quantity:	369	FT
		Work Order No:	159425			

Customer Order No:	Donation	Product:	Ti 6Al-4V 0.500" +/-0.001" Dia. Bridgealloy X 15'-20' lengths Straight lengths - no hooks
Specification:	ASTM B1009 Class 130 (2020)		
		Condition:	Annealed 1400 F - 2 hours

Chemistry Wt %	ASTM E 1447:	Post processing Hydrogen Determination		H: .0007	
Metallographic Examination: Etchant: PER1 & PER2	ASTM E407:	Microstructure -	Equiax alpha-beta	ASTM E 407: Surface Contamination -	No alpha case 500x

Mechanical Properties ASTM E8/EN 2002-001:2005E	Tensile Strength	.2% Yield Strength	Elongation 4D		
Condition	ksi	ksi	%		
As Shipped	152.4	137.1	11		
	150.4	135.9	13		

Bend Tests acceptable.
Calculated cross sectional area = 0.1899 in2
Tensile Modulus = 15.2 Msi

This is to certify that all test results conform to the specifications listed above and that all tests required were performed by Perryman Company.
The material did not come in contact with Mercury or radioactive contamination at Perryman.
Attached is a copy of the Ingot Chemistry. All testing performed at room temperature unless otherwise noted.
The test results relate only to the lots tested and are contained in the records of Perryman Company. The Certified Test Report cannot be reproduced except in full,
without written approval. Made in USA.

8/9/2021
Zachary S. Degan
Laboratory Manager

Nadcap
ACCREDITED
Materials Testing Laboratory

Page 1 of 1

APPENDIX C: BAR BENDING WORK INSTRUCTIONS

Perryman company	Corporate Address: 213 Vandale Drive Houston, PA 15342 P: 724.746.9390 F: 724.746.9392	Document Title: Bridge Bar Bending Work Instructions
		Document Number: B 9.5 WI
		Revision Number: 1
		Effective:
		Page: 1 of 7

1.0 Scope

    1.1 This work instruction provides a guideline to bend the 90° anchorage hook on the textured or untextured Bridgealloy™ bars.

    1.2 This can also be used as a guideline for general bending of titanium bars.

    1.3 It can be applicable for other angles.

2.0 References

    2.1 PC-1200 Bridgealloy™ Materials Specification

    2.2 CRSI Manual of Standard Practice

3.0 Definitions

    3.1 Leg distance – Straight portion of anchorage hook.

    3.2 Anchorage hook length – Leg length + mandrel radius + bar diameter or measurement from end of hook to outside diameter of perpendicular portion of bar.
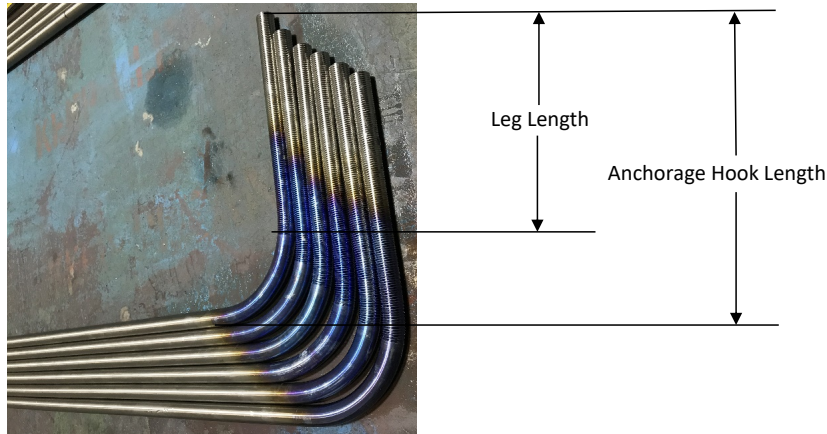
    3.3 Hydraulic rebar bender – Portable machine used to quickly fabricate rebar on the job or at the shop. The machine used at Perryman Company is FASTCUT FR-800 ReBar Bender.

    3.4 Mandrel – A cylindrical rod around which metal or other material is shaped. The mandrels used at Perryman Company were manufactured in house from 304 stainless steel. Mandrel diameter will be dependent on job requirement.

    3.5 CRSI – Concrete Reinforcing Steel Institute

    3.6 Bar size numbers – Rebar size numbering system measured in 1/8" increments. For example, bar size 5 is equivalent to 5/8" diameter.

4.0 Safety
    4.1 Safety glasses.
    4.2 Face shield.
    4.3 Heat resistant gloves.
    4.4 Ear protection.
    4.5 Personal protective equipment on job site as required.

5.0 Responsibilities
    5.1 Bar Mill operators will follow these work instructions.
    5.2 Bar Mill supervisors will make sure operators follow these work instructions.
    5.3 Site contractor and employees will follow these work instructions when bending on site.

6.0 Procedure
    6.1 Calculate cut length of straight bars using the following equation if both ends are being bent: +

$$L=(W-D-2R) + (H-R-D/2)2 + \pi R$$

L = bar length prior to bending
W = Straight length
D = Bar diameter
H = Anchorage length
R = Mandrel radius
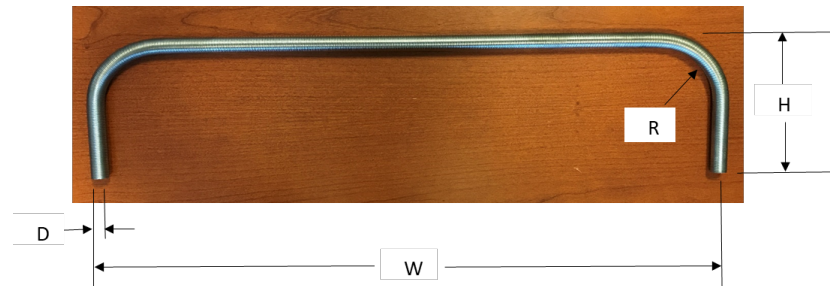
        6.1.1   Cut bars to length.
    6.2 Acquire a scrap bar equivalent in size to prime bars to set up prior to bending prime bars.
        6.2.1   Check bar for irregularities, such as cracks, prior to bending.
    6.3 Set mandrel on hydraulic rebar bender to job required diameter.
    6.4 Set bender for 90° with overbend (2°) to account for spring back.

     6.4.1   Measure angle after bending and adjust as necessary.

6.5 Measure leg distance from center of mandrel to bar stop. For set up of the bar stop, subtract the radius of the bar from the leg length.

     6.5.1   Example:

           Diameter of bar = 0.625"

           Leg length = 3.5"

           Stop position = 3.5 - 0.625/2 = 3.1875" from center of mandrel

           See diagram below:
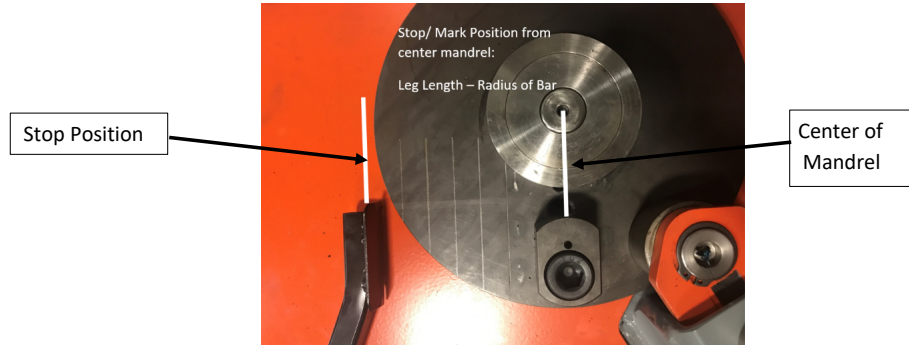
6.6 Turn on hydraulic rebar bending machine.

6.7 Define heating area on the bar starting 3" before the bend area and ending 3" past the bend area.

6.8 Heat bar.

     6.8.1   Use a propane/oxygen torch with rosebud torch tip. Use the hottest point of the torch about 1"-1.5" from tip.

     6.8.2   Proximity of torch heating needs to be close enough to the hydraulic rebar bender for quick transfer.

     6.8.3   The bar needs to be positioned on top of something fire resistant (such as a metal vice) for ease of rotating and stabilizing.

     6.8.4   Heat the bend area while rotating bar until the bar turns blue. For example, a 0.625" diameter bar it should take approximately 1 minute 45 seconds.

6.8.4.1 Straw or yellow color equates to approximately 900°F. Too cold for bending. Continue to heat until blue.
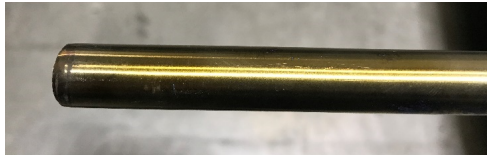
6.8.4.2 Blue color equates to approximately 1200°F. This is the desired color and temperature.

6.8.4.3 If the bar turns red hot, it indicates it is overheated. Contact supervisor for disposition of bar if overheated.

6.8.4.4 If necessary, temperature sticks can be used to confirm temperature.

6.9 Immediately move bar to rebar bender and insert the bar to the stop or a designated mark.
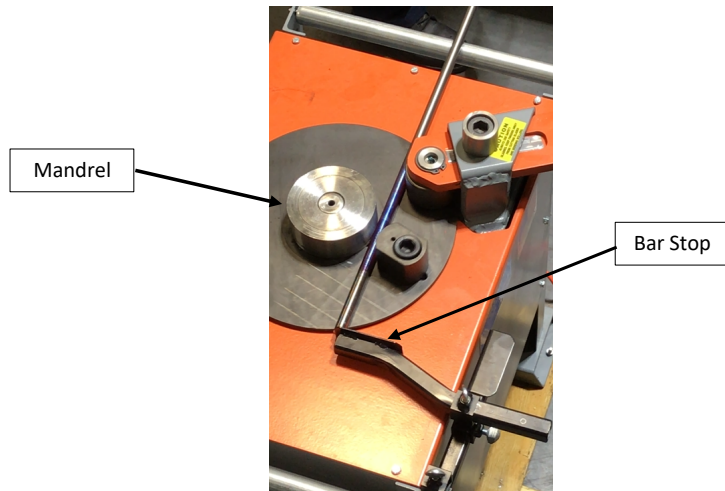
6.9.1 Bend bar immediately while hot.

6.9.2 If one end already has a hook, direction of bar and flatness will be critical. Ensure that hook lays on flat surface while bending the other hooked end.

Uncontrolled Document When Printed Unless Superseded by a Controlled Copy Stamp

6.9.2.1 Flat surface can be any type of table that is on the same plane as the rebar bender.

6.10   Bar can be water quenched for handling purposes.

6.10.1   This can be accomplished with a hose or bucket of water and will cool in seconds once in contact with water.

6.11   Check the bend angle for perpendicularity and anchorage length.

6.11.1   Bend angle can be checked with machinist square.

6.11.2   Per CRSI Manual of Standard Practice, Angular Deviation – maximum +/- 2 ½° or +/- ½ in./ft. but not less than ½ in. on all 90° hooks and bends.

6.11.3   Anchorage hook length can be checked with tape measure.

6.11.4   Per CRSI Manual of Standard Practice, for bar sizes #3 through #11 (see definitions), the dimensional tolerance for leg length = +/- 1". Perryman aims at +/- ¼".   +

6.12   Make necessary adjustments and repeat with scrap bar. When all criteria are met, begin bending prime bars.

6.13   If bars are textured on the bend, use a die grinder assembled with a 40 grit flat wheel to remove the texture on inside diameter of the bend.   +

6.13.1   Grind in longitudinal direction perpendicular to the transverse texture.

6.13.2   Removal amount is approximately 0.010".   +

218

7.0 Revision History

REVISION	DESCRIPTION OF CHANGE
0	Original
1	6.1 Added equation to calculate the straight lengths prior to bending. 6.11 Added photo. 6.13 Changed tool for grinding bend ID and added photos.

APPENDIX D: HILTI EPOXY CURE TIMES

Table 1 — Material properties of fully cured Hilti HIT-RE 500 V3

Bond Strength ASTM C882-13A[1] 2 day cure 14 day cure	10.8 MPa 11.7 MPa	1,560 psi 1,690 psi
Compressive Strength ASTM D695-10[1]	82.7 MPa	12,000 psi
Compressive Modulus ASTM D695-10[1]	2,600 MPa	0.38×10^6 psi
Tensile Strength 7 day ASTM D638-14	49.3 MPa	7,150 psi
Elongation at break ASTM D638-14	1.1%	1.1%
Heat Deflection Temperature ASTM D648-07	50°C	122°F
Absorption ASTM D570-98	0.18%	0.18%
Linear Coefficient of Shrinkage on Cure ASTM D2566-86	0.008	0.008

1 Minimum values obtained as the result of tests at 35°F, 50°F, 75°F and 110°F.

[°F]	[°C]	t_{work}	$t_{cure, ini}$	$t_{cure, full}$
23	-5	2 h	48 h	168 h
32	0	2 h	24 h	36 h
40	4	2 h	16 h	24 h
50	10	1.5 h	12 h	16 h
60	16	1 h	8 h	16 h
72	22	25 min	4 h	6.5 h
85	29	15 min	2.5 h	5 h
95	35	12 min	2 h	4.5 h
105	41	10 min	2 h	4 h

APPENDIX E: EXAMPLE CALCULATIONS

$A_s = 0.4$ in^2
$A_{Ti} = 0.2$ in^2
$b_f = 9.0$ in.
$d_s = 9.9$ in.
$d_{Ti} = 11.6$ in.
$f'_c = 5000$ psi
$f_y = 68$ ksi
$f^*_{yTi} = 131$ ksi
$\alpha_E = 1.0$

$$\beta_{1c} = \frac{A_s f_y + A_{Ti}\alpha_E f^*_{yTi}}{0.85 f'_c b_f}$$

$$M_n = A_s f_y \left(d_{Ti} - \frac{\beta_1 c}{2}\right) + A_{Ti}\alpha_E f^*_{yTi}\left(d_{Ti} - \frac{\beta_1 c}{2}\right)$$

$$P_n = \frac{M_n * 4}{108}$$

Unstrengthened Beam Calculations:

$$\beta_{1c} = \frac{(0.4\ in.^2) * (68\ ksi) + (0\ in.^2) * (1.0) * (0\ ksi)}{0.85 * (5.0\ ksi) * (9.0\ in.)}$$

$\beta_{1c} = 0.7$

$$M_n = 0.4\ in.^2 * (68\ ksi)\left(9.9 - \frac{0.7}{2}\right) + 0.0\ in.^2 * (1.0) * (131\ ksi) * \left(0\ in. - \frac{0.7}{2}\right)$$

$M_n = 260$ k-in

$$P_n = \frac{260\ k-in * 4}{108}$$

$P_n = 9.6$ k

Strengthened Beam Calculations:

$$\beta_{1c} = \frac{(0.4\ in.^2) * (68\ ksi) + (0.2\ in.^2) * (1.0) * (131\ ksi)}{0.85 * (5.0\ ksi) * (9.0\ in.)}$$

$\beta_{1c} = 1.4$

$$M_n = 0.4 \ in.^2 * (68 \ ksi) \left(9.9 - \frac{1.4}{2}\right) + 0.2 \ in.^2 * (1.0) * (131 \ ksi) * \left(11.6 \ in. - \frac{1.4}{2}\right)$$

$M_n = 536$ k-in

$$P_n = \frac{536 \ k - in * 4}{108}$$

$P_n = 19.8$ k

Example l$_{dTi}$ Calculations:

R.HB.30
$f^*_{yTi} = 120$ ksi
$D_{Ti} = 0.5$ in.
$\overline{\mu_u} = 1.0$ ksi

$$l_{dTi} = \frac{D_{Ti}}{4} \frac{\alpha_E f^*_{yTi}}{\overline{\mu_u}}$$

$$l_{dTi} = \frac{(0.5 \ in.)}{4} \frac{1.0 * (120 \ ksi)}{(1.0 \ ksi)}$$

$l_{dTi} = 15$ in.

APPENDIX F: CULLMAN BRIDGE CONCRETE CORE STRENGTHS

Lab NO.	FGR-512-19
Project NO(S):	99-500-680-000-401
Not Sure what this is:	BMT-16. Rev. 10/87
Date Received:	9/27/19
Date Tested:	10/2/19
Tested By:	Weiss/Barker
Testing Engineer:	Steven Ingram

Core Number	Diameter (In.)	Area (in^2)	Load @ Rupture (lb)	Compressive (psi)	Corrected Compressive psi (H/D Ratio)	Length of Core: Capped (in.)
1	2.988	7.012	34300	4890	4690	4.471
2	2.986	7.003	28600	4080	3960	4.868
3	2.989	7.017	28700	4090	(2.00)	5.981
4	2.896	6.587	42000	6370	6050	3.976
5	2.987	7.007	33100	4720	4520	4.347
6	2.987	7.007	31700	4530	4390	4.308